NONSTRUCTURAL COMPONENT FIELD TESTING METHOD FOR THE EVALUATION OF SEISMIC DEMAND INCORPORATING FLOOR RESPONSE SPECTRUM

by

Yan Yang

B.A.Sc., The University of British Columbia, 2011

A THESIS SUBMITTED IN PARTIAL FULFILLMENT OF

THE REQUIREMENTS FOR THE DEGREE OF

MASTER OF APPLIED SCIENCE

in

THE FACULTY OF GRADUATE AND POSTDOCTORAL STUDIES

(Civil Engineering)

THE UNIVERSITY OF BRITISH COLUMBIA

(Vancouver)

April 2014

Abstract

Nonstructural component (NSC) failures due to earthquake events can cause significant economic losses and even life-threatening hazards to occupants. In order to mitigate nonstructural seismic damages, it is critical to assess the seismic force demand which can be utilized to optimize the design of the NSC, and/or to assess methods of rehabilitation on anchorages to enhance seismic strength.

The existing design codes and standards provide guidelines to calculate the minimum lateral earthquake force for designing a new NSC. However, they do not reflect the in-service condition of an existing NSC, which can vary significantly from when it was first installed. This study is intended to develop an easy-to-implement methodology to assess the seismic force demand of an existing NSC under normal operation.

The procedure of the proposed methodology includes two principle phases: 1) field modal identification testing and 2) floor response spectrum analyses using a 3D finite element model (FEM). The practicality of this methodology was assessed through a case study on the U.B.C Hospital Koerner Pavilion building. In this study, the focus is on the machinery and equipment that are critical for the operation of a hospital. During the experimental stage, the fundamental frequencies and damping ratios of eight NSCs were identified. In the second phase, the horizontal floor response spectra (FRS) were constructed from the linear time history analysis results performed on a FEM. Finally, the FRS is used to obtain the lateral seismic force of each NSC corresponding to its dynamic properties. These forces were then compared with those obtained using the NBCC 2010 code equation to demonstrate the effectiveness of this method.

Results from the case study provided evidence that the proposed method is overall a simple and effective tool for diagnosing the in-service modal properties of a NSC. The testing results can be easily applied in FRS analysis to obtain a more realistic nonstructural seismic force than that from the NBCC 2010 approach. The potential applications and limitations of the proposed methodology are also discussed in this dissertation to facilitate engineers to determine the suitability of this method to their specific projects.

Preface

This dissertation was prepared in collaboration between Professor Carlos Ventura and the author. The primary contributions of the author to this research include: establishment of the research methodology, experimental data collection and analysis, development of the analytical model, interpretation of the results and composition of this manuscript.

The concept of this research was initially formed by Professor Carlos Ventura. Similar relevant researches have also been carried out since then. The methodology of this research was partially based on two associated research publications:

1) Seismic performance of Non Structural Components (NSCs) and Operational and Functional Components (OFCs): field observations and shake table testing. H. Juárez García and C.E. Ventura in the 14th World Conference on Earthquake Engineering

2) Modal Testing of Non-Structural Components For Seismic Risk Assessment. M. Archila, C. Ventura, A. Figueira and Y.Yang. in the 30th International Modal Analysis Conference (IMAC).

Professor Carlos Ventura provided guidance and tools for completing the case study, reviewed the case study results and helped with the revision of this manuscript.

Table of Contents

List of Tables

List of Figures

Acknowledgements

First and foremost, I would like to express my uttermost gratification to Dr. Carlos Ventura for his patience in guiding me in my studies and broadening my vision of engineering. His endless passion in seeking for practical solutions to earthquake engineering problems inspired me in many ways during my graduate study to pursue earthquake engineering as a career. His support played an important role in the accomplishment of my study. It has been a great honor working with him. And these life-long lessons that I have learned from him will benefit me in my future career and a person as a whole.

Special thanks are owed to Dr. Liam Finn, for his time and effort on reviewing this thesis and providing insightful comments. The final submission of the thesis would not have been successful without his engagement.

I gratefully acknowledge the financial support from a Strategic Research Grant from the Natural Sciences and Engineering Research Council (NSERC) on Post-Earthquake Functionality of Schools and Hospitals in Eastern Canada that made my research possible.

I would also like to share the credit of my work with Mr. Michael Gong and Mr. Miguel Fraino for their hours of time spent helping me with my research experiments. I would like to thank my lab manager, Mr. Felix Yao, and the lab technician, Mr. Scott Jackson, for their time in training me with the experimental equipment and helping me solve technical issues associated with the testing tools. I thank my labmates from the Earthquake Engineering Research Facility at U.B.C. for sharing their experience and knowledge in related topics.

Special thanks are owed to my husband for his many years of support, spiritually and financially, as well as my parents and my daughter for their love. They have been my rock and source of motivation throughout this journey.

To my family

Chapter 1 Introduction

1.1 Problem Statement

Past earthquake events have shown that the nonstructural component (NSC) damages and failures can cause substantial economic losses and life-threatening hazards to occupants. Thus, evaluation and reduction of nonstructural damages have gained rising awareness in the recent years.

For new buildings, codes and standards are available for the design of NSCs and their anchorage systems. However, these code provisions cannot be applied the same way to NSCs that are already in service in an existing building. For such components, the focus should be on diagnosing their present condition to resist seismic activities.

1.2 Objective

The primary objectives of this study are to 1) develop a methodology for assessing the force demand of a NSC under its in-service state within an existing building, 2) demonstrate the application of the methodology through a case study, 3) evaluate the effectiveness of the methodology by comparing the force demand results with those calculated by lateral force formula provided in the National Building Code of Canada 2010 (NBCC 2010). To accomplish these objectives, the following tasks were carried out:

- Identify NSCs dynamic properties through nondestructive impact testing
- Develop a 3D finite element computer model to carry out linear time history analysis
- Generate floor response spectra in the two principle horizontal directions based on the time history analysis results
- Obtain the NSC lateral seismic force demand in the form of spectral acceleration and comparing the results to those calculated from the NBCC 2010 code formula.
- Evaluate the practicality of this field testing from a practicing engineering standpoint of view.

1.3 Scope and Assumptions

- This study employed floor response spectrum method as a basis for estimating the force demand of a NSC.

- The implementation of the methodology proposed in this study was demonstrated through the U.B.C. hospital case study
- Only the lateral floor response spectrum and lateral force demand were obtained, as the NSCs considered in this study are more sensitive to the lateral vibrations than vertical vibrations.
- The time history analysis does not consider the nonlinearity of the building.
- This study is not intended to assess the stability of the structure. Therefore, the computer model used in the time history analysis is only required to represent the seismic characteristics of the building.

1.4 Thesis Outline

This thesis starts with an introduction chapter that provides a brief overview of the project, which includes the problem statement, the overall objectives and the scope of work. The following chapters establish the main body of the thesis.

Chapter 2 provides background of the nonstructural seismic concerns. It also summarizes the state-of-the-art studies and researches related to this subject. It covers from the current code provisions related to NSCs to a detail review on the floor response spectrum method.

Chapter 3 outlines the methodology developed to assess NSC seismic force demand. It rationalizes the analytical techniques involved.

Chapter 4 demonstrates a step-by-step application of the proposed methodology through the U.B.C hospital Koerner Pavilion case study.

Chapter 5 presents the main results from the analyses including the natural frequencies and damping ratios of NSCs, floor response spectra at the roof level of the building and force demand from the FRS in comparison with that obtained from NBCC 2010 formula.

Chapter 6 is consisted of interpretation of the numerical results from Chapter 5 and evaluation of the effectiveness of the methodology developed in this study.

Finally, Chapter 7 is the conclusion of this thesis. It discusses the overall significance of this study, suggests potential application of the proposed methodology in practicing engineering and outlines future research directions.

All other supporting materials are included in Appendices.

Chapter 2 Background

This chapter provides background information about nonstructural seismic concerns and approaches of damage evaluation through a detail literature review. It includes the definition and classification of NSCs and discusses the primary factors influencing the seismic performance of a NSC. It also reviews the state of the art methodologies for estimating seismic demand of NSCs, of which the results will be used to design NSC anchorage and supporting systems. The most relevant methods for assessing nonstructural seismic demand include code force equations, fragility development and floor response spectrum methods.

2.1 Nonstructural Components Definition

Nonstructural components (NSCs) are defined as components within a structure that do not resist gravity or lateral loading. They are often divided into three primary categories based on their functionality: architectural components, mechanical, electrical and plumbing systems, and the building contents (Canadian Standards Association, 2006). The NSCs can also be classified as acceleration-sensitive and displacement-sensitive components based on its dynamic responses.

NSCs are often referred to as the operational and functional components as they are vital in maintaining the functionality of the building (Canadian Standards Association, 2006). Examples of such components include electrical and mechanical systems, piping, air conditioning ducts, hospital equipment and interior partition walls. In this study, the focus is on the machinery and equipment that are critical for the operation of a hospital.

2.2 NSC Damages

The NSC damages can cause three major consequences: direct and indirect economic losses, life-threatening concerns and interruption of a building's operation.

During earthquakes in 2010, nonstructural damages in earthquakes resulted in billions of dollars of losses (Fierro, Miranda, & Perry, 2011). Some typical nonstructural damages during the Chile earthquake are shown in Figure 2.1.

The direct losses are due to the high capital costs of the NSCs. Damages to these expensive NSCs lead to high repair expenses or even replacement costs. Other losses resulted from closure

or loss of functionality of facilities due to nonstructural damages were also reported from past earthquakes.

Nonstructural seismic damages can be catastrophic. Life-threatening NSC failures during earthquakes include injuries and casualties due to falling objects, blockage of emergency exits and toxic or explosive material spillage (Canadian Standards Association, 2006).

The loss of building functionality is another major concern of nonstructural failure. After the 2010 Chile earthquake, two main airports (Santiago Airport Arturo Merino Benitez and Concepcion airport) were closed down due to extensive nonstructural damages. Hospitals and clinics were also forced to shut down as a result of the nonstructural damages (Miranda, Mosqueda, Retamales, & Pekcan, 2012). The monetary impact due to loss of building functionality is obvious for business institutions. More importantly, for "post-disaster" buildings like hospitals and other health facilities, the post-earthquake operation continuity is required to ensure immediate medical treatment to save lives. The interruption of the services and operation of these facilities can have immeasurable impact and should not be compromised.

Figure 2.1 **Anchorage failure of HVAC equipment (left) and joint failure of sprinkler pipe (right) in Santiago International Airport. Reprinted from "Performance of Nonstructural Components during the 27 February 2010 Chile Earthquake" by Miranda, Mosqueda, Retamales, & Pekcan, 2012.**

2.3 Factors Affecting the Seismic Force Demand of NSC

The seismic force demand of a NSC is sensitive to several factors: 1) natural frequencies of the NSCs relative to the primary structure, 2) dynamic interaction between nonstructural and structural systems, 3) damping of the structure and NSCS, and 4) nonlinearity of the structural and nonstructural components (Villaverde (1997), Medina, Sankaranarayanan, & Kingston (2006), (Shooshtari, Saatcioglu, Naumoski, & Foo (2010) and Rodriguez, Restrepo, & Carr (2001)). Each of these factors is discussed in the following sections.

2.3.1 Natural Frequency Ratio between the NSC and the Primary Structure

Dynamic response of a NSC is directly related to the ratio of its natural frequency to that of the primary structure (Medina, Sankaranarayanan, & Kingston, 2006) & (Fisher, 1988). When the ratio is less than 1.0 and approaches to zero, it indicates that the component is much more flexible compared to the supporting structure. Thus the ground motions are transmitted directly to the component without amplification. The component behaves as if connected directly to the ground. When the ratio is greater than 1.0 and approaches to infinity, the component is considered as a rigid component, its response acceleration represents the peak acceleration of the floor at which the component is attached to. When the ratio is near 1.0, the seismic force is amplified significantly. Therefore, it is advantageous to investigate the natural frequencies of the NSCs and of the structure for predicting the seismic damage of the components.

2.3.2 Dynamic Interaction between NSC and Primary Structure

The response of a NSC during an earthquake can modify the response of its supporting structure, which in turn affects its own response (Villaverde, 1997). This is referred to as the dynamic interaction effects between the NSC and the structural system. The interaction effects can be accounted for by analyzing the combined model of the primary and secondary systems. However, developing a coupled model is challenging due to the great difference in structural and nonstructural dynamic properties, the massive number of degrees of freedom and the uncertainties in attachment conditions of the NSCs (Fisher, 1988).

The significance of the interaction depends on the mass ratio of the NSC to supporting system. Amin et al. (1971) have recommended that the coupling effects can be neglected if the mass of

the NSC is less than 1% of the total mass of the structure. Toro et al. (1989) have pointed out that the interaction may be significant if component-to-structure mass ratio is above 0.1%.

The coupling effect is also dependent on the frequency ratio between the NSC and the structure. Chen and Soong (1988) have demonstrated through their study that the coupling effect is most significant when the ratio approaches to 1.0. In their study, a floor acceleration response spectrum was plotted for both the decoupling and coupling analyses for the same primary and secondary systems, as shown in Figure 2.2. At the period ratio of secondary system to primary system (Ts/Tp) equals 1.0, the maximum acceleration response from the decoupling analysis is almost three times higher than that from the coupling analysis. On the contrary, the difference reduces when Ts/Tp moves away from 1.0. This indicates that when the fundamental frequency of a NSC is close to the structural natural frequencies, decoupling analysis can significantly overestimate the acceleration response which can lead to over-design of the component.

In this study, the NSCs considered are significantly lighter than the primary structure (i.e. mass ratio is less than 0.1%). Furthermore, the NSC natural frequencies are expected to be much higher than that of the primary structure. Therefore, it is deemed appropriate to develop an independent structure model to be used in the floor response spectrum analysis (FRS).

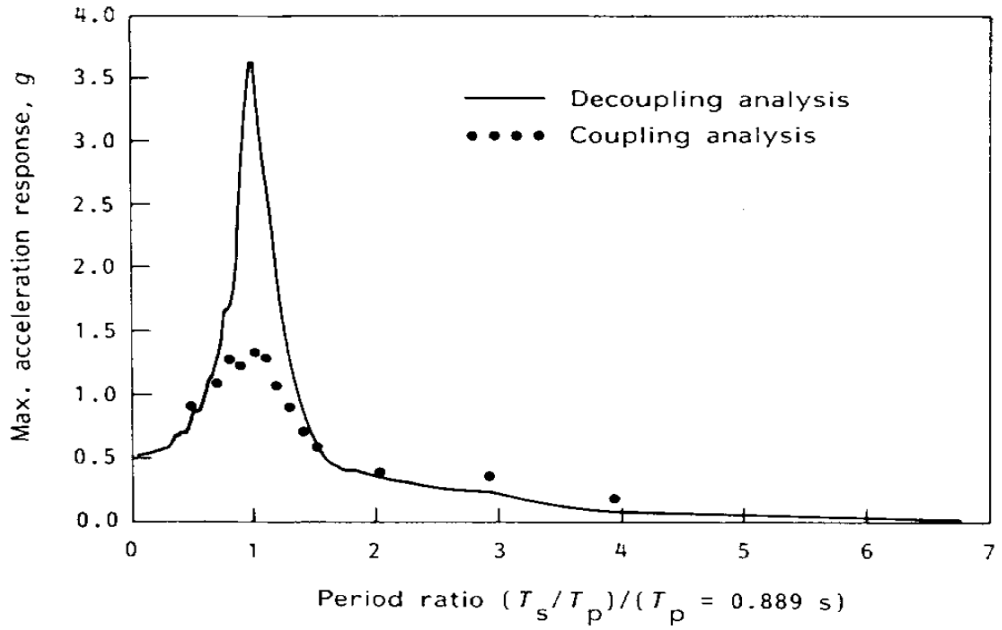

Figure 2.2 **Floor acceleration response spectrum from decoupling and coupling analysis. Reprinted from "State-of-the-Art Review: Seismic response of secondary systems" by Chen & Soong, 1988.**

2.3.3 **Damping**

When a structure is subjected to the energy input caused by ground shaking, its damage level is affected by how well the energy can be absorbed and dissipated. Due to energy-conservation, the energy input should equate the summation of kinetic and potential energy temperately stored in the structure and the energy dissipated through damping (Zahrah & Hall, 1984). The kinetic and potential energy are directly related to the dynamic response parameters (displacement and acceleration). The more energy that can be dissipated through damping, the less energy will be transformed into kinetic and potential energy, and in turn the dynamic responses can be reduced. This is true for both structural and non-structural damping. The damping effect on dynamic responses of a NSC is more pronounced near the region of its fundamental frequency (Medina, Sankaranarayanan, & Kingston, 2006). Therefore, investigating the damping level in both primary structure and the components is desired.

2.3.4 **Nonlinearity**

The other way for a structure and a NSC to dissipate energy is through inelastic deformation. When the structure or the NSC undergoes nonlinear motions subjected to seismic loading, the energy of the excitation is dissipated through its hysteresis behaviour.

Nonlinearity was not considered since this study was conducted on a hospital building where both the structural and nonstructural components were expected to remain elastic subjected to seismic loading. However, for other types of structures, nonlinearity plays an important role in the responses of the NSCs and primary structure. Therefore, future research can be conducted to incorporate the nonlinear effects.

2.4 Development of Code Provisions

Due to the massive and complex NSC inventory in a building, it is impractical and unnecessary to apply rigorous design procedures for each of these components especially for buildings where NSC failures are not so severe (Singh M. P., Moreschi, Suarez, & Matheu, 2006). Therefore, a number of building codes around the world have been developed to "prescribe the seismic design requirements in their simplest form" (Singh M. P., Moreschi, Suarez, & Matheu, 2006, p.1525). These code provisions are usually in a form of force equation, which are derived based on

historical data from previous earthquakes (McKevitt, 2003). In the following sections, three relevant design code provisions are reviewed: UBC (1997), IBC (2006) and NBCC (2010).

2.4.1 **Uniform Building Code**

In the United States prior to 1993, seismic requirements were based on the Uniform Building Code (UBC) (Applied Technology Council, 2008). In the earliest version of the 1930's, the lateral design force on nonstructural components was calculated by multiplying the weight of the component by a factor of 0.05 or 0.25 depending on the type of component. The subsequent versions started to account for the regional seismicity, importance of the building and the rigidity of the considered components (Applied Technology Council, 2008). The development of the code provisions regarding seismic design of NSCs were slow until the Olive View Hospital was forced to shut down due to nonstructural failure following the 1994 Northridge Earthquake event. This event has led to a substantial change in the formula for lateral force on nonstructural components in the 1997 UBC, as shown below.

$$F_p = \frac{a_p C_a I_p (1+3h_x/h_r)}{Rp} W_p \qquad \textbf{Equation 2-1}$$

Where a_p= component amplification factor ranging up to 2.5, but typically equal to1.0 for rigid items;

C_a = a seismic coefficient related to soil profile and seismic zone, with a value up to 0.88 on soft soil sites in the near-field, and equal to 0.4 for competent soil sites in areas of high seismicity outside near-field,

I_p = importance factor of the component,

h_x = elevation of the component measured from the ground

h_r = elevation of the component measured form uppermost level

Rp = a component response modification factor ranging from 1.5 to 4.0, with a typical value of 3.0 assigned to most ductile components and attachments.

The formula accounts for amplification for rigid items, seismicity and soil conditions, importance of the building, and ductility of the components (Applied Technology Council, 2008).

2.4.2 **International Building Code**

The first National Earthquake Hazard Reduction Program (NEHRP) provisions for seismic design of new buildings was introduced in 1985 (Singh, Moreschi, & Suarez, 2006). A few revisions have taken place since then. The latest equation for calculating sesimic design force adopted by International Building Code 2006 (IBC) is presented below (International Code Council, 2003).

$$\boldsymbol{F_p = \frac{0.4 a_P S_{DS} I_P W_P}{R_P}\left(1 + 2\frac{z}{h}\right)} \qquad \textbf{Equation 2-2}$$

Where Ip, Wp, and Rp are the same as those defined in 1997 UBC, S_{DS} is the spectral acceleration at short period (0.2 second)

The 2006 International Building Code (IBC) distinguishes the difference between force-and displacement-controlled nonstructural components. It also includes additional requirements on functionality of the components with hazardous contents and equipment following an earthquake (Applied Technology Council, 2008)

The current 2003 NEHRP Provisions for NSCs, adopted by the 2006 IBC and SEI/ASCE 7-02 Standard provide a conservative estimate of the NSC seismic design forces. However, studies showed that more rigorous methods are necessary to account for the higher mode effects, especially on tall buildings that have the possibility of low damping ratios, irregularities as well as variations in the ground motion characteristics (Miranda & Taghavi, Approximate Floor Acceleration Demands in Multistory Builidng. II: Application, 2005).

2.4.3 **National Building Code of Canada**

The National Building Code of Canada (National Research Concil of Canada, 2010)[1] seismic design force equation was based on the uniform hazard spectrum approach used for the design of structures (McKevitt, 2003). The equation is in a similar format as the IBC 2003, as shown in Equation 2-3.

$$V_P = 0.3 F_a S_a(0.2) I_E S_P W_P \qquad \textbf{Equation 2-3}$$

Where F_a = acceleration-based site coefficient

$S_a(0.2)$ = spectral response acceleration value at 0.2s,

I_E = importance factor of the building

$S_p = C_p A_r A_x / R_p$ (the maximum value of S_p shall be taken as 4.0 and the minimum value of S_p shall be taken as 0.7), where

C_p = element or component factor

A_r = element or component force amplification factor

A_x = height factor (1+2 hx / hn),

R_p = element or component response modification factor,

and W_p = weight of the component or element

Figure 2.3 below illustrates the values of C_p, R_p, A_r, A_x, and V_p for mechanical and electrical components in a typical building in Vancouver. The NBCC 2010 code equation takes into account the seismicity of the site, location of the attachment, importance level of the component, ductility and rigidity of component, and fundamental period of the structure.

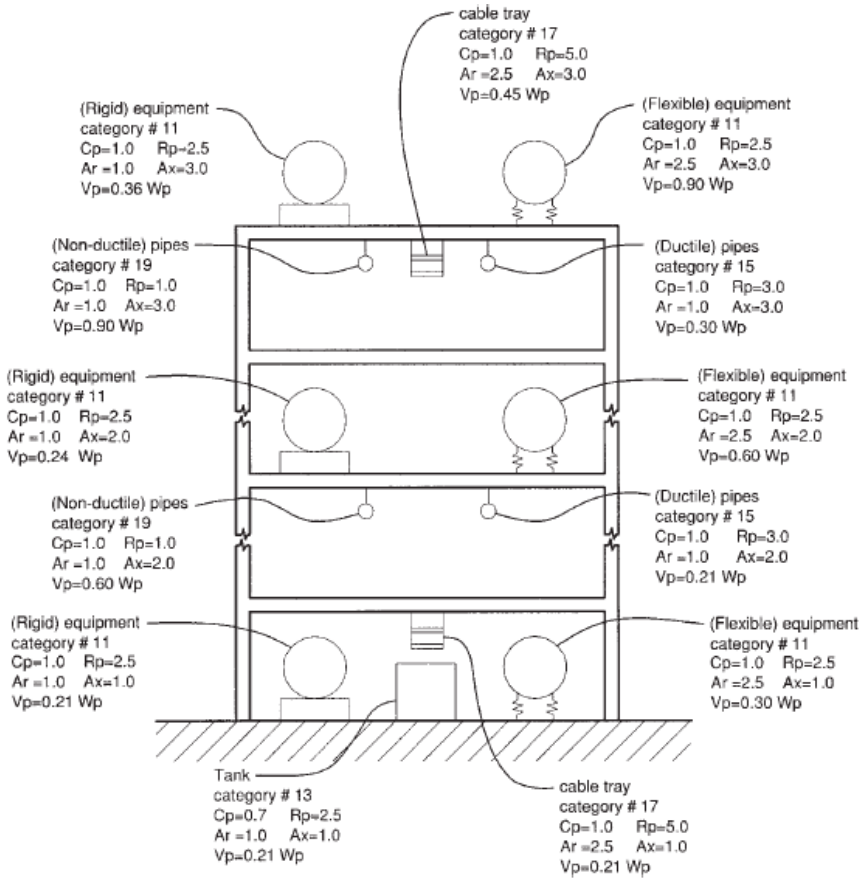

Figure 2.3 Typical values for Cp, Rp, Ar, Ax, and Vp in a building in Vancouver. Reprinted from "Proposed Canadian code provisions for seismic design of elements of structures, nonstructural components, and equipment" by McKevitt, 2003.

2.4.4 **Issues with current code equations**

Although the current code equations for estimating seismic forces of NSCs can provide a rapid tool for NSC design, the issues associated with these simplified equations are quite significant.

The contribution of higher modes of the structure has been neglected in the current code provisions. And this can lead to considerable underestimation of the floor acceleration demands (Miranda & Taghavi, 2005).

The correlation between the force demand and the floor height is dependent on the building dynamic characteristics: modal frequency and mode shapes (Chaudhuri & Hutchinson, 2004). The mode shapes reflect the acceleration distribution within a structure, which implies that the forces at different elevations can vary considerably. The NSC force equation in NEHRP (2003) and IBC (2006) NSC was derived based on the assumption of a linear acceleration distribution along the structure height (Akhlaghi & Moghadam, 2008). This assumption can lead to unrealistic results as higher mode effects are neglected.

The damping and nonlinearity of the structural and nonstructural systems were neglected in the current equations. These two parameters are related to the energy dissipation of the structure and the NSC when subjected to earthquake loading. Neglecting their effects can cause significant error in estimating the seismic forces of the components.

Also, the code equations do not provide guidance on how to assess the vulnerability of an in-service NSC. It does not provide insight on the current state of the NSC.

Thus, the recognition of these limitations associated with the design code provisions promotes the need for developing a methodology to assess the NSC seismic demand which would account for its operational dynamic characteristics, higher mode effects of the structure and damping and nonlinearity effects.

2.4.5 **CSA standard**

The CSAS S832-06 Standard (Canadian Standards Association, 2006) exclusively deals with seismic related issues for operational and functional components (OFCs). The OFCs are part of the nonstructural system and they are critical for maintaining the building's function. A schematic view of typical OFCs within a building is shown in Figure 2.4. This Standard demonstrates general seismic damage reduction procedures for both new and existing buildings.

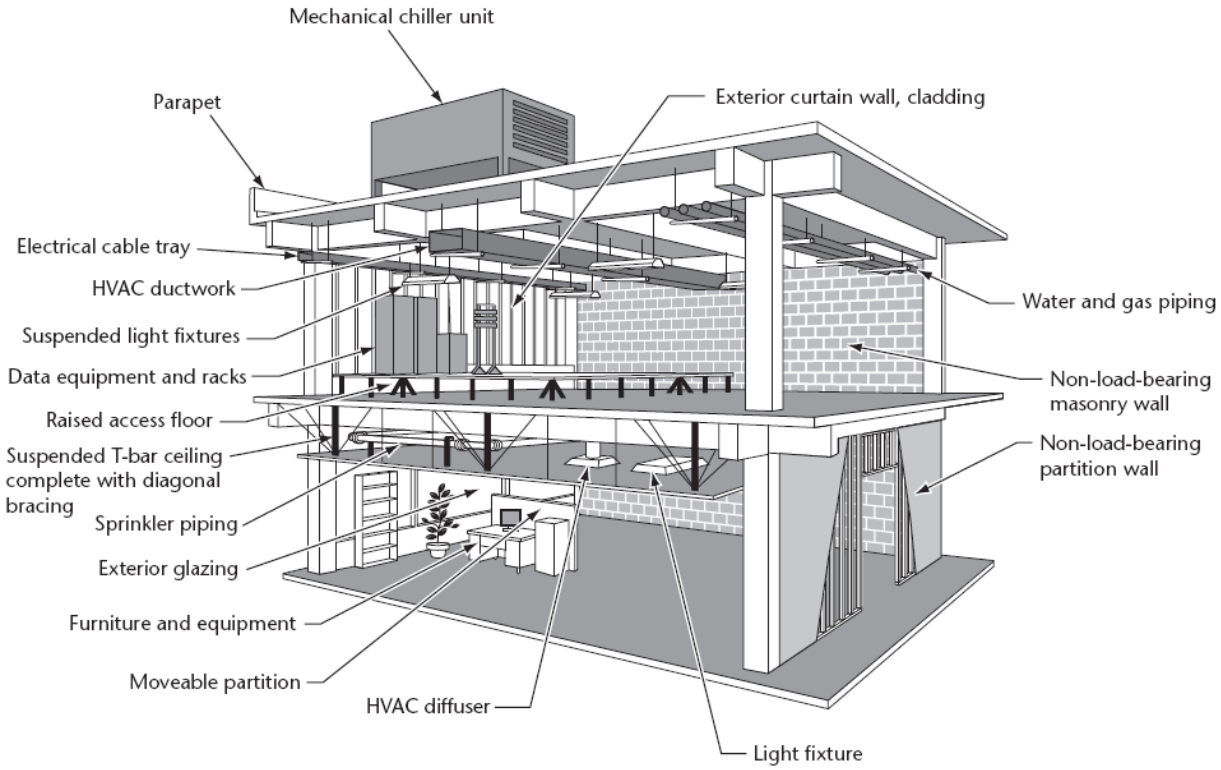

Figure 2.4 Operational and functional components of buildings. Reprinted from "S832-06: Seismic Risk Reduction of Operational and Functional Components (OFCs) of Building" by CSA, 2006.

It is pointed out in the Standard that the damage evaluation and mitigation planning strategies are highly dependent on the building performance objective. For a high-level performance objective, it requires more rigorous damage evaluation method and more robust design or retrofit plan than other performance levels. This is to ensure OFC damages are kept at minimal, so that the building's operation is not interrupted. In comparison, the life safety performance level is considered as the minimum requirements of which the goal is to avoid life-threatening failures, and the Immediate/continued occupancy is higher than the minimum objective (Canadian Standards Association, 2006).

Typical OFC's issues and mitigation techniques are listed in this document to help develop seismic reduction plan suitable for the considered case. More importantly, it introduces a methodology for initial risk assessment of NSCs. The outcome of the NSC risk assessment is measured by "risk index", "which is determined as the product of the OFC's seismic vulnerability (probability of failure) and the consequences of failure (probability of death, injury, or loss of building functionality)" (Canadian Standards Association, 2006, p. 11). The risk index provides a basis for ranking the mitigation priority to help with more efficient planning and reduce the costs.

However, it was also noticed that the Standard "does not explicitly address the characteristics of OFCs and/or their integral components either during or after an earthquake" (Canadian Standards Association, 2006, p.3). In order to do so, more comprehensive analysis and testing should be done.

The Standard also requires the assessment of the seismic demand to be conducted through either application of industry guidelines and compliance with published standards (prescriptive method) or analytical methods including floor response spectrum analysis (Canadian Standards Association, 2006). The methodology employed in this study is consistent with this guideline.

2.5 Floor Response Spectrum

Floor response spectrum (FRS) method is an analytical approach, which uses the responses of the primary structure generated at support locations of a secondary component as the input to the secondary component to determine its response behaviour (Chen & Soong, 1988). The FRS often employs a time history analysis or a response spectrum analysis of the primary structural system as a basis for obtaining the response at the locations at which the NSCs are attached to (Chen & Soong, 1988).

FRS methods have been broadly accepted in industry practice and research activities as it is simple in concept and provides reasonable results for secondary systems with negligible masses compared to the primary structure and with natural frequencies much different than those of the primary structure ((Villaverde, 1997) & (Soong & Chen, 1988)).

2.5.1 **Simplified Method for Generating FRS**

Another alternative method for estimating linear floor acceleration demand was developed by Miranda (2005). This simplified method approximates the first three vibration modes of a building based on a continuum model simulating both flexural and shear deformations, as shown in see Figure 2.5. This method computes rapidly the modal responses for each of the approximated mode and superimposes the modal responses to obtain the overall solution of the building at any given floor level.

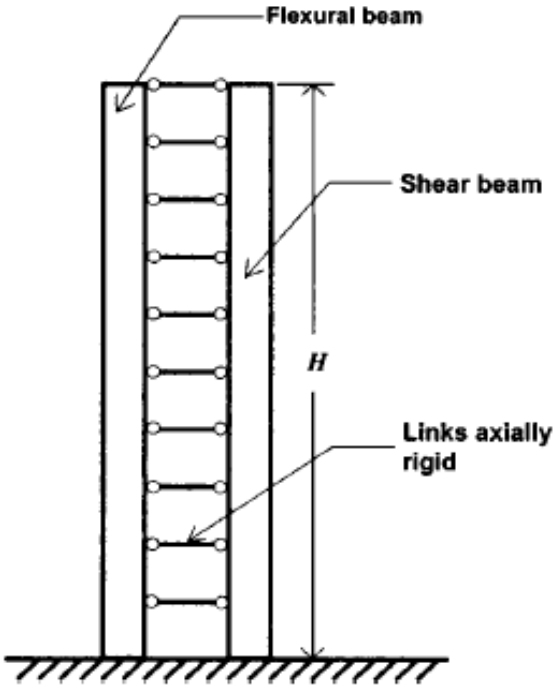

Figure 2.5 **Continuum model to estimate dynamic properties of a multistory building. Reprinted from "Approximate Floor Acceleration Demands in Multistory Buildings. I: Formulation" by Miranda & Taghavi, 2005.**

Based on the fundamental equation of motion for a structural system when subjected to a lateral ground motion, Miranda derived the partial differential equations for this simplified continuum model. The mode shapes solved from the differential equations are only controlled by the level of contribution of flexural and shear rigidity of the structure system. The corresponding natural periods and modal participation factors are also dependent on the relative flexural and shear rigidity. Modal superposition method is used to obtain the total linear response at a given time instance (Miranda & Taghavi, 2005). Miranda also compared the results obtained from this method to those suggested by the current NEHRP provisions (FEMA 356 and FEMA 368).

His parametric studies indicated that the current codes neglected parameters that can have significant influence on acceleration demands on NSCs. Such parameters include fundamental period, damping and nonlinearity of the structure. Thus, the distribution of acceleration demands determined using his proposed method was found quite different from those from the code formula.

Although the simplified FRS method generally captures the dynamic characteristics of the structure, it ignores the torsional deformations. The case study building in this research was expected to be torsional sensitive due to its plan irregularities. Therefore, the conventional FRS based on linear time history analysis was employed in this study.

2.6 Fragility Development

Another way of expressing NSC damages is though "fragility functions". The fragility functions are defined as "statistical distributions that indicate the conditional probability of incurring a damage state given a value of demand." (Applied Technology Council, 2011, p.3-16). Fragility functions can be a relationship between the probability of incurring a specific level of direct economic loss, as well as downtime and casualties at given a damage state (Applied Technology Council, 2011). The development of a fragility function for a component is based on test data or data collected from real earthquake experience for similar component.

The significance of structural and nonstructural fragility development has been widely recognized in the performance-based earthquake design field. Through the fragility curves, the seismic performance values are translated into more meaningful parameters for decision makers. This allows the stakeholders to identify the desired performance level so that the design will reflect the overall performance objective of the stakeholders' interest. The Pacific Earthquake Engineering Research Center (PEER) has undertaken the NSCs fragility development project (Whittaker & Soong, 2003).

A fragility function can be used as a rapid tool for assessing the seismic performance of the components. However, due to the nature of statistic studies, the process is time consuming and the outcome is highly dependent on the quality of the data. It also requires explicit definition of the fragility groups of which the fragility function is calculated for. With the NSCs' increasing complexity and continuous development of new components, constantly updating the fragility

functions is necessary. The proposed methodology in this study can be used for speeding up the fragility development process.

2.7 Shake-table Simulation

A number of shake-table tests have been carried out at various earthquake engineering research institutions across the world. The purpose of such a shake-table experiment is to investigate the dynamic behaviour of the component under consideration. Such experimental approaches can provide more realistic prediction of the damages during an earthquake event than that obtained from analytical approach. However, the setup cost and effort of such a test becomes a major obstacle of its application. Also, the findings can only reflect a specific setting and cannot be applied to general cases. In view of its limitations, the shake-table test approach is often used to validate the findings from an analytical approach.

Chapter 3 Methodology

The primary objective of this study is to develop a methodology that can rapidly assess the seismic force of a NSC in an existing building under its operating condition. This proposed methodology consists of two major components: 1) on-site modal identification testing and 2) floor response spectrum (FRS) analysis based on linear time history simulation.

From the literature review, the natural frequency of a NSC relative to its supporting structure and the damping are the most critical parameters for assessing the nonstructural seismic forces. These dynamic properties can vary significantly with its material properties, boundary conditions, installation methods, operation conditions and many other factors. Thus, these characteristics are best captured experimentally. The uniqueness of the methodology introduced here is that it employs a nondestructive on-site testing technique to gather the modal properties of existing NSCs and the supporting structure. The testing phase includes two main tasks:

- Identification of the natural frequencies and damping ratios of the NSCs through Hammer Impact Modal Testing (HIMT) approach;
- Validation of the natural frequencies of the structure through Ambient Vibration Testing (AVT) approach.

The second phase of this study was to assess the seismic force level of the NSCs through a FRS analysis. The FRS analysis was performed in such order:

- Establishing a 3D linear FE model of the structure;
- Performing time history analysis with a group of ground motions;
- Constructing the FRS for various damping levels.

With the natural frequencies and damping ratios determined from the experiments, the seismic force demand for each NSC can be estimated from the FRS plots.

Each of the major tasks is described in the following sections. The application of this methodology is demonstrated through a case study on a reinforced concrete hospital building located in Vancouver, B.C. and will be discussed in Chapter 4.

3.1 Modal Identification Testing

Following sections describe the technical background of the experimental approaches employed in this study and demonstrate the step-by-step procedure to perform the testing.

3.1.1 Background of Modal Testing Technique

A number of analytical and experimental modal identification measures have been developed in the past decades and applied widely in vibration related fields, such as structural health monitoring, modal updating and damage identification (Giraldo, Song, Dyke, & Caicedo, 2009), (Vu, Thomas, Lafleur, & Marcouiller, 2012) & (Trebuna, Simcak, Hunady, & Pastor, 2013).

The basis of the modal identification tests is that the relation between the input force(s) exerted on a structure and the resulting linear responses is a reflection of the structure's modal properties (Devriendt & Guillaume, 2008). The Newton's equations of motion for a multiple degrees-of-freedom system are given by:

$$M\ddot{x}(t) + C\dot{x}(t) + Kx(t) = f(t) \qquad \textbf{Equation 3-1}$$

Where M, C and K are the mass, damping and stiffness matrices respectively and x(t) is the response displacement of the structure subjected to external forces f(t). Transforming this equation into a frequency-domain equivalent, the time variant response becomes:

$$X(s) = H(s)F(s) \qquad \textbf{Equation 3-2}$$

$$H(s) = X(s)F^{-1}(s) \qquad \textbf{Equation 3-3}$$

$$\text{Also,} \quad H(s) = (Ms^2 + Cs + K)^{-1} \qquad \textbf{Equation 3-4}$$

Where H(s) is defined as a frequency response function (FRF) matrix, also known as a transfer function, and X(s) and F(s) are the output response and input force expressed in the frequency domain, respectively. The time-domain-to-frequency-domain transformation can be performed based on the Faster Fourier Transfer (FFT) algorithm (Chopra, 2007). The FRF can be plotted as the frequency domain relationship between the input and output signals. Now, consider the transfer function H(s) in the modal format:

$$H(j\omega) = \sum_{j=1}^{n} \left(\frac{1}{j\omega - \lambda_i}\right) \{\nu_i\}\langle l_i^T \rangle \qquad \textbf{Equation 3-5}$$

Where ω is the circular frequency; n is the number of modes; $\{\nu_i\}$ are the modal vectors; $\langle l_i^T \rangle$ are the modal participation vectors; and $\lambda_i$are the eigenvalues that are related to natural frequencies $\omega_i$and damping ratios ξ_i as follows:

$$\lambda_i, \lambda_i^* = -\xi_i \omega_i \pm j\sqrt{1 - \xi_i^2}\,\omega_i \qquad \textbf{Equation 3-6}$$

From the above equations, the FRF is related to the mode shapes, modal participation factors, modal frequencies and the damping ratios of the structure. These parameters can be determined once the FRF plots are obtained from the input-output spectrum relationship. This modal identification method is classified as an input-output approach. The Hammer Impact Modal Testing employed in this study is a typical input-output approach.

The other type of modal identification testing method is the output-only approach. Under some conditions where it is not feasible to excite the structure with a measurable impact due to cost, safety issues and/or undesired disturbance of the structure's operation, the input-output approach cannot apply. Only the response vibration can be measured and this type of modal identification method is so called the output-only approach.

The most common application of an output-only method is the Ambient Vibration Testing (AVT) approach. The AVT is most applicable to large structures since excitation of such a structure to exceed its ambient excitation is often expensive and unsafe (Devriendt & Guillaume, 2008, p347). Therefore, the AVT approach was applied in this study for the modal identification of the case study building.

3.1.2 **Hammer Impact Modal Testing for NSCs**

A Hammer Impact Modal Testing (HIMT) approach involves applying an impact force to the tested object by an instrumented hammer with a built-in force transducer. The input signals are measured by the built-in force transducer, and the output signals are measured by external vibration sensors. The recorded input-force and output signals are then processed to extract the fundamental frequency and damping of a NSC.

The general procedure of a HIMT in this study includes the following steps:

- Compiling a NSCs inventory for testing
- Conducting a foot-survey for determining the feasibility of the on-site testing
- Selecting the appropriate equipment
- Proceeding data acquisition
- Extracting modal frequencies and damping ratio from the experimental data using FRF analysis and logarithm decrement algorithm, respectively.

3.1.2.1 Selection of NSCs for Testing

It is impossible to conduct modal testing for every NSC in the building. The selection of the NSCs to conduct the modal identification tests was based on their importance level, vulnerability to seismic damages and accessibility for testing.

The FEMA E-74 report "Reducing the Risks of Nonstructural Earthquake Damage – A Practical Guide" (Federal Emergency Management Agency, 2011) pointed out that "prioritization may be based on budget constraints, risk considerations (i.e., those elements that pose the greatest risks to safety, property or function are retrofitted first), availability of unoccupied space, or to achieve the highest cost to benefit ratio" (FEMA, 2011, p8-10). Therefore, the priority assignment can vary between buildings depending on their use and it is important to consult the in-house expert's opinion. During this study, an in-person interview with professionals from the Maintenance and Facility Management department of the hospital was conducted to determine the priority of the candidate components. Some examples of the NSCs that were identified as high-importance level in this medical building are: fire sprinkler systems, medical air supply system, water pipes, and etc.

Vulnerability of the component to earthquake damages should also be considered. A component with high priority rating may not experience severe damages during an earthquake. For these items, modal testing was not necessary.

Although some NSCs were considered as high-priority items and vulnerable to seismic damages, HIMT was not practical due to limited access. For example, medical equipment in the operation rooms is critical to the hospital's continuous service during and after an earthquake. Modal

information about these items is beneficial for preventing seismic damages of such equipment. However, due to restricted access to the operation rooms, the tests for these items could not be carried out.

3.1.2.2 Initial Foot-survey

A foot-inspection was conducted to access the feasibility of the modal testing for the components on the list. The on-site observations include:

- Determined the accessibility of the components; e.g.: for elements that were high up in the ceiling, the modal testing was performed on a similar component within reach.
- Investigated any potential safety issues during testing; e.g.: if the tested objects contain hazardous or toxic materials, the impact hammer testing was considered unsafe and the tests were not conducted for these components.
- Identified component anchorage condition: whether it's free-stand or mounted to the structure. For free-stand elements, modal testing was not necessary.

3.1.2.3 Testing Equipment

The next step is to select the appropriate equipment for testing. A set of preliminary tests were carried out on site to determine the most suitable equipment. The main criteria for selecting the equipment include the sensitivity of the sensor to the low level vibrations, measurement amplitude range, frequency range, compatibility with the impulse hammer system and its own mobility at the testing site. The specifications of three candidate sensors considered for this experiment and their specifications are listed below. Figure 3.1 shows the dimensions of the devices.

Dytran Model 3035BG:

Uniaxial accelerometers

Size:	*see Figure 3.2 below*
Weight:	*2.5 grams*
Sensitivity:	*100 mV/g (±10%)*
Measurement Range:	*± 50 g*
Frequency range:	*0.5 to 10k Hz (±5/%)*

SENSR CX-1:

Tri-axial accelerometer

Size:	*see Figure 3.3 below*
Weight:	*570 grams*
Measurement accuracy:	*0.05 mg*
Measurement range:	*± 50 g*
Frequency range:	*DC to 200 Hz*

MicroStrain G-Link:

Tri-axial wireless accelerometer

Size:	*see Figure 3.3 below*
Weight:	*40 grams*
Measurement accuracy:	*10 mg*
Measurement range:	*± 10 g*
Frequency range:	*1-512 Hz*

Note: dimensions showing in inches

Dytran 3035 BG **SENSR CX1** **MicroStrain G-Link**

Figure 3.1 Accelerometer dimensions. Reprinted from Dytran Instruments, Inc. Outline/Installation Drawing; SENSR- CX1 Specifications; Lord MicroStrain, GLink Specifications.

A series of trial impact tests were carried out using the three types of accelerometers to determine the most appropriate equipment for this study. The typical setup for each type of accelerometers is shown in Figure 3.2.

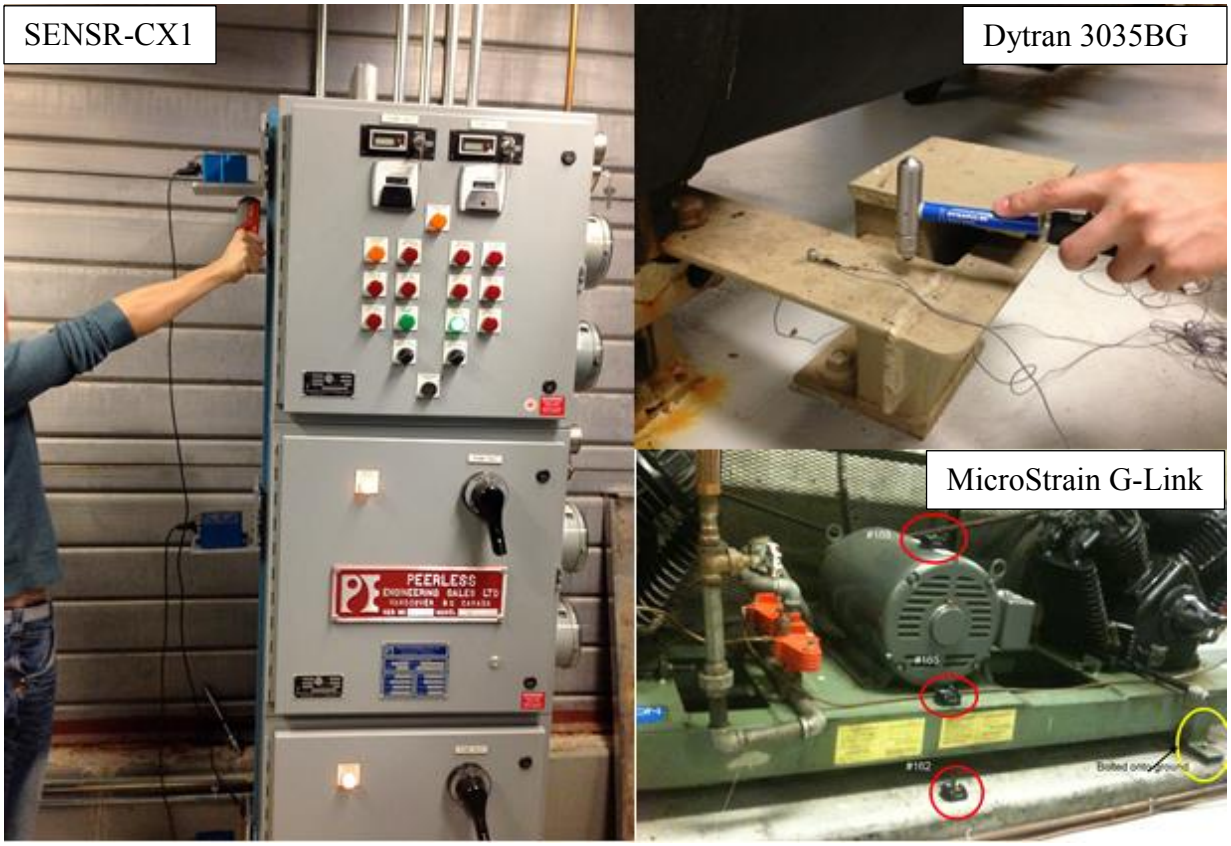

Figure 3.2 Pictures showing the test setup using the three candidate devices

The trail tests have found that the MicroStrain G-Link wireless sensors don't have an adequate level of sensitivity for capturing such a low level vibration whereas SENSR-CX 1 and Dytran 3035BG sensors both meet this criteria.

The weight of SENSR-CX1 sensors is significant relative to the weight of the NSCs. This may affect the NSC dynamic properties obtained through testing. It is difficult to attach the SENSR-CX1 sensors onto the NSCs without flat surfaces. As shown in Figure 3.2, L-shaped angle plates with magnetic were used to attach the sensors onto the relay rack.

In contrast, the Dytran 3035 BG sensors are small and light and can be easily attached to the testing object by some adhesive clay-like material. They are also compatible with the Dytran impact hammer. This allows both input force and response signals to be recorded simultaneously with one data acquisition device. Therefore, the Dytran 3035BG accelerometers were selected over the SENSR-CX1 accelerometers.

To choose the impact hammer, one must ensure that the impact force applied by the hammer is sufficient to excite the component to exceed its natural excitation. There were two impact hammers used in this study: 1) Dytran Model 5850B impulse hammer for lighter components and 2) Dytran Model 5803A for heavier components. The details of these two hammers are included in Table 3.1 below. The adequacy of the impact can be determined by the ratio of the impact force to the weight of the component. Tirelli (2011) suggested that a ratio greater than 0.1% to 0.5% should be sufficient to expect adequate results (Tirelli, 2011). Therefore, the Dytran Model 5850B is good for a component with weight of up to 10 tonne and Dytran Model 5803A is good for a component up to 100 tonne.

Table 3.1 Specifications of A) Dytran Model 5850B impulse hammer and B) Dytran Model 5803A impulse hammer. Reprinted from "Specifications, Model 5850B Three-Range Impulse Hammer" by Dytran Instruments, Inc.

A) Dytran Model 5850B impulse hammer

SPECIFICATION	VALUE			UNITS
SWITCH POSITION	100	10	1	
RANGE (for +5V out)	50	500	5000	Lbs F
SENSITIVITY, ±10%	100	10	1	mV/Lb
MAXIMUM INPUT FORCE	1000	6000	8000	Lbs F

Note: switch position was set to 100 for all tests.

B) Dytran Model 5803A impulse hammer

SPECIFICATION	VALUE	UNITS
RANGE, NOMINAL FOR +5 VOLTS OUT	5000	LBS
SENSITIVITY, ±10%	1.0	mV/LB
MAXIMUM INPUT	10,000	LBS

A schematic view of each impact hammer is included in Figure 3.3 and 3.4. When applying the impact, the impact force at the tip of the hammer is measured by the built-in force sensor. The input and output signals are consequently sent to a data logger through the BNC connector. The data is then downloaded from the data logger and stored in the computer for post-processing.

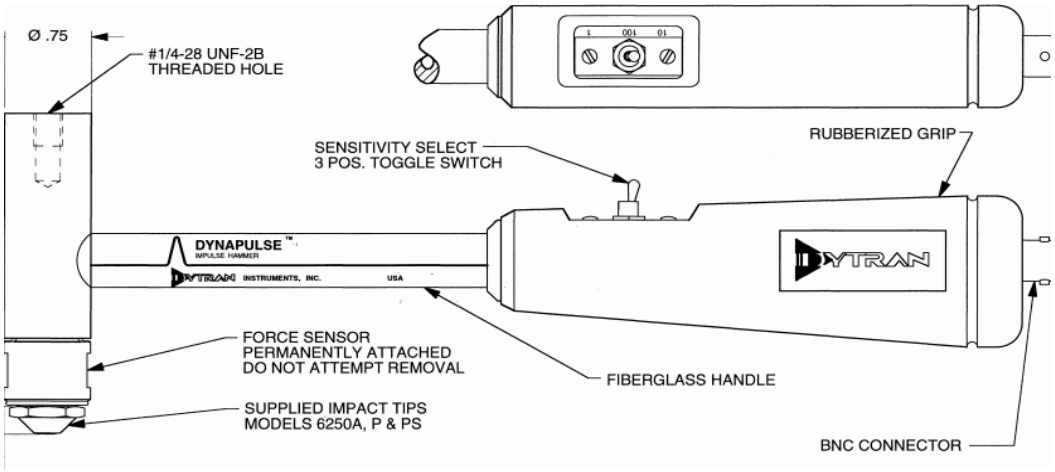

Figure 3.3 Schematic view of the Dytran 5850B impact hammer. Reprinted from "Outline/Installation Drawing, Impulse Hammer 5850B" by Dytran Instruments, Inc.

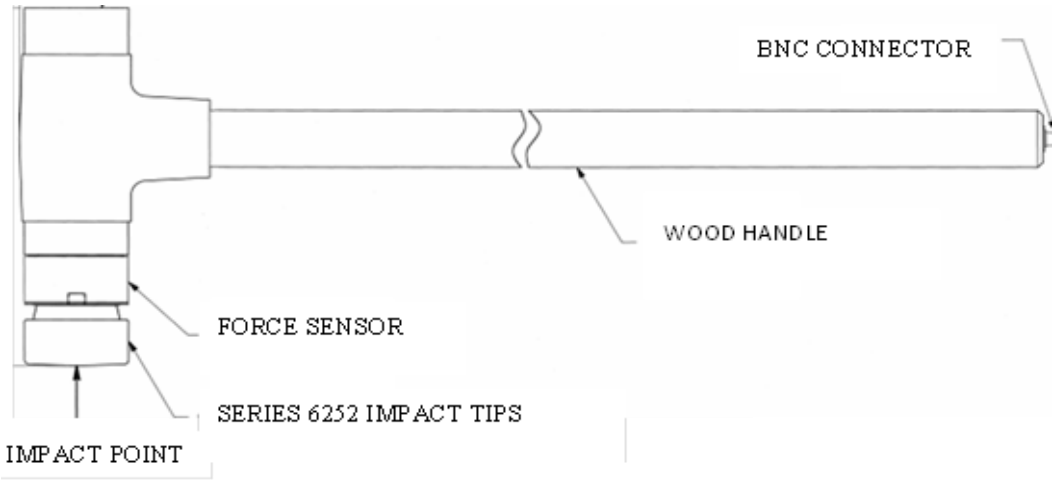

Figure 3.4 Schematic view of the Dytran 5803A impact hammer Reprinted from "Outline/Installation Drawing, Model Series 5803A impulse hammers" by Dytran Instruments, Inc.

3.1.2.4 Data Acquisition

The data acquisition of the HIMT includes placing the response sensors at the selected locations on the NSCs, applying impacts with the hammers to excite the component and recording the excitation and response data with proper sampling rate and duration. Figure below shows a typical HIMT experiment setup for a vertical pipe on the left, and the recorded input and output time history signals for one impact on the right.

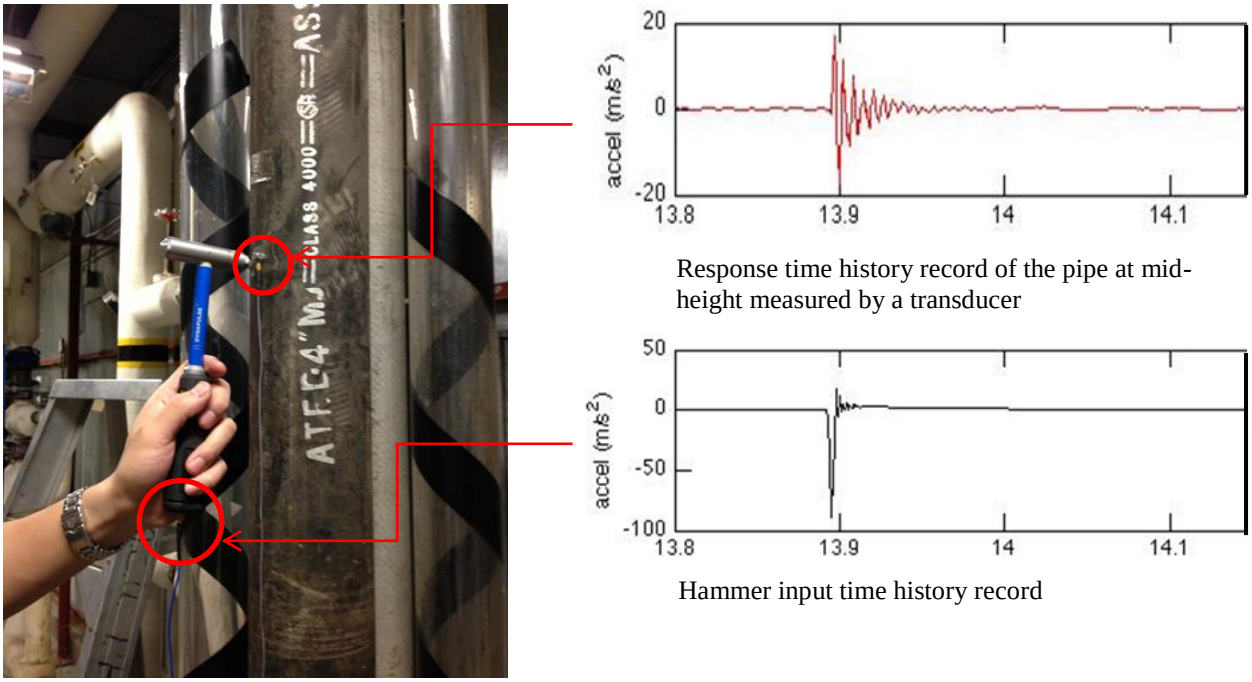

Figure 3.5 Typical HIMT test setup for a vertical pipe.

The direction and location of the impact can affect the results greatly. The impact force should be exerted in a way so that the fundamental mode of the component can be excited. In addition, an appropriate location for measuring the response must ensure that the recorded vibration due to the excitation can reflect the modal deformation of the NSC. Therefore, the test setup is optimized if the mode shapes can be predetermined. For some components with simple geometries, their fundamental mode shapes can be predicted through computer modeling (see details in Chapter 4).

The sampling rate to be used in the HIMT is determined based on the natural frequency range of the tested objects. The Nyquist sampling theorem stated that the proper sampling rate is required to be a minimum of twice the frequency of the contained signal (Smith, 1997). In this study, the natural frequency range of a NSC was predicted to be between 0~100 Hz. The sampling rate of 1280 Hz used throughout all tests was deemed adequate.

During a HIMT, continuous recording was carried out to cover multiple impacts instead of individual recording for each impact. This approach can reduce the inconsistency between setups so that the quality of the data is improved. Each continuous recording usually lasted for about 1~ 2 minutes depending on the duration of a complete impact cycle. A complete impact

cycle is from the time of the impulse till the excitation is damped out. Thus, it is dependent on the damping of the components. In the case study, each two consecutive impacts are generally 10-15 seconds apart to allow the excited motions to be damped completely.

3.1.2.5 Modal Property Extraction Analysis

The last stage of the HIMT process is the data processing, which aims at extracting the fundamental frequencies and the damping ratios of the NSCs. The procedure includes conducting the FRF analysis to obtain fundamental frequencies and calculating damping ratios

3.1.2.5.1 Fundamental Frequency

This study employed Matlab program (The Mathworks, 2009) for obtaining the fundamental frequencies of the NSCs (see Appendix A.2 for details). The Matlab worksheet was set up to read the input and output signals in the form of acceleration time histories. From the time history plots, the best three impacts for each test were selected for further processing. The signals during each of these impacts were transformed to Fast Fourier Transform (FFT) functions. A Power Spectral Density (PSD) was then estimated by taking the magnitude of the squared FFT. Following the transformation, A FRF was calculated by dividing the response FFT by the input FFT and taking the magnitude.

Peeters & Ventura have demonstrated through mathematical equations that "under the conditions of low damping and well-separated eigenfrequencies, the FRFs reach a local maximum around an eigenfrequencies" (Peeters & Ventura,2003, p.968). This characteristic of an FRF plot makes it simple to identify the modal frequencies just by tracing the peaks on the plot. This is so-called the peak-picking (PP) technique. Thus, from the FRF plots obtained from the above steps, the fundamental frequencies can be easily extracted by identifying the peaks. The PP technique was employed throughout the modal identification process in this study.

The peak-picking is not always straightforward. The noises with high frequency content, such as operation of a machine nearby will also appear as a "peak" in the FRF plots. It is important to distinguish the modal frequencies from these noise frequencies. For some components with simple geometry and known material properties, simple computer models can be developed to perform modal analysis. The analytical results can then be used to validate the frequencies extracted from the PP process. The accuracy of the analytical predictions is related to the

component properties (stiffness and mass) and boundary conditions defined in the model. For components with little information, this approach is not practical.

The other alternative is to identify the operation frequencies from the Ambient Vibration Tests (AVT) carried out on the floor slabs, as described in Section 3.1.6. The vibrations of the floor due to machine operation were captured in the time history recordings. The operational frequencies of these machines appeared to be "sharp" peaks in the PSD plots and were usually observed in signals in all three directions. Examples to demonstrate this approach are included in Chapter 4. With the noise frequencies known, the NSC frequencies found in the HIMT can be validated.

The application of the FRF analysis for obtaining the NSC fundamental frequencies is described in more detail in Chapter 4.

3.1.2.5.2 NSC Damping Ratio

Damping corresponding to the fundamental mode of a NSC is obtained using logarithm decrement algorithm. The logarithm decrement method is a convenient approach as it deals with the time-domain measurements and does not require a time-domain-to-frequency- domain transformation. After the fundamental frequency is obtained from the previous step, a band pass filter can be applied to the original response time histories to generate the free vibrations only near the fundamental frequency. An ideal free decay oscillation is shown in Figure 3.6.

The logarithmic decrement is defined as the average natural logarithmic value of the ratio between two peak values in free decay vibration as shown in Equation 3-7 and 3-8.

$$\delta = \frac{1}{n}\, ln \left|\frac{x_1}{x_{n+1}}\right| \qquad \textbf{Equation 3-7}$$

Where δ is the logarithmic decrement, x_1 the initial response value from the time history and $x_{n+1}$is the response value of n+1th cycle of oscillation. The damping ratio can be calculated by the following formula

$$\zeta = \frac{\delta}{\sqrt{4\pi^2+\delta^2}} \qquad \textbf{Equation 3-8}$$

The responses x_1 and x_{n+1} can be obtained from the signal and applied to the above equations to calculate the damping ratio. An example of calculating the damping ratio for a vertical pipe in this study is described in Chapter 4. The damping ratios for all components being studied in this research are represented in Chapter 5.

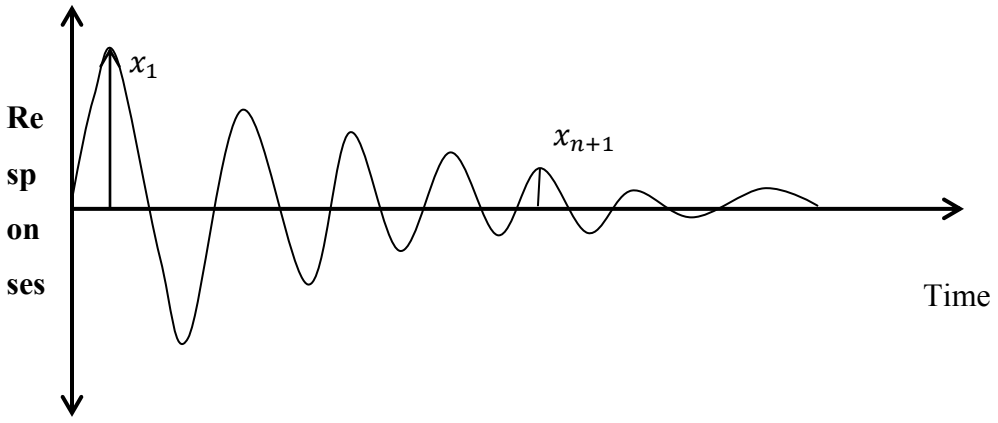

Figure 3.6 Free vibration at frequency f_n for calculating the damping ratio ζ%.

3.1.3 **Ambient Vibration Testing for Modal Validation**

The Ambient Vibration Testing (AVT) was primarily conducted to identify the natural frequencies of the primary building and in turn, to validate these values obtained from computer model. The secondary intent of the AVT was to detect the harmonic noises due to the operation of machines so that the true natural frequencies of the NSCs from the HIMT can be separated from these noise frequencies.

The AVT procedure includes:

- measuring the floor response at the floor of interest using SENSR-CX1 accelerometers during the normal operation of the building
- constructing the PSD plots using the FFT algorithms,
- Identifying the natural frequencies of the structure and frequencies associated with harmonic excitation due to running machinery using peak-picking (PP) technique.

The AVT is defined as a measure to record only the response of the structure under ambient excitations such as wind and traffic. Ideally, the ambient excitation can be treated as white noise, which corresponds to a constant power spectral density within any frequency band, so that the response spectrum is reflective to the modal properties of the structure. The excitation with limited bandwidth and low amplitudes can lead to the extraction of inaccurate modal properties (Giraldo, Song, Dyke, & Caicedo, 2009). Therefore, the response signals should be recorded over a long duration to ensure that the excitation contains a broad range of vibration frequencies.

SENSR- CX1 accelerometers were used for these tests (see Section 3.1.2.3 for equipment specifications). Each setup takes 10 to 15 minutes, with a sampling rate of 1000 Hz. The accelerometers were directly connected to a computer through a USB connection so that the data can be reviewed immediately after each recording. Figure 3.7 is a photo showing a typical test setup. All other test setup photos and figure related to this analysis are included in Appendix B.

The time history measurements were transformed into PSDs using FFT technique in the SeismoSpect program (Seismosoft Ltd., 2002). The PP technique was used to identify the natural frequencies of the structure with respect to the following criteria:

- The concrete floor slab was assumed to perform as a rigid diaphragm, thus the translational deformation at any location at the same floor level should be consistent. This implies that if a "peak" is corresponding to the structural natural frequency it is expected in the PSD plots throughout all locations in the direction of interest.
- If the "peak" is narrow and with high amplitude and appears in all three directions, it is clear that this is an operating frequency of a machine nearby the test location.

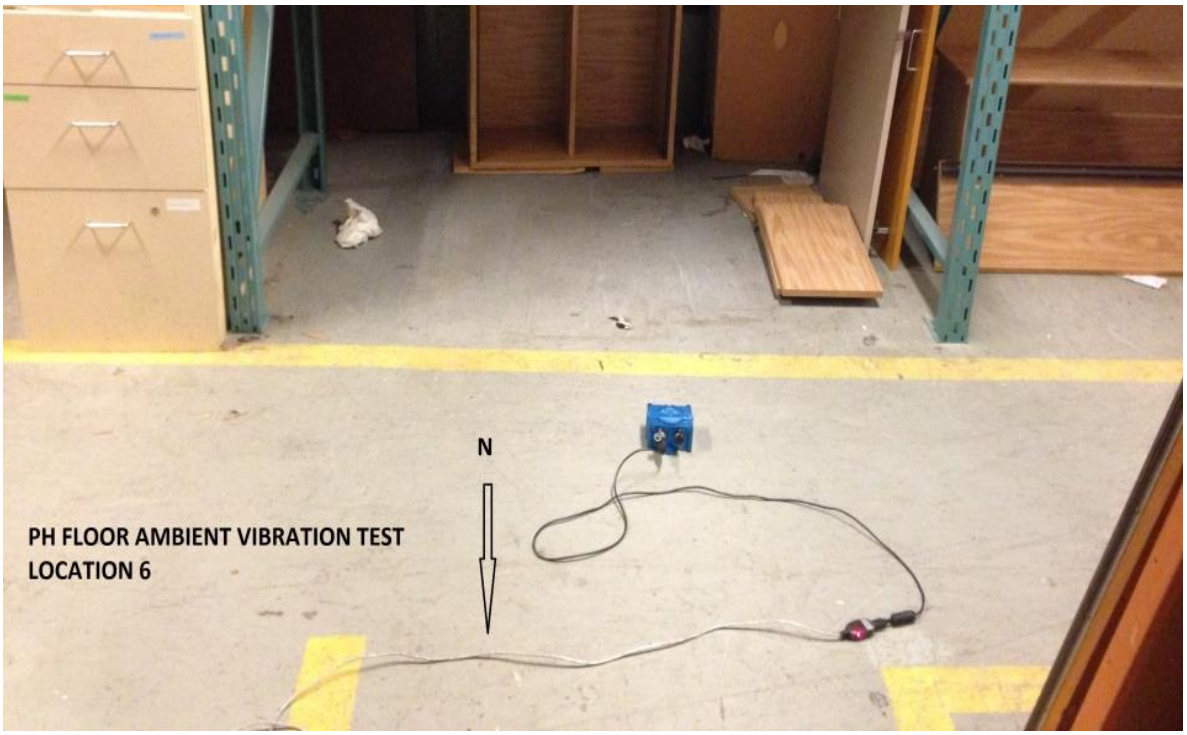

Figure 3.7 Test setup for floor ambient vibration experiment

3.2 Analytical Structure Model for Obtaining FRS

During the second phase of the study, a 3D finite element model of the primary building was developed for FRS analysis. The key steps to complete this analytical phase are discussed here.

3.2.1 Preparation of the 3D FE Model

From the previous discussions, the dynamic behavior of a structure is related to its mass, stiffness and damping ratio. Therefore, these parameters should be properly accounted for in the FE model. The key considerations for establishing the model are discussed below.

3.2.1.1 Stiffness of the Lateral Force Resistance System (LFRS)

The lateral force resistance system (LFRS) refers to the structural components that provide lateral strength for the structure to withstand lateral loads, such as earthquake and wind. Thus, the first step in preparing the 3D model for dynamic analysis is to identify its LFRS.

The adequacy of LFRS to resist the seismic force is dependent on its lateral stiffness, which is based on the material and section properties defined for the members. In this model, only the linear behavior was considered, so that only the uncracked concrete properties were used in the model. In other words, no section stiffness reduction was considered.

The lateral loads are transferred between lateral resisting elements (shear walls, braced frames, moment frames and etc.) through diaphragms at each story level. Depending on the rigidity of the diaphragms, the lateral loads are distributed differently throughout the structure. If the floor is defined as rigid diaphragm, the load is distributed to the lateral resisting members depending on their relative stiffness; whereas for a flexible diaphragm, the lateral loads are divided into portions based on tributary areas. In the case study building, the floor slab systems consist of a minimum 200 mm reinforced concrete slab. This implies that the in plane bending is negligible for these floor slabs; thus, it is reasonable to assume that they are rigid diaphragms. To model the rigid diaphragm, rigid constraints were assigned to all nodes at each floor level so that only translational movements were allowed.

3.2.1.2 Dynamic masses

The earthquake-induced force acting on the structure is a direct function of the natural period, which is in direct relationship with the structure's stiffness and mass. Thus, the dynamic model must properly include the dynamic masses of the building. In the NBCC 2010, the sources of seismic mass of a building include the dead load and the snow load as shown below:

$$W = 100\%\ DL + 25\%\ SL \qquad \textbf{Equation 3-9}$$

Where DL refers to the dead load of the structure which includes:

- the weight of the member itself,
- the weight of all materials of construction incorporated into the building to be supported permanently by the member,
- the weight of partitions
- the weight of permanent equipment, and
- the vertical load due to earth, plants and trees

The specified snow load (SL) was determined in accordance with Article 4.1.6.2 in NBCC 2010. The equation is shown below:

$$S = I_s[S_s(C_b C_w C_s C_a) + S_r] \qquad \textbf{Equation 3-10}$$

Where

Is = importance factor for snow load,

Ss = 1-in-50-year ground snow load, in kPa,

Cb = basic roof snow load factor,

Cw = wind exposure factor,

Cs = slope factor

Ca = shape factor

Sr = 1-in-50-year associated rain load, in kPa

Self-weight of the structural members were automatically accounted for in the computer model when defining for its member section, and any additional weight were applied as directional joint masses. Details of added masses are included in Chapter 4.

3.2.1.3 Damping of the structure

Damping of the structure is an important parameter to the dynamic behavior of the building. For linear systems with classical damping, the damping can be approximated as a function of the mass and stiffness matrices (Chopra, 2007).

For an existing building, damping is also dependent on the stress level of the building during earthquake motions (Stevenson, 1980), therefore is also a function of its ductility. It is incorrect to approximate such damping as mass or stiffness-proportional. Ideally, structural damping should be estimated experimentally based on the recorded earthquake motions of similar structures. However, the earthquake data is not always available and the cost and time associated with such experiment is significant (Chopra, 2007).

Newmark and Hall (1982) have come up with recommended damping values for various types of structures under two stress levels as shown in Table 3.2. They suggested a damping ratio of 3-5% for reinforced concrete structures under stress level below half of its yield stress. For hospital buildings, the damage level is anticipated to be low and a maximum of 5% damping is

appropriate. Also, in most building codes, "typically a 5% damping ratio is implicit in the code-specified earthquake forces and design spectrum" (Chopra, 2007, p 453). Therefore, a damping of 5% was imputed in the dynamic analysis of this study.

Table 3.2 Recommended damping ratios for structures. Reprinted from Earthquake Spectra and Design by N.M. Newmark, and W. J. Hall, Earthquake Engineering Research Institute, Berkeley, California, 1982

Stress Level	Type and Condition of Structure	Damping Ratio (%)
Working stress, no more than about $\frac{1}{2}$ yield point	Welded steel, prestressed concrete, well-reinforced concrete (only slight cracking)	2–3
	Reinforced concrete with considerable cracking	3–5
	Bolted and/or riveted steel, wood structures with nailed or bolted joints	5–7
At or just below yield point	Welded steel, prestressed concrete (without complete loss in prestress)	5–7
	Prestressed concrete with no prestress left	7–10
	Reinforced concrete	7–10
	Bolted and/or riveted steel, wood structures with bolted joints	10–15
	Wood structures with nailed joints	15–20

3.2.2 **Time History Analysis**

This section describes two essential steps for carrying out the time history analysis after the 3D FE model is established: 1) selecting the input ground motions and 2) performing Modal Superposition Time History Analysis (MSTHA).

3.2.2.1 Input Ground Motions

The set of ground motions inputted in the time history analysis should best characterize the seismicity of the site for a given hazard level. In this study, the ground motions were selected from the Pacific Earthquake Engineering Research Center (PEER) strong motion database (PEER, 2011) following the procedure listed below.

- Defining the Uniform Hazard Spectrum (UHS) associated with the hazard level of interest. The spectral accelerations can be generated from the Natural Resources Canada online hazard calculator (Natural Resources of Canada, 2013);
- Determining the site classification to select the appropriate ground motion amplification factors and adjust the spectral accelerations;
- Choosing the magnitude and epicenteral distance range of the shaking that can cause the most significant damages based on disaggregation studies of the site;
- Selecting the period range to match the target spectrum, which are most likely to present the natural period of the building under consideration.

With these criteria specified, the PEER website searches for the best matched ground motions. The original time history records can be downloaded and then scaled to match the target spectral acceleration using the SeismoMatch program (Seismosoft Ltd., 2002).

Ground motions can act in any lateral directions. To provide adequate design values, NBCC 2010 requires applying the ground motions in each of the principle directions independently if the LFRS are oriented in two orthogonal directions. In this study, the two horizontal components of the input ground motions were applied in both the principle horizontal directions.

3.2.2.2 Modal Superposition Time History Analysis

Modal superposition time history analysis (MSTHA) employed in this study is a computationally inexpensive approach for calculating the linear dynamic response of the structure. To perform the (MSTHA), modal analysis of the building was performed using SAP2000 (Computers and Structures, Inc., 2012), based on Ritz-vector approach. The results can provide information about natural periods, modal shapes and mass participation factors of the structure. It is critical to ensure sufficient modes are included in the MSTHA. The number of modes is deemed adequate if their accumulated mass participation factor add up to be more than 90% (National Research Council Canada, 2010 [2]).

The accuracy of the responses calculated from the MSTHA is related to how well each of the significant modes was predicted. Misrepresentation of the structure's properties in the finite element model can lead to excessive errors in predicting the natural modes, which in turn can cause false response estimates. Therefore, it is necessary to verify the modal analysis results

with those obtained through AVT. The experiment procedure was discussed previously in Section 3.1.4.

3.2.3 **Construction of FRS**

The construction of FRS was completed in the SeismoSpec program (Seismosoft Ltd., 2002). The final FRS to represent the response of the floor was achieved by the following steps:

- Calculating response spectrum for each of the time histories at a constant damping ratio,
- Obtaining the mean response spectrum at every point of interest in each of the horizontal direction by averaging the responses from all input ground motions,
- Obtaining the mean floor response spectrum in each of the horizontal directions by averaging the response spectra from all points of interest
- Enveloping the mean floor response spectra in the two principle horizontal directions to obtain the final floor response spectrum used to evaluate the NSC's seismic force.
- Repeat the above steps for each of the damping levels under consideration.

The mean floor response spectrum is intended to help identifying the seismic demand of NSCs located anywhere at this floor level. Thus, the points of interest selected to calculate the mean FRS should be well spread out within the floor plan so that the mean response from these points captures the overall behavior of the floor. It is also important that these points are away from a joint of structure members (e.g. beam-column connection or girder-beam connection) to avoid high local responses.

The damping levels selected to generate the FRS should cover the range of the damping values predicted from the modal testing of the NSCs.

Chapter 4 UBC Hospital Building Case Study

4.1 Case Study Overview

A simple methodology was developed in this study for evaluating the nonstructural seismic force demand in existing buildings. It consists of an on-site modal testing process and a floor response spectrum analysis, as described in Chapter 3. To demonstrate the application of this methodology, a case study was conducted on the U.B.C. Hospital Koerner Pavilion located in Vancouver, BC. The results were then compared with those obtained using the NBCC 2010 code equation to evaluate the effectiveness of this approach.

The reason in choosing the hospital building as the demonstration of this methodology is obvious: hospitals are defined as post-disaster buildings that are required to remain functional during and after seismic activities, which indicates that the requirements on the nonstructural performance during earthquakes are also strict. In a recent study conducted by Achour, Miyajima, Kitaura, & Price (2011), data were collected on the structural and nonstructural damages to 34 healthcare facilities across the world due to earthquakes occurred between 1994 and 2004. The findings illustrated that the NSC concerns in hospitals are vital for its overall damage control during and after an earthquake event.

It was observed in the same study that the different facilities experienced similar equipment and utility supply system damages because the setup and installation of these components are similar among health service buildings (Achour, Miyajima, Kitaura, & Price, 2011). This implies that if implementing this proposed methodology is practical for assessing the nonstructural seismic demand in the case study hospital building, the same or similar procedure can be used when studying other health facilities.

This chapter provides a step-by-step description of the case study procedure. The limitations of this case study are also discussed in this chapter in order to facilitate the future use of the methodology.

4.2 Deliverables

The final deliverables of this study include:

- 15 sets of the NSCs test data in the format of time histories
- The natural frequencies and corresponding damping ratios obtained from power density spectrum analyses based on Fast Fourier Transform algorithm.
- Modal analysis results of the 3D SAP2000 finite element model of the case study structure, which identifies the natural periods and mode shapes of the building.
- The time history results in the format of acceleration time histories at multiple points of interest.
- The FRS generated for each time history set and the mean and enveloped FRS for the floor under consideration.
- The final seismic force demand values extracted from the FRS method and the difference between these values and those found in NBCC 2010 formula.

4.3 Description of the Building

4.3.1 General

The Koerner Pavilion is the main component of the U.B.C. Hospital buildings. It is located on the U.B.C Point Grey Campus. Figure 4.1 is a satellite view of the Koerner Pavillion showing its geometry and orientation. The Koerner Pavilion hosts not only the acute services but also serves for a wide range of other medical needs. It currently has about 800 staff in total, and sees about 21,600 clinic visits annually.

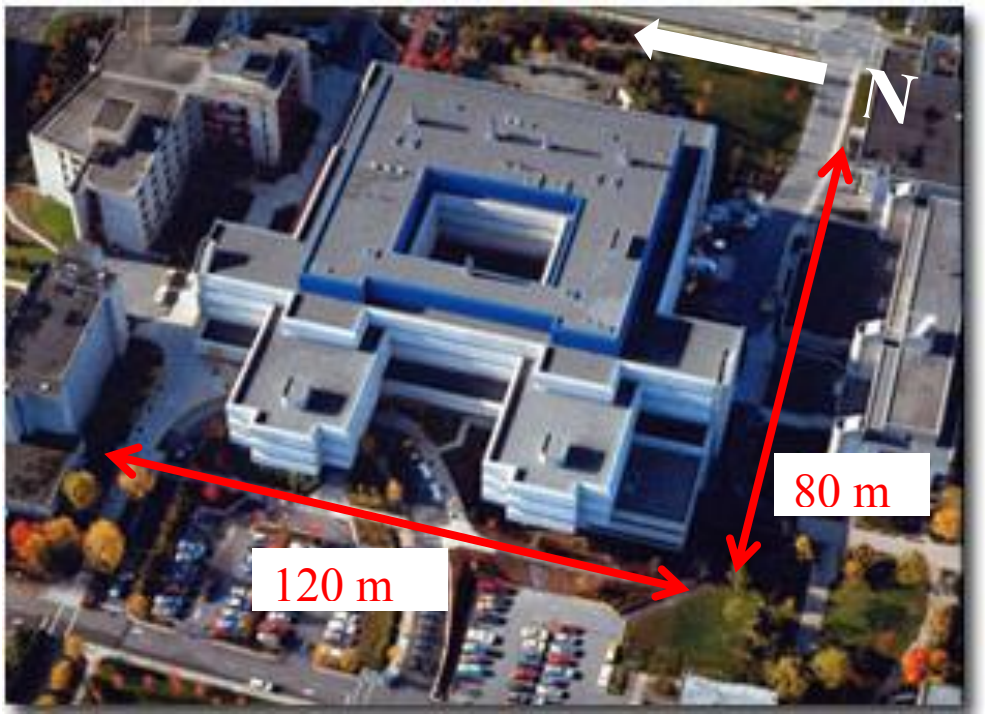

Figure 4.1 Satellite view of the U.B.C Hospital Koerner Pavilion showing its geometry and orientation.

4.3.2 Structural System

According to the original structural drawings, the Koerner Pavilion building is classified as a reinforced concrete moment frame structure. The building contains of 6-stories plus a penthouse level. The NSCs studied here are located in the mechanical room on the roof level. The total height of the structure is 27 meters. Each typical story is 4.5 meter in height, except for the ground floor with a 5.5 meter story height and the penthouse level that is mainly 4 meter high. The main structural elements include:

- columns with a 400 mm diameter or 450 mm diameter,
- beams and joist with a typical depth of 450mm,
- concrete floor slabs with 200 mm thickness,
- concrete walls with a thickness of 200 mm or 250 mm that form the stairwells and elevator shafts.

Figure 4.2 below is a 3D view of the FE model containing the main structural members without the floor slabs. The floor slabs were not modeled as finite elements to save computation time in

time history analysis. The modeling details are included in Section 4.6. Figure 4.3 is a typical elevation view of the structural model showing the storey levels. The roof floor plan and a typical floor plan are included in Figure 4.4.

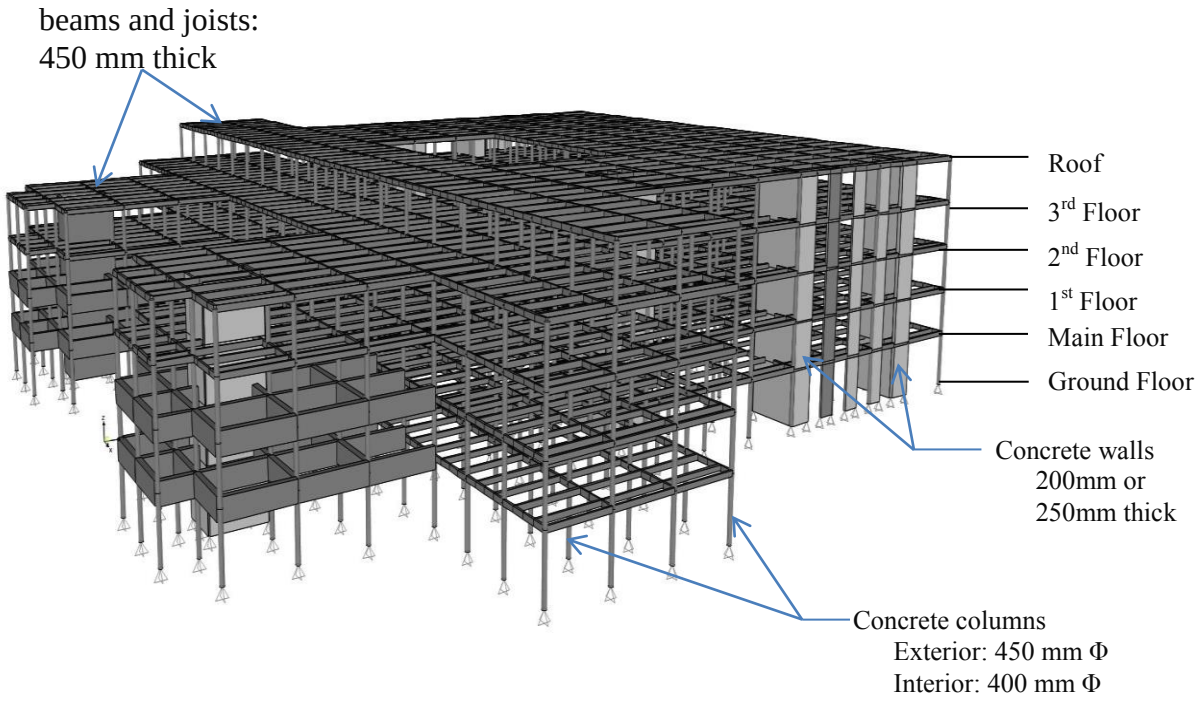

Figure 4.2 A 3D overview of the structural model of the U.B.C. Koerner Pavilion.

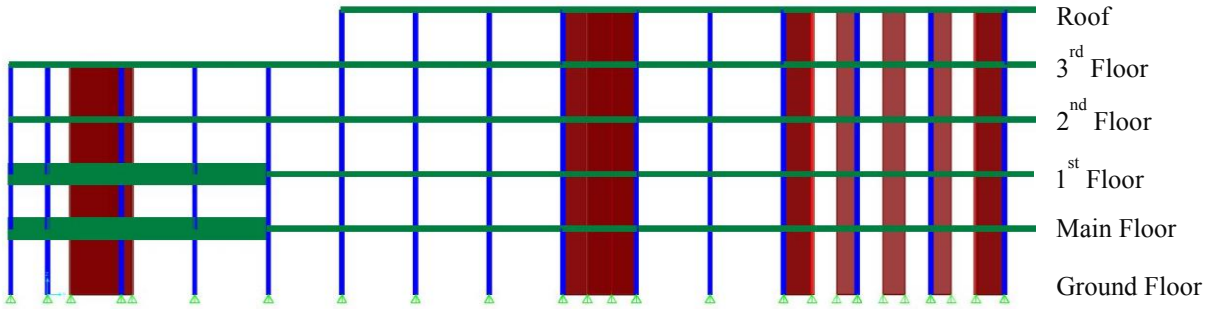

Figure 4.3 A typical section cut of the structural model.

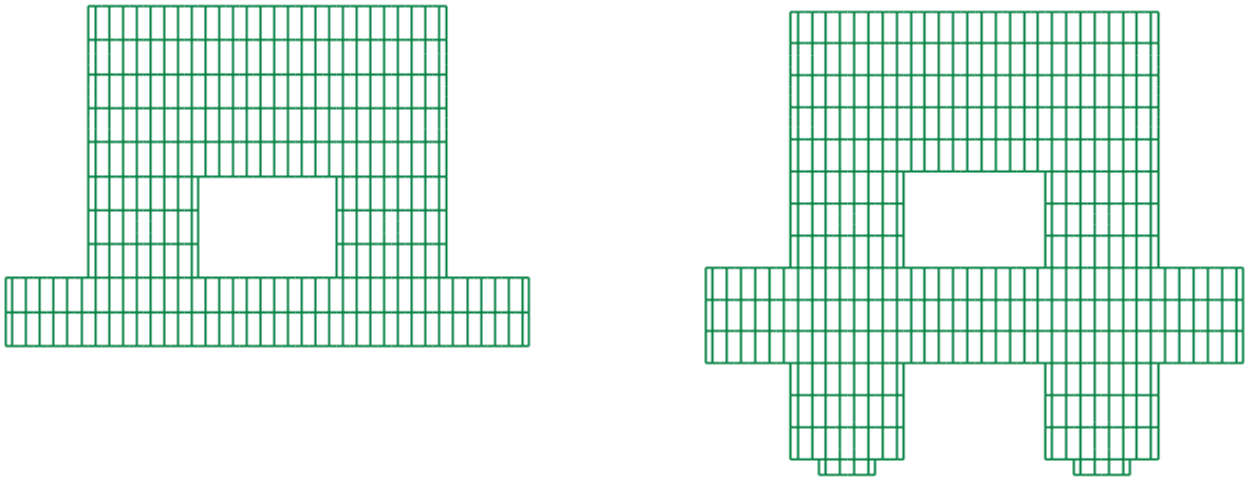

Figure 4.4 **A plan view of the roof level (left); a plan view of a typical floor below the roof (right)**

4.4 Modal Identification of the NSCs

The case study started with the Hammer Impact Modal Testing (HIMT) to identify NSC natural frequencies and damping ratios. The test followed the procedure outlined in Chapter 3. Below is a summary of the key steps involved in the HIMT.

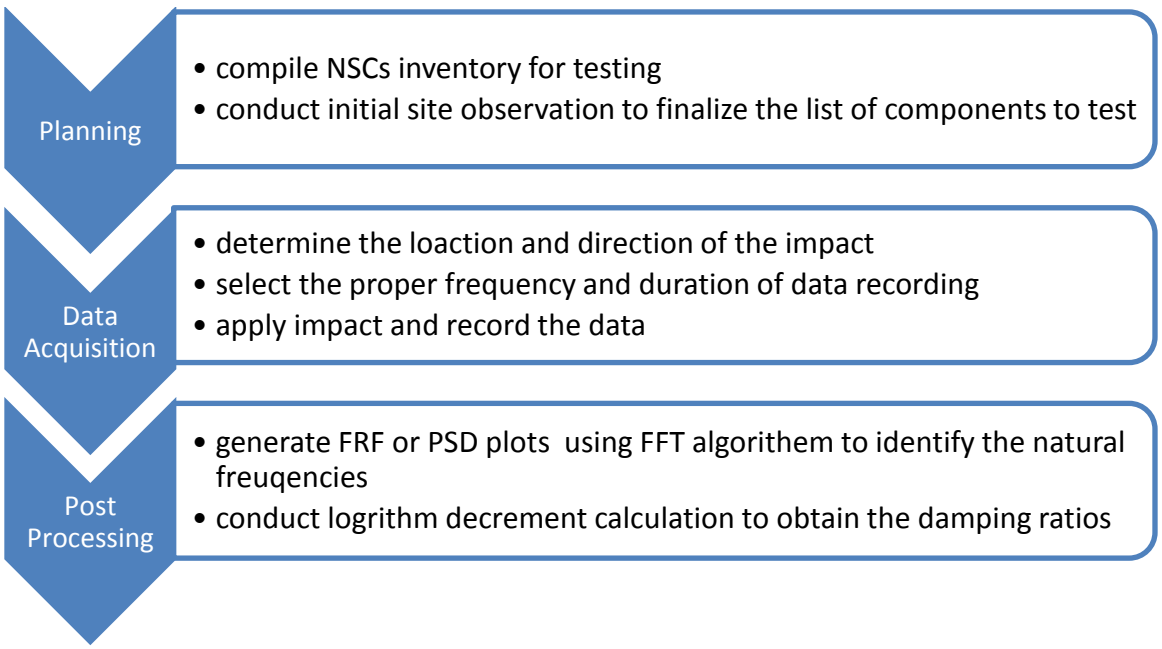

4.4.1 **Nonstructural component inventory**

Based on the criteria discussed in Chapter 3, the final tested components are listed in Table 4.1 below. They were selected in collaboration with the professionals from the maintenance and facility management group of the U.B.C. Hospital. Pictures of the tested components are included in Figure 4.5 and 4.6. All of these NSCs are located in the mechanical and electrical room on the roof floor level.

Table 4.1 List of the final tested NSCs

Component Number	Component Description
COMP1	Pump Assembly
COMP2	Air Handler Unit
COMP3	Relay Rack
COMP4	Dry Air Vacuum Unit
COMP5	Medical Air Vacuum Unit
COMP6	Concrete Pump Deck
COMP7	Vertical Pipe
COMP8	Medical Air Cylinder Rack
COMP9	Service Air Vacuum Unit

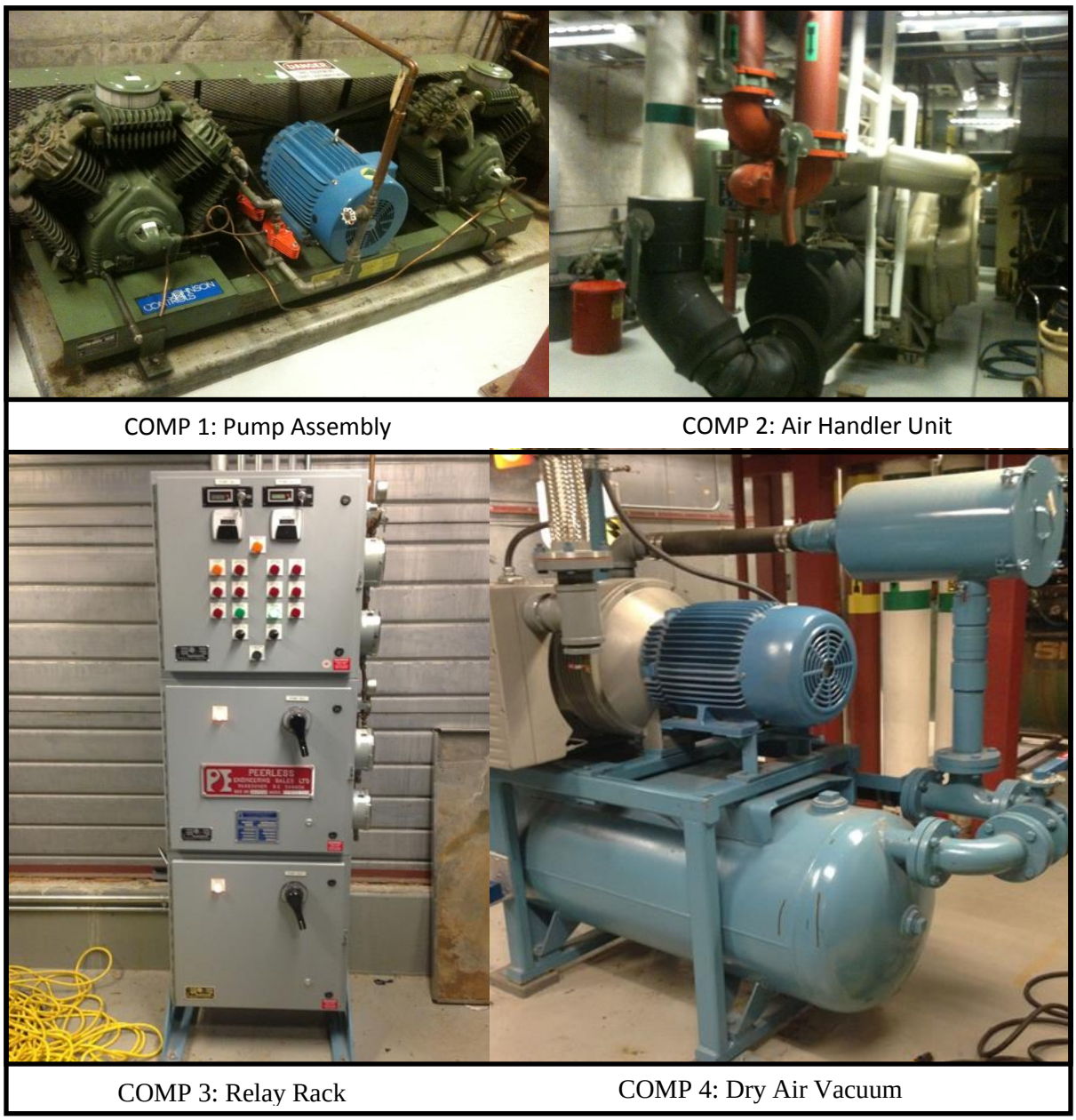

Figure 4.5 Pictures of COMP1 to COMP4

COMP 5: Medical Air Vacuum Unit

COMP 6: Concrete Pump Deck

COMP 7: Vertical Pipe

COMP 8: Medical Air Cylinder

COMP 9: Concrete Pump Deck

Figure 4.6 Pictures of COMP5 to COMP9

4.4.2 Data Acquisition

During the data acquisition, the vibrations were measured with three Dytran Model 3035BG uniaxial accelerometers. Dytran Model 5850B (50 lbf range) and Dytran Model 5803A (5000 lbf range) impulse hammers for applying the excitations. The recorded data stored was saved as .svn files and was converted into text files for post-processing.

4.4.2.1 Sampling frequency and duration

A sampling rate of 1280 Hz was used throughout the HIMT. A sample set of the time history measurements for the entire test duration is shown in Figure 4.13. Figure 4.14 is an enlarged view of the signals measured during the first impact. All the recorded data are stored in .txt format. File name convention includes the component ID, setup number in impact direction as shown in Table 4.2.

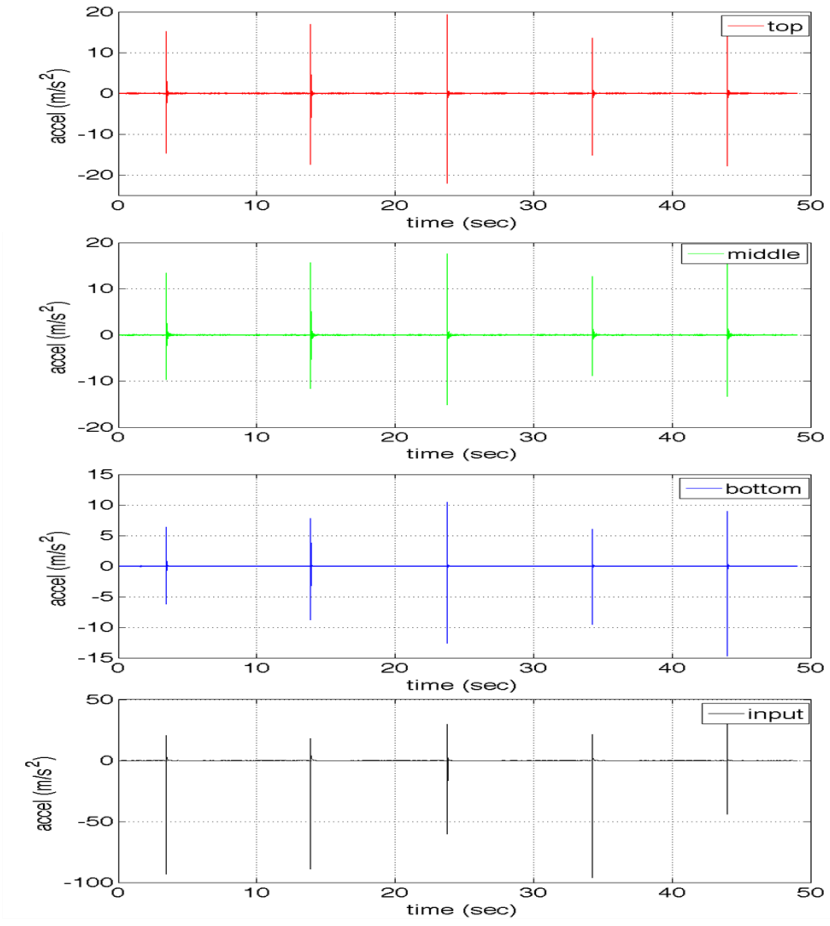

Figure 4.7 Original acceleration time histories measured at top, mid-height and bottom and the input force for COMP 7.

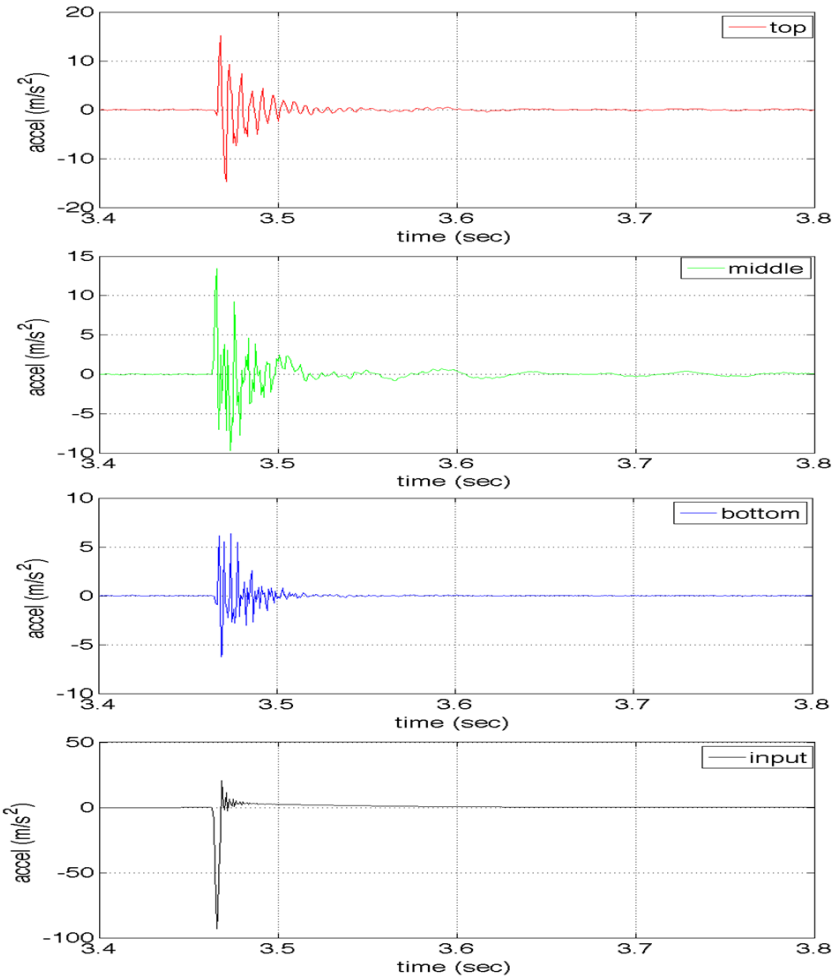

Figure 4.8 **Enlarged view of the acceleration time histories measured at top, mid-height and bottom and the input force of COMP 7- the vertical pipe force for the first impact.**

Table 4.2 Summary of the test data

Record Number	Component Number	Component Description	impact direction / location	File Name	Hammer Used
1	COMP1	Pump	Lateral	comp1_setup1_lat.txt	5850B
2	COMP1	Pump	Longitudinal	comp1_setup1_long.txt	5850B
3	COMP2	Air Handler Unit	Middle	comp2_setup1_mid.txt	5803A
4	COMP3	Relay Rack	location 1 (bottom)	comp3_setup1_hit1.txt	5850B
5	COMP3	Relay Rack	location 2 (mid)	comp3_setup1_hit2.txt	5850B
6	COMP3	Relay Rack	location 3 (top)	comp3_setup1_hit3.txt	5850B
7	COMP4	Dry Air Vacuum	hit 1 lateral	comp4_setup1_lat.txt	5850B
8	COMP4	Dry Air Vacuum	hit 2 longitudinal	comp4_setup1_long.txt	5850B
9	COMP5	Medical Air Vacuum Unit	lateral	comp5_setup1_lat.txt	5850B
10	COMP5	Medical Air Vacuum Unit	longitudinal	comp5_setup1_long.txt	5850B
11	COMP6	Concrete Pump Deck	lateral	comp6_setup1_lat.txt	5803A
12	COMP6	Concrete Pump Deck	longitudinal	comp6_setup2_long.txt	5803A
13	COMP7	Vertical Pipe	location 1 (bottom)	comp7_setup1_hit1.txt	5850B
14	COMP7	Vertical Pipe	location 2 (mid)	comp7_setup1_hit2.txt	5850B
15	COMP7	Vertical Pipe	location 3 (top)	comp7_setup1_hit3.txt	5850B
16	COMP8	Medical Air Cylinder Rack	lateral	comp8_setup1_lat.txt	5850B
17	COMP8	Medical Air Cylinder Rack	longitudinal	comp8_setup1_long.txt	5850B
18	COMP9	Service Air Vacuum Unit	lateral	comp9_setup1_lat.txt	5803A
19	COMP9	Service Air Vacuum Unit	longitudinal	comp9_setup2_long.txt	5803A

4.4.2.2 Validation Models

For components with simple geometries such as COMP3, COMP4 and COMP 7, computer models were developed in SAP2000 (Computers and Structures, Inc., 2012) to validate the experimental results. The mode shapes obtained from the computer models were used to determine the proper impact location and direction. The input parameters for each model include: geometric dimensions, material properties, masses and boundary conditions.

COMP 3: Relay Rack

Dimension: see Figure 4.8

Material:

Aluminum 6061T6:

Unit weight: 26.6 kN/m^3

Elastic modulus: 68.9 GPa

No additional mass was assigned.

Boundary condition: assume pinned at the bottom by anchoring bolts.

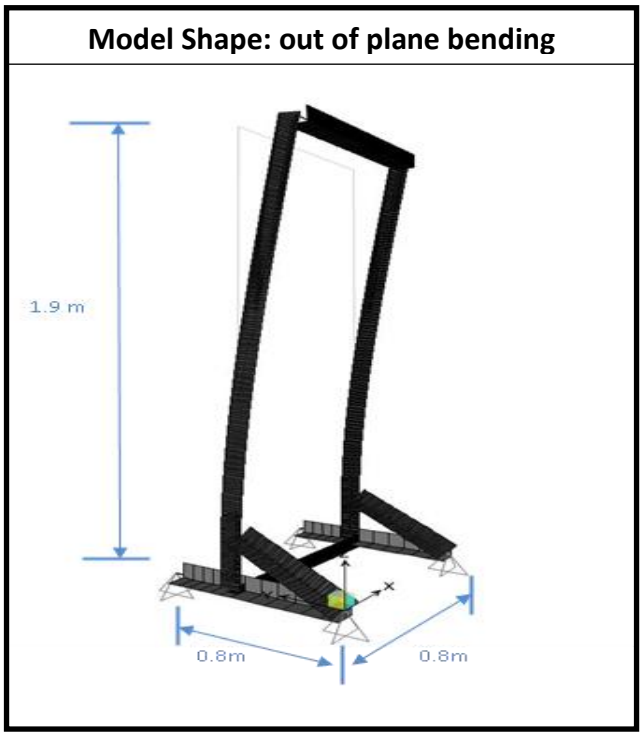

Figure 4.9 Fundamental mode shape and natural frequency for COMP3 from the computer model.

It was observed from the model that the dominant mode for COMP 3 was out of plane bending with the maximum displacement at the top of the rack, as shown in Figure 4.7. Therefore, the impact force was applied at the top of the relay rack in the out-of-plane direction.

COMP 4: Dry Air Vacuum (model only includes the supporting frame)

Dimension: 1.0 m (W) x 1.2 m (L) x 0.8 m (H)

Material:

Aluminum 6061T6:

Unit weight: 26.6 kN/m3

Elastic modulus: 68.9 GPa

A total of 200 kg additional masses were assigned at each corner at the top of the supporting frame to account for the weight of the vacuum unit attached to the frame structure.

Two boundary conditions considered:

1) Pinned connection at the base of the frame
2) Fixed connection at the base of the frame

COMP4 is a dry air unit supported by a four-leg frame structure as shown in Figure 4.8 below. The base connection of the frame structure that supports the dry air unit to the concrete floor slab is also shown in the figure. The actual fixity of the connection is unknown. Therefore, a fixed base connection (stiffest) and a pinned base connection (softest) were considered to provide an upper bound and a lower bound of the fundamental frequency. The average frequency of the two extremes was used to compare with experimental result (see Chapter 6). For each of these two boundary conditions, the frame structure exhibited two dominant modes: 1) sway motion in the lateral direction and 2) sway motion in longitudinal direction. Figure 4.9 shows the fundamental modes in the two principle directions and for both fixed and pinned connections. Therefore the impact force was applied in the direction and location as shown in Figure 4.10.

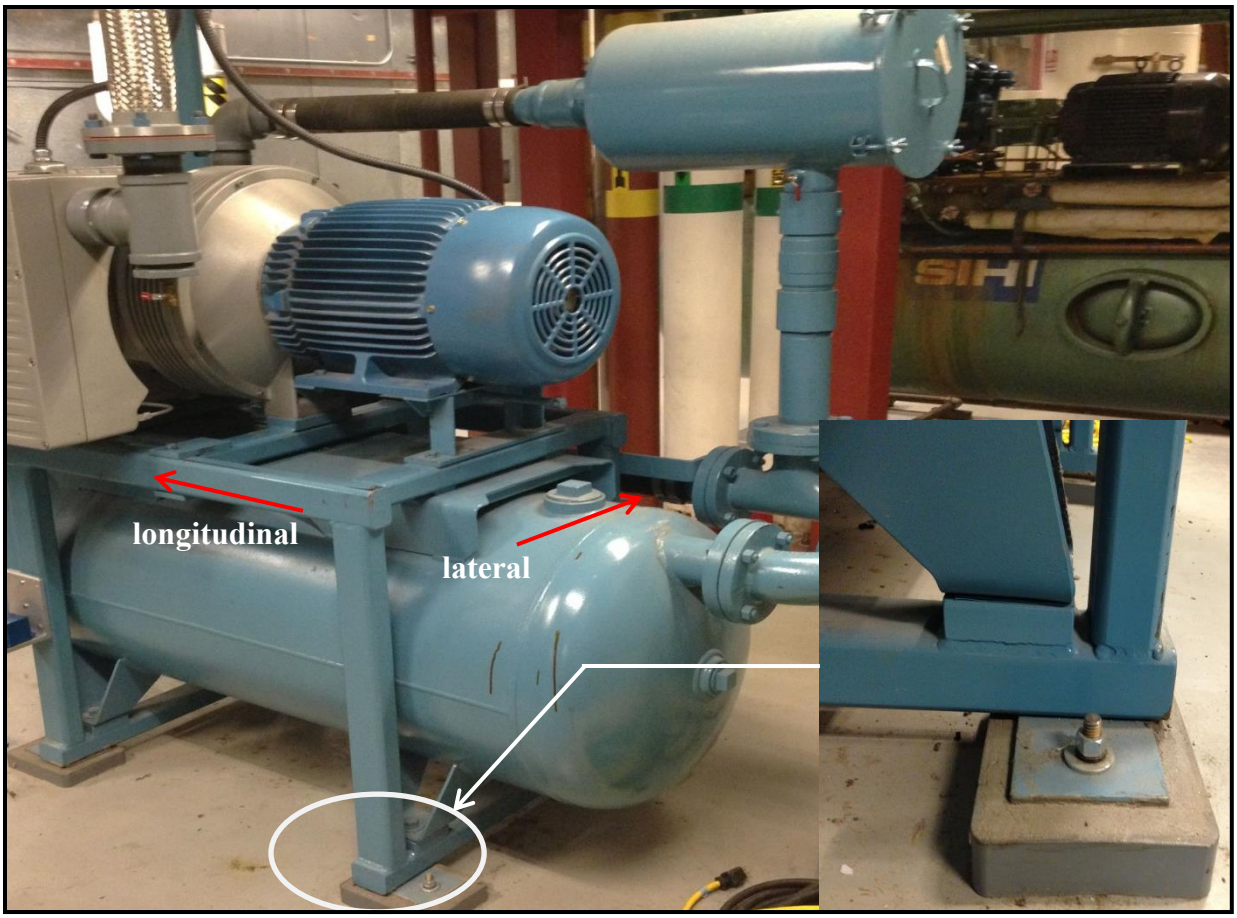

Figure 4.10 **Overview of COMP4 and a blown-up view of the base connection of the frame structure**

Pinned Mode shape: lateral sway (in y dir.) $f_n = 22.6\ Hz$	Fixed Model shape: lateral sway (in y dir.) $\mathbf{f_n = 11.3\ Hz}$
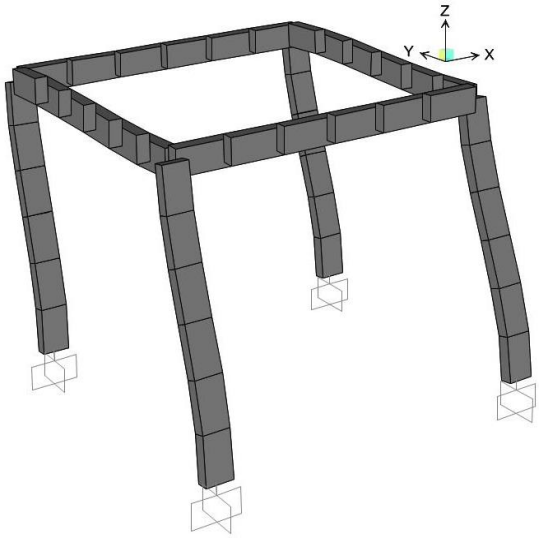	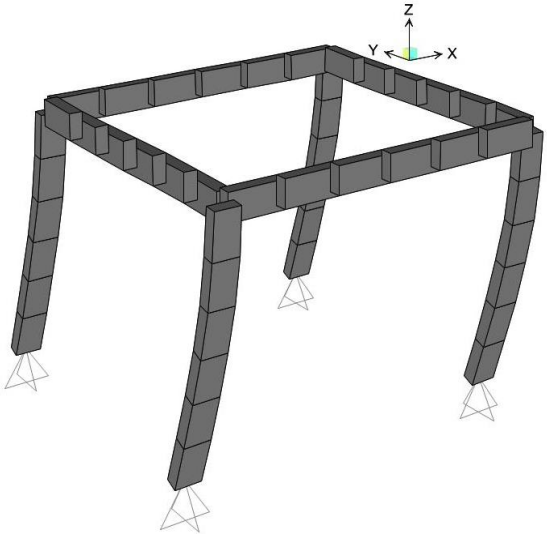
Pinned Mode shape: longitudinal sway (in x dir.) $f_n = 39.0\ Hz$	Fixed Mode shape: longitudinal sway (in x dir.) $f_n = 19.0\ Hz$
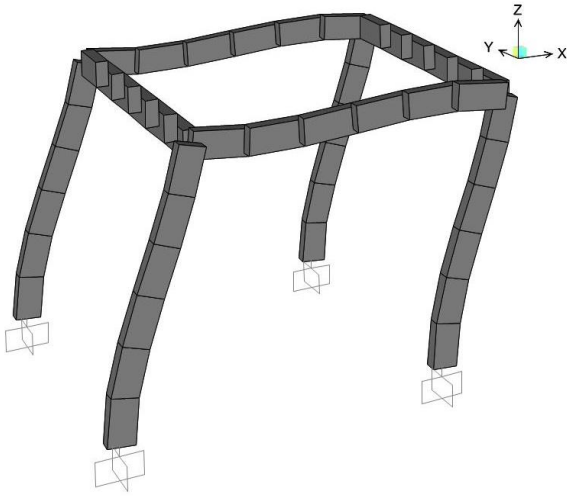	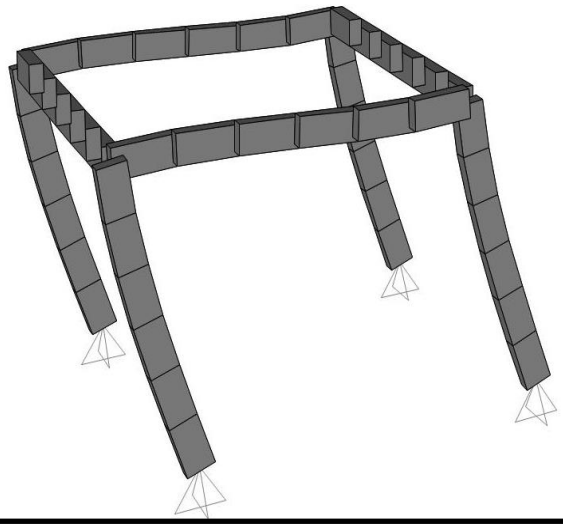

Figure 4.11 Fundamental mode shapes (in x and y direction) and corresponding natural frequencies for COMP4 from the computer model for both pinned and fixed bottom connection.

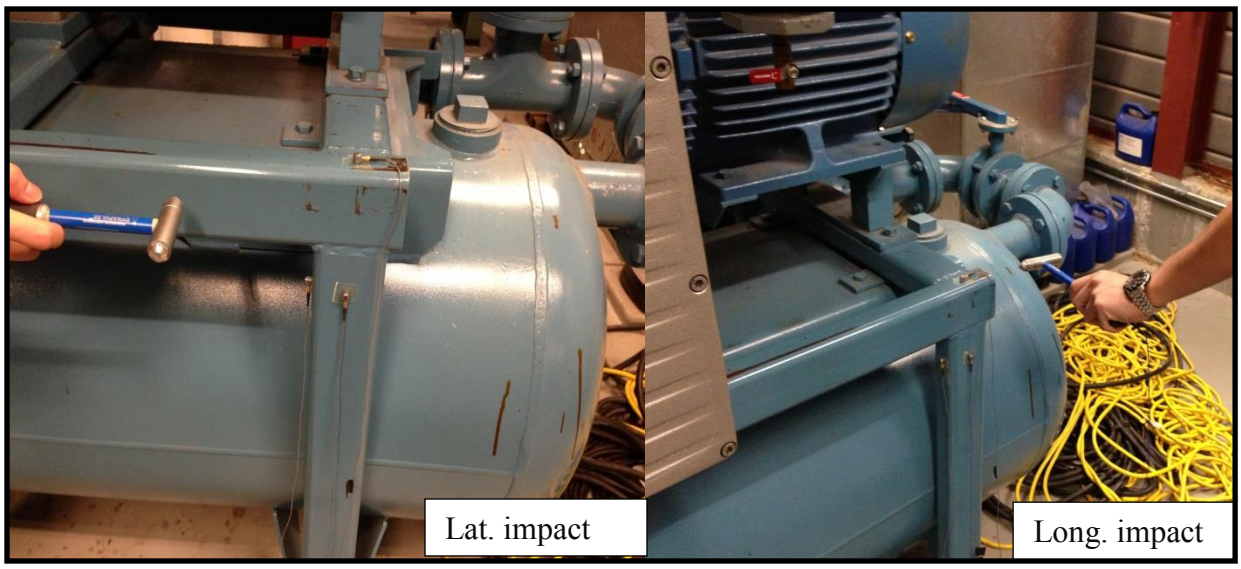

Figure 4.12 Hammer impact applied on COMP4 in lateral direction and longitudinal direction, respectively.

COMP 7: Vertical Pipe

Dimension: length=3.6 m; diameter =150 mm; pipe wall thickness = 6 mm

Material: Steel

Unit weight: 26.6 kN/m3

Elastic modulus: 68.9 GPa

No additional mass was assigned.

Two boundary conditions considered:

1) Fixed-roller connection if the pipe is fixed at the base and runs continuously through a considerable height;
2) Fixed-free connection if the pipe is fixed at the base and not restrained at the top;

COMP7 is a vertical water pipe fixed at the bottom, and the restraint at the top is unknown as shown in Figure 4.11. Therefore, computer models for two possible boundary conditions were developed. A fixed-free connection (i.e. fixed at the bottom and not restrained at the top) was considered if the pipe is not continuous at the top and not restrained. A fixed-roller connection (i.e. fixed at the bottom and only restrained vertically at the top) was considered if the pipe runs continuous at the top. The mode shapes and corresponding frequencies for the two extreme conditions are included in Figure 4.12 below. For both conditions, out-of-plane bending was the

fundamental mode. The impact force was applied in the lateral direction along the height of the vertical pipe (i.e. bottom, mid-height and top).

Figure 4.13 Top portion of COMP7 - vertical pipe showing that the pipe extends beyond the ceiling

Fixed-free (Not continuous and not restrained at top) $f_n = 10.6$ Hz	Fixed-roller (Continuous at top) $f_n = 17.2$ Hz
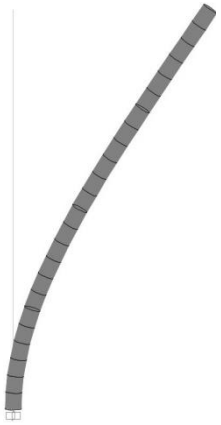	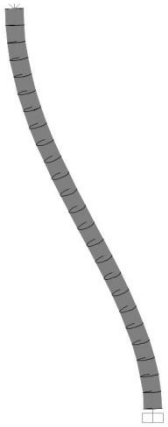

Figure 4.14 Fundamental mode shapes and natural frequencies for COMP7 from the computer model for fixed-free and fixed – roller boundary conditions

4.4.3 **Data Processing**

The data processing followed the procedure described in Chapter 3. It involved transforming time-domain signals into frequency-domain measurements using Fast Fourier Transform (FFT) technique. The calculations were carried out in the Matlab program. The frequency-domain measurements were expressed in the form of power spectral density (PSD) plots. Figure 4.15 is a sample of the PSD plot with three response signals and the input force signal for COMP7-the vertical pipe. A perfect impulse should be applied for an infinitely small duration so that constant energy throughout the entire frequency range was inputted. The input PSD in the plot is nearly a horizontal line, which indicates a good quality impulse.

Following the transformation, the output-input relationship known as the FRFs was also plotted in Matlab, as shown in Figure 4.16. For this example, the first local maximum of the FRF plot was around 14.4 Hz. Thus, the fundamental frequency of this pipe was estimated to be 14.4 Hz. The analytical results from the computer model discussed in Section 4.4.2.1 showed a fundamental frequency of 10.9 Hz for the fixed-free condition and 17.2 Hz for the fixed-pinned condition, respectively. The actual support condition of this pipe is expected to be between these two idealized situations; therefore the average value (13.9 Hz) was used to compare with the experimental value. The difference between the analytical and experimental values was 3.5% which confirms that the HIMT captured the fundamental frequency of COMP7 accurately. A couple of other well defined peaks at higher frequencies were also observed from the same plot. These peaks most likely represent the higher modes of the NSC. From the computer model, the first mode contributes greater than 90% of the mass participation. Thus the higher mode effects on NSCs were negligible, it was deemed adequate to identify only the dominant mode in this study.

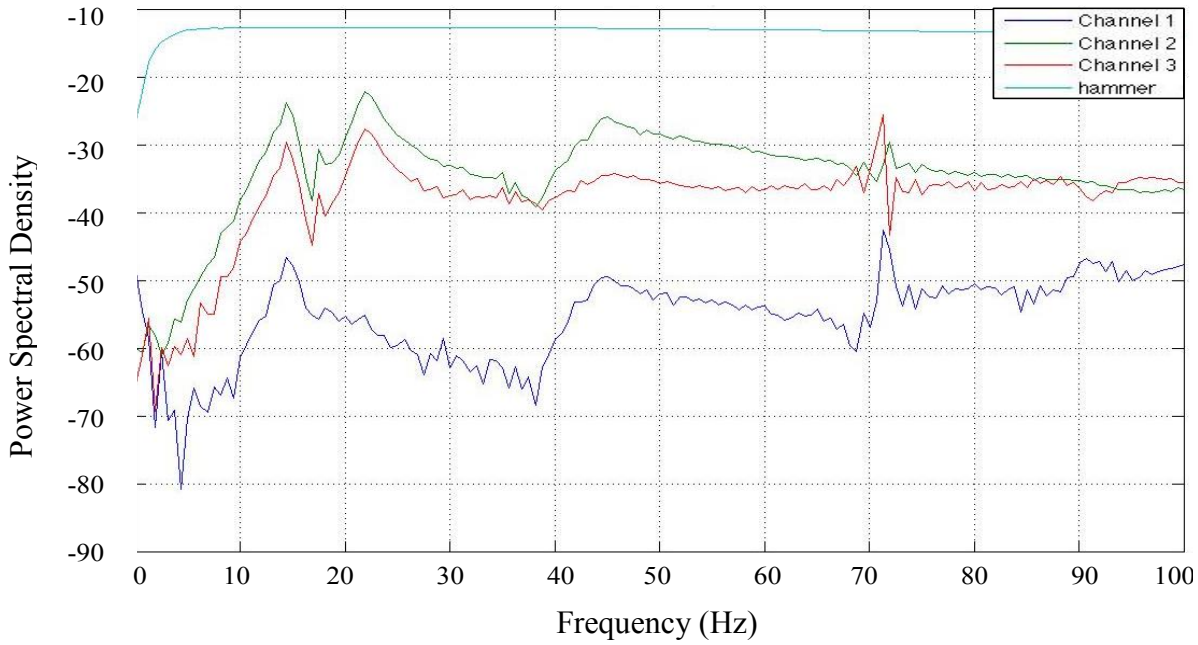

Figure 4.15 **Power spectral density plots (PSD) for the response measurements and the applied impulse (hammer) from 0 to 100 Hz for COMP7. Channel 1, 2 and 3 are responses measured at bottom, mid-height and top of the vertical pipe, respectively.**

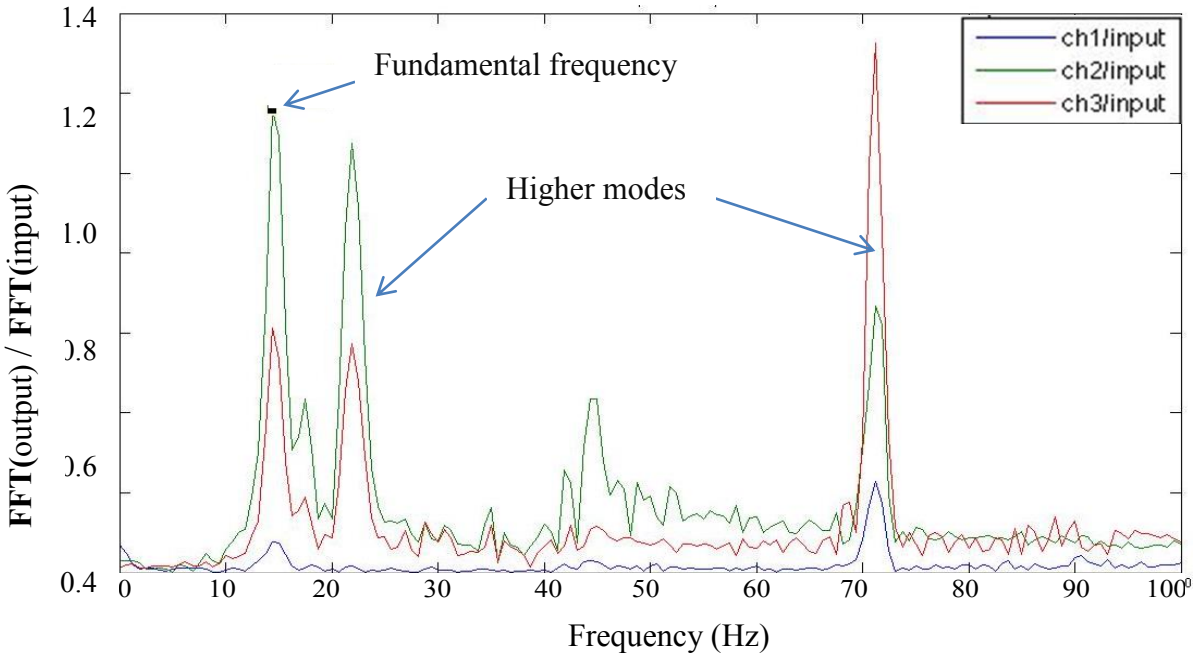

Figure 4.16 **Frequency response spectrum plots (FRF) for the response measurements and the applied impulse (hammer) from 0 to 100 Hz for COMP7. Channel 1, 2 and 3 are responses measured at bottom, mid-height and top of the vertical pipe, respectively.**

Damping was evaluated based on the logarithm decrement algorithm discussed in Chapter 3. Figure 4.17 shows the plot of the free vibration of COMP7 after the impact using the Geopsy program (Marc Wathelet, 2011). The initial and the 18th response values were found to be 2.10 and 0.05, respectively. These values were plugged into Equation 3-7 and 3-8 and the calculated damping ratio was 3.5%. The same calculations were carried out for all other components and the results are summarized in Chapter 5.

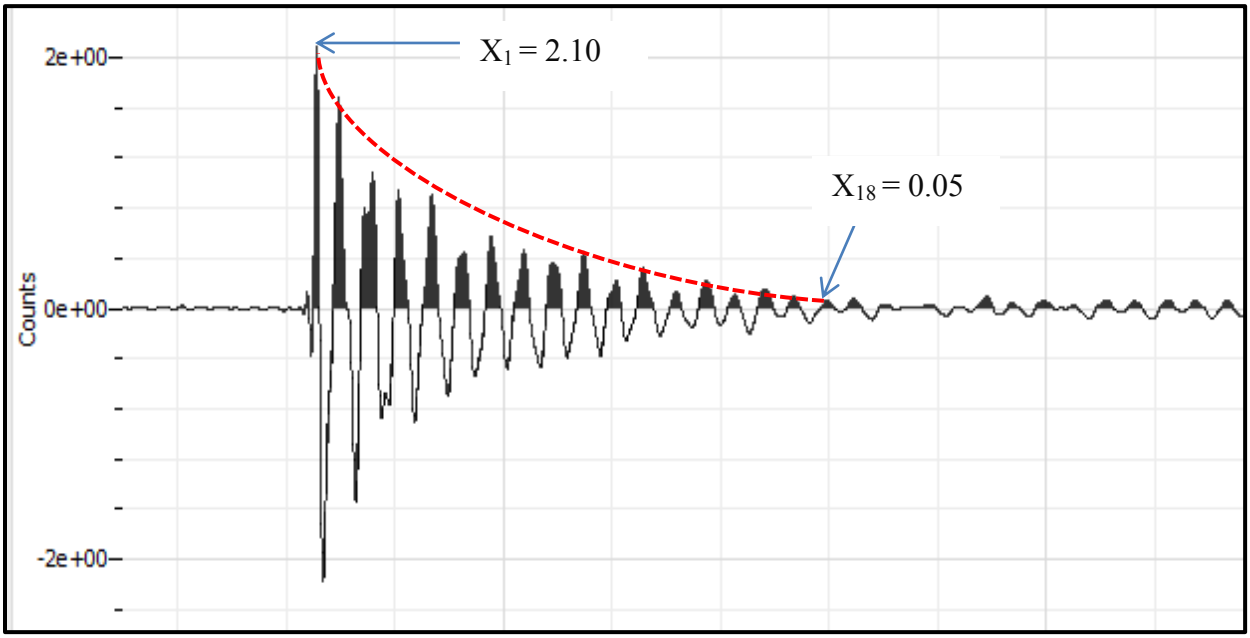

Figure 4.17 Free vibration time history measurement for COMP 7.

4.4.4 Challenges of the HIMT

Although this field testing experience was found to be generally time-efficient and economic, following challenges and limitations were still confronted in this study. In order to evaluate its appropriateness in engineering practice, these associated shortcomings are addressed in this section. Some alternative solutions to overcome these issues are also discussed here.

The most common issue throughout the testing was that it was difficult to excite the fundamental mode shapes of components with large size or with complex geometry. COMP2 (air handler unit) was one example of this situation as shown in Figure 4.18.

The component was too large to excite with the "small" hammer (Dytran 5850B). A solution to this issue was to use a larger hammer (Dytran 5803A). Figure 4.18 and 4.19 show the impact test setup with the "big" hammer. One shortcoming of using the larger hammer was that the input signals from the hammer could not be recorded, and hence the output/input transfer function was not calculated. Therefore, only the response PSD plots were generated to obtain the natural frequencies, which make the peak-picking process more difficult.

The other situation where the HIMT was difficult to carry out was when the component has an irregular geometry, which makes it challenging to predict the mode shape. COMP5 (medical air vacuum unit) shown in Figure 4.20 below is an example. In this situation, the resultant experimental frequency may not be associated with the natural modes of the component but rather due to the local vibration excited by the hammer. Therefore, the experimental results should either be used with careful considerations or other modal identification techniques should be considered.

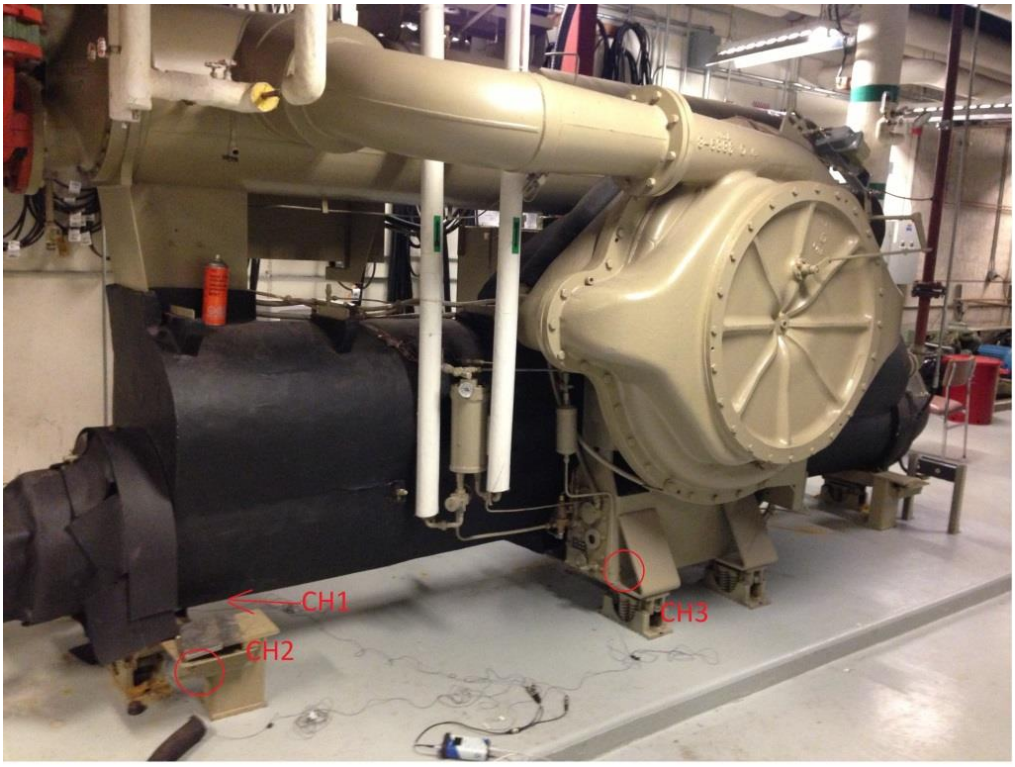

Figure 4.18 Accelerometer setup for COMP2: air handler unit.

Figure 4.19 A colleague applying the big hammer impact to excite COMP2.

Figure 4.20 An overview of COMP5: medical air vacuum unit.

Another major challenge of this experiment is distinguishing between the natural free vibration frequency and the noise frequencies due to machine's operation. In the mechanical room where the tests took place, a number of machines were in operation. This caused tremendous vibration noises that were reflected in the FFT analysis. To overcome this challenge, a floor ambient testing was employed to identify the frequencies of these operating machines. Subsequently band filters were applied to the original recording to extract the natural free vibrations.

Although these techniques can be helpful for separating the natural frequency from the operational frequencies to some extent, the results can still be misleading. More importantly, when the operating machine is too close by or the magnitude of vibration is too high, the impact excitation is overpowered by the "noise". Under this situation, the impact testing approach cannot provide useful information. This problem was observed during the testing for COMP6, the concrete pump deck. During the experiment, two of the pumps on the deck that were in operation produced vibration that suppressed the hammer impact. A sample of the measured acceleration time histories is shown in Figure 4.21 below. Therefore, "noisy" surroundings can largely amplify the amount of work associated with post-experiment analysis. In worse cases, this impact testing method is not even applicable.

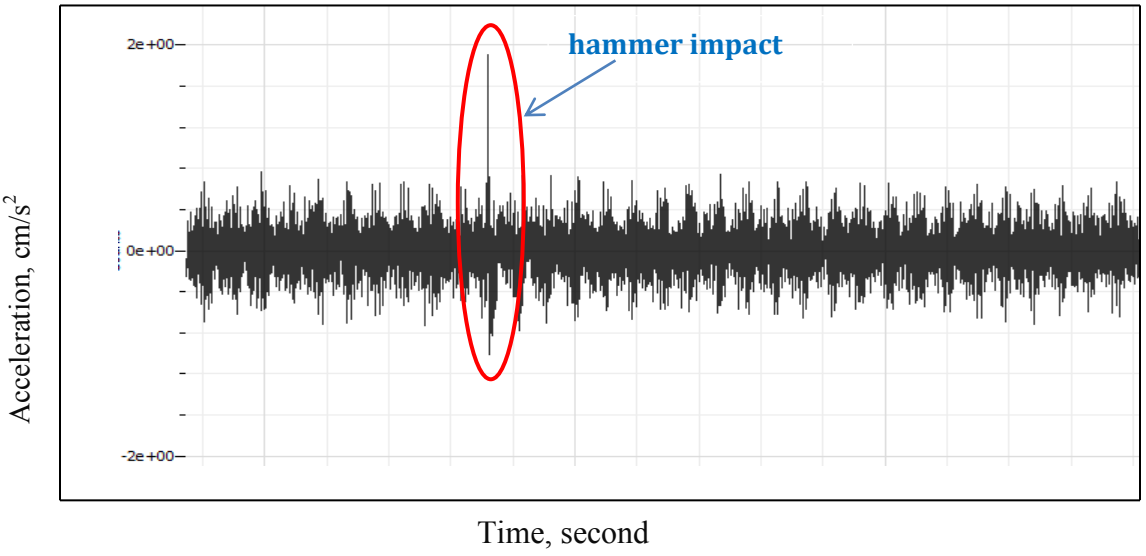

Figure 4.21 A section of the time history record from impact test on COMP6 showing the noise overpowering the intended forced vibration

4.5 Ambient Floor Testing

Following the HMIT for the NSCs, the Ambient Vibration Tests (AVT) were carried out at the roof level of the U.B.C Hospital Koerner Pavilion for two purposes:

- The primary use of the AVT results was to identify the natural frequencies of the structure and in turn, to validate these values calculated in the computer model;
- The secondary intent of the AVT was to detect the harmonic noises due to the operation of machines so that the true natural frequencies of the NSCs from the HIMT can be separated from the frequencies due to noise.

4.5.1 Test procedure

The test procedure was introduced in Chapter 3 and summarized again below:

- Measuring the floor responses using accelerometers at various locations during the normal operation of the building;
- Constructing the PSD plots using the FFT algorithms;
- Identifying the natural frequencies and harmonic excitation due to running machinery using peak-picking (PP) technique.

The accelerometers used here to measure the ambient floor vibration were the SENSR-CX1 sensors. The equipment specifications are included in Section 3.1.2. There were eight tests performed in total with 10 to 15 minutes time for each recording at a sampling rate of 1000 Hz.

In order to capture the global modal behavior of the floor slab, the sensors were set at multiple locations throughout the floor, as shown in Figure 4.22. Figure 4.23 shows the original acceleration time history signals in X, Y and Z directions measured at location #1. It was important to avoid setting up the sensor too close to a column or a wall since the local behavior of the vertical member would also be measured and provide misleading information about the floor slab behavior.

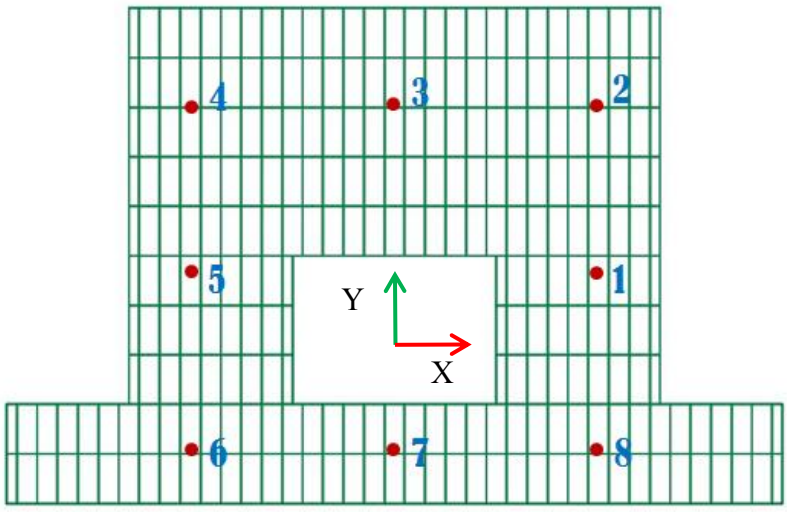

Figure 4.22 Locations of the ambient floor vibration testing at the roof level.

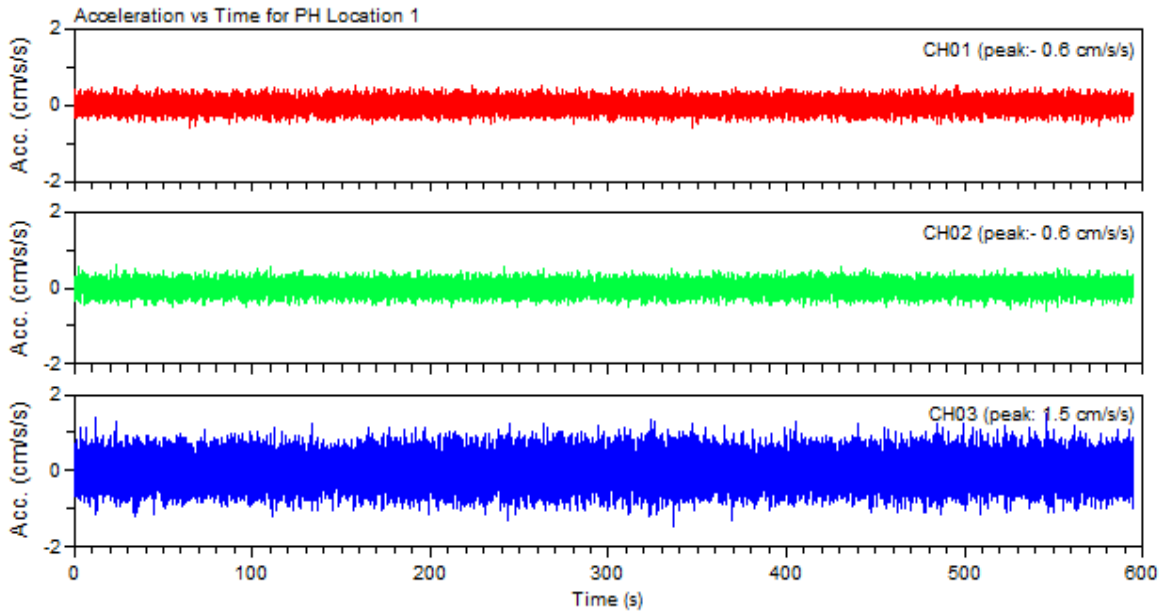

Figure 4.23 Acceleration time histories measured at location 1 in X (CH01), Y (CH02) and Z(CH03) direction, respectively.

4.5.2 Identification of the Structural Natural Frequencies

Each time history measurement contains 600,000 data points (600 seconds at 1000 Hz) per channel. A frequency range of 0 ~ 50 Hz was considered adequate for identifying the natural frequencies of the structure. Therefore, the original data was decimated from 1000 Hz to 100 Hz using Matlab (The Mathworks, 2009). Subsequently, the decimated time histories were

transformed into PSDs using FFT technique in the SeismoSpect program (Seismosoft Ltd., 2002). A sample PSD plot for signal in X (N-S) and Y (E-W) direction is shown in Figure 4.24 and 4.25, respectively. Peak-picking (PP) technique was applied to identify the natural frequencies of the building. The range of natural frequencies was expected to be below 10 Hz; therefore, a close-up view of each PSD plot between 1 to 10 Hz was obtained. All the PSD plots are included in Appendix B.

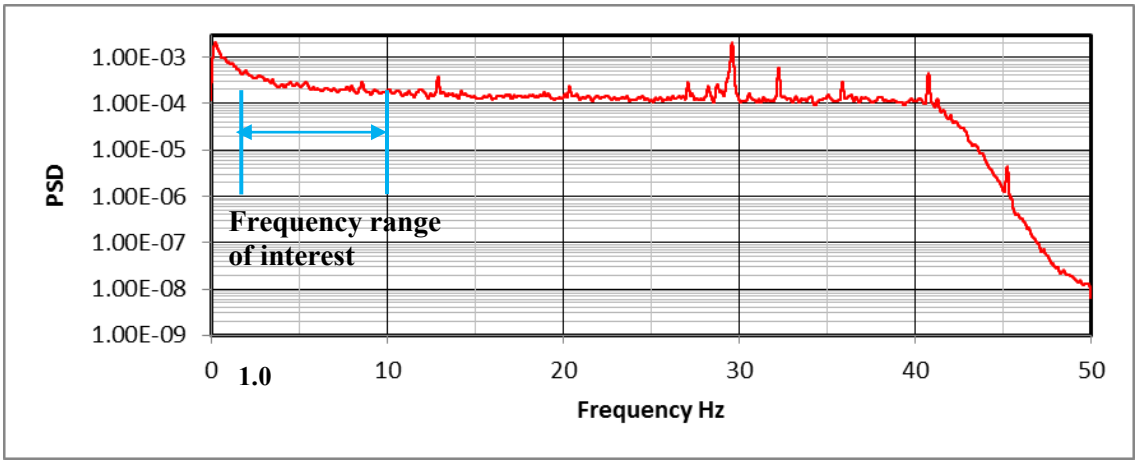

Figure 4.24 Sample power spectral density plot for measurement in N-S (X) direction.

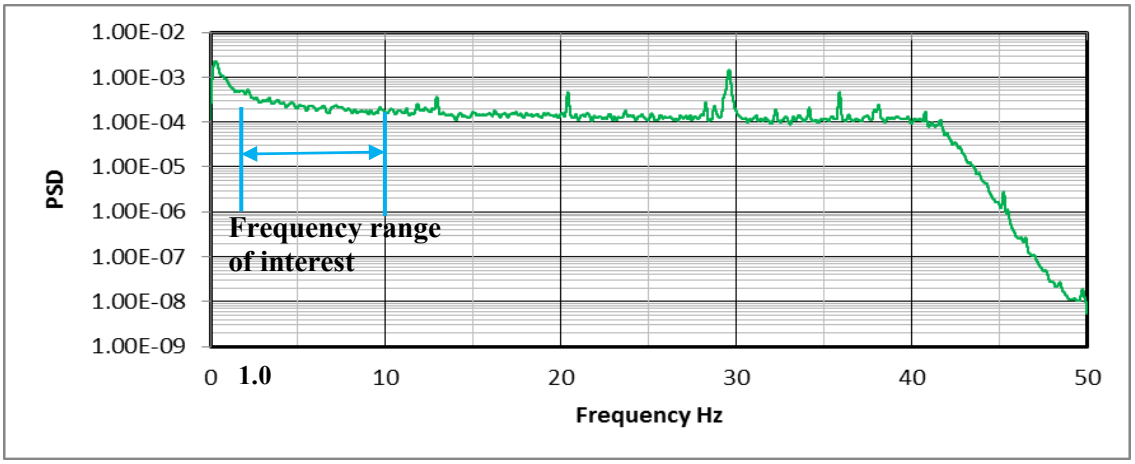

Figure 4.25 Sample power spectral density plot for measurement in E-W (Y) direction.

In the PP process, the common local peaks observed throughout all locations were identified as natural frequencies of the structure. In the N-S direction, peaks were observed in all PSD plots near frequencies: 1.38 Hz, 1.72 Hz and 4.60 Hz. In the E-W direction, common peaks were found in PSDs for all locations near frequencies of 1.40 Hz and 6.00 Hz. Figure 4.26 and 4.27 include the sample enlarged PSD plots in log-log scale showing the identified natural

frequencies. Table 4.3 shows the comparison between the modal frequencies estimated through experiments and through analytical model for the first five modes.

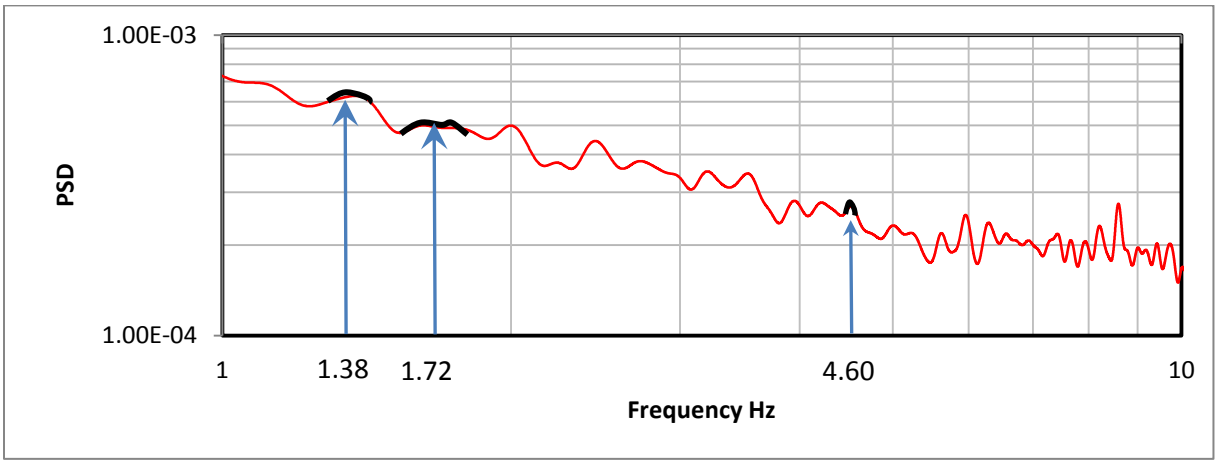

Figure 4.26 **Sample power spectral density plot for 1 ~ 10 Hz in N-S (X) direction showing the estimated natural frequencies.**

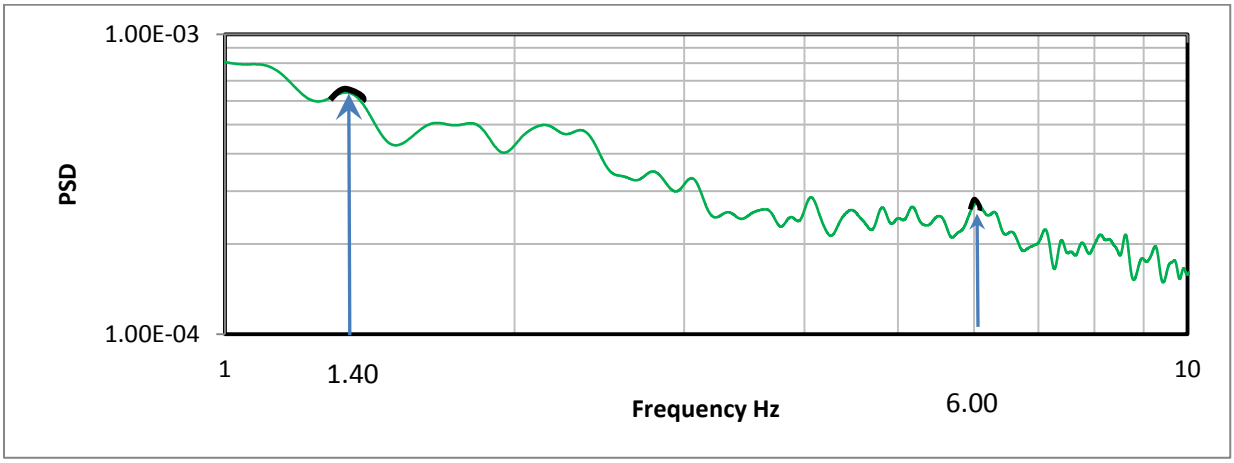

Figure 4.27 **Sample power spectral density plot for 1 ~ 10 Hz in E-W (Y) direction showing the estimated natural frequencies.**

Table 4.3 **Comparison of modeled and experimental structural natural frequencies**

Mode	Mode Shape Description	Natural Frequencies (Hz)		Difference	
		Modeled	Experimental	(Hz)	(%)
1	Torsional and Translational in N-S	1.32	1.38	0.06	5
2	Translational in E-W	1.35	1.40	0.05	4
3	Torsional and Translational in N-S	1.65	1.72	0.07	4
4	Torsional and Translational in N-S	4.55	4.60	0.05	1
5	Translational in E-W	5.42	6.00	0.58	10

The experimental values are 1~ 10% higher than the computer model values for all the modes considered. The model was developed based on the layout and the specified material properties included in the original drawing. Therefore, the difference between the experimental and analytical values can be an explained by the fact that the model did not account for the façade of the structure, which may contribute to the overall structural stiffness.

In addition, the concrete is known as a time-varying material of which the elastic modulus can increase over time (The International Federation for Structural Concrete (FIB), 2012). Realizing that the building was built roughly 50 years ago, the time impact on the concrete material is clear and should have caused a higher stiffness than that calculated with the material properties specified from the original drawings.

Another possible reason for the frequencies in the model being lower is that the weight of the structure used in the model was overestimated. As mentioned in Chapter 3, the weight of the structure was determined by including the dead load and a portion of the snow load. The detail calculation is included in Section 4.5.2. There was no snow load at the time when the experiments were carried out. In addition, it is almost impossible to calculate the actual weight of each member, partition, equipment and other components that would have added weight to the structure. The simplified approximation was likely to cause overestimation of the weight.

Since the difference between the theoretical and the experimental values was within an expected range (below 10%), the model is considered sufficient for capturing the dynamic characteristics of the actual building.

4.5.3 **Machine Operating Frequencies**

In the PSD plots generated from the floor vibration tests, a few narrow and sharp peaks (high spectral density amplitude) were observed, as shown in Figures 4.28 to 4.30. They occur in measurements in all three directions. These peaks were identified as operational frequencies of the machines near the tested location as shown in Table 4.4.

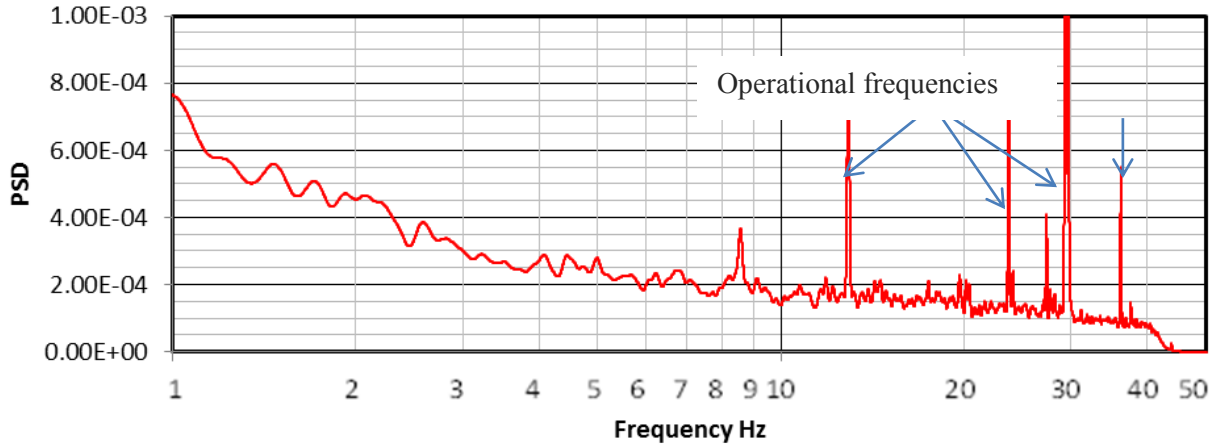

Figure 4.28 **A sample power spectral density plot in N-S direction showing the machine operational frequencies**

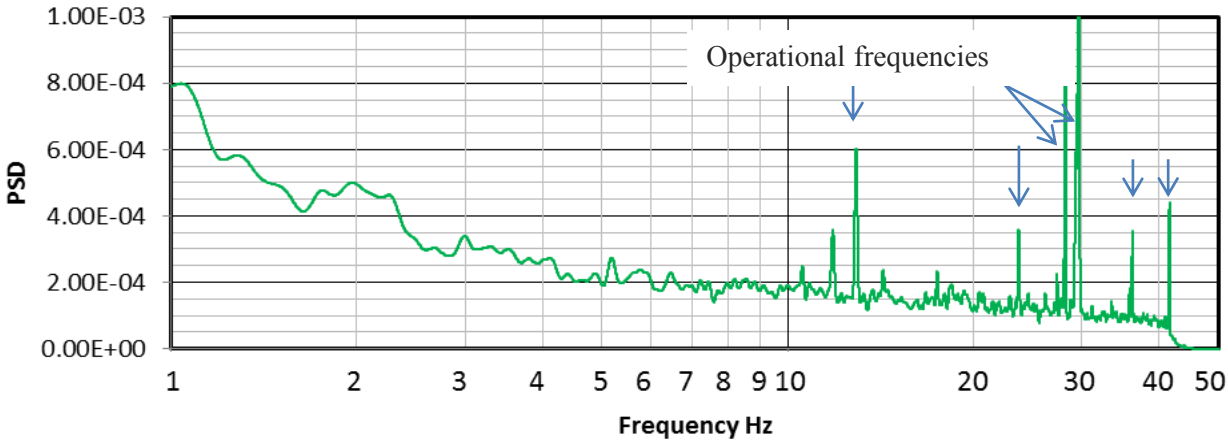

Figure 4.29 **A sample power spectral density plot in E-W direction showing the machine operational frequencies**

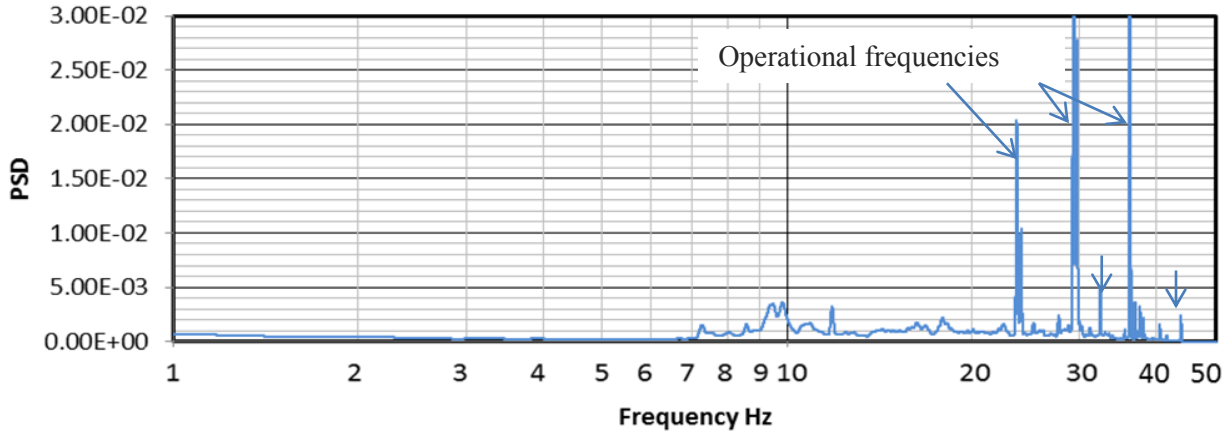

Figure 4.30 **A sample power spectral density plot in vertical direction showing the machine operating frequencies.**

Table 4.4 Detected machine operating frequencies

Frequency Number	Operation Frequencies (Hz)
1	12.9
2	23.8
3	27.2
4	29.5
5	36.2

4.6 Preparation of the 3D FEM

Since coupling effects are not significant for this case as discussed in Chapter 2, an independent 3D FE structural model was developed in SAP 2000 (Computers and Structures, Inc., 2012) to simulate the dynamic response of the structure.

This section describes the key steps for establishing the computer model including: definition of the material and section properties, assignment of directional masses, setup of boundary condition and coordinate system.

A time history analysis (THS) using modal superposition approach was performed in this case study. This section will also demonstrate the procedure for selecting and scaling the input ground motions used in the THS. A constant damping ratio of 5% was assigned in the structural model as discussed in Chapter 3. To apply the modal superposition, a modal analysis using Ritz vector method was carried out. The modal information including the natural frequencies, mass participation factors (MPF) and mode shapes for the modes with at least 5% MPF in the principle horizontal directions are also presented in this section.

4.6.1 Material and section properties

The material and section properties were obtained based on the original structural drawings. The following is a summary of the material properties applied in the model.

a) Concrete:

Specified compressive 28 day strength: 35 MPa

Density: 240 kg/m^3

Modulus of Elasticity: 25 GPa

Poison's Ratio: 0.2

b) Steel:

Yield Strength: 345 MPa

Density: 785 kg/m^3

Modulus of Elasticity: 200 GPa

Poison's Ratio: 0.3

An efficient FE model should be formed with the least number of elements possible without losing the accuracy. For this reason, the key components included in the model are:

- Concrete columns modeled as frame members
- Concrete beam joists modeled as frame members
- Concrete walls modeled as thick shell elements.

Modeling the floor slabs as actual shell elements can significantly increase the computational time for the linear time history analysis and meshing shells properly can be tedious. Since each floor was predicted to behave as a rigid diaphragm. A series of rigid diaphragm constraints were assigned at each the node on the same floor level. The weight of the slabs was accounted for by assigning masses to the joints.

4.6.2 **Sources of mass**

The dynamic mass of the structure should include its self-weight and also the weight of its permanent equipment and attachment. Therefore, the following sources of dynamic mass were considered in the model:

- Self-weight of the modeled elements generated automatically based on the material density and element dimensions;
- Self-weight of the floor slab at each floor level calculated based on the material density and volume of slab, e.g.: 200 mm thick floor slab is equivalent to 4.8 kPa dead load;

- Superimposed dead load to account for the weight of equipment, building contents and attachment per Table 4.1.5.3 in NBCC 2010, e.g.:an average of 2.0 kPa at each floor;
- 25% of the snow load at the roof level. Snow pressure was equal to 2.0 kPa and the applied snow load was 0.5 kPa;

In summary, a joint load of 288 kN was applied at each column location for the roof level and 248 kN for the lower floor levels. The calculation details are included in Appendix D.

4.6.3 **Boundary condition**

From the structural drawings, the bottom floor of the building is below ground level. This underground portion of the structure was not included in the model. The surrounding soils were assumed to provide lateral and vertical restraints to the building but are rotationally flexible. Therefore, to account for the rotational flexibility of the soils around the structure, pin supports were assigned at each node at the base of the ground floor. Thus, the simplified model is consisted of 5 stories and pinned at the bottom. The zero height in the model starts from the ground level.

4.6.4 **Coordinate System**

Figure 4.31 below is a 3D view of the model showing its coordinate system. The origin of the model is located at the ground level, at the center along X direction. The ground motions were applied along the X (North-South) and Y (East –West) directions. The FRS generated and discussed in later sections will refer to the same coordinate system.

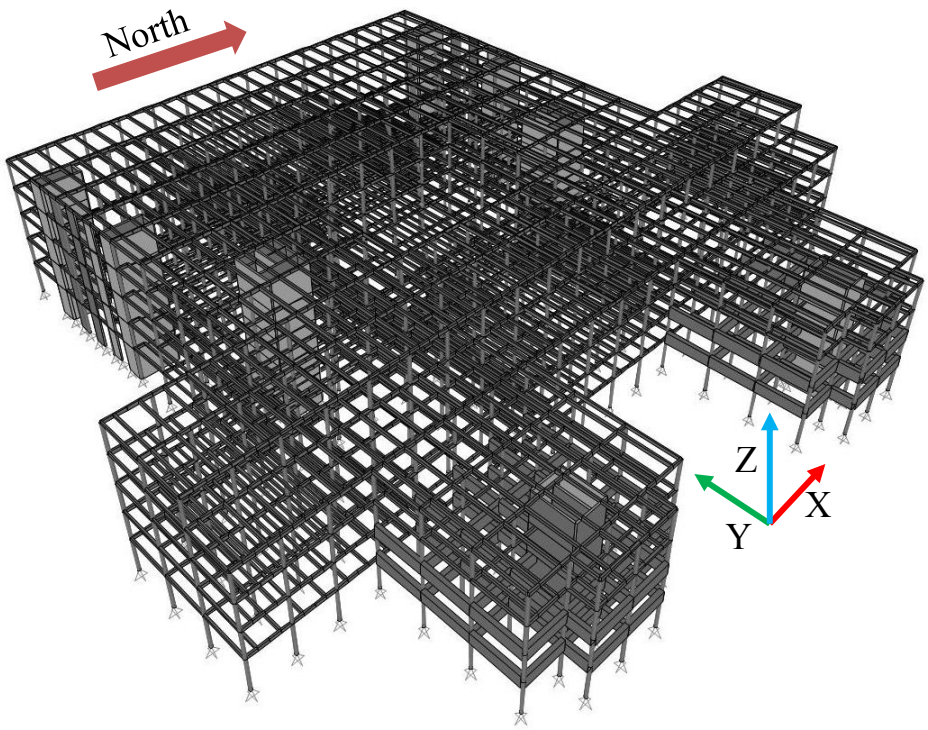

Figure 4.31 3D overall view of the model showing the coordinate systems

4.6.5 Selection of ground motions

The ground motions selected to conduct the linear time history analysis of the U.B.C Koerner Pavilion are based on the 2% in 50 years (1/475 year) hazard level and site class D (V_{30} = 180~360) for its geological location. The most current spectral values adopted in the Canadian code to define the hazard level were provided by Geological Survey of Canada (Natural Resources of Canada, 2013). These values are presented in Table 4.5 below.

Table 4.5 Spectral values used for matching the ground motions

Site Class	PGA	Sa(0.2)	Sa(0.5)	Sa(1.0)	Sa(2.0)
C	0.461	0.939	0.651	0.338	0.174
D	0.507	1.033	0.755	0.392	0.202

A seismic hazard deaggregation analysis is a tool for assessing the contribution of earthquake sources in terms of the magnitude and distances for a given spectral value and a probability of exceedence (Halchuk, Adams, & Anglin, 2007). Deaggregation studies conducted by Halchuk,

Adams, & Anglin (2007) on seismic hazard with a probability of exceedence of 2% / 50 years in Vancouver have shown that earthquakes with magnitude from 6.0 to 7.5 and with an epicenter distance of 40 to70 km contribute the most to the hazard.

The building period of interest was set to 0.2 to 2 seconds. The scaling factors were limited to 0.5 to 2 to obtain realistic ground motions. Figure 4.32 below shows the search criteria entered in the PEER database.

Based on these criteria, seven ground motions were selected from the PEER Strong Ground Motion Database (PEER, 2011) as shown in Table 4.6 below. Each component contains three components (i.e.: fault parallel, fault normal and vertical). These original ground motions were scaled to match the target spectrum defined in Table 4.6. The scaling was done using the SeismoMatch program (Seismosoft Ltd., 2002). Figures 4.33 and 4.34 are the original and matched acceleration spectra for all three components of GM#1: Chi-Chi CHY 036 with respect to the NBCC 2010 UHS, respectively. The complete input ground motion database is included in Appendix C.

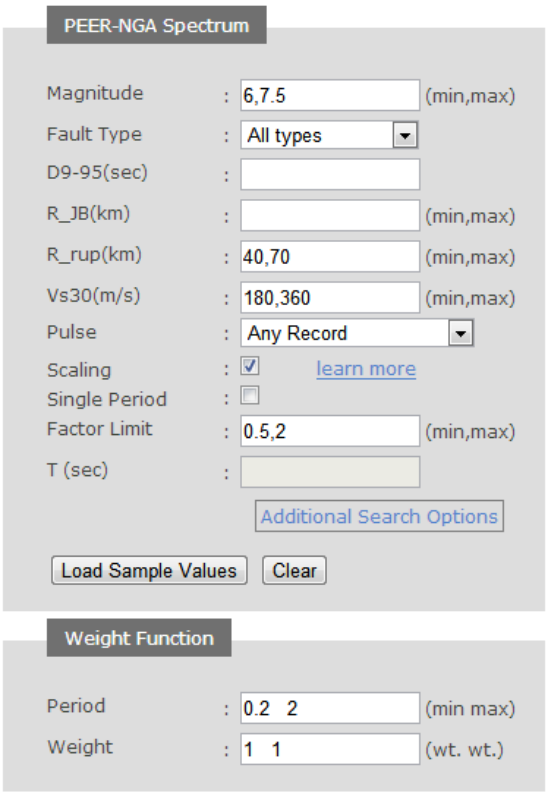

Figure 4.32 Screenshot of the PEER strong ground motion database online. Reprinted from http://peer.berkeley.edu/peer_ground_motion_database

Table 4.6 Ground motions selected for the time history analysis

GM #	NGA #	Event	Year	Station	Magnitude	Rjb(km)	Vs_{30}(m/s)
1	3275	Chi Chi	1999	CHY036	6.3	45.1	233.1
2	733	Loma Prieta	1989	APEEL 2E Hayward Muir Sch	6.93	52.5	271.1
3	1762	Hector Mine	1999	Amboy	7.13	41.8	271.4
4	799	Loma Prieta	1989	SF Intern. Airport	6.93	58.5	190.1
5	3276	Chi Chi	1999	CHY037	6.3	52.8	212.1
6	832	Landers	1992	Amboy	7.28	69.2	271.4
7	956	Northridge	1994	Buena Park - La Palma	6.69	59.4	308.6

Note: **NGA # refers to the designation of each ground motion within the PEER ground motion database.**

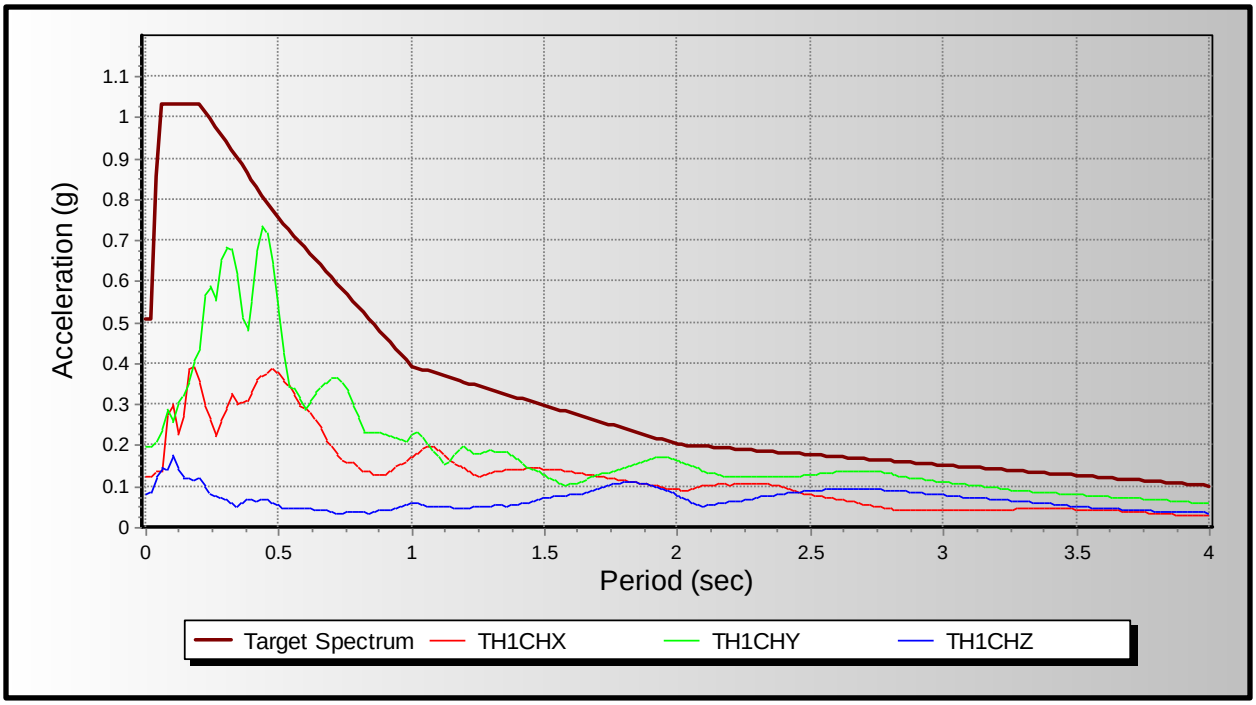

Figure 4.33 **Original Acceleration Spectra vs. Target Spectrum (NBCC 2010 UHS) for GM#1: Chi Chi CHY036 component X, Y and Z.**

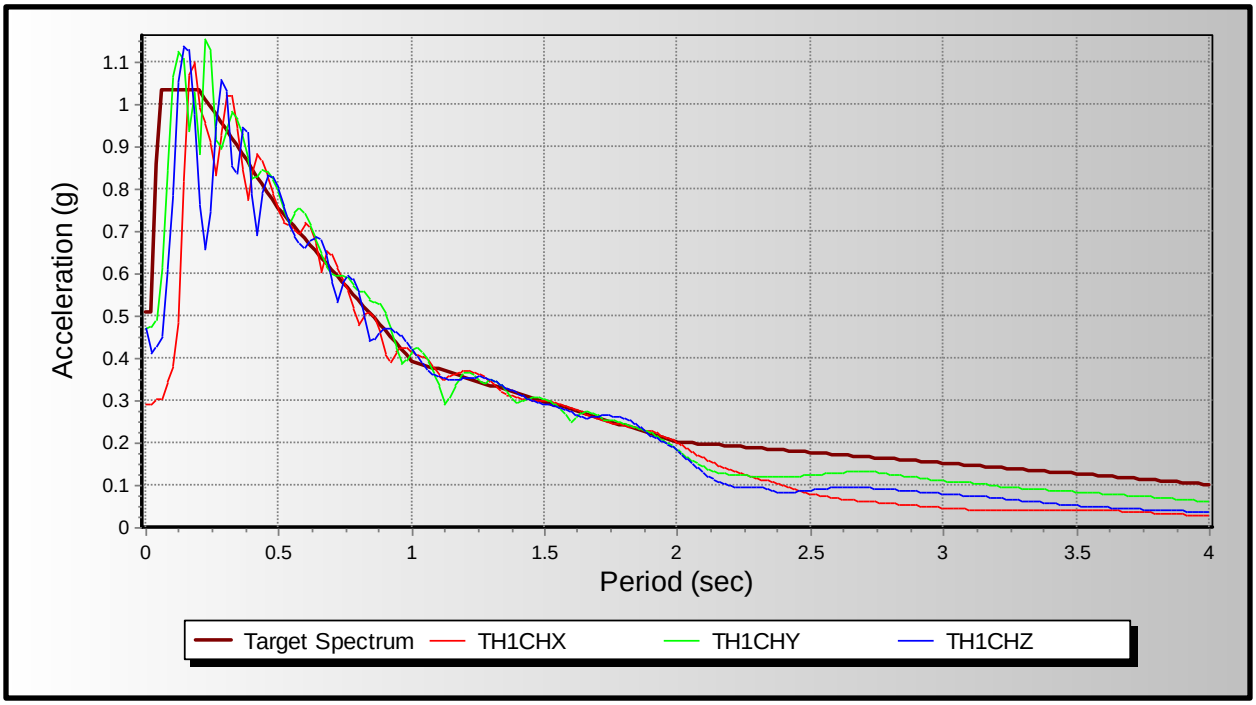

Figure 4.34 **Original Acceleration Spectra vs. Target Spectrum (NBCC 2010 UHS) for GM#1: Chi Chi CHY036 component X, Y and Z.**

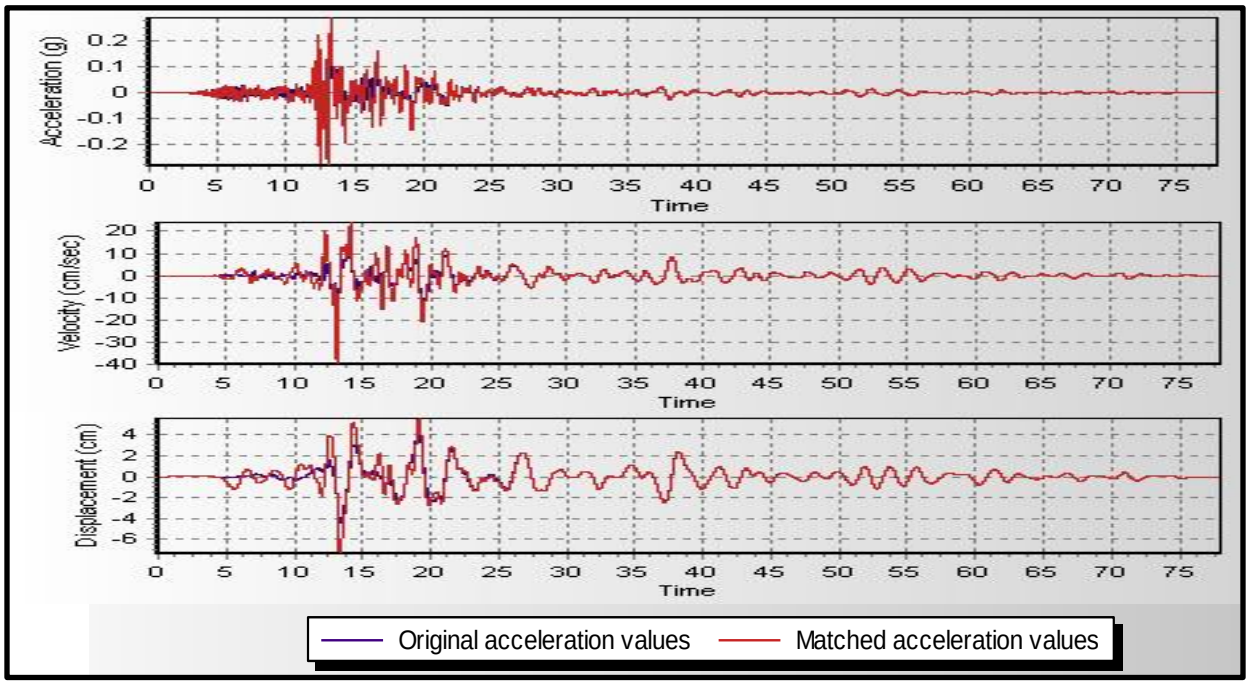

Figure 4.35 Original and Matched acceleration, velocity and displacement time histories for GM#1: Chi Chi CHY036 component X.

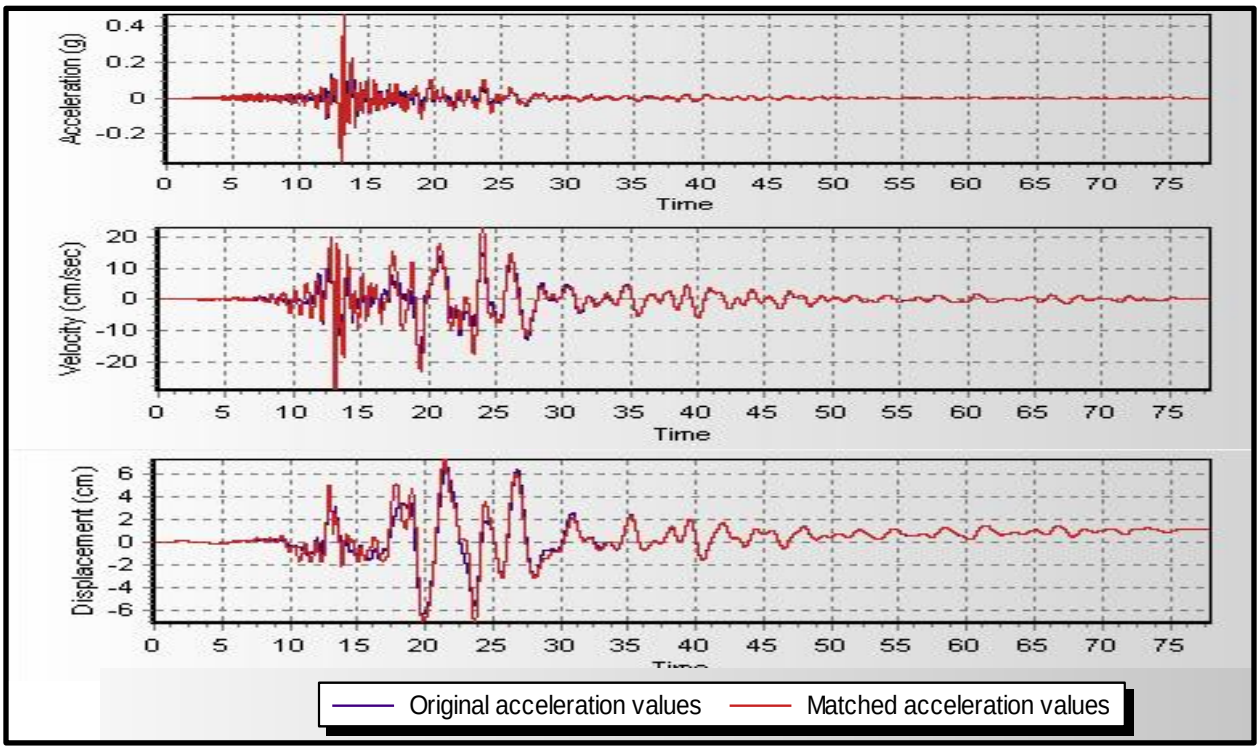

Figure 4.36 Original and Matched acceleration, velocity and displacement time histories for GM#1: Chi Chi CHY036 component Y.

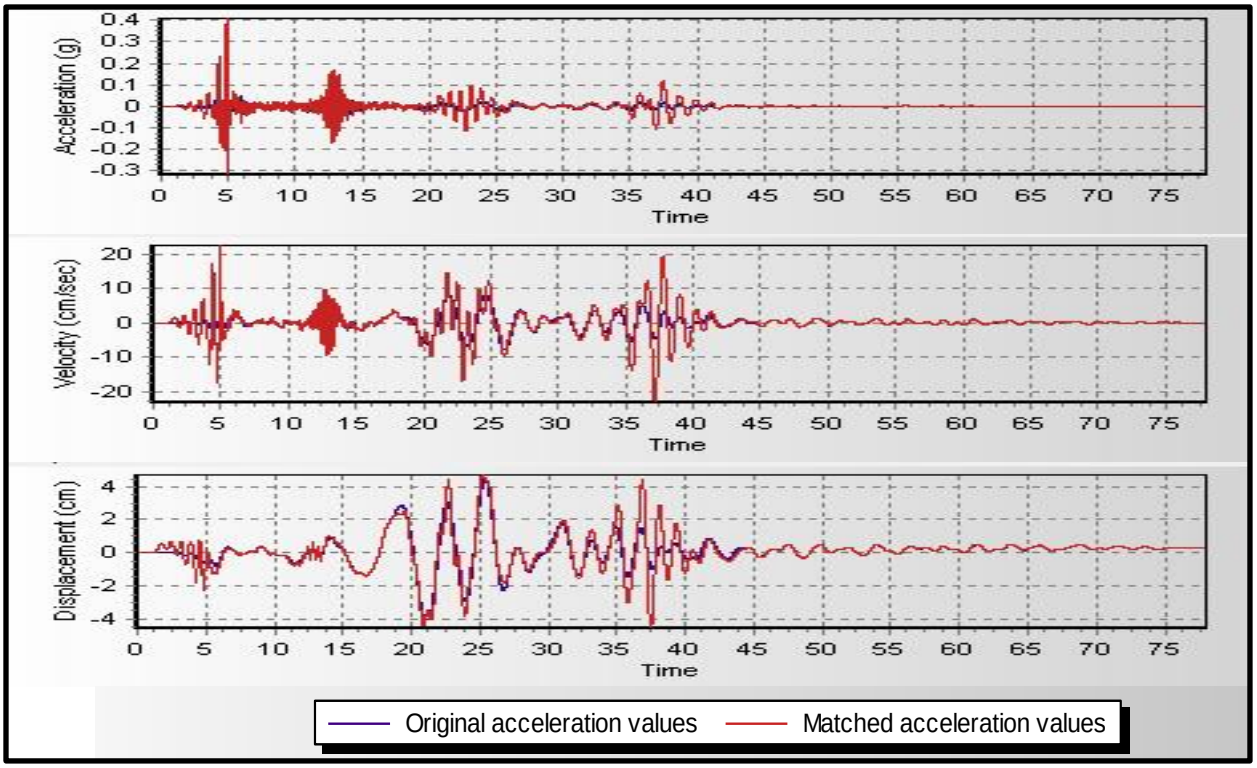

Figure 4.37 Original and Matched acceleration, velocity and displacement time histories for GM#1: Chi Chi CHY036 component Z.

4.6.6 **Modal analysis**

Once the 3D FE model was developed, a modal analysis was carried out to serve the following purposes:

- Check for discontinuity and instability of the model
- Obtain modal frequencies and corresponding mode shapes that can help understand response mechanisms of the building subjected to dynamic loading
- Determine the minimum number of modes required for the model superposition time history analysis to account for at least 90% of the cumulative mass participation in all three principle directions.

Table 4.7 shows the modal information of the significant modes with at least 5 % of the MPF in the principle horizontal directions. The natural periods, frequencies, corresponding mass participation factors (MPF) and brief descriptions of the mode shapes are tabulated here. The mode shapes for these modes are shown in Figure 4.38.

Table 4.7 Modal periods and corresponding mass participation factors

Mode	Period Sec	Frequency Hz	MPF	Mode Shape
1	0.759	1.318	37%	Torsional and Translational N-S
2	0.742	1.347	73%	Translational E-W
3	0.608	1.645	35%	Torsional and Translational N-S
4	0.220	4.546	10%	Torsional and Translational N-S
5	0.185	5.417	21%	Translational E-W
6	0.129	7.755	11%	Translational N-S direction

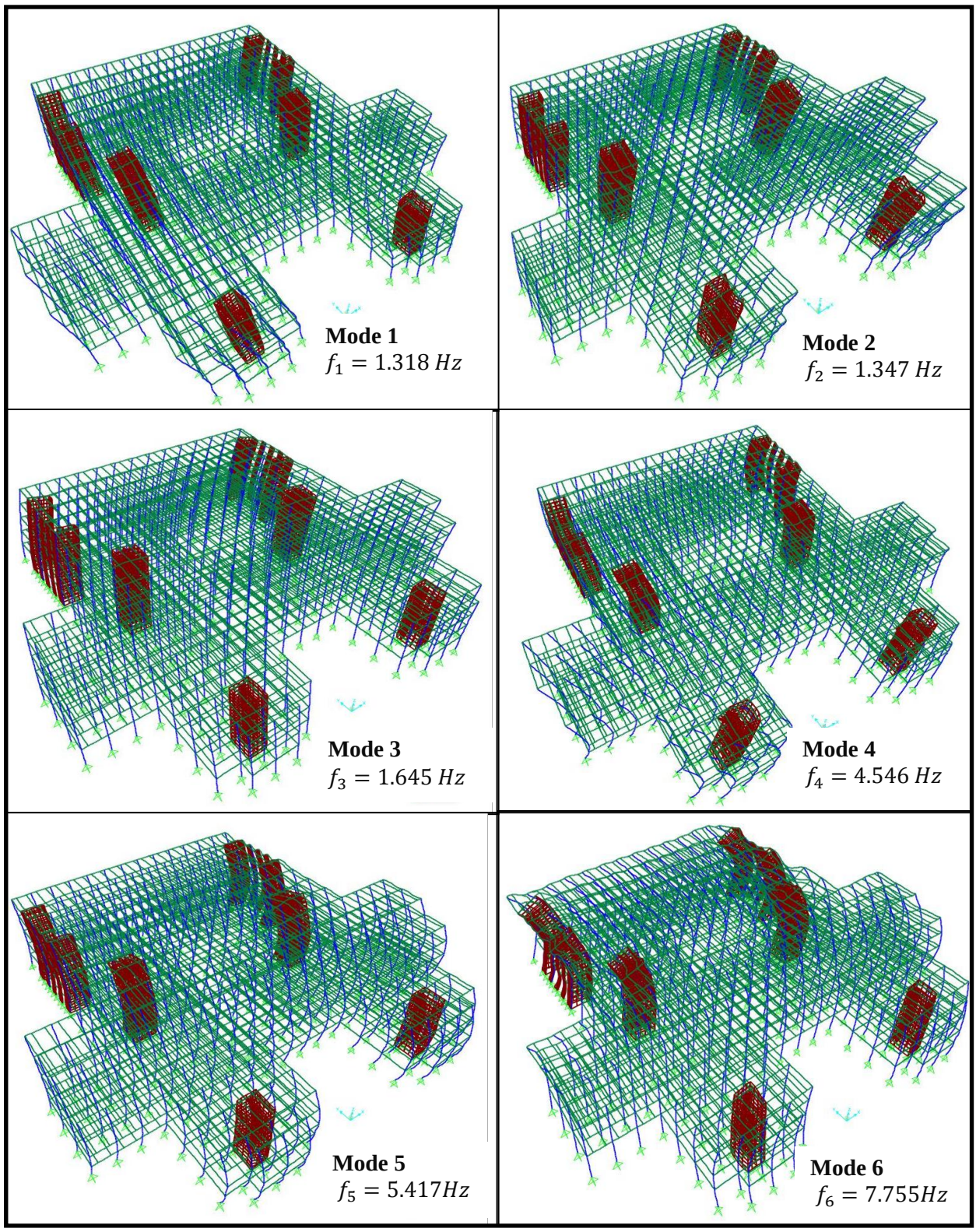

Figure 4.38 Mode shapes with MPF more than 5% in the E-W and N-S direction.

4.7 Generation of the FRS

To construct the FRS from the time history analysis for a series of damping levels of interest, the SeismoSpec program (Seismosoft Ltd., 2002) was employed in this study. The final outcome of this phase is the horizontal FRS at various damping levels, which is the envelope of the mean FRS in the two horizontal directions. The damping levels selected to generate the FRS should cover the range of the damping values predicted from the modal testing of the NSCs.

4.7.1 Selecting Points of interest

The time history responses at any location of structure can be exported from the computer model. Multiple locations, which were expected to capture the overall floor behavior within the roof floor, were selected for conducting the floor response spectrum analysis. Figure 4.39 below is a plan view of the roof level showing the layout of these points of interest (POI). POIs: RF2, RF4 and RF6 were deemed adequate for generating the FRS in X direction whereas POIs: RF3, RF4 and RF7 were chosen for computing the FRS in Y direction.

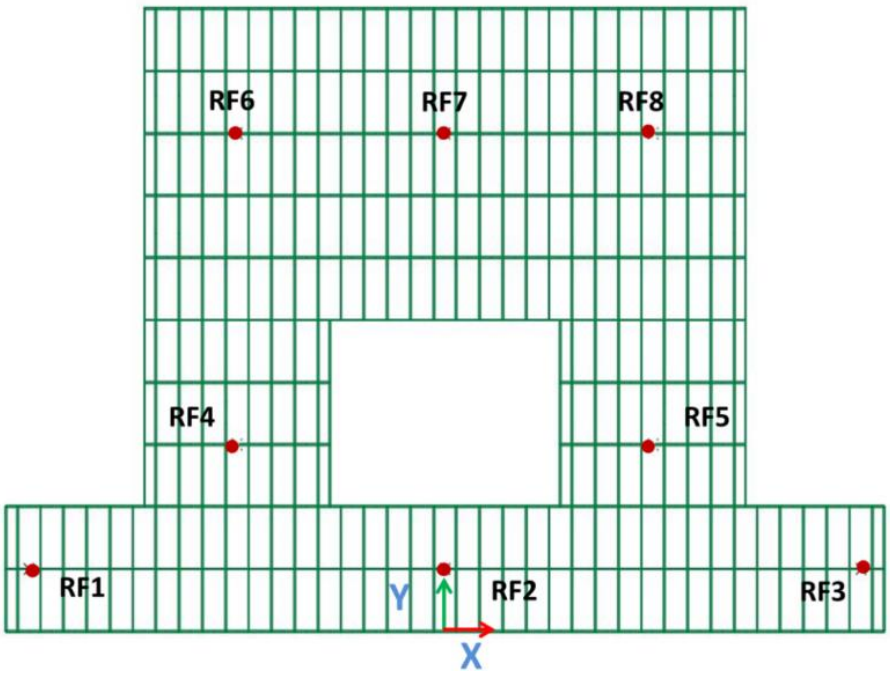

Figure 4.39 Locations of the points of interest relatively to the roof floor plan.

4.7.2 **Combining FRS at POI**

From the linear time history analysis, a total of 42 response time histories (7 sets of two-component response time histories at three locations) were generated. These resultant time histories were then inputted to the SeismoSpect program and converted into response spectra. In Figure 4.40, these individual response spectra at one damping level are shown as dashed lines and the combined spectra at each POI is shown as solid lines. Finally, the bold black line represents the combined FRS by averaging the three mean response spectra.

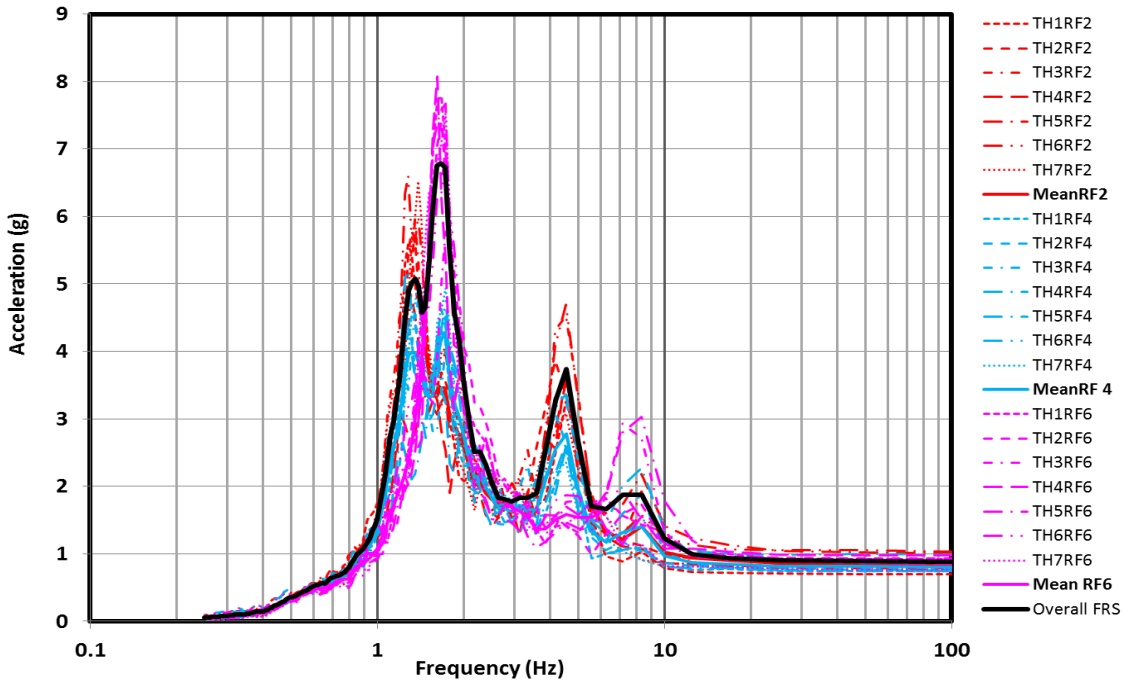

Figure 4.40 Sample response spectra corresponding to 7 sets of ground motions in one horizontal direction at three different locations on the floor of interest

4.7.3 **Obtaining FRS at Various Damping Levels**

According to the NSC modal identification analysis, the damping ratios detected by the experiment were found to be between 1 to 9%. Therefore, FRS for damping ratios of 1%, 2%, 5% and 10 % were calculated to cover the damping levels of all the components under consideration. The built-in tools for interpolating the FRS at different damping levels were available in the SeismoSpect program. Figure 4.41 is a sample plot to show the mean FRS for one horizontal direction for the four damping levels under consideration.

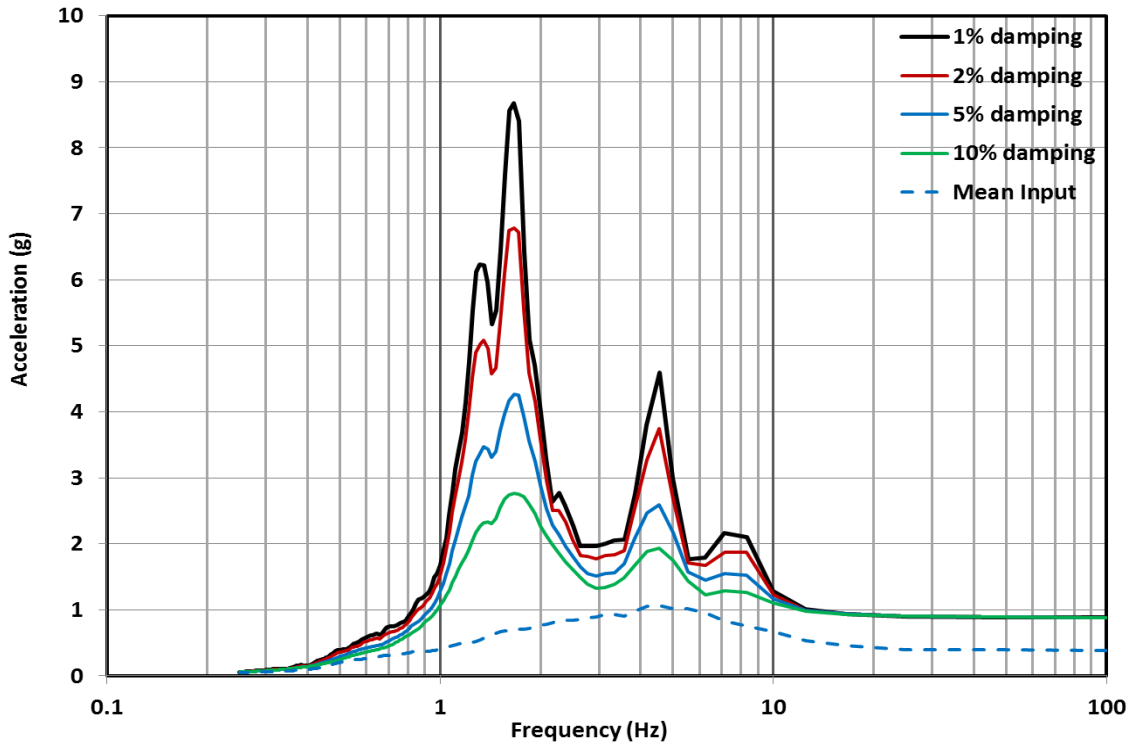

Figure 4.41 Mean FRS at four damping levels for X direction with the mean input spectra plotted as reference

4.7.4 Combining FRS in two directions

As the actual orientation of the ground motions is unknown, the final horizontal FRS should be established by enveloping the X and Y mean FRS. This accounts for the effect due to the direction variation in which the ground motions were applied. The final horizontal FRS is included in the results section in Chapter 5.

4.8 Lateral Force Demand

The final outcomes of this case study are the nonstructural lateral forces generated from the FRS plot for the corresponding fundamental frequencies and damping ratios. In order to validate the methodology followed in this case study, these lateral forces were compared with those calculated using the NSC lateral force formula from NBCC 2010. Results are presented in Chapter 5.

4.8.1 **FRS Approach**

The horizontal FRS represents the seismic force demand in the form of spectral acceleration in a unit of g (equivalent to the fraction of the component weight) with respect to the component fundamental frequency and damping. From the HIMT, the fundamental frequency and the damping ratio of COMP 7 were estimated to be 14.4 Hz and 3.5%, respectively. By simply tracing these values on the final horizontal FRS plot, the lateral force demand was found to be 1.3 W_p for all damping levels, as shown in Figure 4.42. A summary of the force demand found for all components are presented in Table 5.3 in Chapter 5.

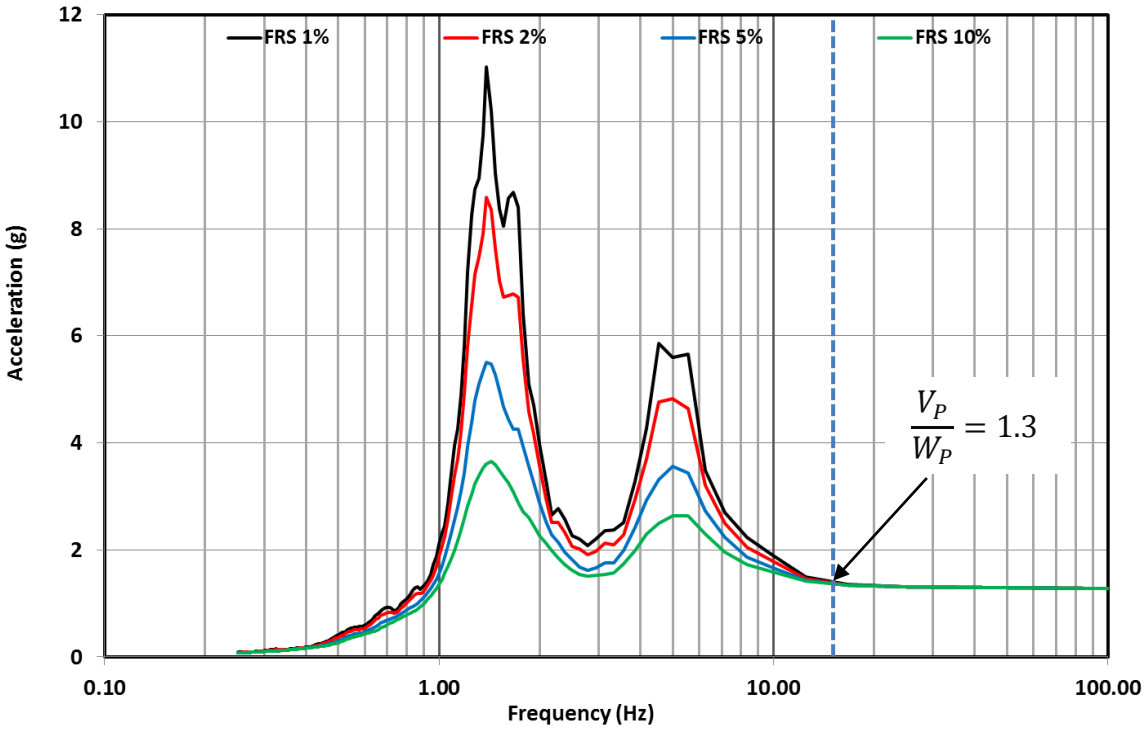

Figure 4.42 Horizontal FRS showing the force demand for COMP 7

4.8.2 **NBCC Code Equation Approach**

The lateral force formula for calculating the NSC seismic force demand specified in the current NBCC 2010 Code Clause 4.1.8.18 is presented in Equation 4-1. The formula can be reformatted into the form of fraction of the component's weight as shown in Equations 4-2 and 4-3. Definition of each variable was described in Section 2.4.3. The values of these design

parameters were determined in accordance with Sentence 4.1.8.18 based on the component category listed in Table 4.1.8.18 in the NBCC 2010.

$$V_P = 0.3F_aS_a(0.2)I_ES_PW_P \quad \textbf{Equation 4-1}$$

$$\frac{V_P}{W_P} = 0.3F_aS_a(0.2)I_ES_P \quad \textbf{Equation 4-2}$$

$$where \quad S_p = C_pA_rA_x/R_p \quad \textbf{Equation 4-3}$$

All components under consideration except for COMP7, were identified as Category 11-machinery, fixtures, equipment, ducts and tanks (including contents). This category was further divided into two subcategories: 1) rigid and rigidly connected components and 2) flexible or flexibly connected components (National Research Council Canada, 2010).

The dynamic amplification factor, Ar, and the response modification factor which accounts for the ductility of the component, Rp, differ significantly between these two types as listed below:

- "rigid" components: Ar = 1.00, Ar = 2.50;
- "flexible" components: Rp = 1.00, Rp = 2.50 .

The code defines the "rigid" component as components with a fundamental period less than or equal to 0.06 seconds. Due to the large differences in the Ar and Rp values between the two subcategories, knowing the fundamental frequencies of the NSCs is advantageous.

Instead of using one of the two values, one can be more precise when assigning the Ar and Rp factors. The amplification factor, Ar, is defined as a function of the frequency ratio between the component and the structure, as shown in Figure 4.43 (McKevitt, 2003). The structure fundamental frequency from the computer model was 1.3 Hz, and all the NSC fundamental frequencies were found to be at least 5.9 Hz (Tp/T < 0.2). Therefore, Ar should be taken as 1.0 for all NSCs.

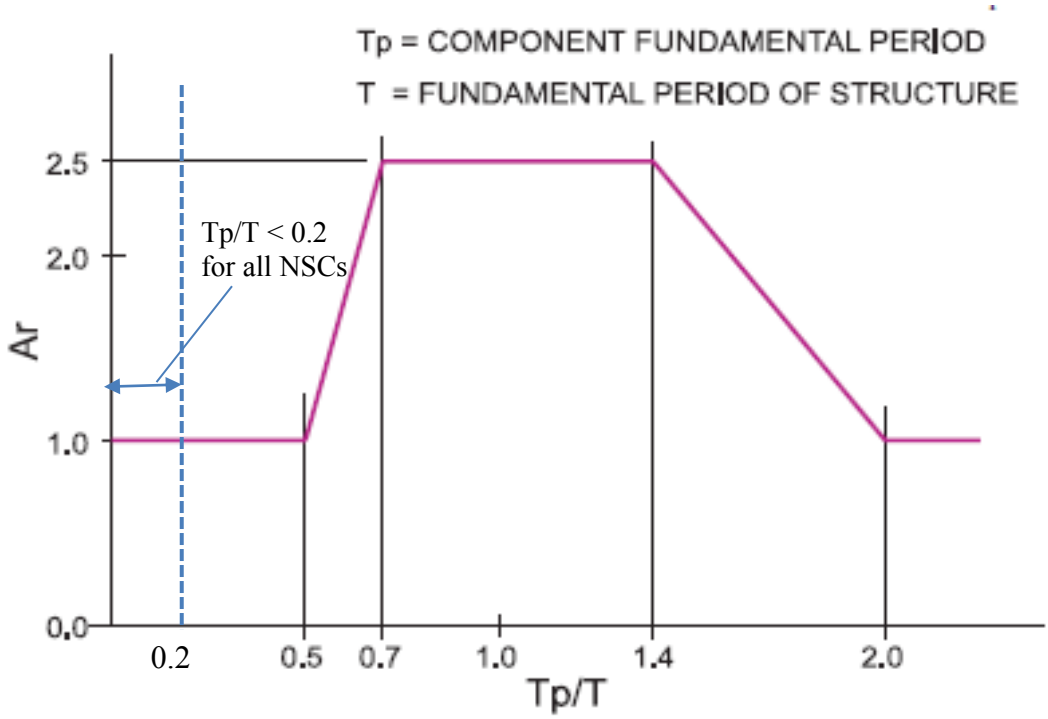

Figure 4.43 Component amplification factor Ar versus period ratio Tp/T. Reprinted from "Proposed Canadian code provisions for seismic design of elements of structures, nonstructural components, and equipment" by McKevitt, 2003.

The response modification factor, Rp accounts for the ductility of the component and its connection with the structural element. The recommended Rp value for "rigid and rigid connected" components from Table 4.1.8.18 in NBCC 2010 was 1.25. However, since the exact depth of embedment of the anchors and the installation methods were not clear for the NSCs studied, the ductility of the component and of the connection is unknown. For hospital buildings, the critical NSCs are required to perform elastically so that little ductile behavior is expected. With these considerations, it was more appropriate to apply an Rp of 1.0 to account for the lack of ductility of such components and/or their connections to the structure in this case.

Apart from Category 11 components, COMP7, which is the vertical water pipe, was classified as "pipes, ducts, cable trays" (Category 15). The corresponding design parameter values and the resultant lateral forces for these two types of components are listed in Table 4.8 below. A comparison of these final force demand values with those obtained from the FRS method will be summarized in Chapter 5.

.

Table 4.8 Design parameter values for components classified as category 11 & 15

Parameters in Sentence 4.1.8.10 (NBCC 2010)	Category 11	Category 15
F_a	1.1	1.1
S_a (0.2)	0.939	0.939
I_E	1.50	1.50
$A_x = 1+2\ h_x/h_n$	2.70	2.70
R_p	1.00	3.00
A_r	1.00	1.00
C_p	1.00	1.00
V_p/W_p	**1.3**	**0.4**

Chapter 5 Analysis Results

This chapter summarizes the analytical and experimental results of the case study. Through modal testing, the dynamic properties of the NSCs (i.e. natural frequencies and damping ratios) were extracted and the results are listed in Section 5.1. From the linear time history analysis, the acceleration responses at the selected locations on the roof level of the building were obtained and saved as .txt files in the project database. A series of response spectra for these time histories were calculated at various damping levels: 1%, 2%, 5% and 10%. Section 5.2 contains the mean FRS plots in both X and Y directions and the envelope of the two to represent the overall seismic force demand. Section 5.3 summarizes the final seismic force for each NSC generated from the proposed methodology. These values were compared to the ones calculated by NBCC 2010 equation. The comparison results are also included in Section 5.3.

5.1 Natural Frequencies and Damping Ratios of NSCs

The modal frequencies and the corresponding damping ratios obtained from the tests are listed in Table 5.1. The fundamental frequencies found in this analyses range from 5.9 Hz to 77.5 Hz. The damping ratios are within a range of 1.3 % to 8.9 %.

Table 5.1 Fundamental frequencies and damping ratios for the NSCs Tested

Component	Description	Mode	Mode Shape	Natural	Damping
COMP1	Pump 2	1	Lateral	18.8	3.2
COMP1	Pump 2	2	Longitudinal	22.8	4.5
COMP2	Air Handler Unit	1	Lateral	5.9	7.4
COMP3	Relay Rack	1	Fore-and-aft	13.6	1.3
COMP4	Dry Air Vacuum	1	Lateral	16.7	1.7
		2	Longitudinal	26.9	4.9
COMP5	Medical Air Power Unit	1	Lateral	77.5	2.6
		2	Longitudinal	54.4	3.7
COMP6	Pump Assembly	1	Lateral	N/A	N/A
		2	Longitudinal	N/A	N/A
COMP7	Vertical Pipe	1	Horizontal	14.4	3.5
COMP8	Medical Air Cylinder Rack	1	Lateral	42.2	3.4
		2	Longitudinal	15.6	6.4
COMP9	Service Air Vacuum Unit	1	Lateral	17.8	2.6
		2	Longitudinal	20.3	8.9

The modal frequencies for COMP3, COMP7 and COMP9 were validated with FE computer models, as described in Chapter 4. The experimental and analytical fundamental frequencies and mode shapes are presented below for these components. The difference between the experimental and theoretical frequencies is less than 8% and the mode shapes were also found to be consistent between the two methods.

Table 5.2 Experimental and modeled fundamental frequencies for

Component	Mode shape	Fundamental Freq. (Hz)		Difference (%)
		Experimental	Modeled	
COMP3	Out-of-plane bending	13.6	14.0	3.0
COMP4	lateral	16.7	17.0	1.8
	longitudinal	26.9	29.0	7.8
COMP7	lateral	14.4	13.9	3.5

5.2 Floor Response Spectra

For each individual acceleration response time history exported from the structural model, a response spectrum was computed at four damping levels (1%, 2%, 5% and 10%).
Figures 5.1 – 5.8 present the response spectra for the four damping ratios. The computed mean FRS are presented in Figures 5.9 and 5.10 for X and Y direction, respectively. The final horizontal FRS was obtained by enveloping the two mean FRS, as shown in Figure 5.11.

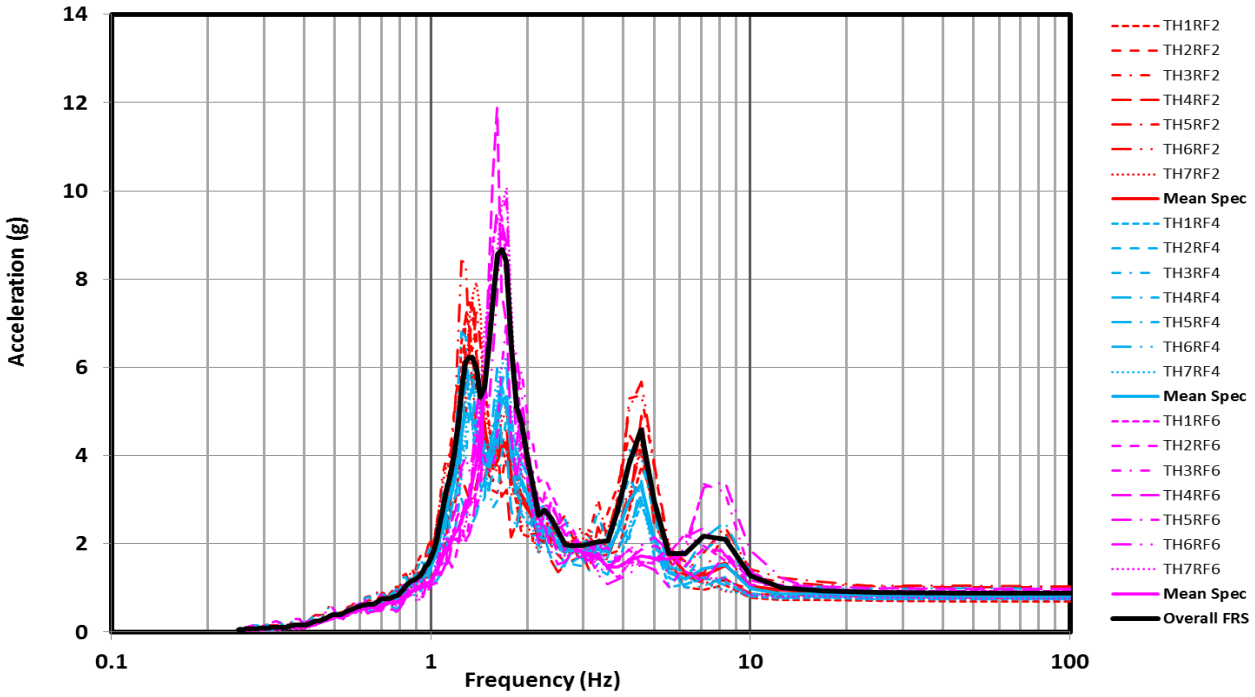

Figure 5.1 Floor response spectrum at roof floor for 1% damping in X direction

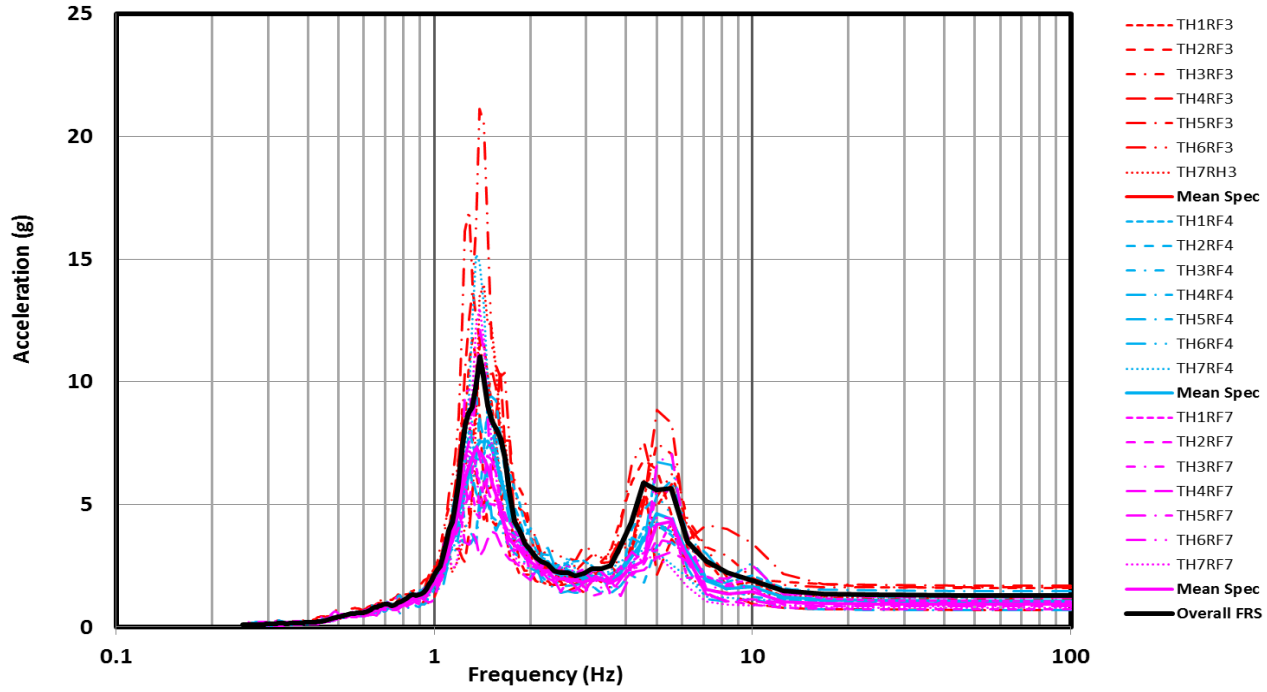

Figure 5.2 Floor response spectrum at roof floor for 1% damping in Y direction

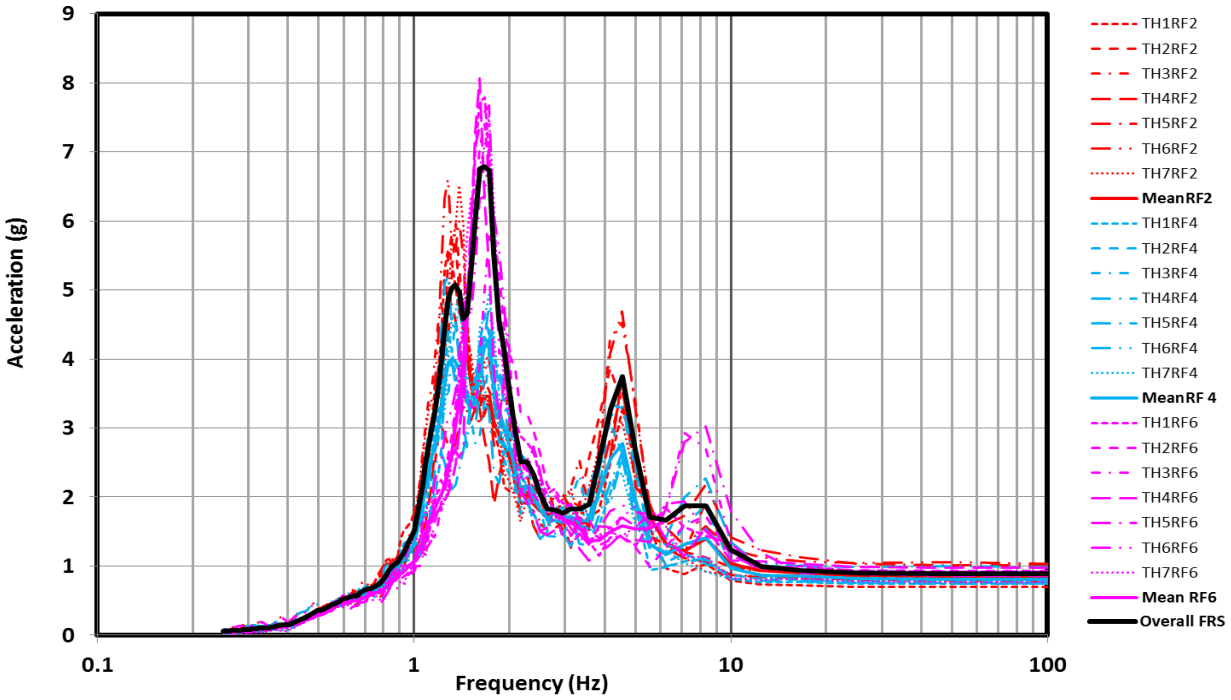

Figure 5.3 Floor response spectrum at roof floor for 2% damping in X direction

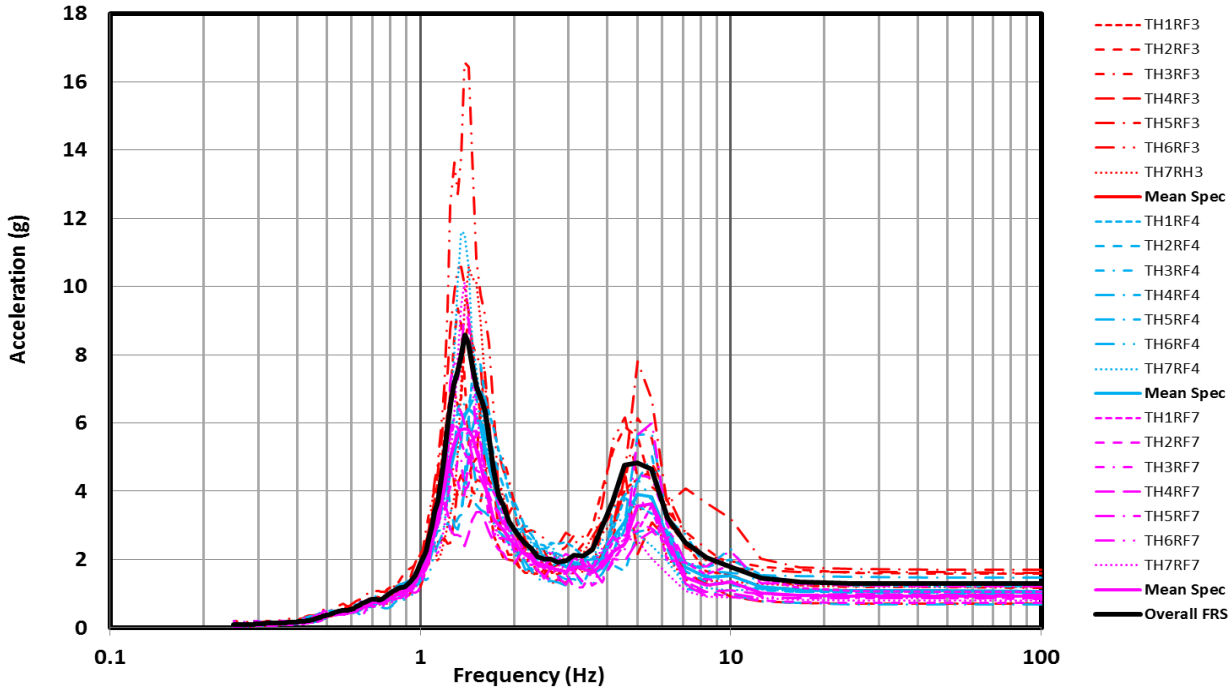

Figure 5.4 Floor response spectrum at roof floor for 2% damping in Y direction

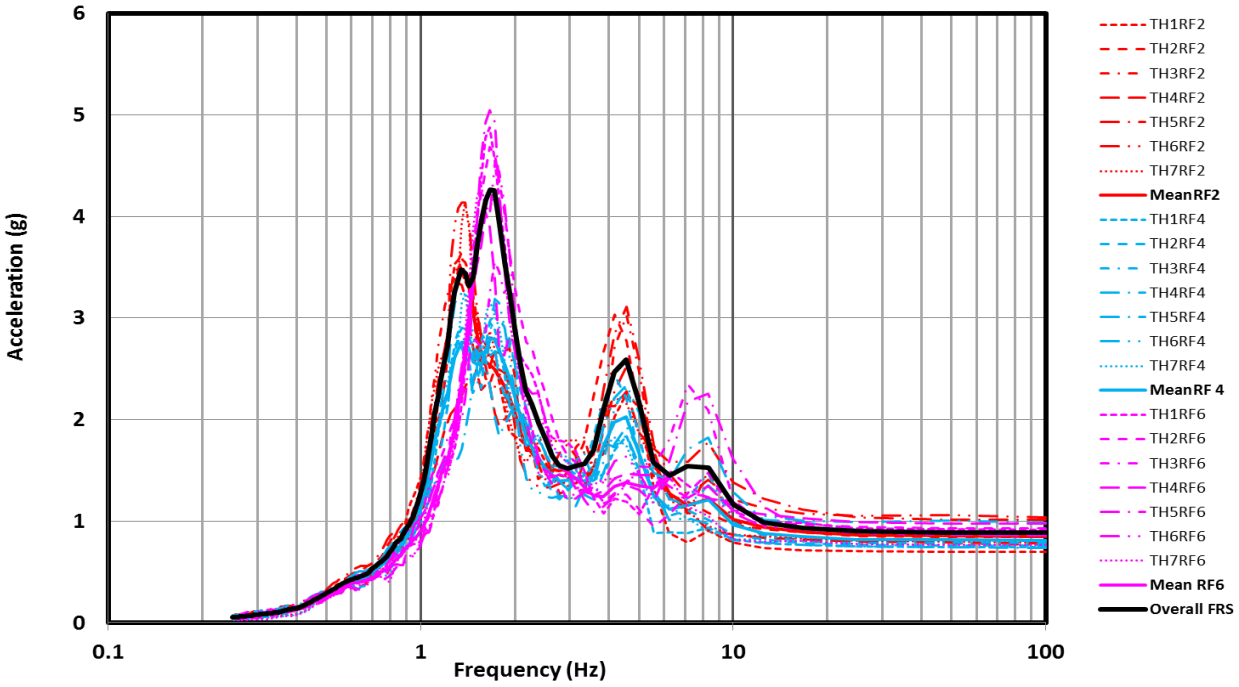

Figure 5.5 Floor response spectrum at roof floor for 5% damping in X direction

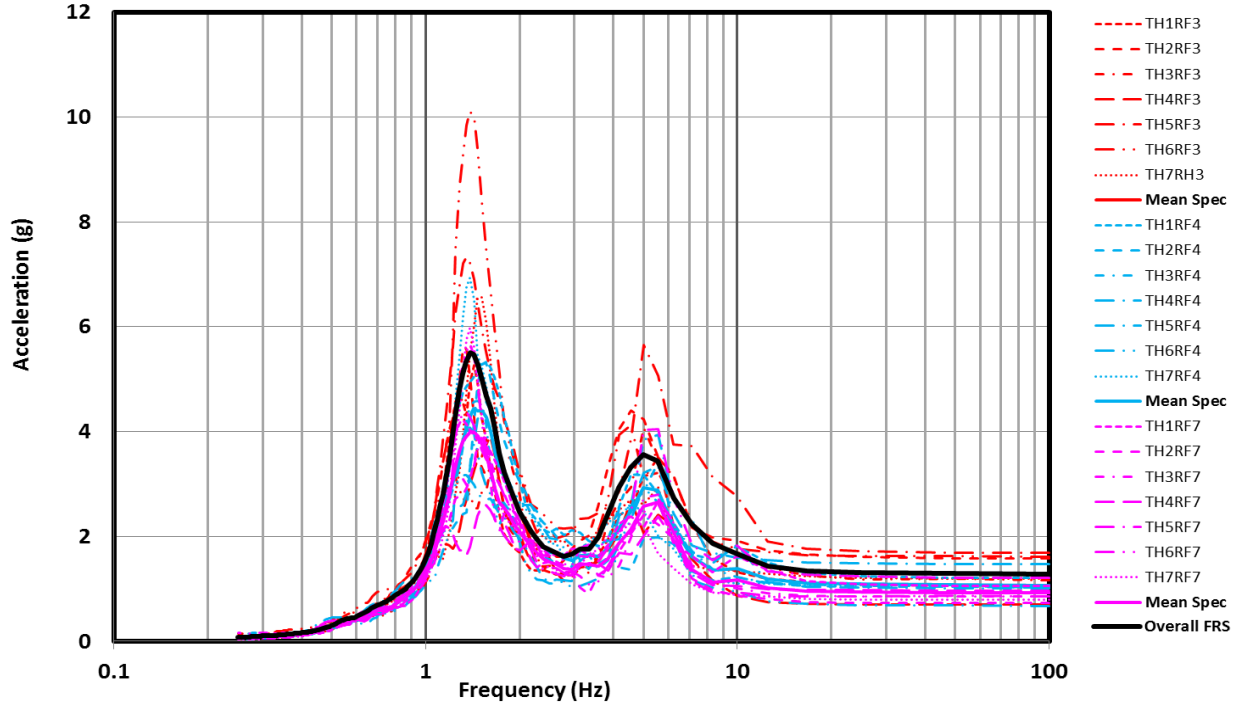

Figure 5.6 Floor response spectrum at roof floor for 5% damping in Y direction

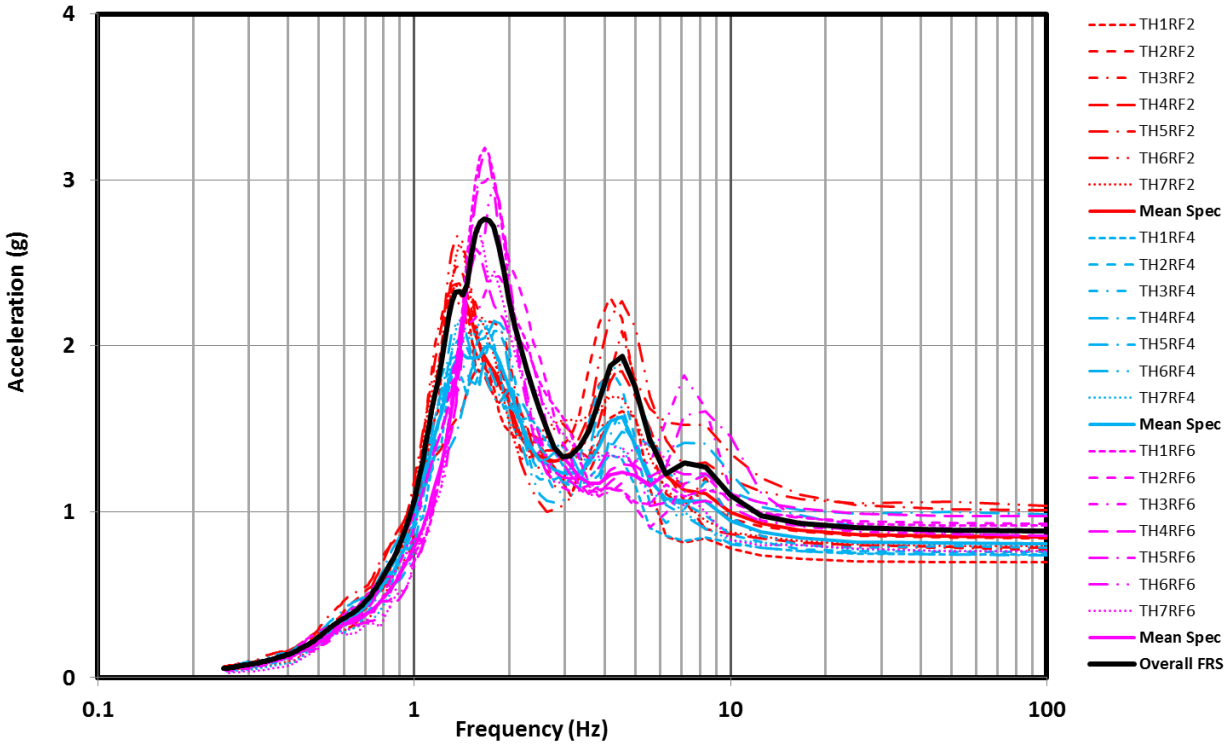

Figure 5.7 Floor response spectrum at roof floor for 10% damping in X direction

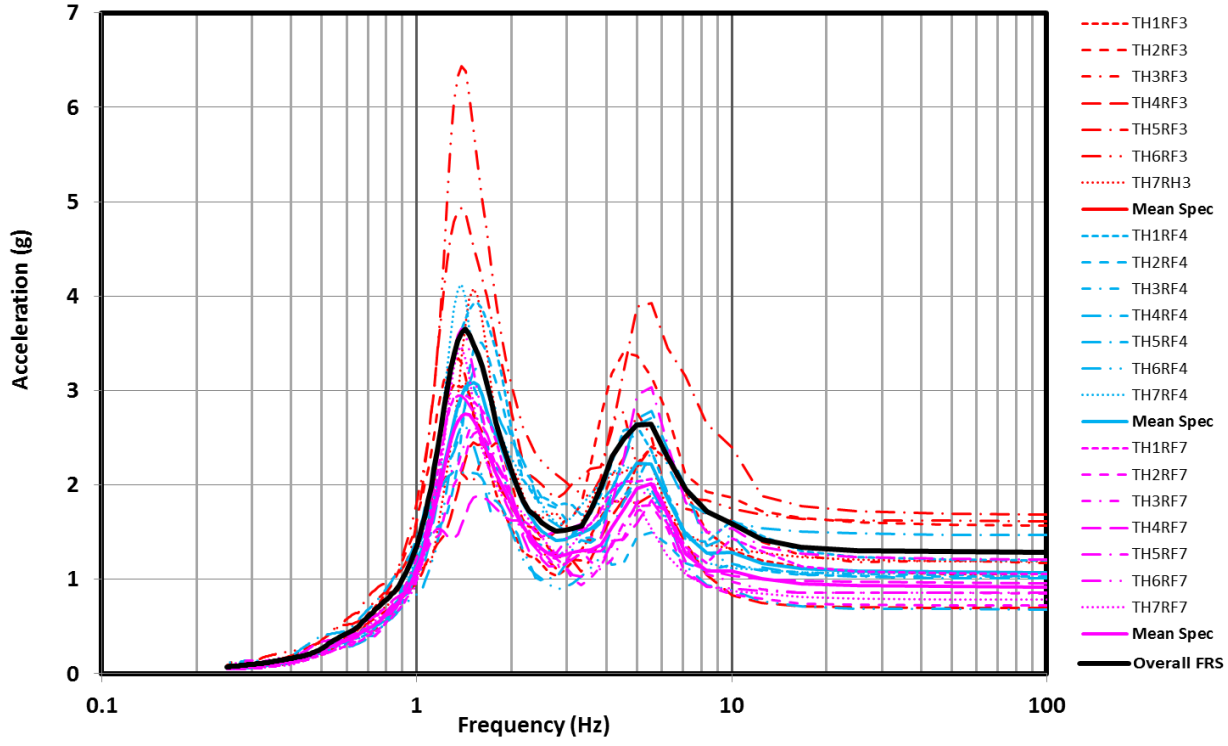

Figure 5.8 Floor response spectrum at roof floor for 10% damping in Y direction

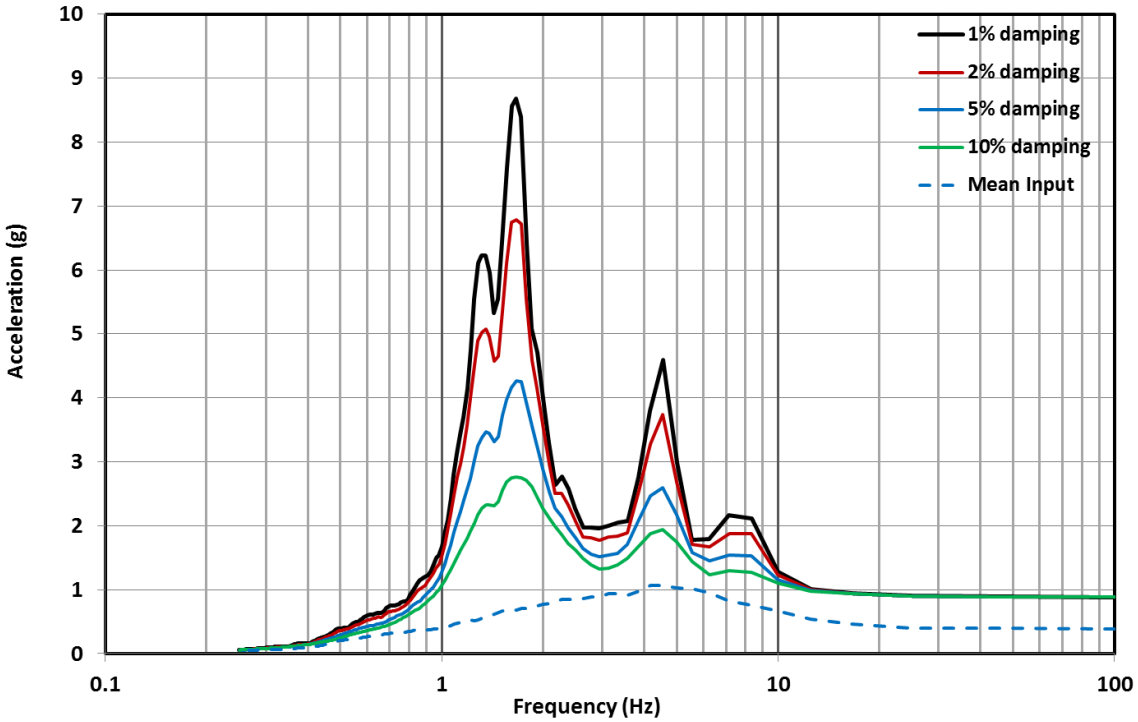

Figure 5.9 **Floor response spectrum of roof floor in X direction with mean input spectrum as a reference**

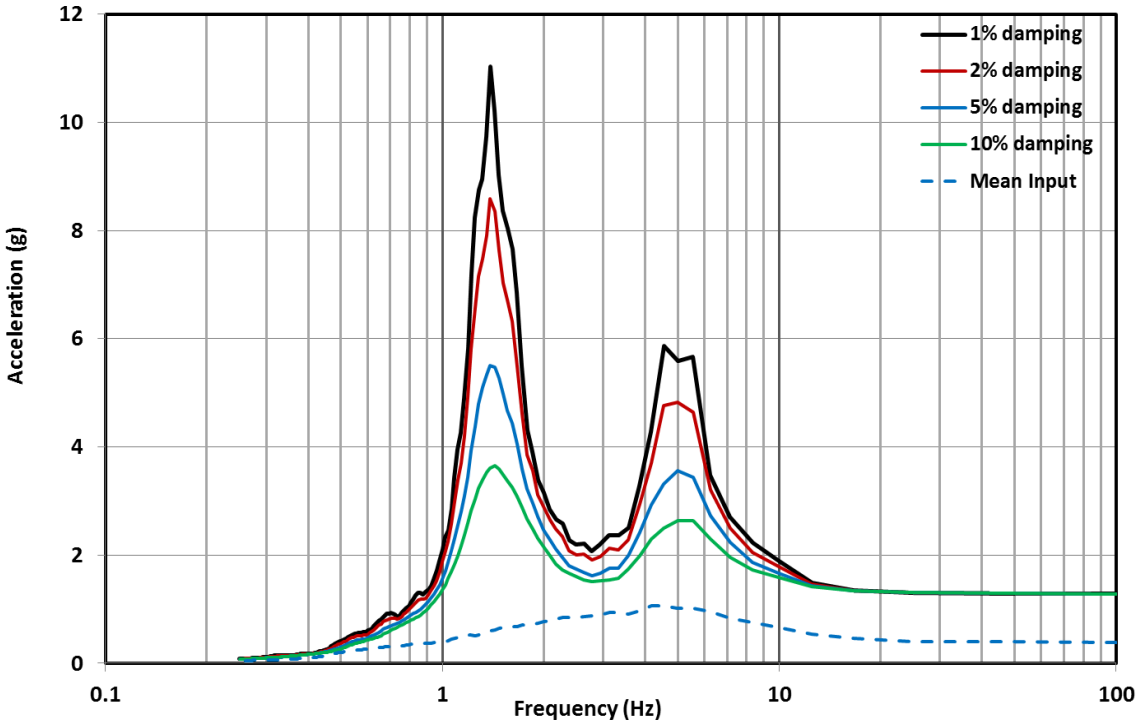

Figure 5.10 **Floor response spectrum of roof floor in Y direction with mean input spectrum as a reference**

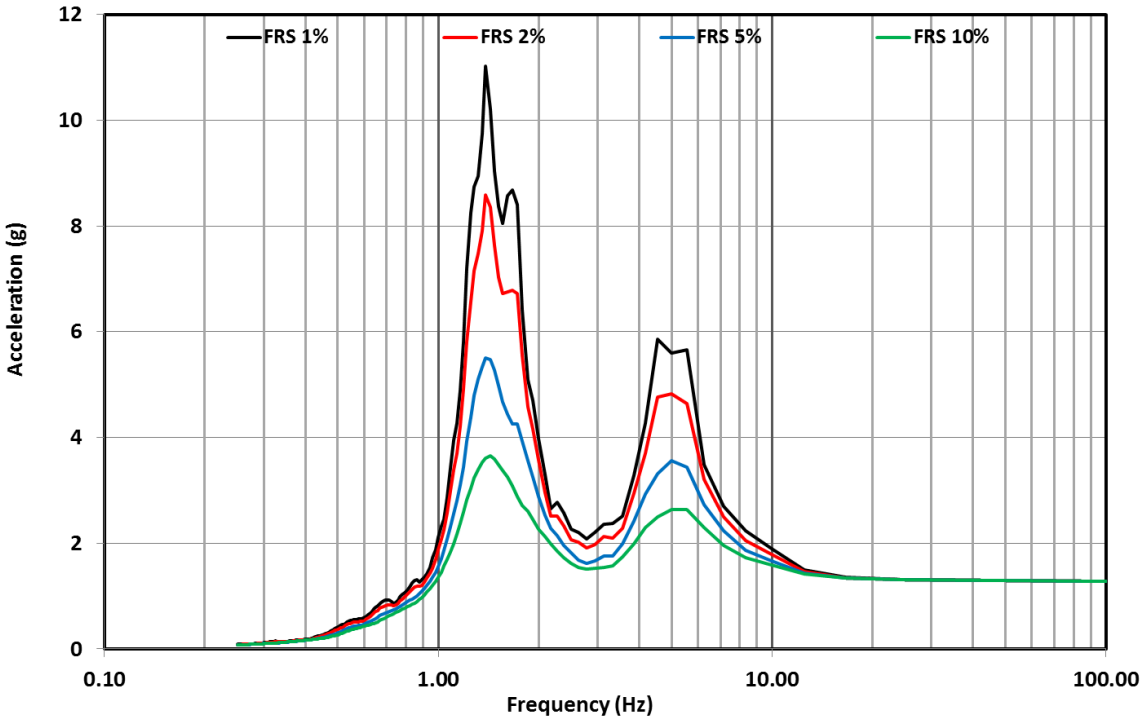

Figure 5.11 Horizontal response spectrum of roof floor (envelope of X and Y)

It was observed from these FRS that the acceleration was most amplified near the dominant frequencies obtained from the modal analysis, as summarized in Table 5.3 below. In high frequency range (greater than 16.0 Hz), the FRS for different damping ratio tends to converge and remain constant around 1.3 g. This is an indication that the acceleration demand is not sensitive to the natural frequency of the NSCs that have a frequency more than 16.0 Hz for this case study. These observations will be discussed in more detail in Chapter 6.

Table 5.3 Modal frequencies of the structure from the FE model

Primary Modal	Mode Number	Natural Frequencies (Hz)
N-S (X)	1	1.32
	2	1.65
	3	4.55
E-W (Y)	1	1.35
	2	5.42

5.3 Seismic Force Demand from FRS and from NBCC 2010 formula

The NSC forces were obtained from the final horizontal FRS, which represents the overall floor response subject to ground motions at a hazard level of 2% in 50 years. To validate the results obtained from the FRS analysis, the lateral forces were compared to these calculated from the NBCC 2010 code formula. The procedure of the code formula approach was described in Chapter 4. The final forces for the two scenarios are included in Table 5.4.

Table 5.4 Summary of the NSC seismic forces from FRS and NBCC 2010 approach

Component Number	Mode	Natural Frequency (Hz)	Damping Ratio (%)	Vp/Wp (FRS)	Vp/Wp (NBCC 2010)	Difference %
COMP1	lateral	18.8	3.2	1.3	1.3	0%
	longitudinal	22.8	4.5	1.3	1.3	0%
COMP2	lateral	5.9	7.4	2.8	1.3	56%
COMP3	Out-of-	13.6	1.3	1.4	1.3	7%
COMP4	lateral	16.7	1.7	1.3	1.3	0%
	longitudinal	26.9	4.9	1.3	1.3	0%
COMP5	lateral	77.5	2.6	1.3	1.3	0%
	longitudinal	54.4	3.7	1.3	1.3	0%
COMP6	lateral	N/A	N/A	N/A	1.3	N/A
	longitudinal	N/A	N/A	N/A	1.3	N/A
COMP7	lateral	14.4	3.5	1.3	0.4	70%
COMP8	lateral	42.2	3.4	1.3	1.3	0%
	longitudinal	15.6	6.4	1.4	1.3	7%
COMP9	lateral	17.8	2.6	1.4	1.3	7%
	longitudinal	20.3	8.9	1.3	1.3	0%

From the table above, the lateral force Vp calculated based on the modal properties obtained from the HIMT and FRS analysis results range from a minimum of 1.3 Wp to a maximum of 2.8 Wp. COMP6 was an exemption since the modal identification using the proposed method was not successful, as discussed in Section 4.4.4.

The results from the FRS analysis were consistent with those from the NBCC 2010 equation for most of the NSCs studied except for COMP2 and COMP7. The lateral forces for COMP2 and COMP7 estimated using the code equation were found to be over 50% lower than that from the FRS method. The rationales for the observed differences between the two analysis methodologies are discussed in the next chapter.

Chapter 6 Discussion of Key Findings

This chapter first rationalizes the major observations from Chapter 5 and evaluates the practicality of the modal testing methodology adopted. It also discusses the potential value of the proposed field modal testing methodology in practicing engineering field related to NSC seismic analysis and design.

6.1 Validation of the Lateral Force Demand Results

To validate the case study results from the proposed methodology, the lateral seismic forces were also calculated based on the NBCC 2010 code provisions. The results were listed in Table 5.3. The lateral forces (Vp/Wp) for most NSCs between the two methods were consistent (within a difference of 7%). However, large differences were observed for COMP2 and COMP7, as shown in Table 6.1. The rationales for the differences are included below.

Table 6.1 NSC seismic forces obtained from the FRS method and the NBCC 2010 equation

Component	Mode	f_p (Hz)	Vp/Wp	Vp/Wp
COMP 2	Lateral	5.9	2.8	1.3
COMP 7	Lateral	14.4	1.3	0.4

6.1.1 Higher mode effects

First of all, the code equation approach was based on the assumption that only one dominant frequency governs the overall dynamic behavior of the structure and higher mode impact was neglected. For "flexible" components in this study, this over-simplification of the dynamic behavior of the structure led to a significant underestimation of the force demand. The higher mode effects were considerably large in this case study. Figure 6.1 below shows the relative location of COMP2 on the horizontal FRS and that it coincides with the second peak, which corresponds to one of the higher natural modes of the structure. As a result, lateral force demand for COMP2 was $1.3W_p$ by the NBCC equation and was $2.8\ W_p$ from the FRS method.

Thus, the FRS method is more effective over the code equation under this consideration, as it captured the higher mode effects. This advantage of the FRS method is more apparent in buildings with some degrees of irregularities and with torsional sensitivities. In the recent

building codes, this issue is limited by restricting the design to avoid irregularity and torsional sensitivities in post-disaster buildings. However, in the case of buildings designed prior to these code provisions, this is still problematic.

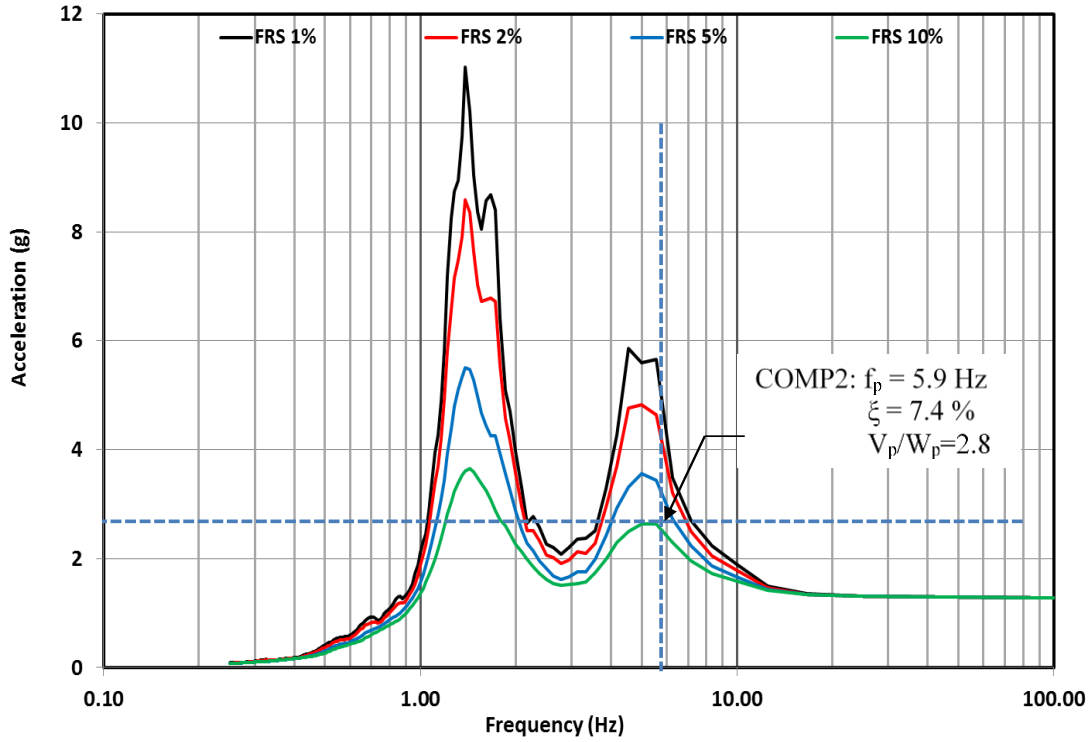

Figure 6.1 FRS showing the natural frequency, damping ratio and lateral force of COMP2

6.1.2 Damping effects

The large difference between the lateral forces obtained from the two methods for COMP7 was due to the high response modification factor, Rp, assigned to the component when using the code formula. To capture the energy dissipation of a NSC subjected to earthquakes, the FRS method considers the structural and nonstructural damping while the code formula assigns a response modification factor R_p to account for the component ductility. The latter is related to the NSC's inelastic deformation capacity. An Rp value of 3.0 was assigned to COMP7 – vertical pipe according to Table 4.1.8.18 in NBCC 2010. This high Rp value indicates that the pipe can undergo large inelastic cyclic deformations due to seismic activities before its capacity is reached. In this study, only the elastic behavior was considered so that Rp should have been taken as 1.0. From this situation, it is clear that the NBCC code equation does not explicitly

address the dynamic characteristics of a specific NSC or the current condition of the NSC. Generalizing the design parameters for NSCs by grouping them into vague categories seems to oversimplify the problem and the results can be misleading.

It is concluded from the case study that the lateral seismic forces obtained using the proposed methodology were reasonable as they generally agree with those calculated from the NSC design force formula in NBCC2010. For the two components of which the results differ significantly, it was due to the exclusion of higher mode effects and damping effects in the code equation. Therefore, the FRS method was more robust than the code equation method for this study.

6.2 Evaluation of the Modal Identification Testing

The focus of this thesis is to develop a methodology for assessing the seismic force demand of NSCs using on-site modal identification testing. The significance of such a testing approach was demonstrated through the case study. To determine its value in practicing earthquake engineering, aspects such as accuracy of testing results, costs, its nondestructive feature and suitability to NSCs are evaluated and discussed here.

6.2.1 Significance of modal identification testing

To correlate the FRS values with the code provision, the spectral forces from the two methods are presented on the same plot, as shown in Figure 6.2. The cutoff frequency of 16.7 Hz for distinguishing flexible and rigid components specified in Sentence 4.1.8.18 (4) in NBCC 2010 was plotted on the FRS to illustrate its relation with the force-frequency relationship suggested by the FRS method.

The FRS, regardless of the NSC damping, exhibits a steady force level for frequencies beyond roughly 17.0 Hz. This is consistent with the code-specified minimum frequency of 16.7 Hz (period of 0.06 seconds) for a rigid component. Since the difference in the values of Ar and Rp factors is significant between “flexible” and “rigid” component, it is critical to distinguish these two categories properly when applying the code equation for calculating the nonstructural seismic force,. The on-site testing approach can provide valuable insights on the rigidity of the component and its connections rapidly so that more accurate Ar and Rp values can be applied.

The FRS plot also shows that the NSCs seismic response was sensitive to its damping, as shown in FRS presented in Figure 6.2. The effect is more substantial as the component's fundamental frequency approaches the fundamental frequencies of the building to which the component is attached. In this case study, the response of a component with a 1% damping ratio was 3 times higher than that with a 10 % damping ratio around the resonance frequencies. When the fundamental frequency of the NSC approaches zero (very flexible component) or when it is larger than 17 Hz (rigid component), the damping effects diminishes.

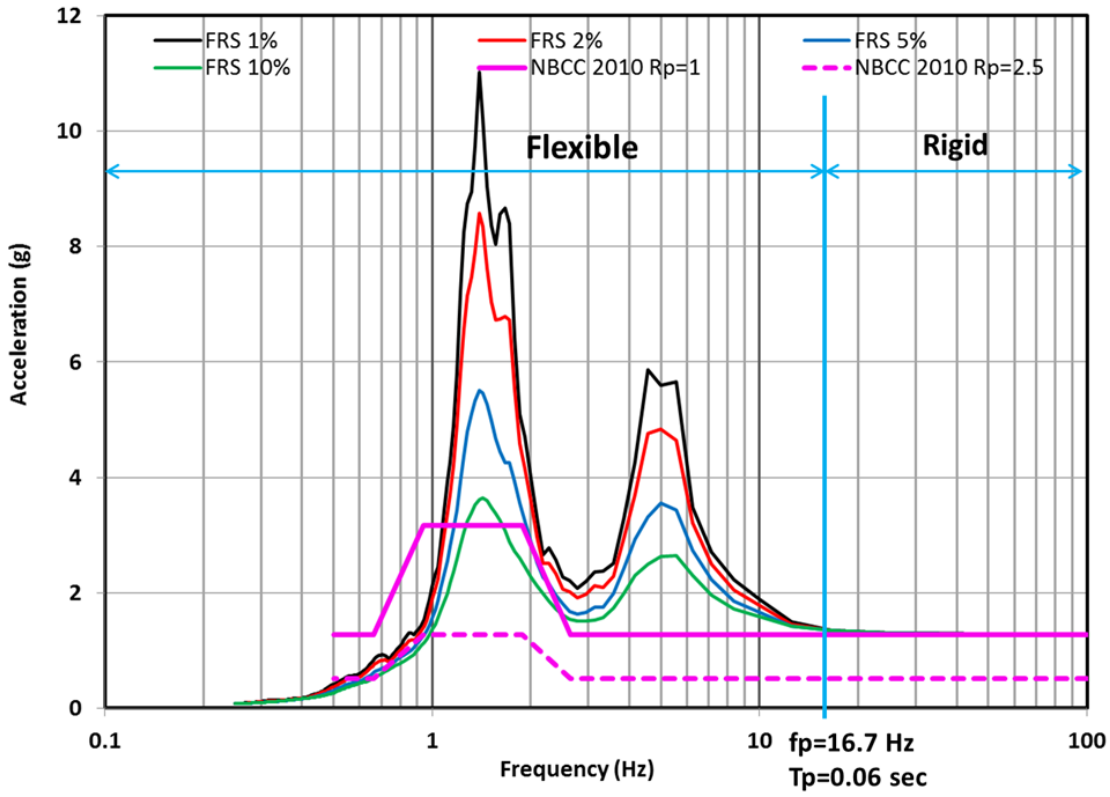

Figure 6.2 Comparison of horizontal floor response spectrum and NBCC 2010 equation

It was demonstrated throughout this study that there is certainly a need for on-site modal identification testing in estimating the lateral force demand of the NSCs in an existing building. The HIMT technique was proposed and applied in this case study to estimate the fundamental frequencies and damping ratios of the NSCs. The implementation of this experimental approach through the case study has proved that it is overall practical and cost-effective.

6.2.2 **Accuracy of testing results**

The HIMT results presented in Section 5.1 have confirmed that such an on-site testing can provide reasonable estimation of the modal properties of the NSCs. The correctness of the results was validated with computer models for components with simple geometry. For other components, validation can be done with more sophisticated data processing tools and technique in future studies.

6.2.3 **Cost of the testing**

One of the major advantages of the proposed methodology is that it is economic in terms of the setup cost, time and manpower required. For this particular case study, two graduate students with engineering background were required to be present at site during each test due to safety regulations of the hospital. A total of 10 visits with 4~5 hours per visit were made by the two students. The testing devices were available at the U.B.C. Earthquake Engineering Research Facility. The data processing was conducted in programs with free access.

6.2.4 **Nondestructive testing**

Another key feature of the HIMT is that it is usually carried out in a nondestructive manner, which means that the tested component is not required to shut down or removed from its original location so that there is no interruption of operation. Currently, another commonly adopted modal identification technique for NSCs is the shake table testing method. This is widely recognized as an effective method that serves NSC design purposes. However, this type of testing is not applicable for diagnosing the components' in-service dynamic properties. Also, the setup for a shake table test can be expensive and time consuming. For the purpose of assessing an existing working component, the on-site impact testing is more appropriate.

6.2.5 **Suitability to component types and conditions**

Although this field testing method was advantageous in many ways, it was not always applicable depending on the component type and condition. As discussed in Chapter 4, the modal identification was not successful for COMP6 due to high noise level. The impact excitation was

overpowered by the vibration of the operation machines. The free vibration after the impact diminished so quickly that the recorded data were not useful for extracting the modal properties.

Another case where this method was not ideal was COMP5. The frequencies found for COMP5 (medical air vacuum unit) using the HIMT method were 77.5 Hz in longitudinal direction and 54.4 Hz in lateral direction. These values were much higher than other components. The reason could be that this component has a complex structure and the impact may have not excited its fundamental mode. Instead, the results were likely to reflect the local vibration at the base support where the impact was applied. For this scenario, the natural frequencies could be overestimated, which can lead to underestimation of the force demand.

Based on the above findings, the HIMT applied in this study is overall an easy-to-implement technique for modal identification of an existing NSC that is attached to an existing structure. The testing procedure followed in this case study, was found effective and well-planned. Thus it can be adopted for other similar projects in recognition of its case-specific nature. The results can be utilized in either FRS method or equations available in code provisions for generating the lateral force demand of the NSCs. For this study, the FRS method provided captured the higher modes effects and damping effects especially for components near the resonance conditions.

Chapter 7 Conclusion and Recommendation

7.1 Conclusion

With the increasing awareness of the impact of NSC seismic damages, a number of ongoing NSC seismic analysis techniques have been developed in recent years. The proposed methodology in this study employed an on-site modal identification testing technique and the FRS method (see Chapter 3) for assessing the lateral seismic force demand of existing NSCs. The main steps include:

- conducting Hammer Impact Modal Tests to estimate the natural frequencies and damping ratios of the NSCs;
- developing a 3D FE model of the primary structure and validating its natural frequencies using the Ambient Vibration Testing technique;
- performing time history analyses with a series of ground motions selected to reflect the seismic hazard characteristics specified in NBCC 2010;
- constructing the floor response spectra for various damping levels;
- estimating the seismic demand of the NSCs from the floor response spectra based on their natural frequencies and damping ratios obtained from the modal testing step.

The effectiveness of the proposed method was demonstrated by applying it to the U.B.C Hospital Koerner Pavilion case study. The NSC force demand from the FRS method was compared with those obtained from NBCC 2010. The key findings of this research are:

1) The fundamental frequencies and damping ratios of NSCs greatly influence to the overall seismic performance of the NSCs. When excitation of the NSC without destruction of its operation is possible, the Hammer Impact Modal Testing technique proposed in this study can provide reasonable results with low cost. For cases when the hammer force applied is not sufficient due to the setting and/or size of the components, or the components contains toxic or hazardous materials, this testing method is not practical.

2) The testing results can be used together with either the FRS method or code equations to evaluate the seismic demand values. Herein, the FRS method using time history analysis was employed. Results showed that the FRS in this study provided more realistic results

than the code formula because it captured higher mode effects and damping effects. The FRS method was also computationally inexpensive since nonlinearity of the structural and nonstructural components was not a concern for this case.

7.2 Limitation of the research

For a health facility, past experience has shown that critical nonstructural failures can occur anywhere in the building. It can be the suspended ceiling falling down in the hallway, toppling of storage cabinets and failure of sprinkler system near a nurse station, or dropping of an overhanging monitor in a patient room. This research project only focused on machines and equipment in the mechanical room due to limited access to other areas, such as operation rooms and patient rooms.

The other major limitation of this research project is that it is difficult to correlate the analytical and experimental results. Although the modal properties of some NSCs found through testing were confirmed by analytical models in this study, it is impossible for most cases to develop computer models for the NSCs where their in-service properties, such as boundary conditions and material strength, are unknown. When this is the case, other testing techniques should be employed and the results can be compared to those obtained from the HIMT method.

7.3 Potential Application in Engineering Practice

The proposed experimental approach for NSC modal identification can be utilized as a rapid tool for practicing engineers to diagnose the in-service condition of the components in an existing building.

This on-site testing approach is also useful to validate the modal properties of the newly designed NSCs to exam the sufficiency of the anchorage design. As the dynamic properties of the NSCs are sensitive to installation methods, it is necessary to examine the actual dynamic properties after it is installed.

Furthermore, when the building code equations are used to determine the nonstructural seismic forces, it is important to distinguish the “flexible” and “rigid” NSCs in order to obtain more realistic design factors, as discussed in Chapter 5. The proposed methodology provides rapid estimation on the flexibility of the candidate components with very little cost. The results can

help design engineers to assign more realistic design factors and to avoid overdesign of the NSCs, which can be impractical and costly. Thus, conducting a simple modal testing on site can reduce significantly the project costs associated with NSC design.

There is also a potential to establish a database containing the modal properties of typical NSCs in a hospital through the proposed on-site testing method with consideration of various nonstructural and structural configurations. The benefit of compiling such a database is to expedite the NSC design process. The database can also be utilized to improve the current code equation.

In view of the experimental-based nature of this methodology, engineers should take following considerations when applying it to any of the above uses:

- sufficient testing data must be obtained to achieve a high confidence level of the results;
- testing results should be validated by other measure or by previous experience for similar components.

7.4 Recommendation for Future Research

Realizing the limitations within this research, future studies should be conducted to cover a broader range of NSCs in a hospital building and possibly in other types of building as well. This is important for observing possible obstacles and issues associated with the proposed methodology in a more general manner. The information can be used to enhance the testing procedure. Additionally, similar studies on various structure systems can help understand the correlation between structure configuration and seismic demand of NSCs.

Nonlinearity is a major influence on the dynamic response of a NSC and its supporting structure. For the future, nonlinear analysis can be conducted following the similar procedure as described in this study to incorporate its impact on NSC behavior.

Future research can also include comparison study on different testing techniques. The intent is to explore options for improving the accuracy of the modal properties extracted from the measure data.

References

Achour, N., Miyajima, M., Kitaura, M., & Price, A. (2011). Earthquake-induced strucutral and nonstructural damage in hospitals. *Earthqauke Spectra , 27*, 617-634.

Akhlaghi, H., & Moghadam, A. (2008). Height-Wise Distribution of Peak Horizontal Floor Acceleration (PHFA). *The 14th World Conference on Earthquake Engineering.* Beijing, China.

Amin, M., Hall, W., Newmark, N., & Kasswara, R. (1971). Earthquake response of multiply connected light secondary systems by spectrum methods. *Proceeding of the 1st national conference on pressure vessels and piping*, (pp. 103-29).

Applied Technology Council. (2008). *ATC-69 Reducing the Risks of Nonstructural Earthquake Damgae: State-of-the-Art and Practice Report.* Redwood City, California.

Applied Technology Council. (2011). *Seismic Performance Assessment of Buildings Volume 1- Methodology (ATC-58-1).*

Canadian Standards Association. (2006). S832-06: Seismic Risk Reduction of Operational and Functional Components (OFCs) of Buildings.

Chaudhuri, S., & Hutchinson, T. C. (2004). Distribution of peak horizontal floor acceleration for estimating nonstructural element vulnerability. *13th World Conference on Earthquake Engineering.* Vancouver.

Chen, Y., & Soong, T. T. (1988). State-of-the-Art Review: Seismic response of secondary systems. *Engineering Structures* , 218-228.

Chopra, A. k. (2007). *Dynamics of Structures: Theory and Applications to Earthquake Engineering* (3rd ed.). Upper Saddle River, New Jersey: Pearson.

Computers and Structures, Inc. (2012). SAP2000 Version 15.

Devriendt, C., & Guillaume, P. (2008). Identification of modal parameters from transmissibility measurements. *Journal of Sound and Vibration* , 343-356.

Dytran Instruments, Inc. (2013, March). SPECIFICATIONS, MODELS 3035BX & 3035BXG.

Federal Emergency Management Agency. (2011). *FEMA E-74: Reducing the Risks of Nonstructural Earthquake Damage—A Practical Guide, Fourth Edition.*

Fierro, E. A., Miranda, E., & Perry, C. L. (2011). Behavior of Nonstructural Components in Recent Earthquakes. *Architectural Engineering Conference* (pp. 369-377). Oakland: ASCE.

Fisher, F. (1988, August). Generation of Earthquake Response Spectra for Production Equipment. *SPE Production Engineering* , 292-298.

Giraldo, D. F., Song, W., Dyke, S. J., & Caicedo, J. M. (2009). Modal identification through ambient vibration: comparative study. *Journal of Engineering Mechanics* , 759-770.

Halchuk, S., Adams, J., & Anglin, F. (2007). Revised Deaggredation of Seismic Hazard for Selected Canadian Cities. *Ninth Canadian Conference on Earthquake Engineering* . Ottawa, Ontario: Earthquakes Canada website.

International Code Council. (2003). International Building Code. Whittier, California.

Lord MicroStrain. (2013). *G-Link® -LXRS® Specifications*. Retrieved November 24, 2013, from Lord MicroStrain Sensing Systems: http://www.microstrain.com/wireless/g-link

Marc Wathelet. (2011). Geopsy Version 2.9.0. ISTerre, Grenoble, France.

McKevitt, W. (2003). Proposed Canadian code provisions for seismic design of elements of structures, nonstructural components, and equipment. *Canadian Journal of Civil Engineering* , 366-377.

Medina, R. A., Sankaranarayanan, R., & Kingston, K. M. (2006). Floor response spectra for light components mounted on regular moment-resisting frame structures. *Engineering Structures* , 1927-1940.

Miranda, E., & Taghavi, S. (2005). Approximate Floor Acceleration Demands in Multistory Buildings. I: Formulation. *Journal of Structural Engineering @ ASCE* , 203-211.

Miranda, E., & Taghavi, S. (2005). Approximate Floor Acceleration Demands in Multistory Builidng. II: Application. *Journal of Structural Engineering* , 212-220.

Miranda, E., Mosqueda, G., Retamales, R., & Pekcan, G. (2012). Performance of Nonstructural Components during the 27 February 2010 Chile Earthquake. *Earthquake Spectra, Volume 28, No. S1 , 28* (1), S453-S471.

National Research Concil of Canada. (2010)[1]. National Building Code of Canada 2010. Ottawa, Ontario, Canada.

National Research Council Canada. (2010)[2]. Commentary J - Deisgn for Seismic Effects. In *User's Guide - NBC 2010 Structural Commentaries (Part 4 of Division B).*

Natural Resources of Canada. (2013, 06 26). *Determine 2010 National Building Code of Canada seismic hazard values*. Retrieved from Natural Resources of Canada Web Site: http://www.earthquakescanada.nrcan.gc.ca/hazard-alea/interpolat/index_2010-eng.php

Newmark, N. M., & Hall, W. (1982). *Earthquake Spectra and Design.* Berkeley, California: Earthquake Engineering Research Institute.

PEER. (2011). *PEER Ground Motion Database*. Retrieved 2013, from Pacific Earthquake Engineering Research Centre Web site: http://peer.berkeley.edu/peer_ground_motion_database

Peeters, B., & Ventura, C. (2003). Comparative study of modal analysis techniques for bridge dynamic characteristics. *Mechanical Systems and Signal Processing* , 965-988.

Rodriguez, M., Restrepo, J. I., & Carr, A. J. (2001). Earthquake-induced floor horizontal accelerations in buildings. *Earthquake Engineering and Structural Dynamics* , 693-718.

Seismosoft Ltd. (2002). SeimoSpect Version 2.1.0.

SENSR Intelligent technology. (2013). *CX1 Structural Dynamic Monitor*. Retrieved November 24, 2013, from SENSR Intelligent technology. Measured results.: http://www.sensr.com/products/civil-and-structural/cx1.php

Shooshtari, M., Saatcioglu, M., Naumoski, N., & Foo, S. (2010). Floor response spectra for seismic design of operational and functional components of concrete buildings in Canada. *Canadian Journal of Civil Engineering* , 1590-1599.

Singh, M. P., Moreschi, L. M., Suarez, L., & Matheu, E. E. (2006). Seismic Deisng Forces. I: Rigid Nonstructural Components. *Journal of Structural Engineering @ ASCE* , 1524-1532.

Smith, S. W. (1997). *The Scientist and Engineer's Guide to Digital Signal Processing.* California Technical Publishing.

Soong, T., & Chen, Y. (1988). State-of-the-art Review: Seismic Response of Secondary Systems. *Engineering Structures , 10*, 218-228.

Stevenson, J. (1980). Structural Damping Values as a Function of Dynamic Response Stress and Deformation Levels. *Nuclear Engineering and Deisgn* , 211-237.

The International Federation for Structural Concrete (FIB). (2012). *Model Code for Concrete Structures 2010 - Final draft, Volume 1.*

The Mathworks. (2009). Matlab R2009b.

Tirelli, D. (2011). *JRC Scientific and Technical Reports: Modal Analysis of Small & Medium Structures by Fast Impact Hammer Testing Method.* Institute for the Protection and Security of the Citizen.

Toro, G., McGuire, R., Cornell, C., & Sewell, R. (1989). *Linear and nonlinear reponse of structures and equipment to California and Estern United States earthquakes.* Palo Alto (CA): Electric Power Research Institude.

Trebuna, F., Simcak, F., Hunady, R., & Pastor, M. (2013). Identification of pipes damages on gas compressor stations by modal analysis methods. *Engineering Failure Analysis* , 213-224.

Villaverde, R. (1997). Seismic Deisgn of Secondary Structures: State of the Art. *Journal of Structural Engineering* , 1011-1019.

Vu, V., Thomas, M., Lafleur, F., & Marcouiller, L. (2012). Towards an automatic spectral and modal identification from operational modal analysis. *Journal of Sound and Vibration* , 213-227.

Whittaker, A., & Soong, T. (2003). An overview of nonstructural components research at three US Earthquake Engineering Research Centers. *Seminar on Seismic Design, Performance, and Retrofit of Nonstructural Components in Critical Facilities.* Applied Technology Council - Multidisciplinary Center for Earthquake Engineering Research.

Zahrah, T. F., & Hall, W. J. (1984). Earthquake energy absorption in SDOF structures. *Journal of Structural Engineering* , 1757-1772.

Appendices

Appendix A

Hammer Impact Modal Testing Photos and Data Processing Figures

This appendix includes the detail information for the hammer impact vibration experiments for identifying the modal properties of the nine NSCs. It is consisted of the following subsections:

A.1 Testing setup photos and descriptions

A.2 Sample Matlab calculation worksheets for obtaining the power spectral density (PSD) and frequency response function (FRF) plots for each test setup

A.3 Acceleration time history measurements for the full recording duration and for one impact duration; PSD and FRF plots of the best impact of each set of data to show the fundamental frequencies

A.1 Experiment Setup Photos and Description

This section includes the photos and brief description of each experiment setup. The photos show the locations of the accelerometers (marked as channels) and the direction in which the impact forces were applied.

Figure A.1.1 Test photo for COMP1: Pump.

Description:

Channel 1: vertical
Channel 2: lateral
Channel 3: longitudinal
Channel 4: hammer input
Test #1: impact applied in lateral direction (same as Channel 2)
Test #2: impact applied in longitudinal direction (same as Channel 3)

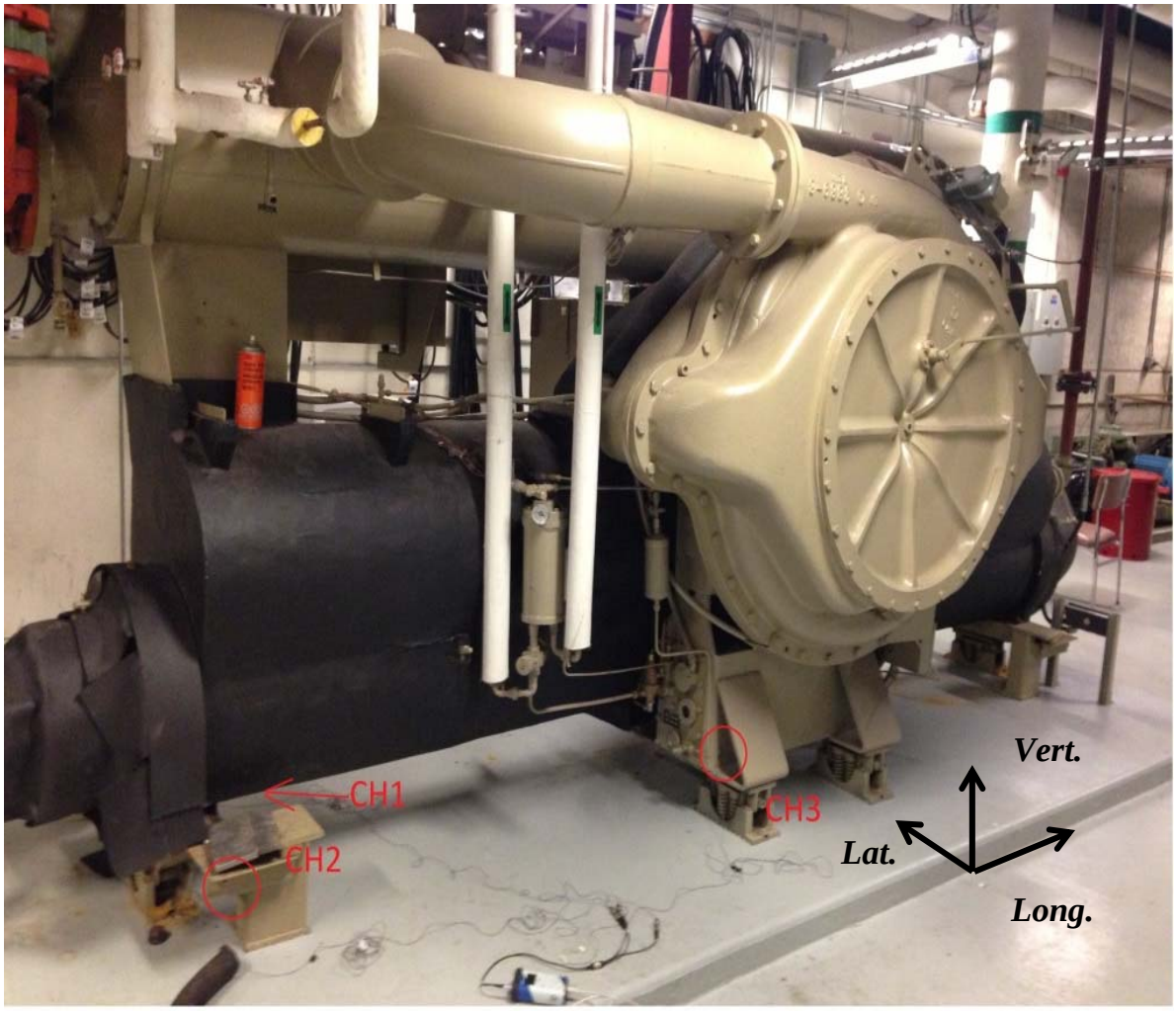

Figure A.1.2 Test photo for COMP2: Air Handler Unit.

Description:

Channel 1-3: lateral

Channel 4: hammer input (not available for the “big hammer” setup)

Impact forces applied in the lateral direction.

Figure A.1.3 Test setup photo for COMP3: Relay Rack.

Description:

Channel 1: out-of-plane (near the bottom)
Channel 2: out-of-plane (mid-height)
Channel 3: out-of-plane (near the top)
Channel 4: hammer input
Test #1: Impact applied in out-of-plane direction near channel 1
Test #2: Impact applied in out-of-plane direction near channel 2
Test #3: Impact applied in out-of-plane direction near channel 3

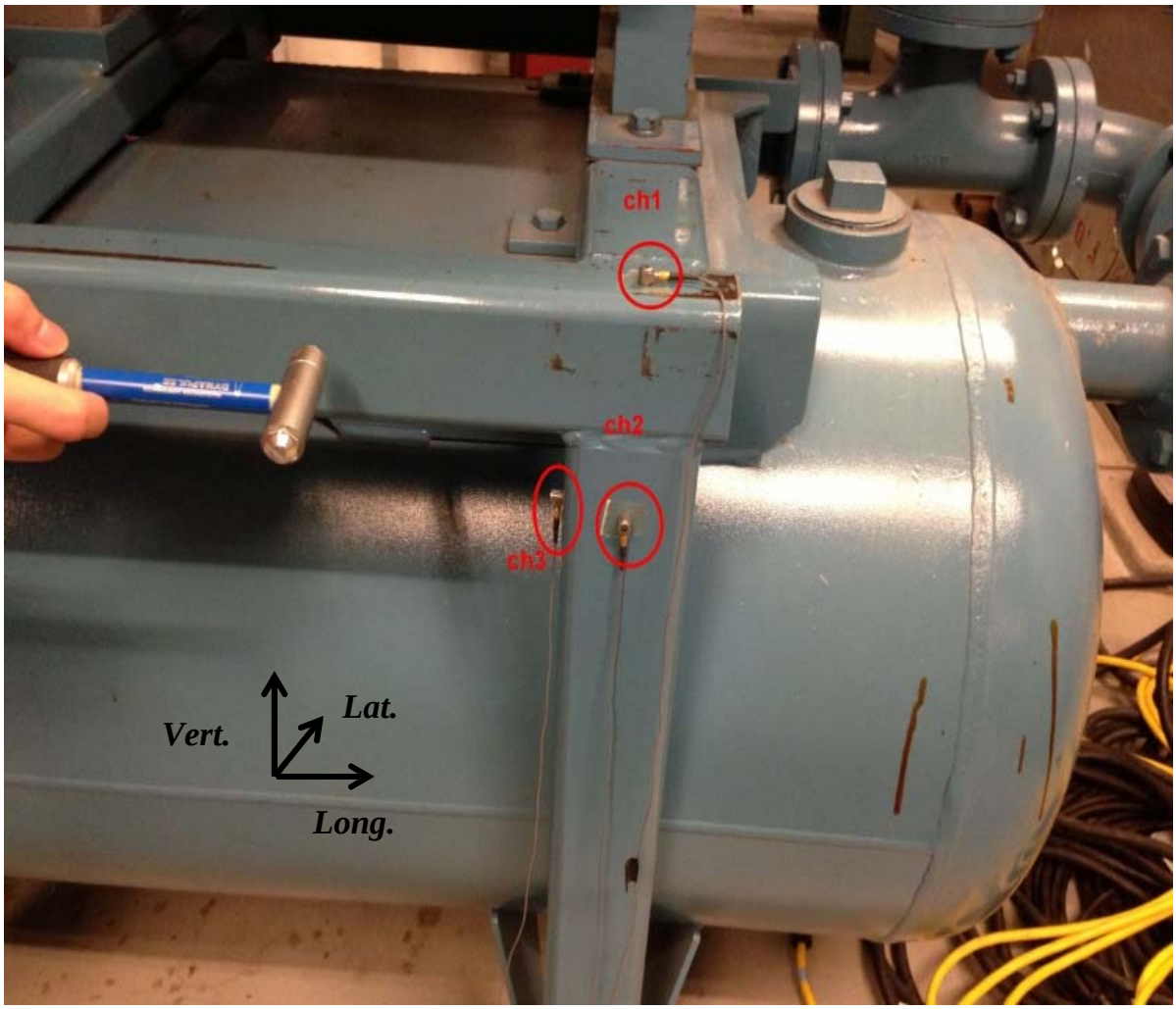

Figure A.1.4 Test setup photo for COMP4: dry air vacuum unit

Description:

Channel 1: vertical
Channel 2: lateral
Channel 3: longitudinal
Channel 4: hammer input
Test #1: Impact applied in lateral direction
Test #2: Impact applied in longitudinal direction

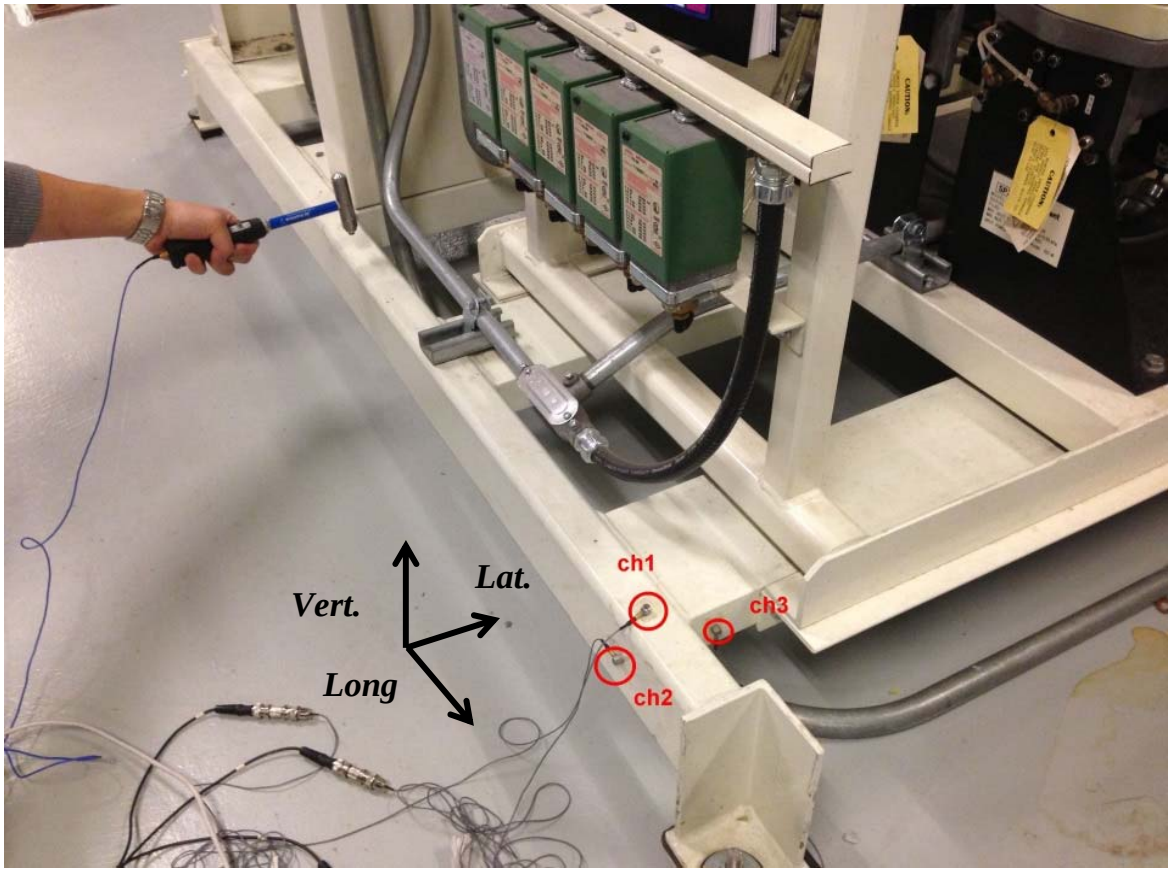

Figure A.1.5 Test setup photo for COMP5: medical air vacuum unit

Description:

Channel 1: vertical
Channel 2: lateral
Channel 3: longitudinal
Channel 4: hammer input
Test #1: Impact applied in lateral direction
Test #2: Impact applied in longitudinal direction
Test #3: Impact applied in vertical direction (as shown in picture above)

Figure A.1.6 Test setup photo for COMP6: concrete pump deck setup #1

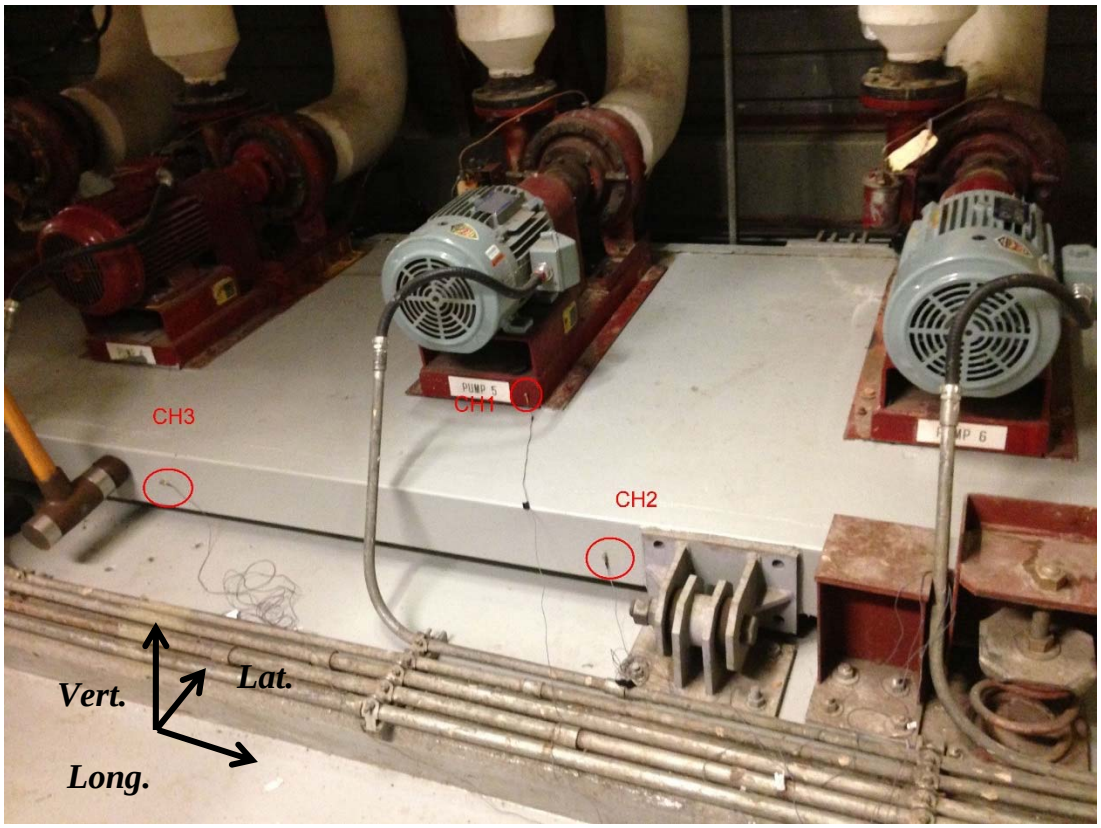

Figure A.1.7 Test setup photo for COMP6: concrete pump deck setup #2

Description:

Test #1: Impact applied in longitudinal direction
- Channel 1: longitudinal
- Channel 2: longitudinal
- Channel 3: longitudinal
- Channel 4: hammer input (not available for “big hammer” setup)

Test #2: Impact applied in lateral direction
- Channel 1: lateral
- Channel 2: lateral
- Channel 3: lateral
- Channel 4: hammer input (not available for “big hammer” setup)

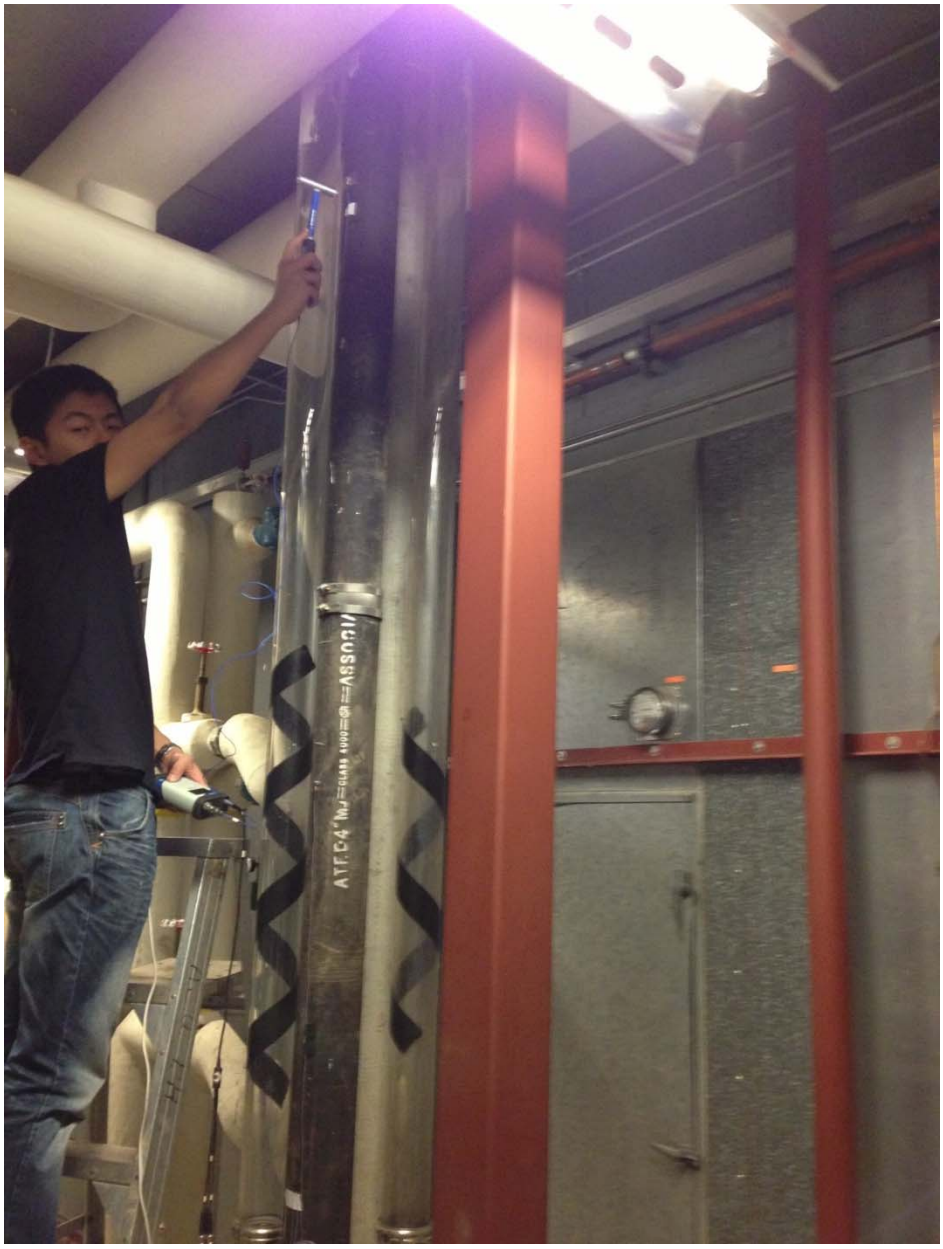

Figure A.1.8 Test setup photo for COMP7: vertical pipe

Description:

Channel 1: lateral (near the bottom)
Channel 2: lateral (mid-height)
Channel 3: lateral (near the top)
Channel 4: hammer input
Test #1: Impact applied in lateral direction near channel 1
Test #2: Impact applied in lateral direction near channel 2
Test #3: Impact applied in lateral direction near channel 3

Figure A.1.9 Test setup photo for COMP8: medical air cylinder rack

Description:

Channel 1: vertical
Channel 2: longitudinal
Channel 3: lateral
Channel 4: hammer input
Test #1: Impact applied in lateral direction
Test #2: Impact applied in longitudinal direction

Figure A.1.10 Test setup photo for COMP9: service air vacuum unit setup #1

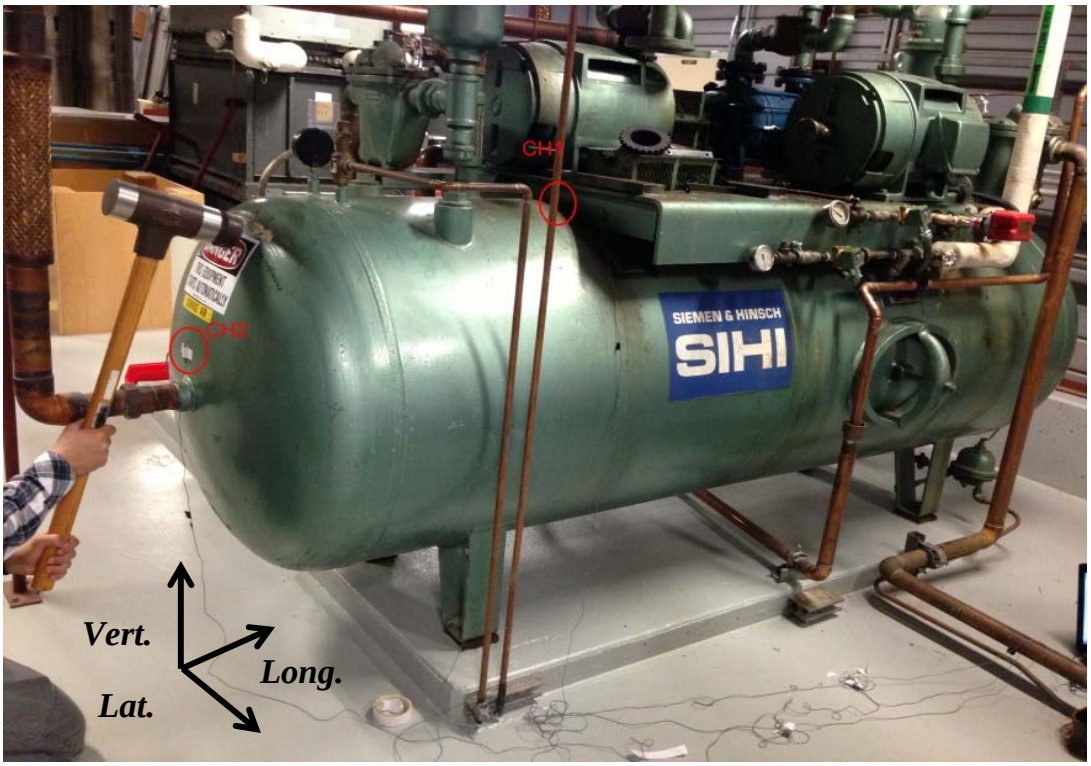

Figure A.1.11 Test setup photo for COMP9: service air vacuum unit setup #2

Description:

Test #1: Impact applied in lateral direction

- Channel 1: lateral
- Channel 2: lateral
- Channel 3: lateral
- Channel 4: hammer input (not available for “big hammer” setup)

Test #2: Impact applied in longitudinal direction

- Channel 1: longitudinal
- Channel 2: longitudinal
- Channel 3: not available
- Channel 4: hammer input (not available for “big hammer” setup)

A.2 Sample Matlab Worksheet for PSD and FRF Calculations

This appendix includes a sample Matlab files for calculating the Power Spectral Density (PSD) and Frequency Response Function (FRF) for the nine components. The calculations are based on the Fast Fourier Transform (FFT) algorithm.

```
% General Description:
% This Matlab worksheet is created for
%   1) plotting the orginal acceleration time records for the NSCs
%   2) Calculating Power Spectrual Density for multiple impact trials
%   3) Generate Transfer Function Amplitude for
%      each of the impact trial selected.

%Description of the experiment setup
%   component #1: pump assembly
%   ch 1, 2 & 3 refer to response measurement in the lateral, longitudinal
%   and vertical direction
%   sampling rate of 1280 Hz
%   duration of roughly 80 seconds
%   see coresponding pictures for sensor locations


%STEP 1: PLOT ACCELERATION TIME HISTORY RECORDS FOR ALL THREE LOCATIONS

load comp1_setup1_lat.txt;


Fs=1280;
T=1/Fs;
N=length(comp1_setup1_lat);
t=(0:N-1)*T;
data=comp1_setup1_lat;

for i=1:4
    lineColor=['b','g','r','k'];
    lgdName=char('Ch1', 'Ch2', 'Ch3', 'Hammer Input','FontSize',14);
 figure (1);

  subplot(4,1,i);
  plot(t,data(:,i),lineColor(i));

  legend(lgdName(i,:));

end
  xlabel('Time (sec)','FontSize',14)
  ylabel('Acceleration (m/s^2)','FontSize',14)
saveas(figure(1),'comp1_setup1_lat_TH')



% STEP 2: OBTAIN PSD AT EACH LOCATION FOR EACH OF THE IMPACT TRIAL

% from observation of the time history plot,
% select impact #1 (t=3.45s to 4.45s), #2 (t=13.90s to 14.90s)
% and #4 (t=34.2s to 35.2s)
% for psd calculation. Each window is set to be 1.0 second long.

t_ini=[5.5 18.5 27.5] ;
t_fin=t_ini+1;
for m=1:3
x=data(t_ini(m)*Fs:t_fin(m)*Fs,:);

nfft=2^nextpow2(length(x));
```

```
Pxx = abs(fft(x,nfft)).^2/length(x)/Fs;

hpsd = dspdata.psd(Pxx(1:length(Pxx)/2,:),'Fs',Fs);
figure(2*m)
plot(hpsd)
grid on;
xlim([0 100])
grid minor;

xlabel('Frequency (Hz)','FontSize',14);
ylabel('Power Spectral Density (dB/Hz)','FontSize',14)

legend('Channel 1','Channel 2','Channel 3','hammer')

saveas(figure(2*m),['comp1_setup1_lat_psd_',num2str(m)])

% STEP 3: PLOT TRANSFER FUNCTION AMPLITUDE AND PHASE ANGLE FOR OUTPUT/INPUT

[T14,f]=tfestimate(x(:,4),x(:,1),length(x),0,nfft,Fs);
[T24,f]=tfestimate(x(:,4),x(:,2),length(x),0,nfft,Fs);
[T34,f]=tfestimate(x(:,4),x(:,3),length(x),0,nfft,Fs);


figure(2*m+1);
plot(f,abs(T14),f,abs(T24),f,abs(T34));
grid on;
xlim([0 100])
grid minor;
xlabel('Frequency (Hz)', 'FontSize',14)
ylabel('FFT(output)/FFT(input)','FontSize',14)
legend('ch1/input','ch2/input','ch3/input')

saveas(figure(2*m+1),['comp1_setup1_lat_tf_',num2str(m)])
end


clearvars
```

A.3 Hammer Impact Modal Testing Data Processing Figures

The power spectral density and transfer function analysis was calculated using the Matlab worksheet presented in the previous appendix. There are a total of 15 sets of records being processed. Following figures include a set of raw time history records (full-duration time histories and enlarged time histories), PSD plots and the FRF plots for each of the 15 recordings. Note that the FRF plots are only available for the "small" hammer case in which the input signals were recorded.

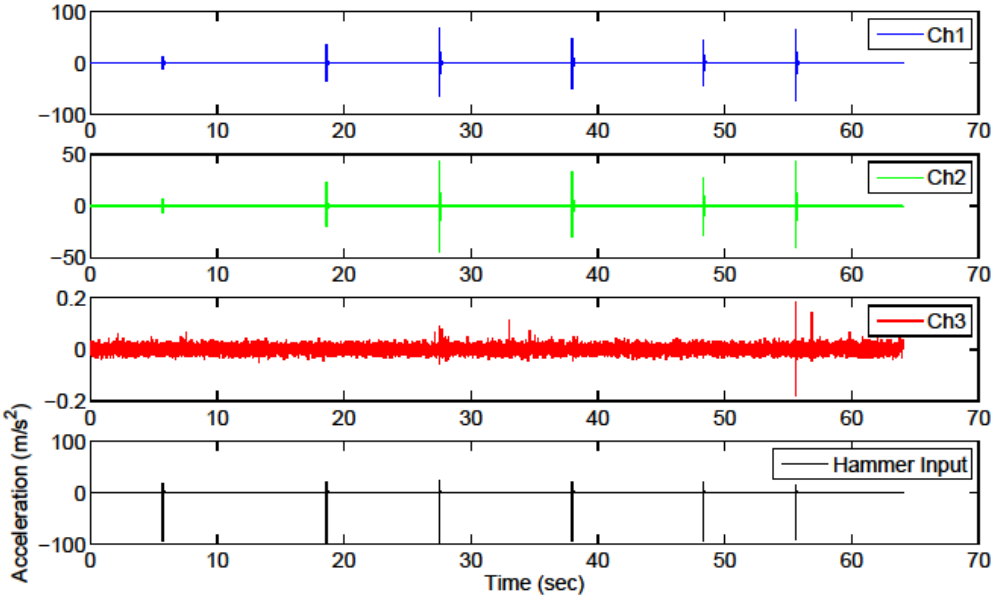

Figure A.3.1 Acceleration time histories for the entire duration for lateral impacts on COMP1.

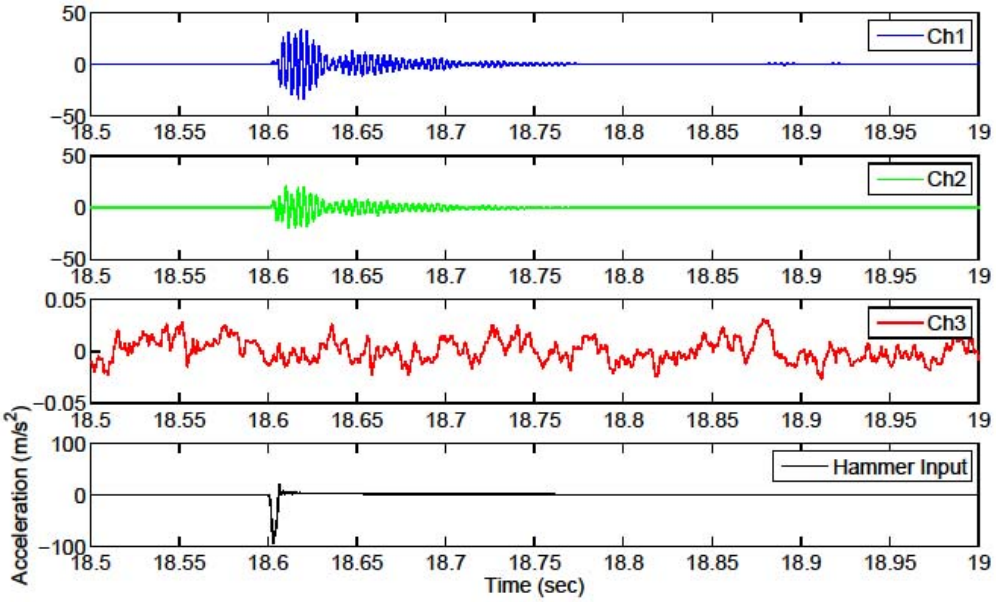

Figure A.3.2 Enlarged acceleration time histories for the best lateral impact on COMP1.

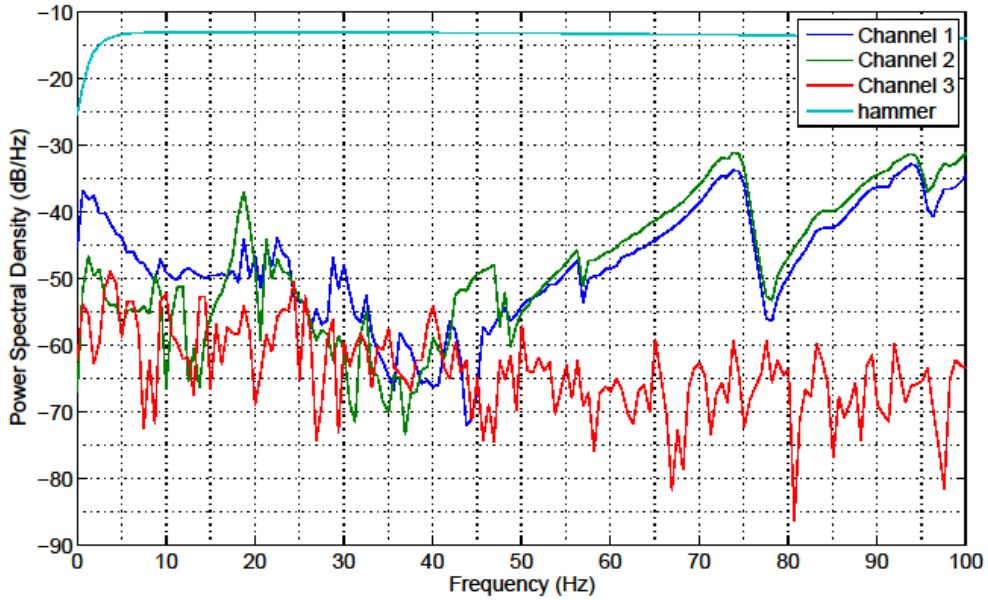

Figure A.3.3 Power Spectral Density plot for the best lateral impact for COMP1

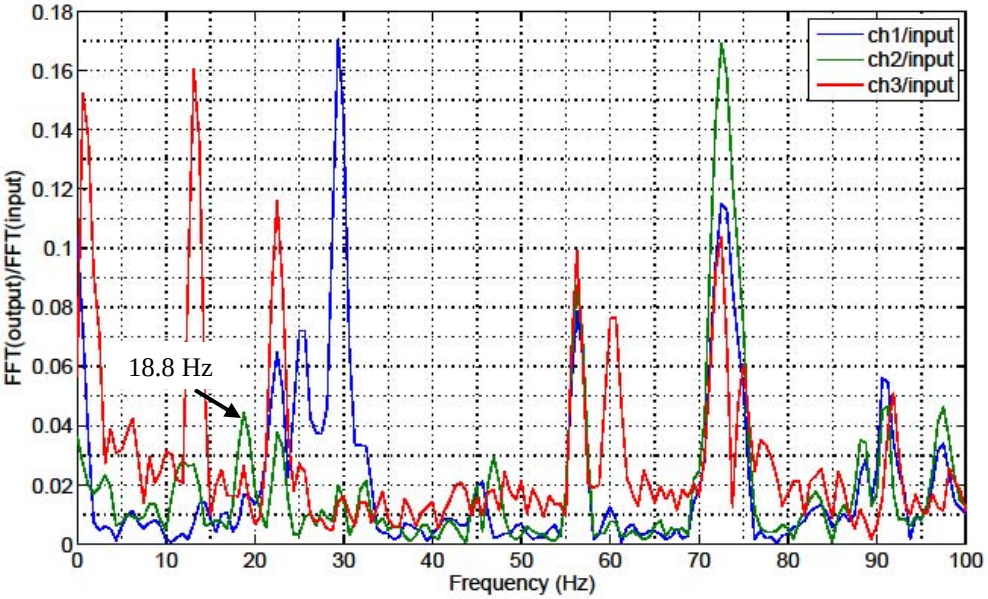

Figure A.3.4 Frequency Response Function plot for the best lateral impact for COMP1

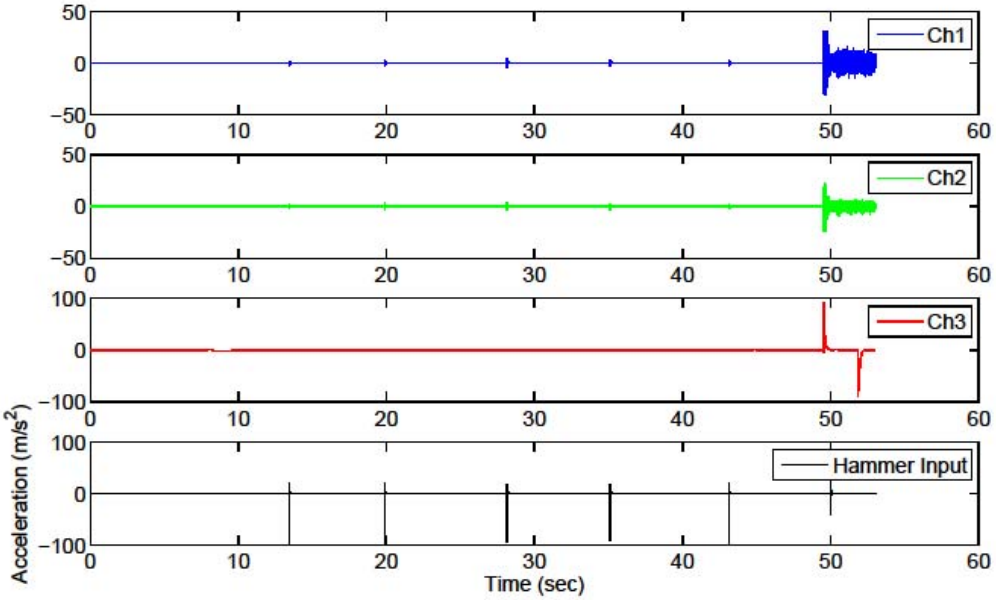

Figure A.3.5 Acceleration time histories for the entire duration for longitudinal impacts on COMP1.

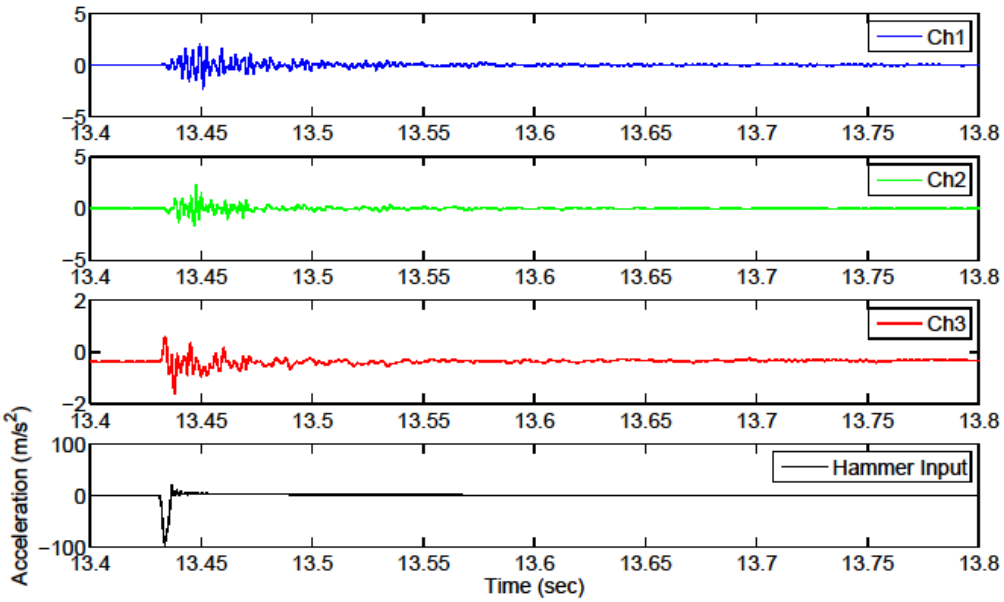

Figure A.3.6 Enlarged acceleration time histories for the best longitudinal impact on COMP1.

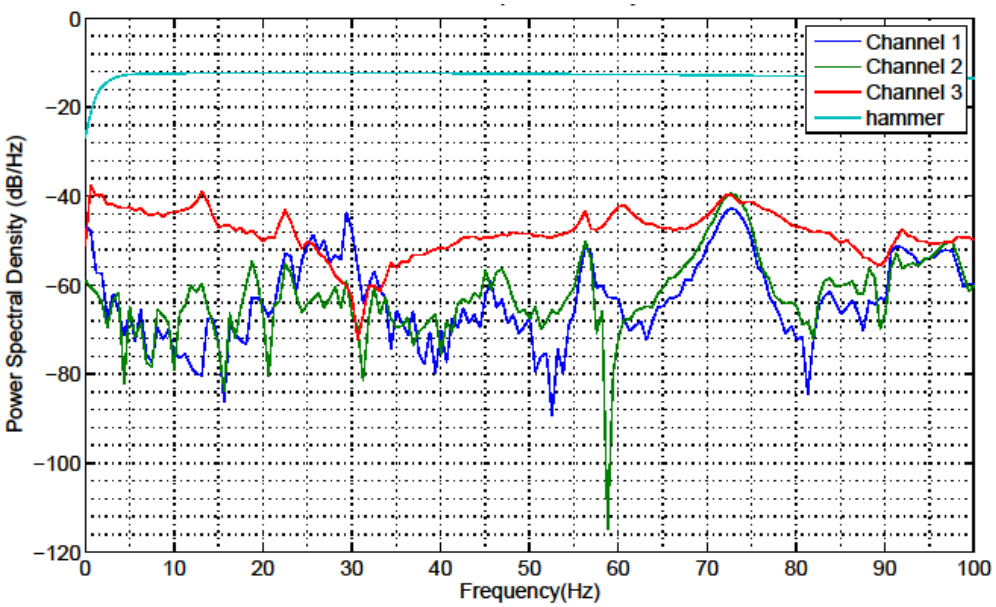

Figure A.3.7 Power Spectral Density plot for the best longitudinal impact for COMP1

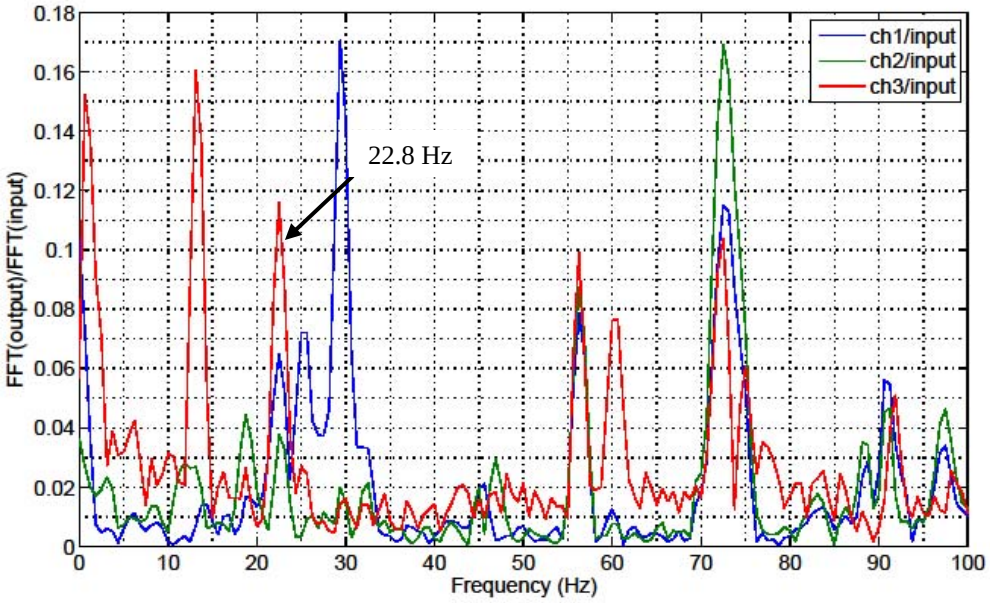

Figure A.3.8 Frequency Response Function plot for the best longitudinal impact for COMP1

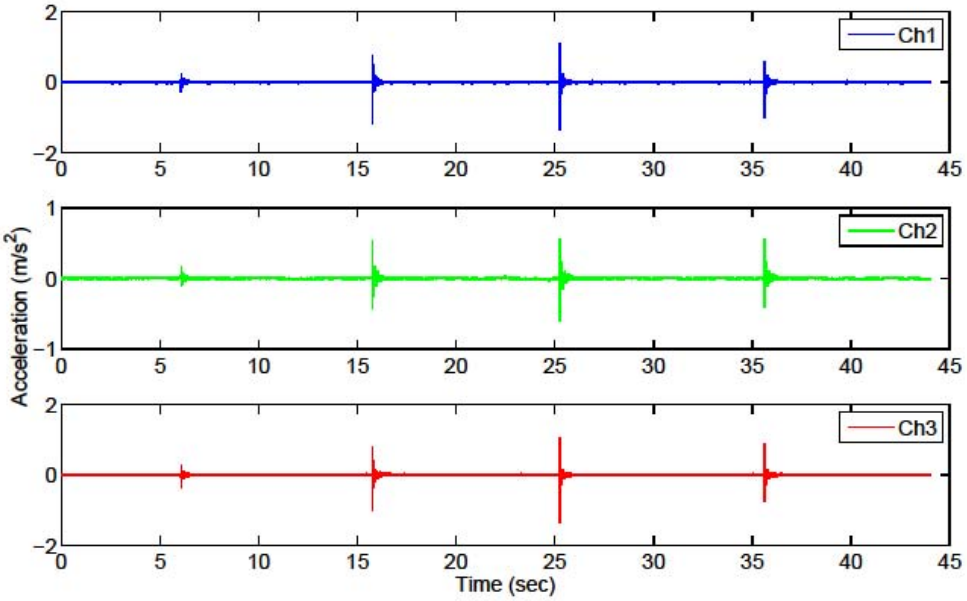

Figure A.3.9 Acceleration time histories for the entire duration for lateral impacts on COMP2

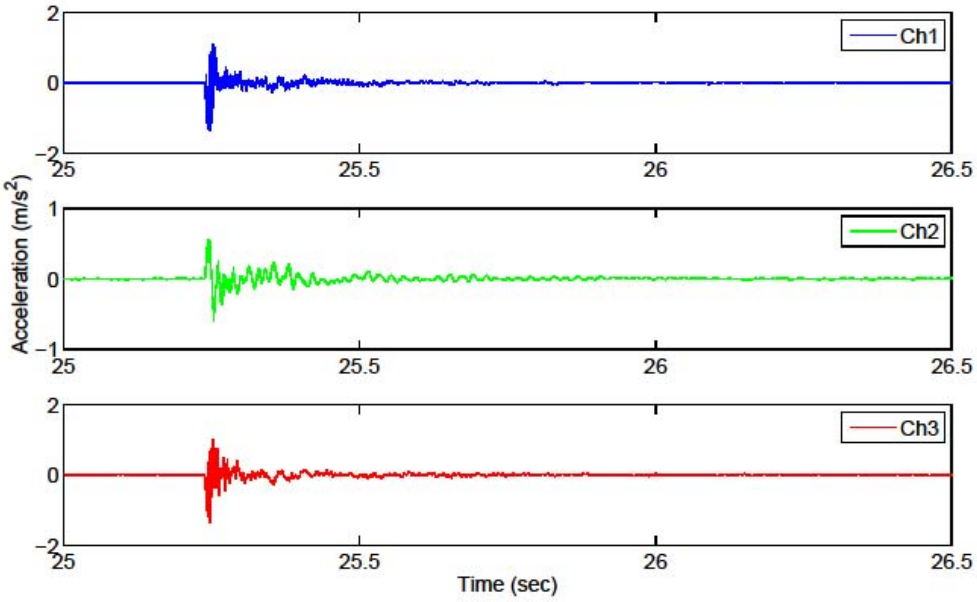

Figure A.3.10 Enlarged acceleration time histories for the best lateral impact on COMP2

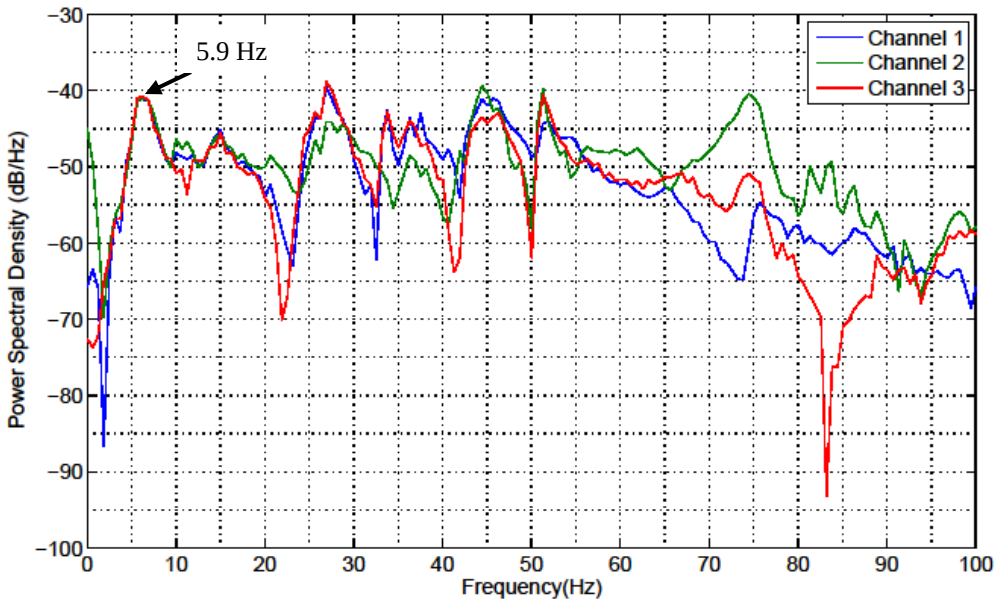

Figure A.3.11 Power Spectral Density plot for the best lateral impact for COMP2

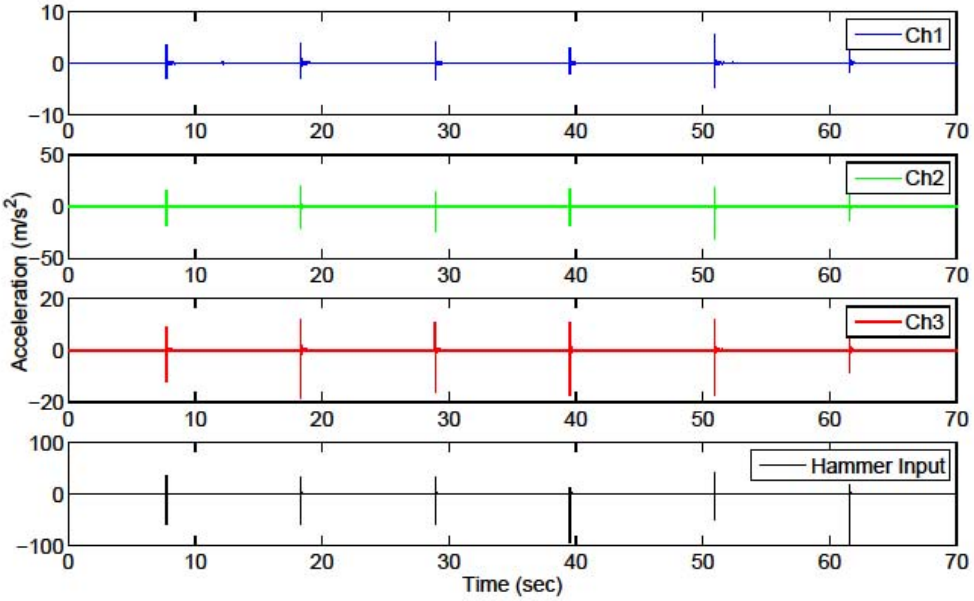

Figure A.3.12 Acceleration time histories for the entire duration for lateral impacts on COMP3

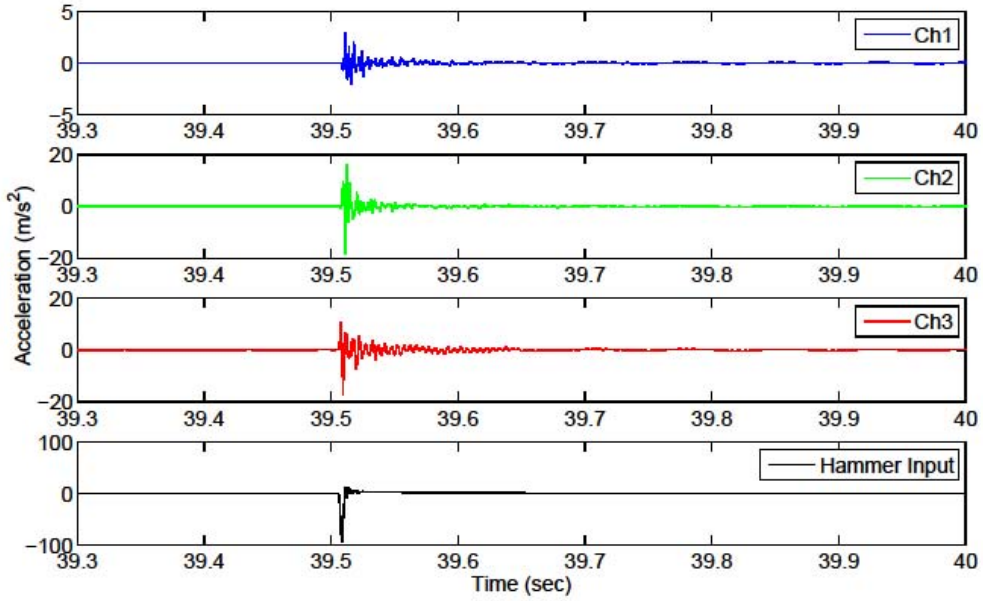

Figure A.3.13 Enlarged acceleration time histories for the best lateral impact on COMP3

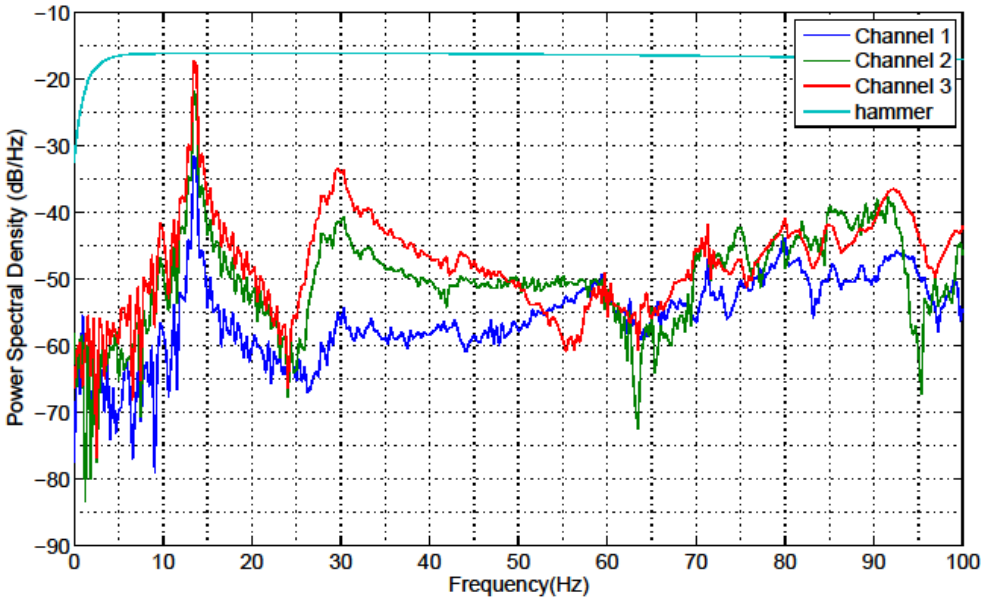

Figure A.3.14 Power Spectral Density plot for the best lateral impact for COMP3

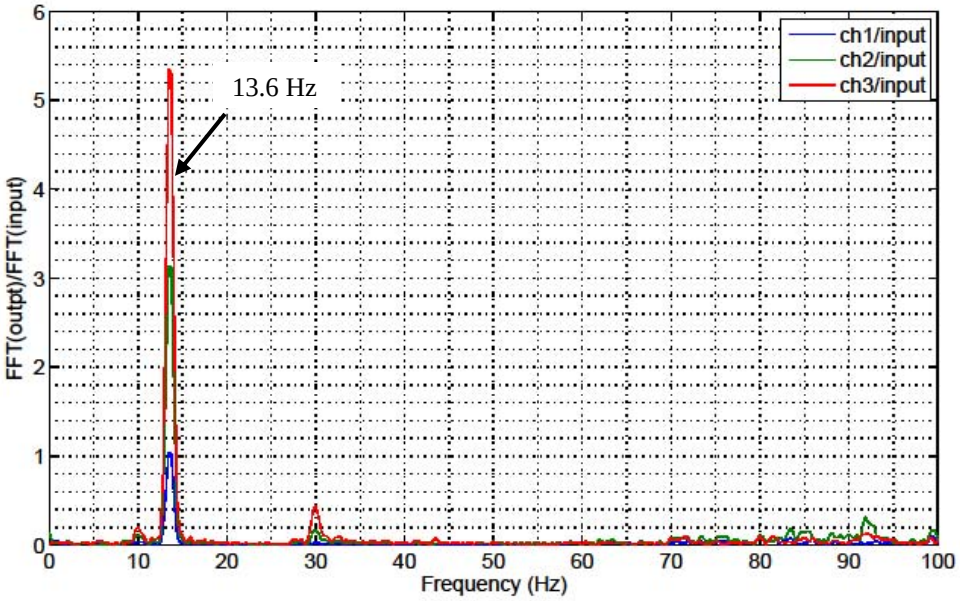

Figure A.3.15 Frequency Response Function plot for the best lateral impact for COMP3

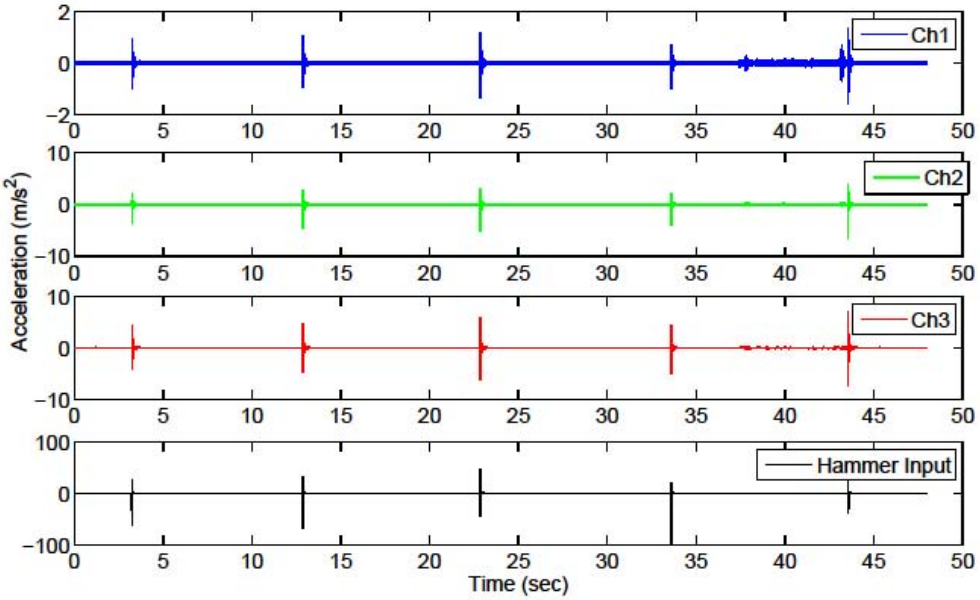

Figure A.3.16 Acceleration time histories for the entire duration for lateral impacts on COMP4

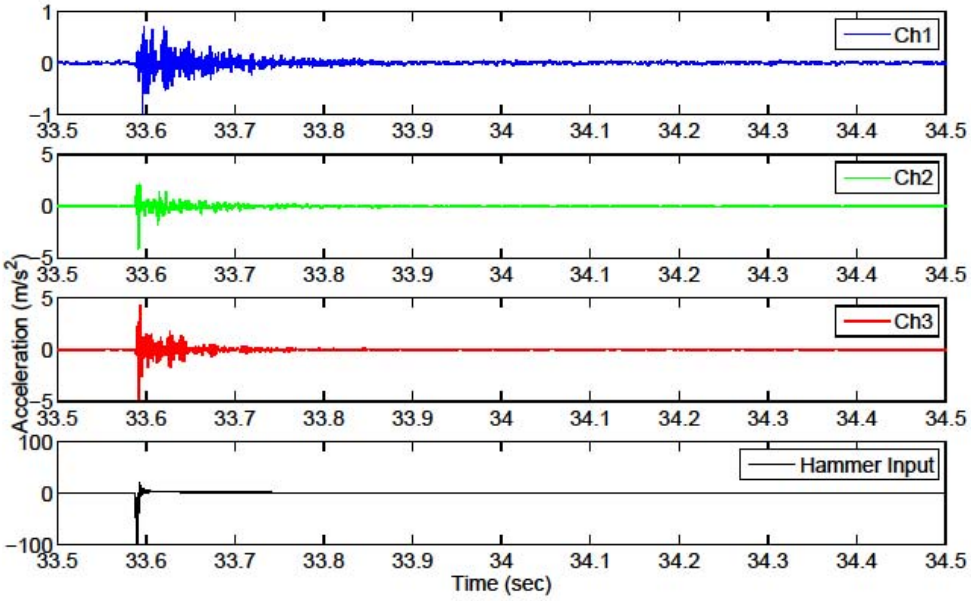

Figure A.3.17 Enlarged acceleration time histories for the best lateral impact on COMP4

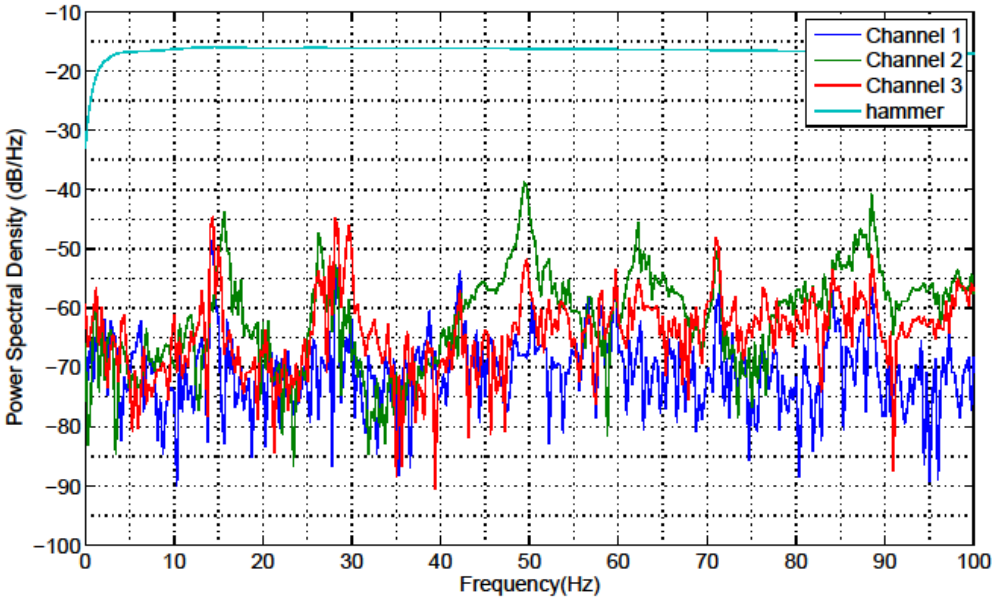

Figure A.3.18 Power Spectral Density plot for the best lateral impact for COMP4

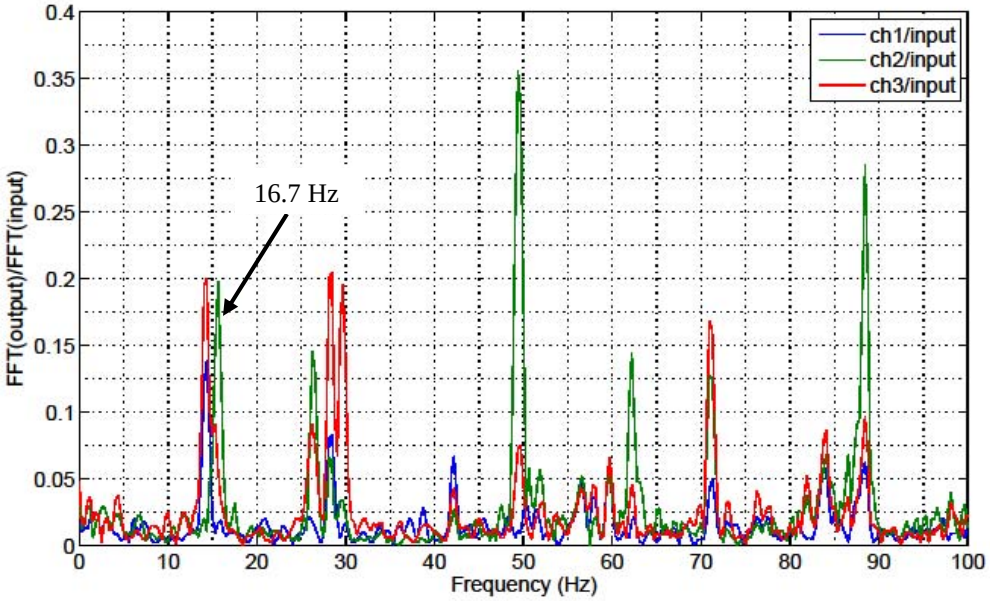

Figure A.3.19 Frequency Response Function plot for the best lateral impact for COMP4

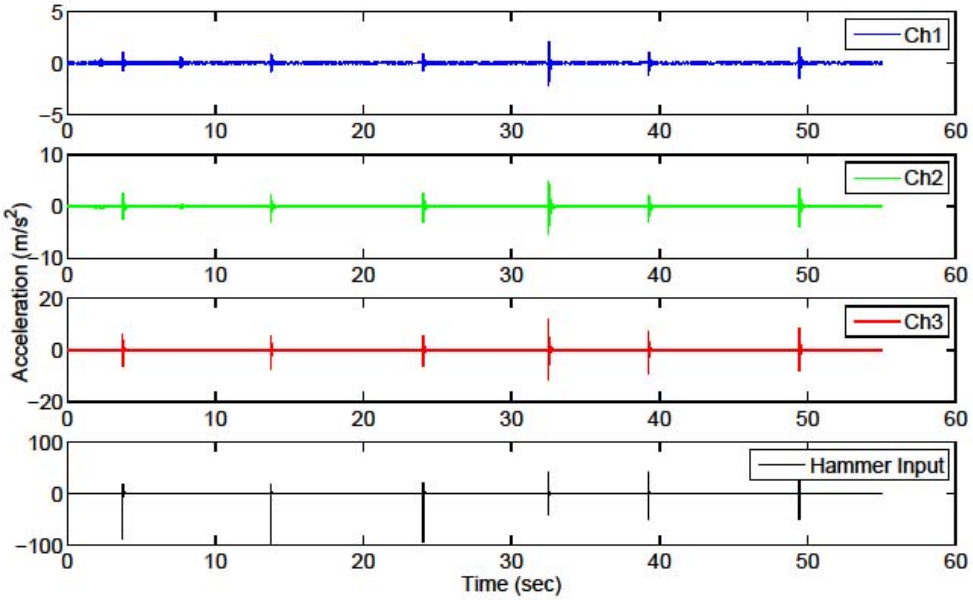

Figure A.3.20 Acceleration time histories for the entire duration for longitudinal impacts on COMP4

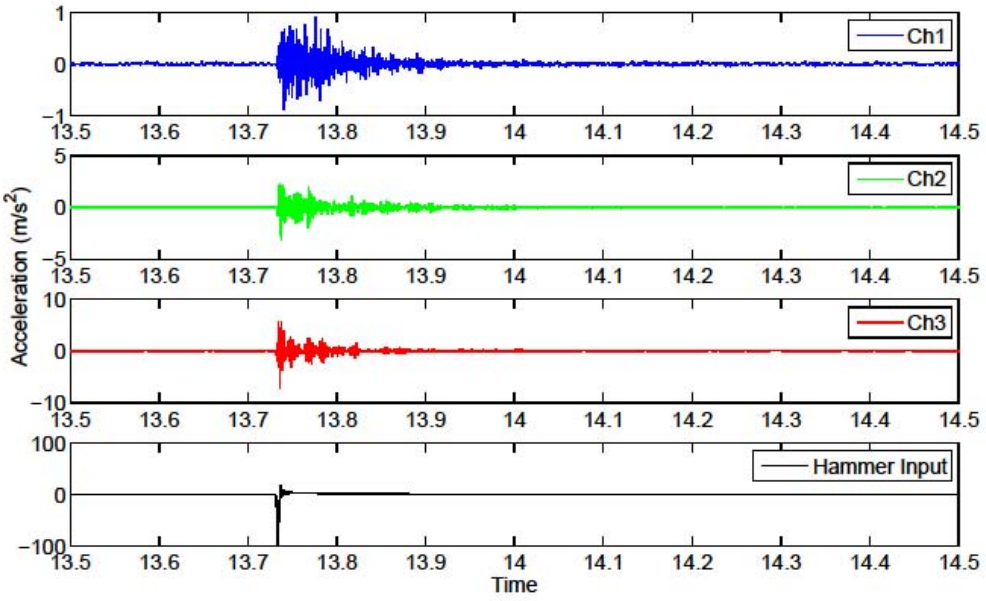

Figure A.3.21 Enlarged acceleration time histories for the best longitudinal impact on COMP4

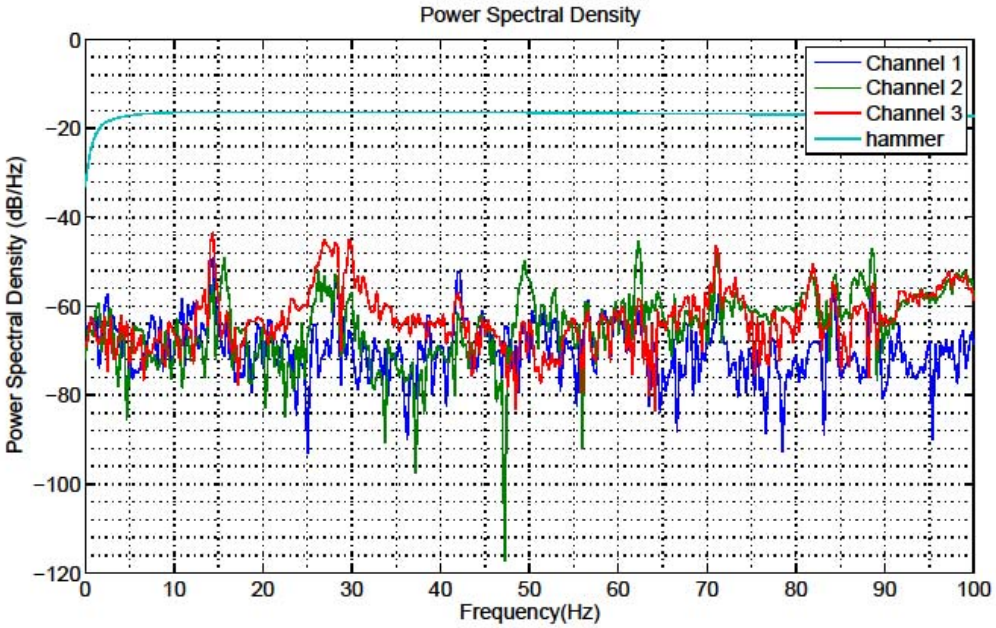

Figure A.3.22 Power Spectral Density plot for the best longitudinal impact for COMP4

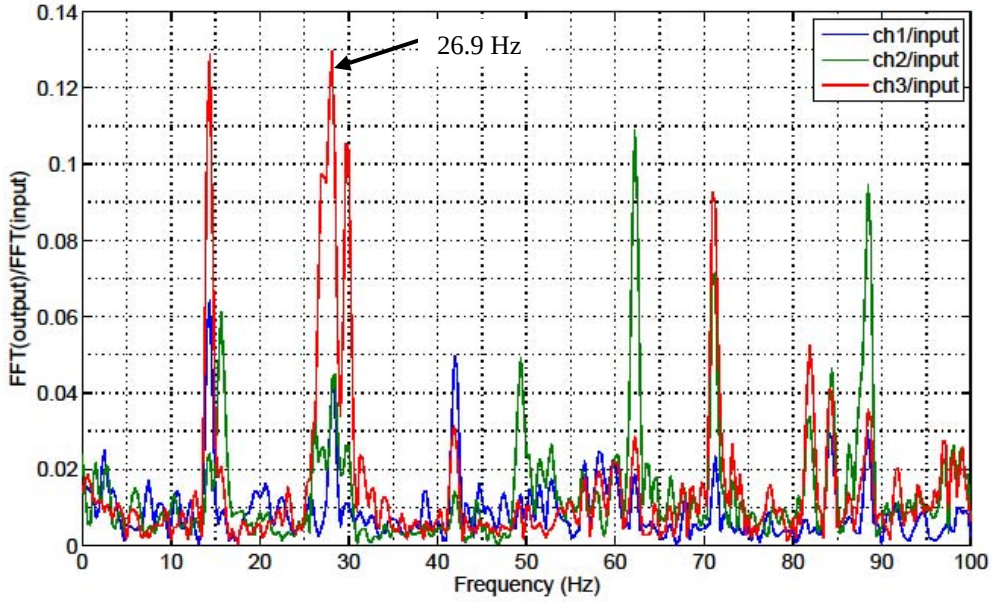

Figure A.3.23 Frequency Response Function plot for the best longitudinal impact for COMP4

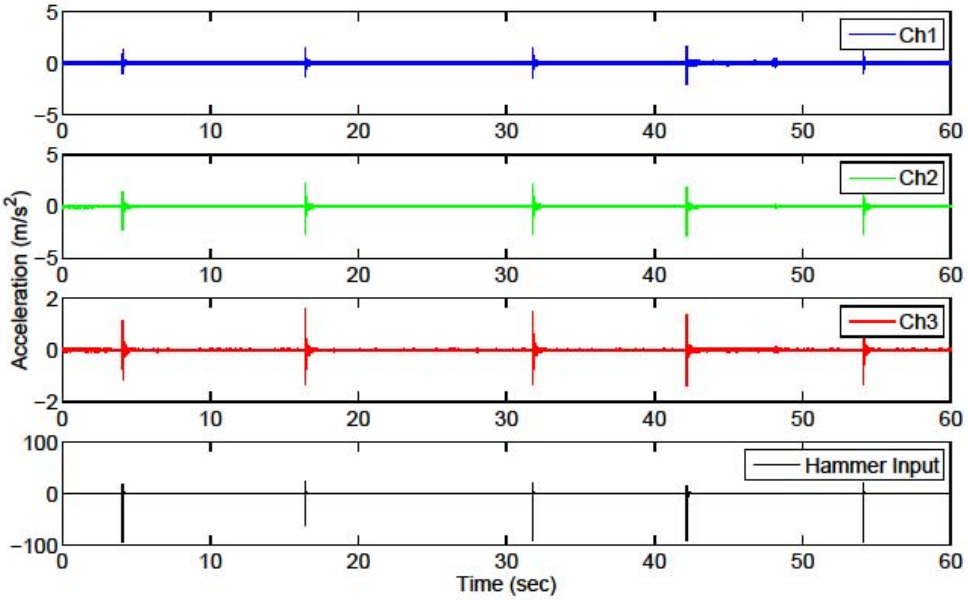

Figure A.3.24 Acceleration time histories for the entire duration for lateral impacts on COMP5

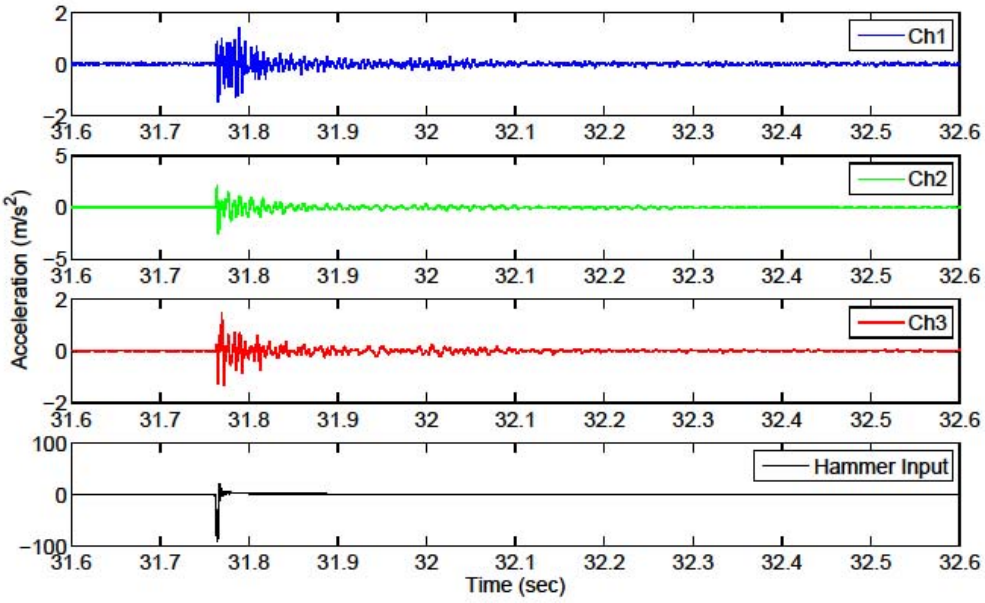

Figure A.3.25 Enlarged acceleration time histories for the best lateral impact on COMP5

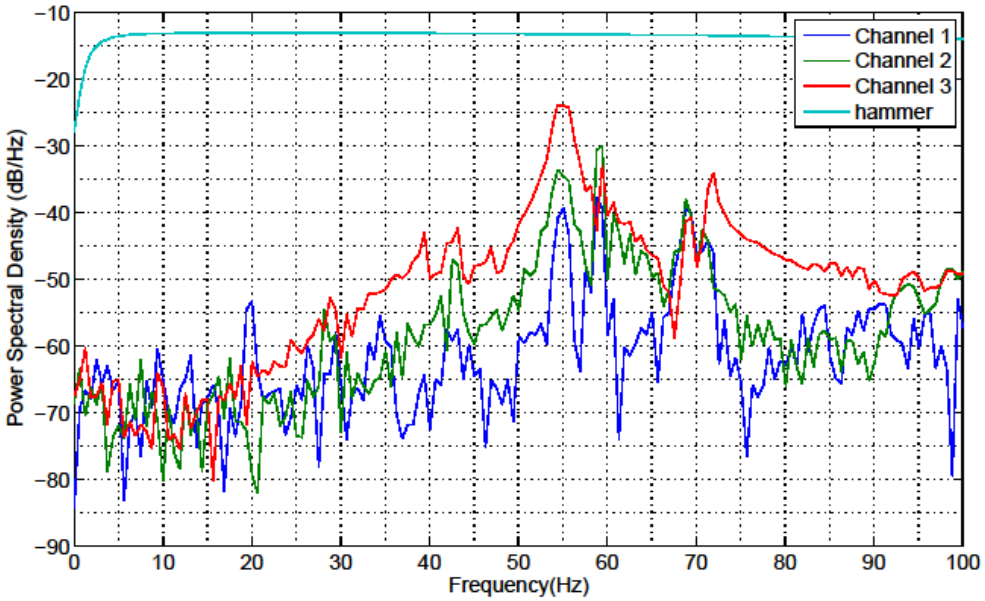

Figure A.3.26 Power Spectral Density plot for the best lateral impact for COMP5

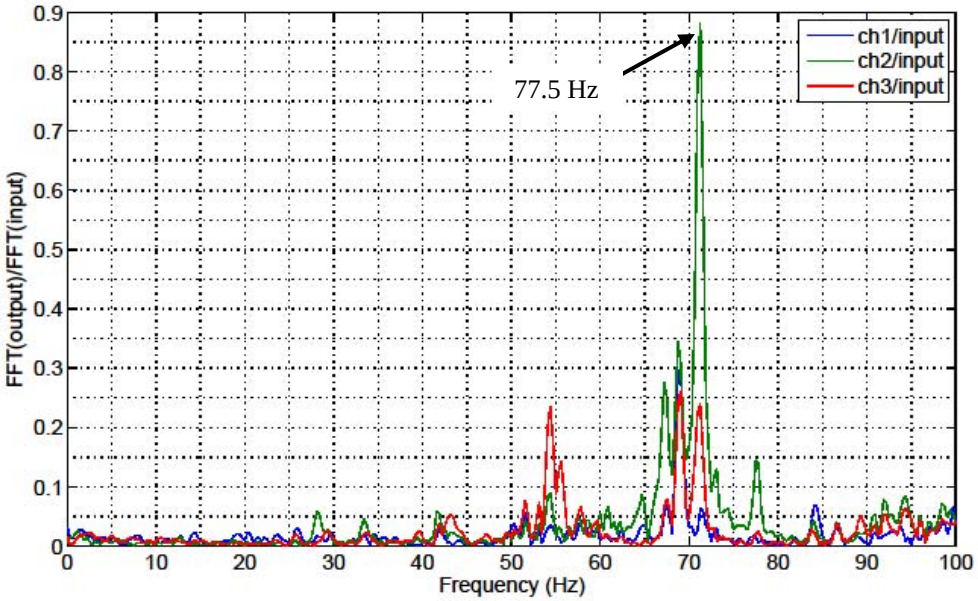

Figure A.3.27 Frequency Response Function plot for the best lateral impact for COMP5

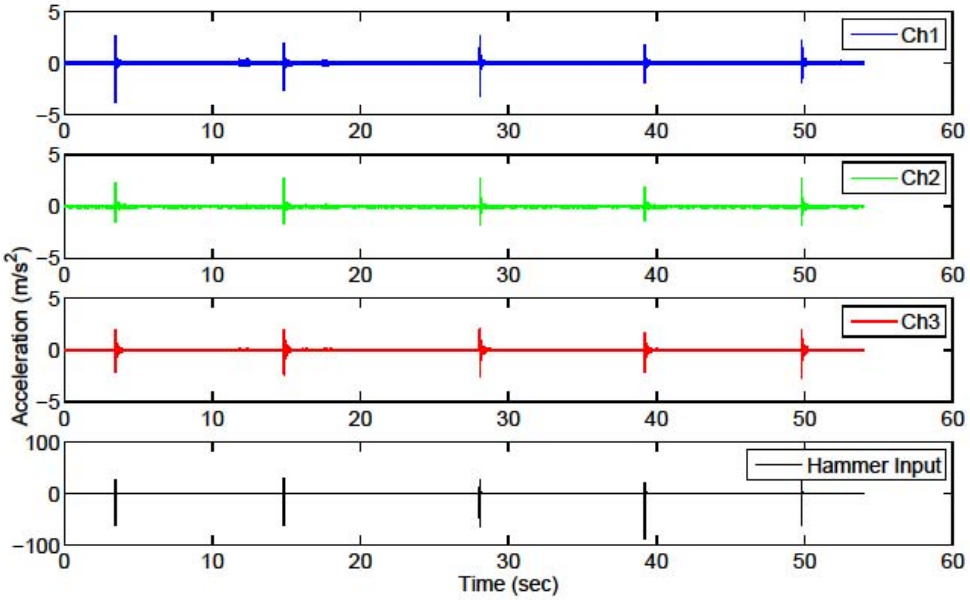

Figure A.3.28 Acceleration time histories for the entire duration for longitudinal impacts on COMP5

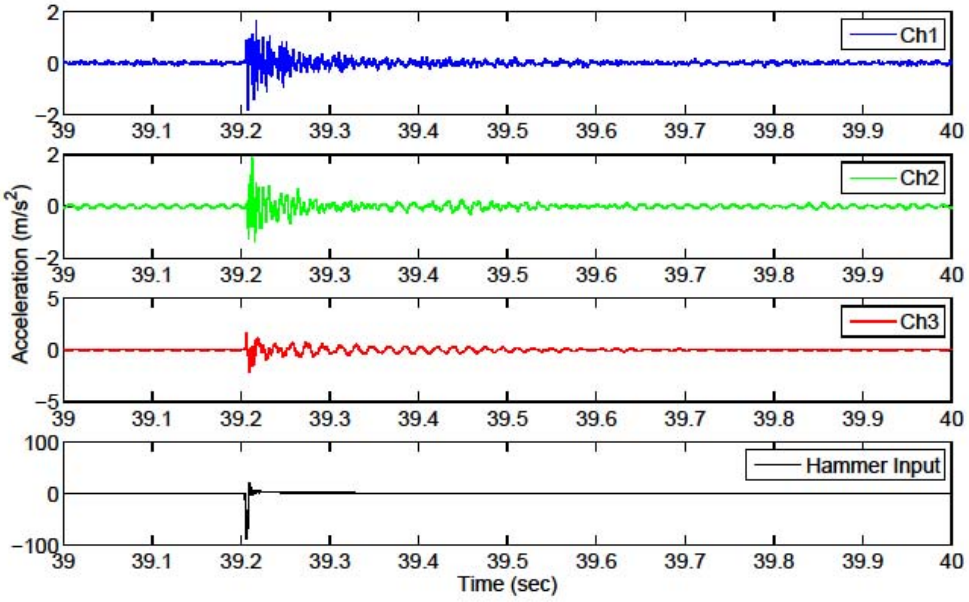

Figure A.3.29 Enlarged acceleration time histories for the best longitudinal impact on COMP5

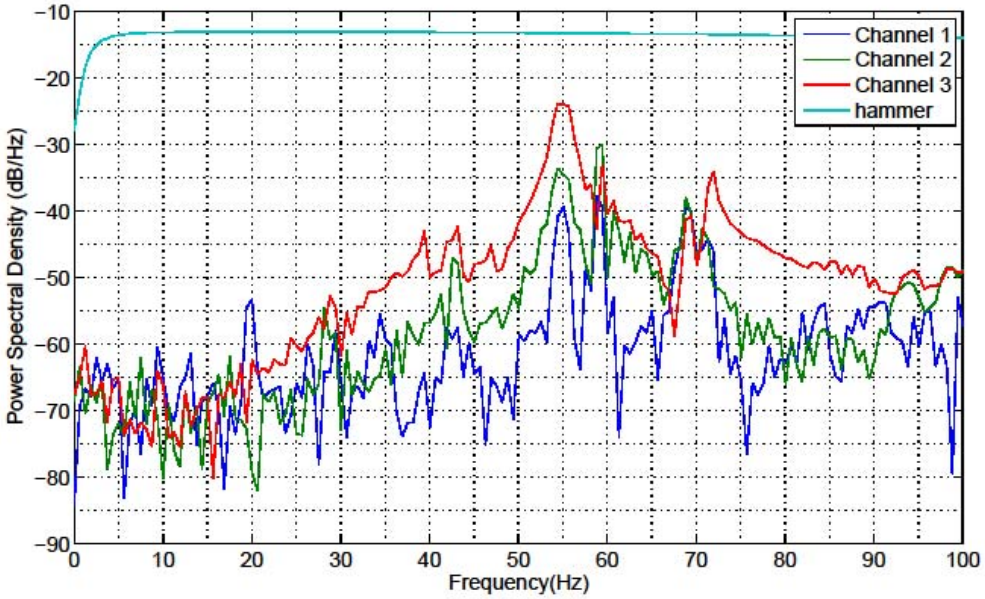

Figure A.3.30 Power Spectral Density plot for the best longitudinal impact for COMP5

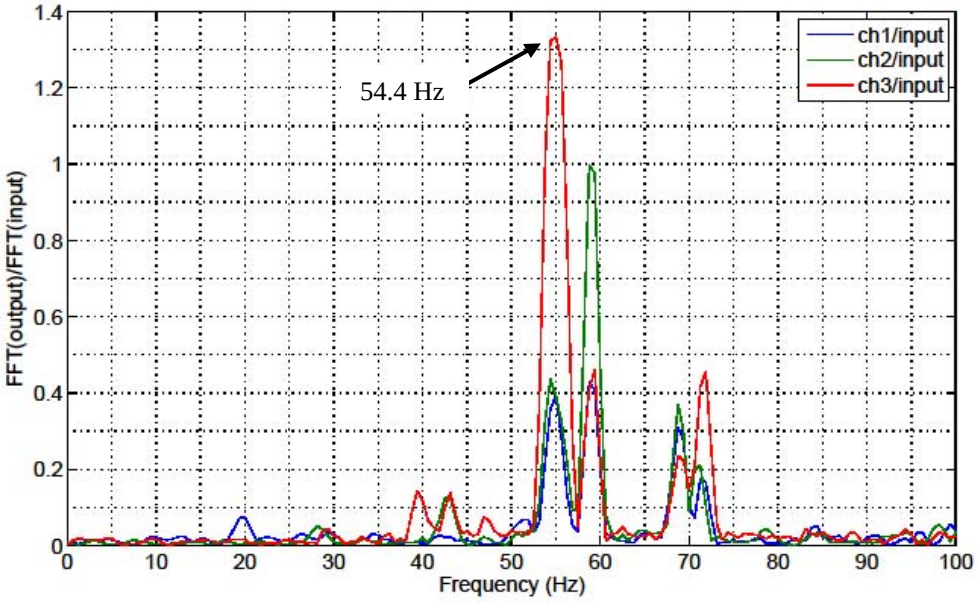

Figure A.3.31 Frequency Response Function plot for the best longitudinal impact for COMP5

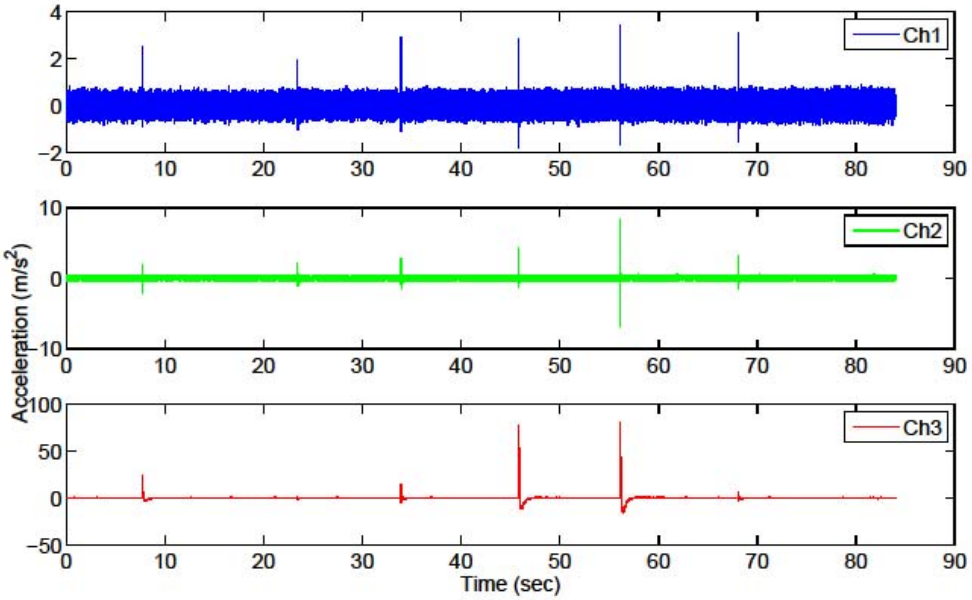

Figure A.3.32 Acceleration time histories for the entire duration for lateral impacts on COMP6

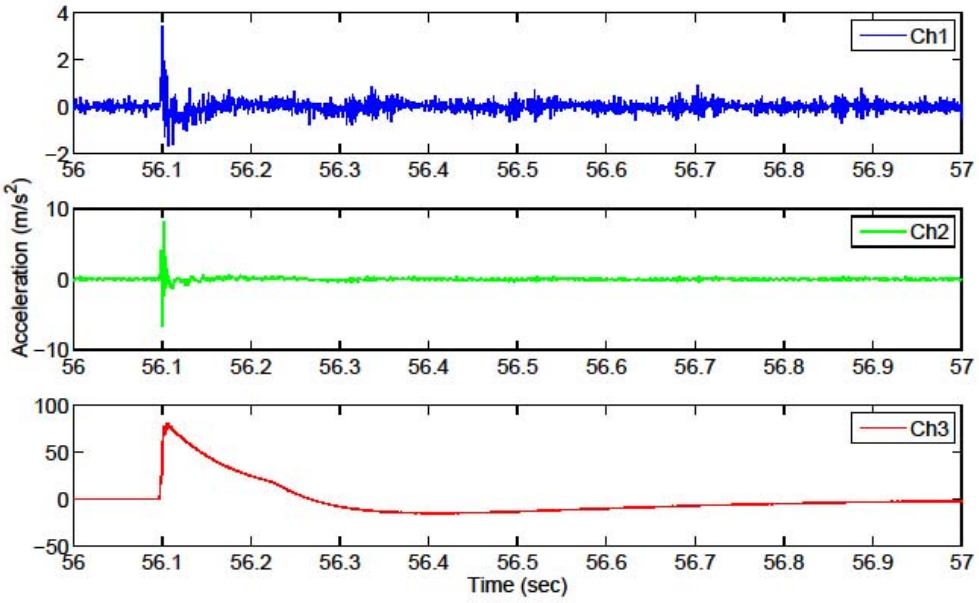

Figure A.3.33 Enlarged acceleration time histories for the best lateral impact on COMP6

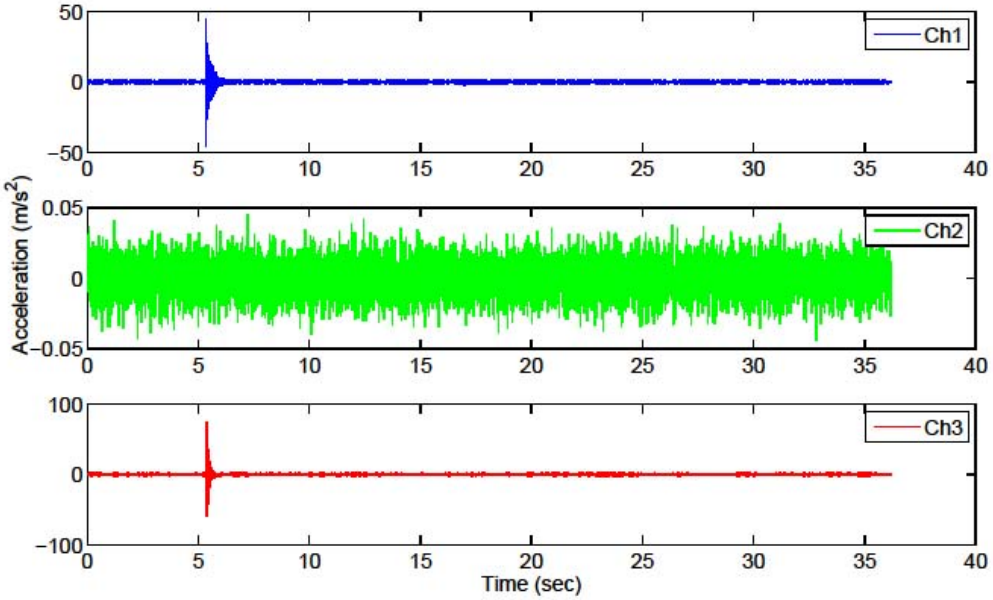

Figure A.3.34 Acceleration time histories for the entire duration for longitudinal impacts on COMP6

Note: The PSD and FRF plots for COMP 6 were not available. The impact tests for this component was not successful.

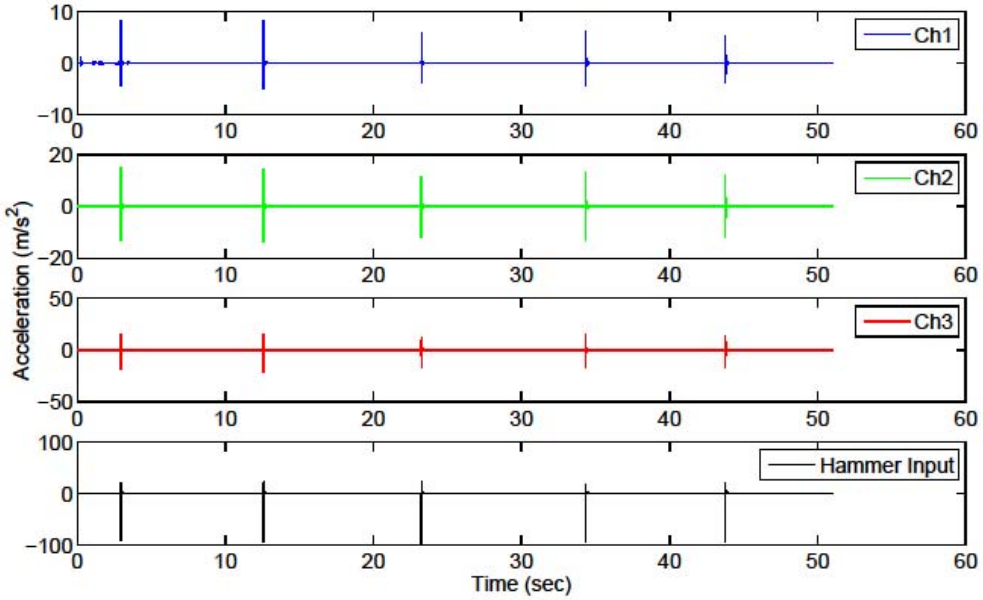

Figure A.3.35 Acceleration time histories for the entire duration for lateral impacts on COMP7

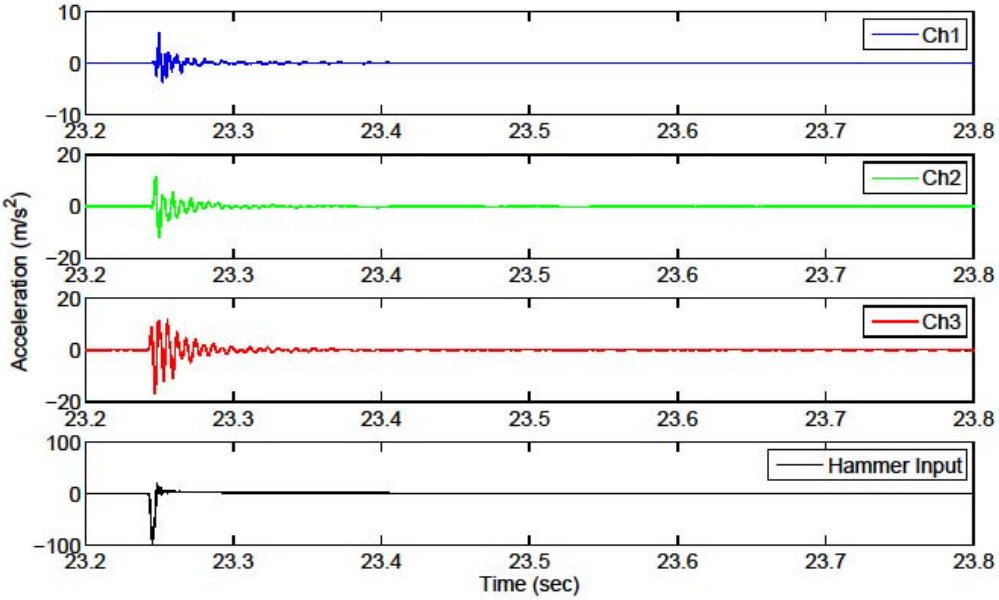

Figure A.3.36 Enlarged acceleration time histories for the best lateral impact on COMP7

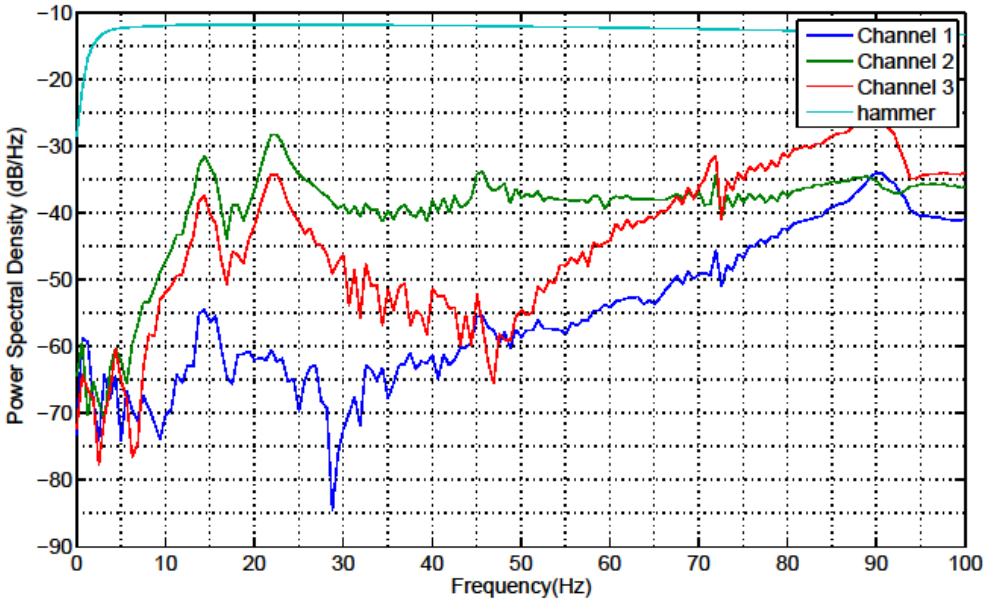

Figure A.3.37 Power Spectral Density plot for the best lateral impact for COMP7

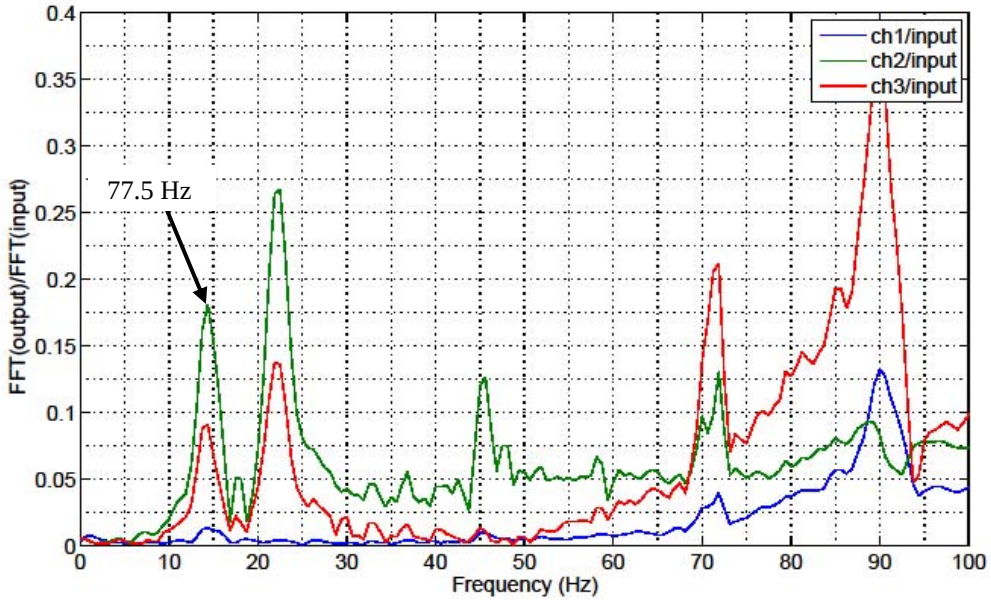

Figure A.3.38 Frequency Response Function plot for the best lateral impact for COMP7

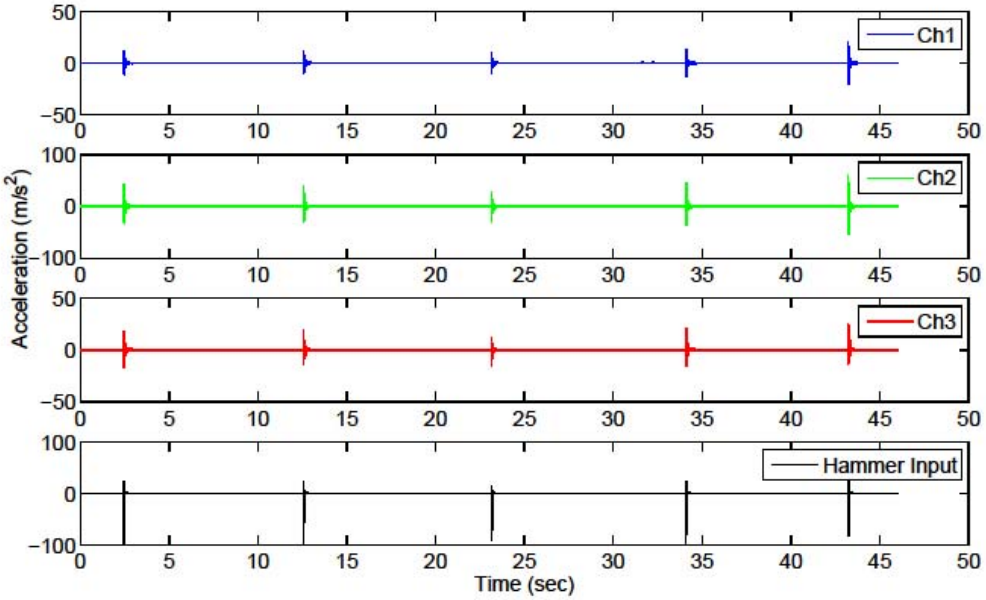

Figure A.3.39 Acceleration time histories for the entire duration for lateral impacts on COMP8

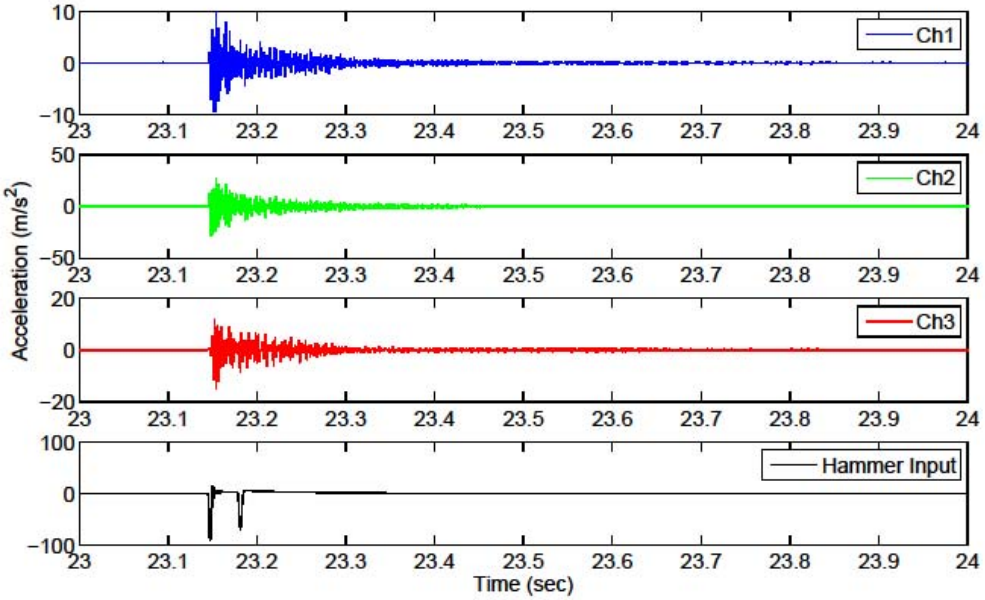

Figure A.3.40 Enlarged acceleration time histories for the best lateral impact on COMP8

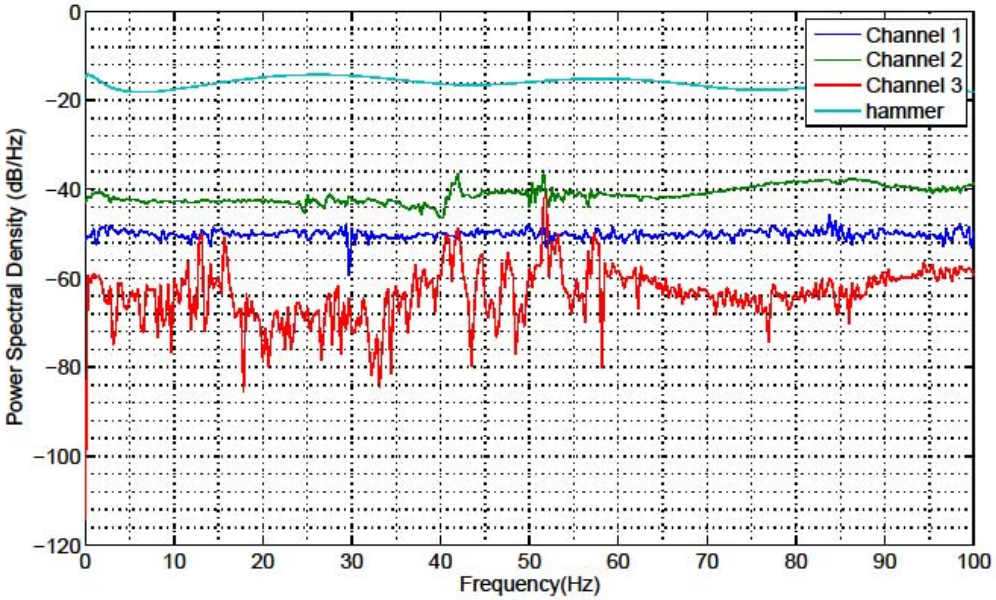

Figure A.3.41 Power Spectral Density plot for the best lateral impact for COMP8

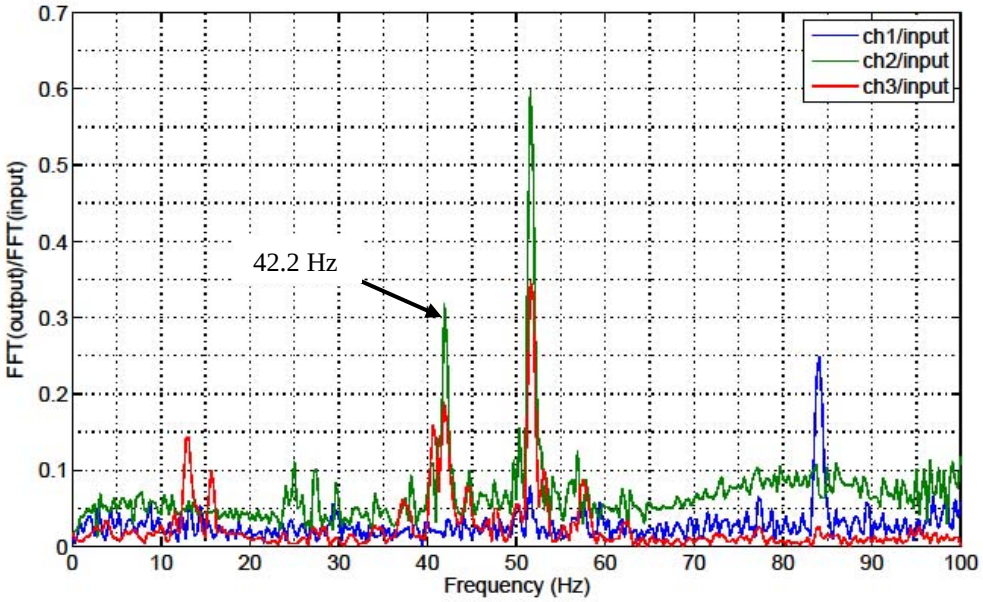

Figure A.3.42 Frequency Response Function plot for the best lateral impact for COMP8

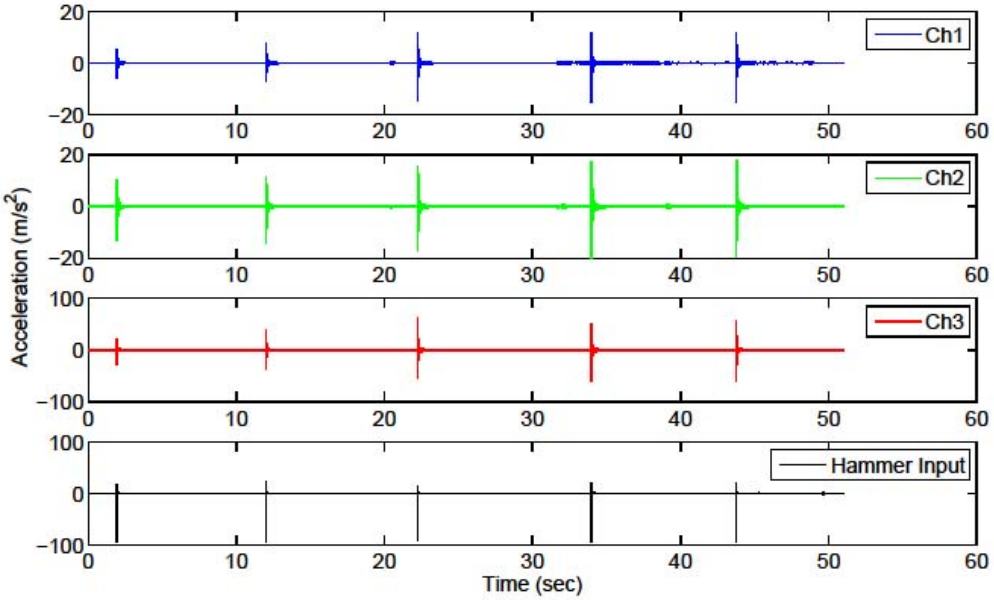

Figure A.3.43 Acceleration time histories for the entire duration for longitudinal impacts on COMP8

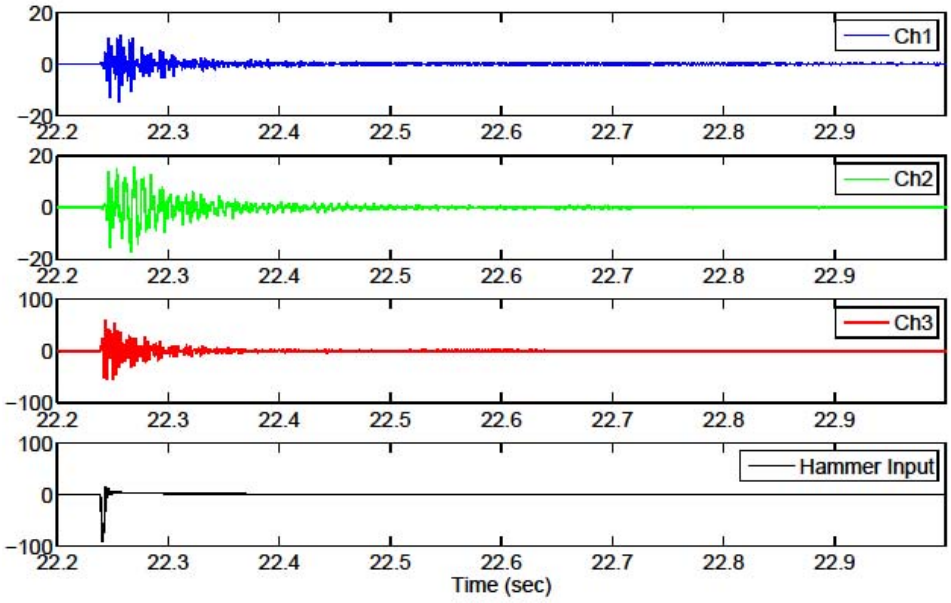

Figure A.3.44 Enlarged acceleration time histories for the best longitudinal impact on COMP8

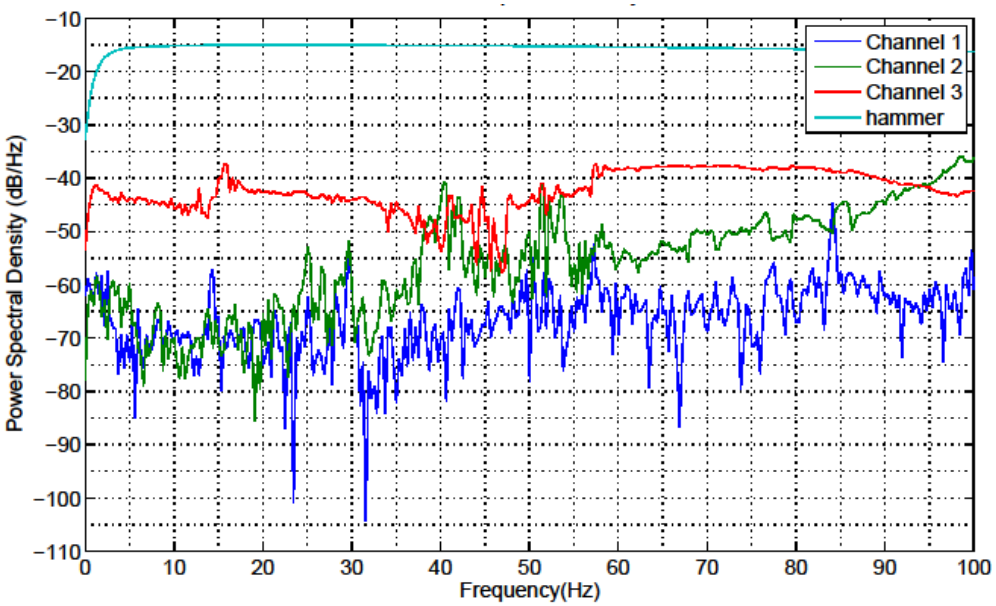

Figure A.3.45 Power Spectral Density plot for the best longitudinal impact for COMP8

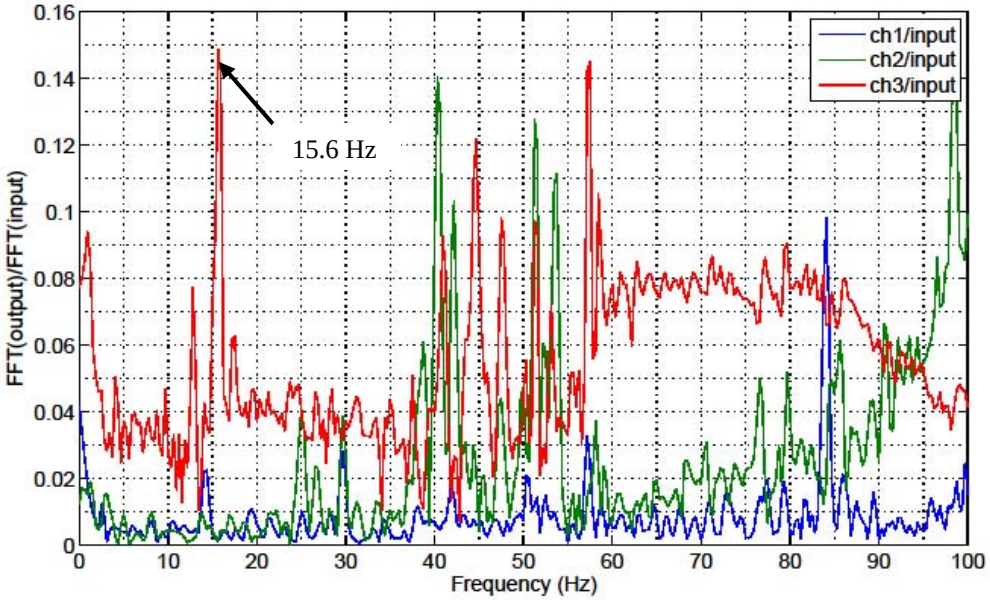

Figure A.3.46 Frequency Response Function plot for the best longitudinal impact for COMP8

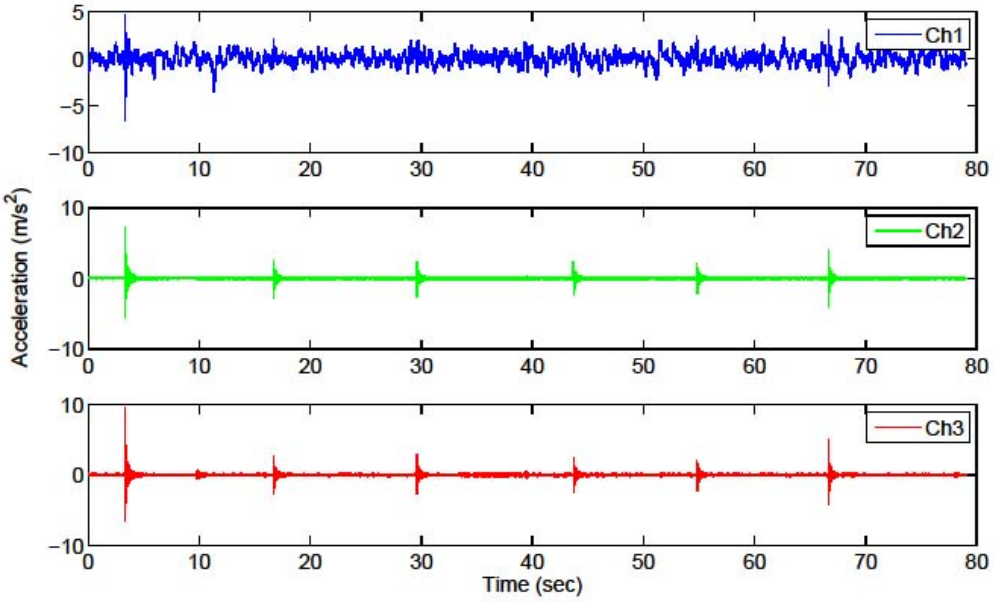

Figure A.3.47 Acceleration time histories for the entire duration for lateral impacts on COMP9

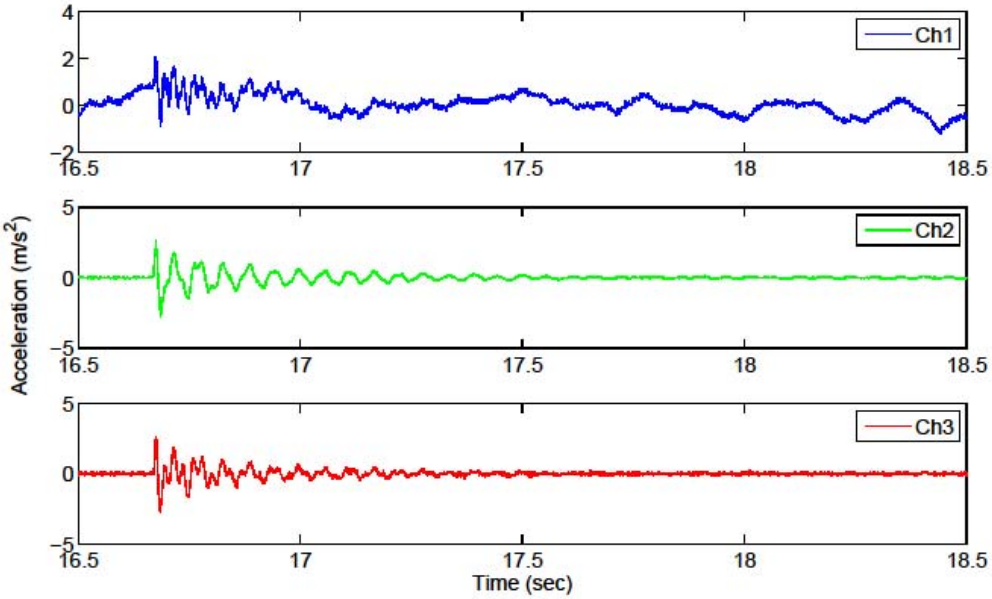

Figure A.3.48 Enlarged acceleration time histories for the best lateral impact on COMP9

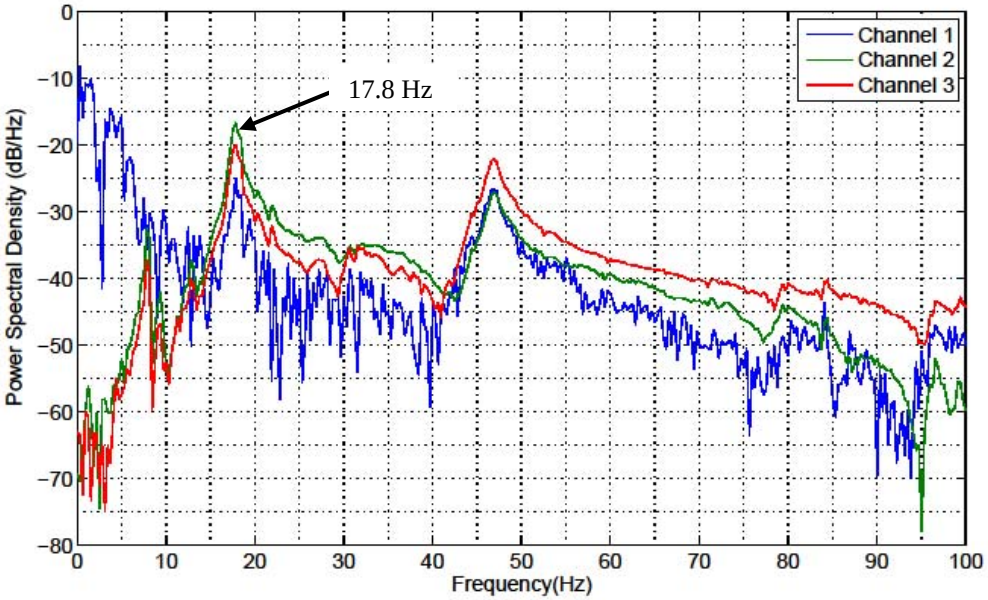

Figure A.3.49 Power Spectral Density plot for the best lateral impact for COMP9

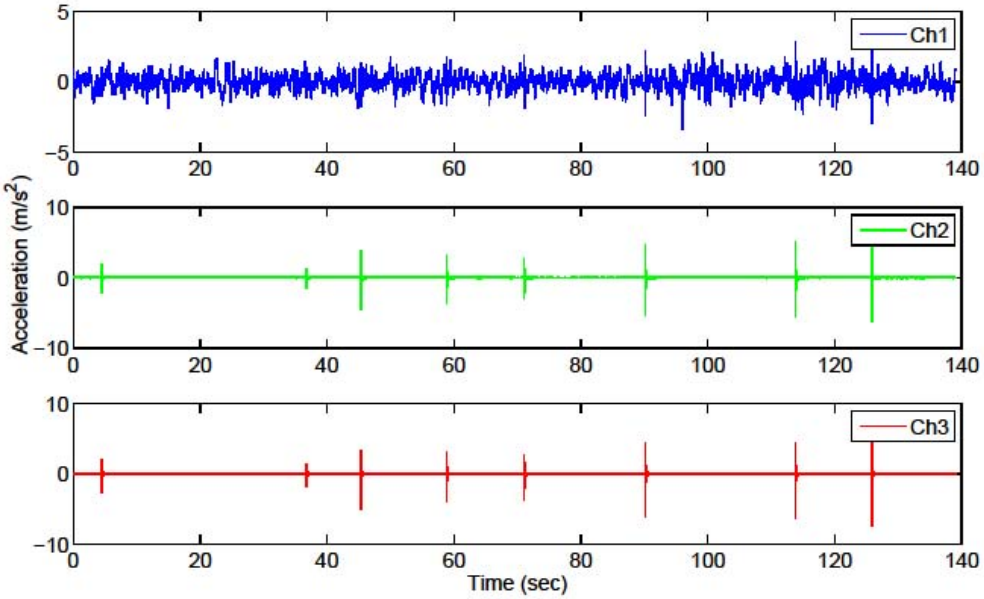

Figure A.3.50 Acceleration time histories for the entire duration for longitudinal impacts on COMP9

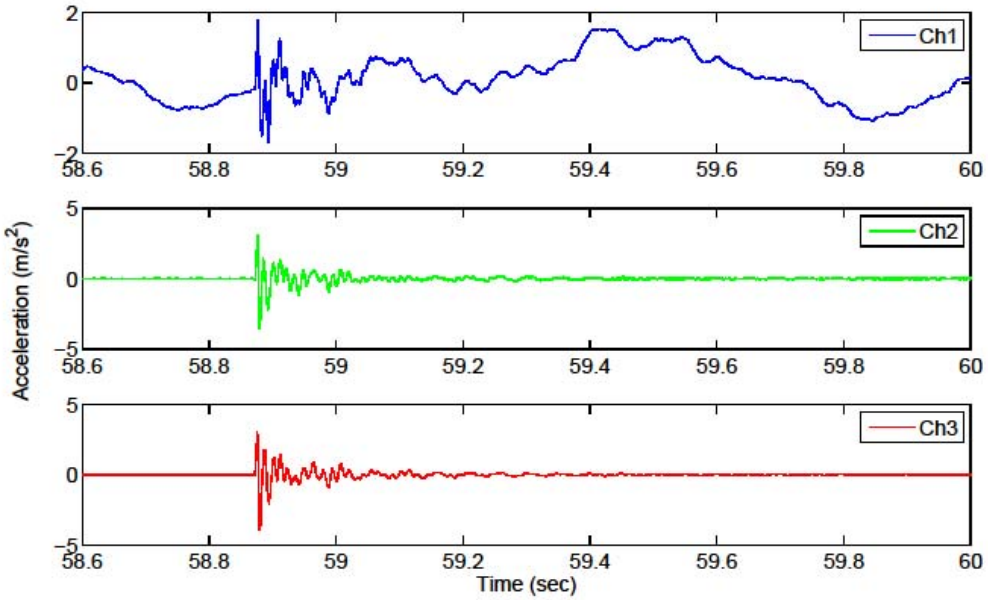

Figure A.3.51 Enlarged acceleration time histories for the best longitudinal impact on COMP9

Figure A.3.52Figure A.3.53

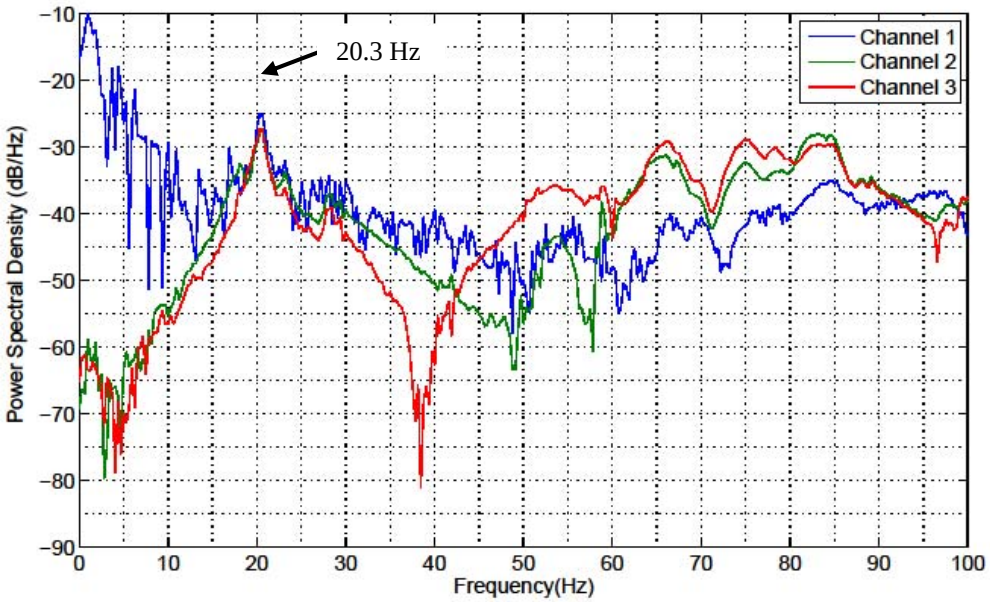

Figure A.3.54 Power Spectral Density plot for the best longitudinal impact for COMP9

Appendix B

Ambient Vibration Testing Photos and Data Processing Figures

This appendix contains the information for the ambient floor vibration testing at the roof level (also referred to as penthouse) as presented below. The results were utilized to identify the dominant frequencies of the building and detect the machine operation frequencies.

B.1 A screenshot of the ViewWave program for generating power density spectrum for the measured signals and a sample set of decimated time histories (acceleration, velocity and displacement time histories)

B.2 Processed power spectral density vs. frequency plots for all 8 testing locations.

Each recording was taken at a sampling rate of 1000 Hz for roughly 10 minutes (600,000 data points). To speed up the data processing, the data was decimated to 100 Hz (60,000 data points). And the decimated sampling rate (100 Hz) was deemed reasonable for the purpose of this testing.

B.1 Testing Setup Photos

This subsection of Appendix B contains the photos taken during the ambient vibration tests at eight locations on the penthouse level of the case study building.

Figure B.1.1 Ambient vibration test setup photos for location #1-3 at penthouse level

Figure B.1.2 Ambient vibration test setup photos for location #4-5 at penthouse level

Figure B.1.3 Ambient vibration test setup photos for location #6-7at penthouse level

Figure B.1.4 Ambient vibration test setup photo for location #8 at penthouse level

B.2 Decimated Time History Data

The raw time history recordings of the ambient tests were decimated down to 100 Hz. Following includes a screenshot of the ViewWave program used to complete the decimation and a sample set of acceleration, velocity and displacement time histories after decimation.

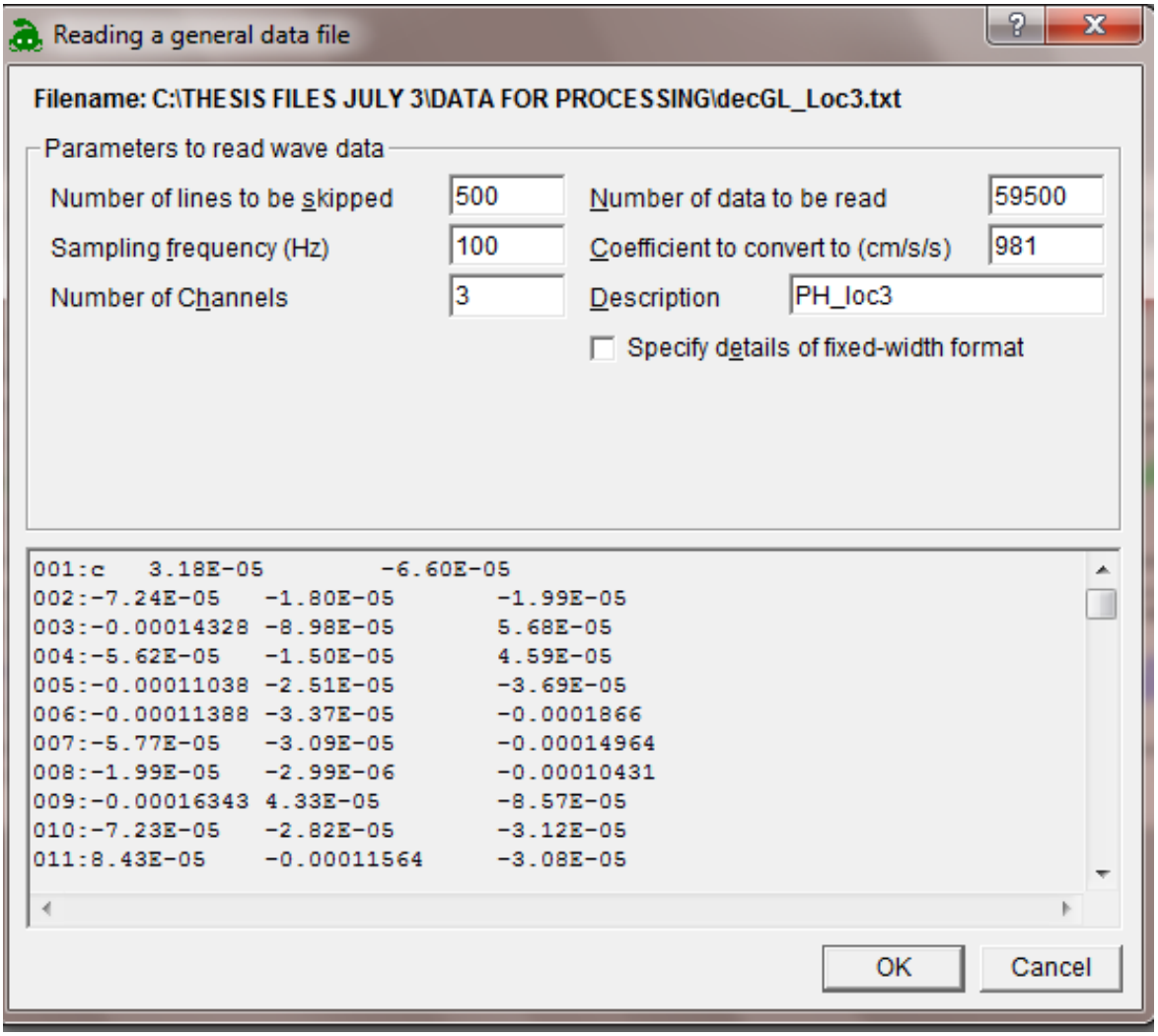

Figure B.2.1 Screenshot of the ViewWave program for generating the PSD plots

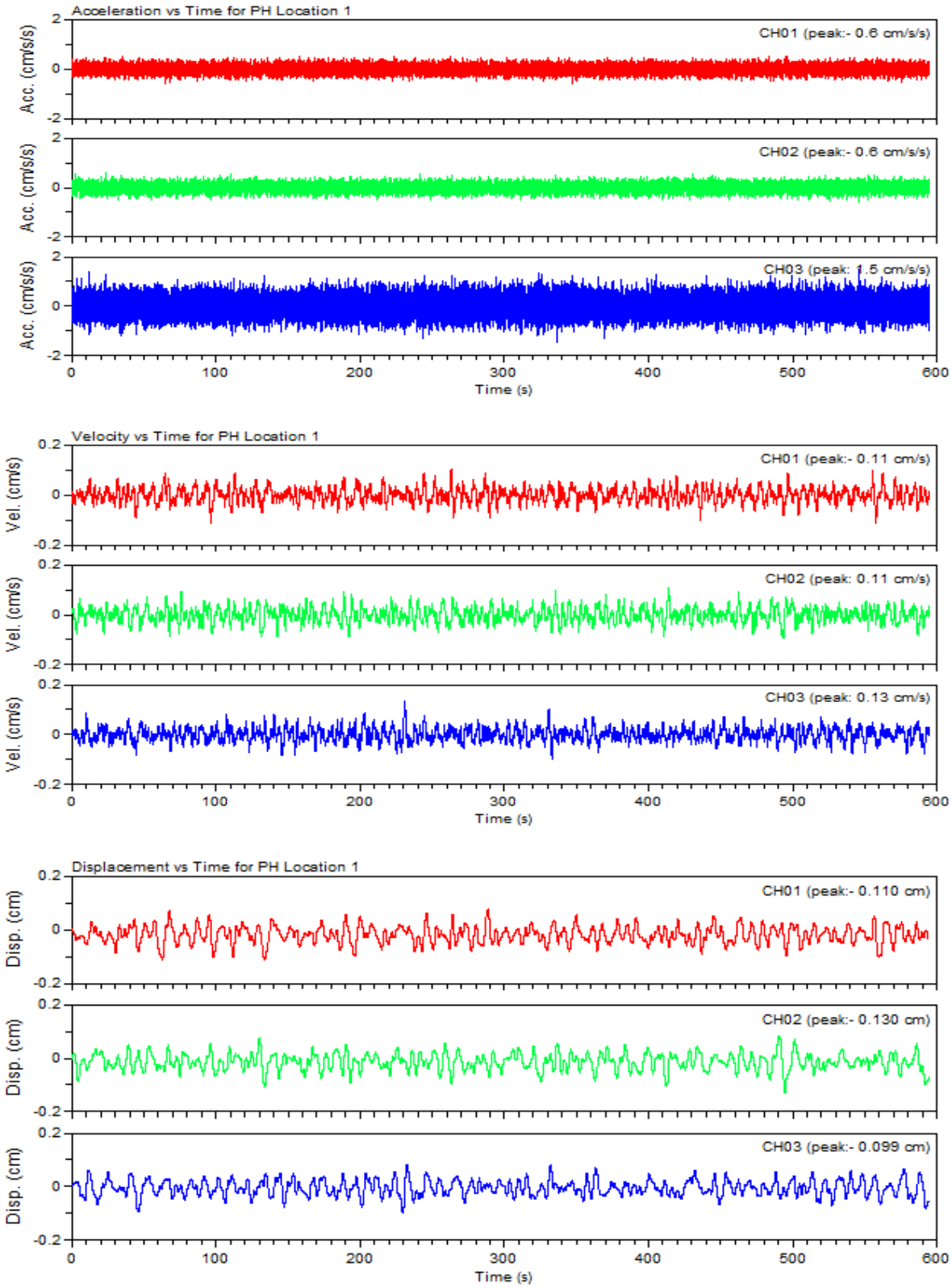

Figure B.2.2 Decimated acceleration, velocity and displacement time histories measured at Location 1

B.3 Log-log Power Spectral Density Plots for Frequency Range 0 to 50 Hz

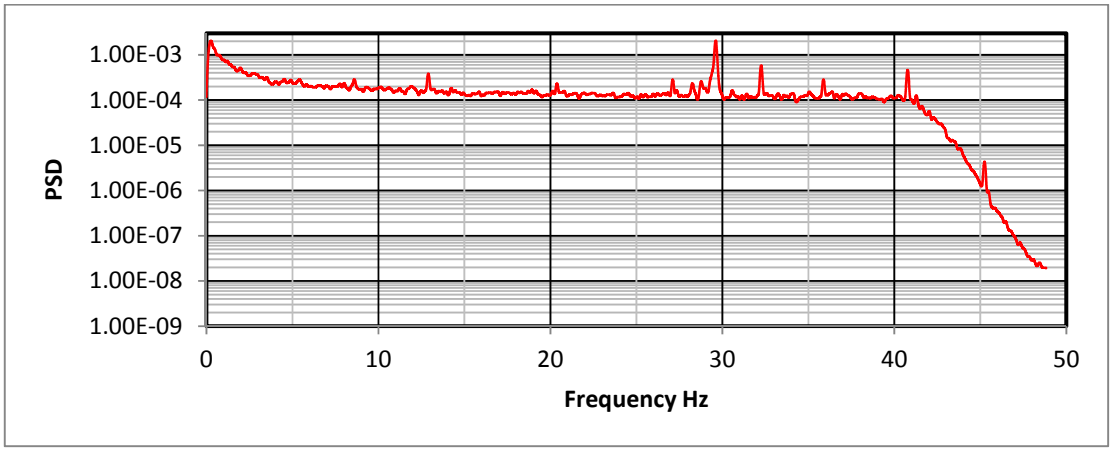

Figure B.3.1 Log-normal PSD plot for N-S direction at Location 1

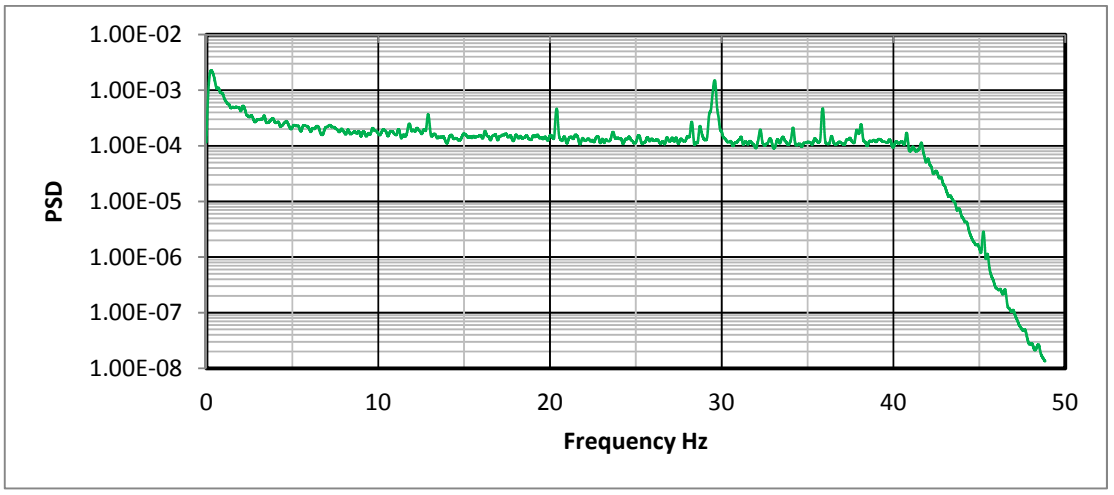

Figure B.3.2 Log-normal PSD plot for E-W direction at Location 1

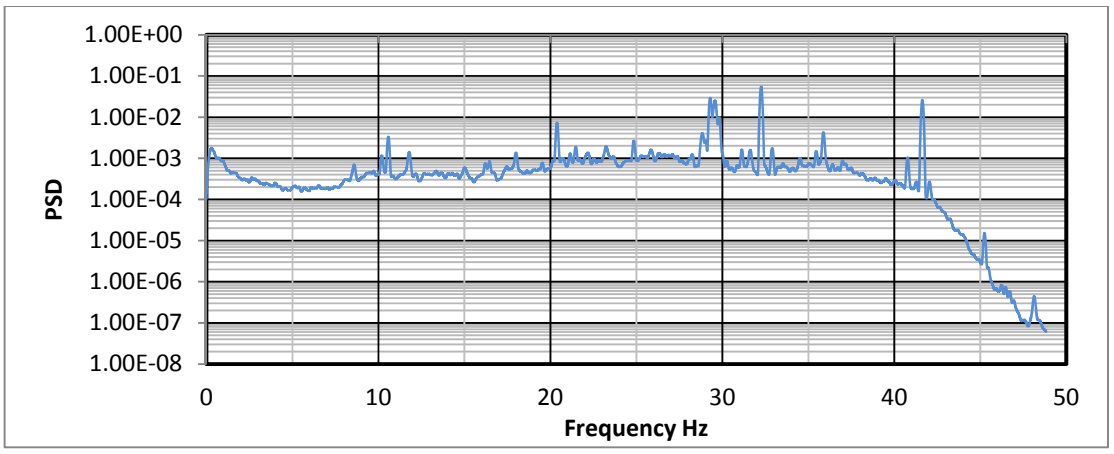

Figure B.3.3 Log-normal PSD plot for vertical direction at Location 1

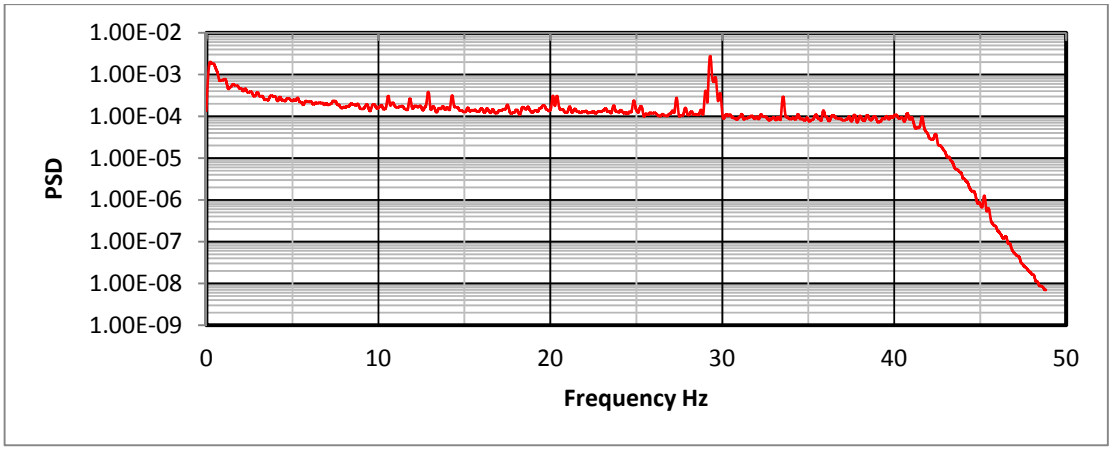

Figure B.3.4 Log-normal PSD plot for N-S direction at Location 2

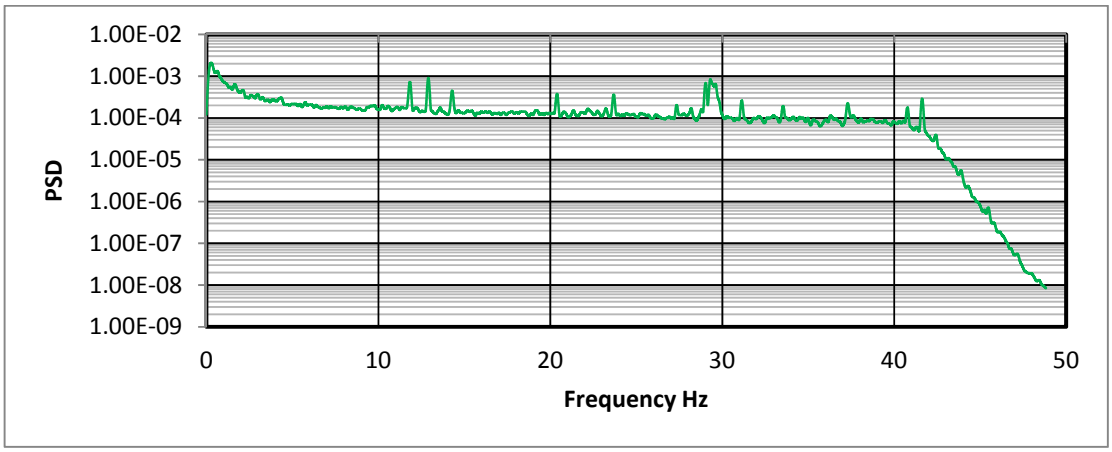

Figure B.3.5 Log-normal PSD plot for E-W direction at Location 2

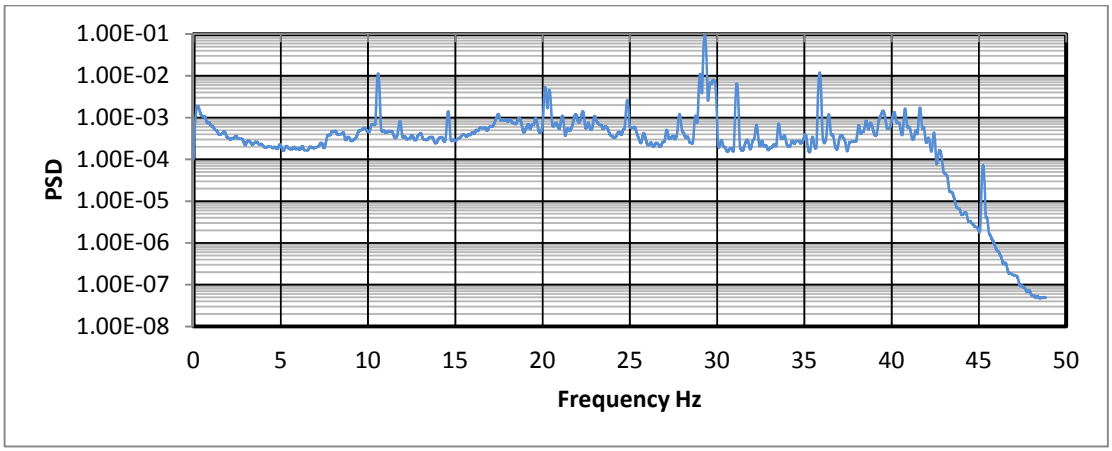

Figure B.3.6 Log-normal PSD plot for vertical direction at Location 2

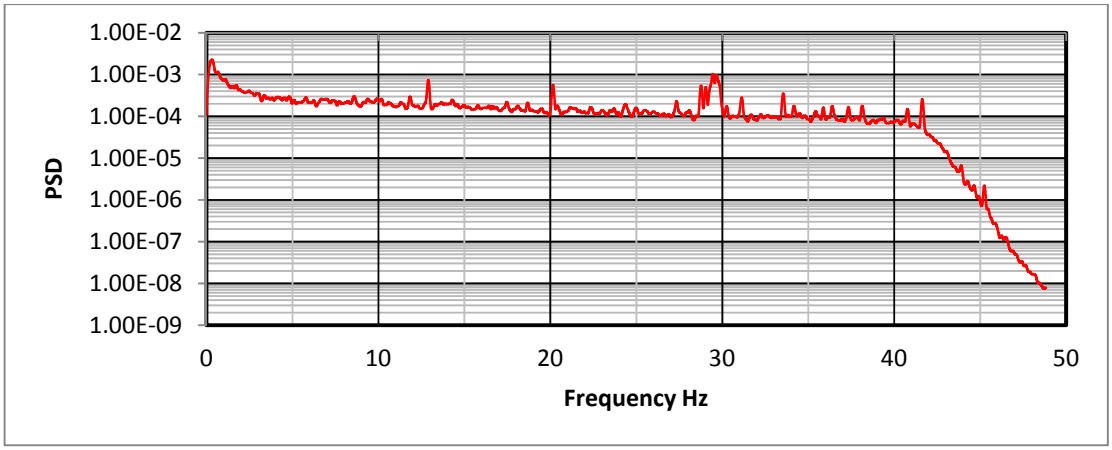

Figure B.3.7 Log-normal PSD plot for N-S direction at Location 3

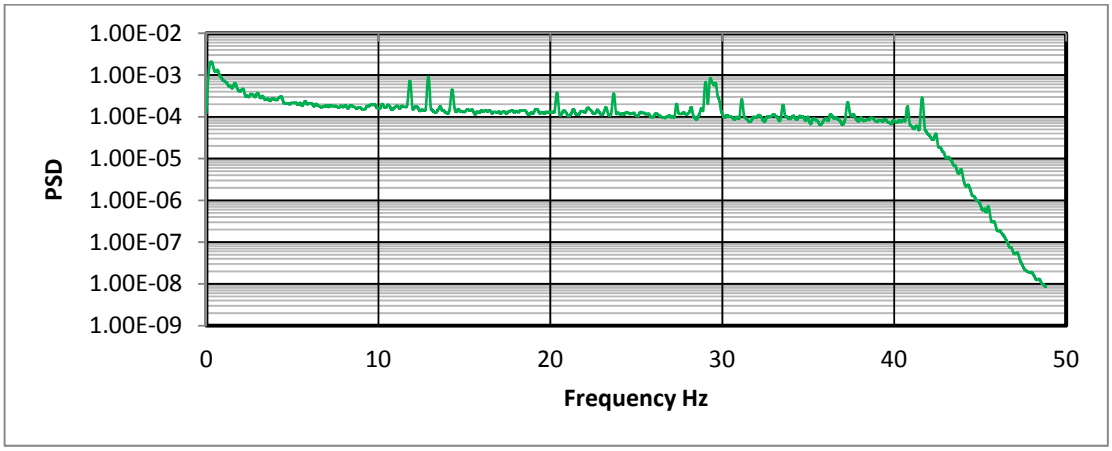

Figure B.3.8 Log-normal PSD plot for E-W direction at Location 3

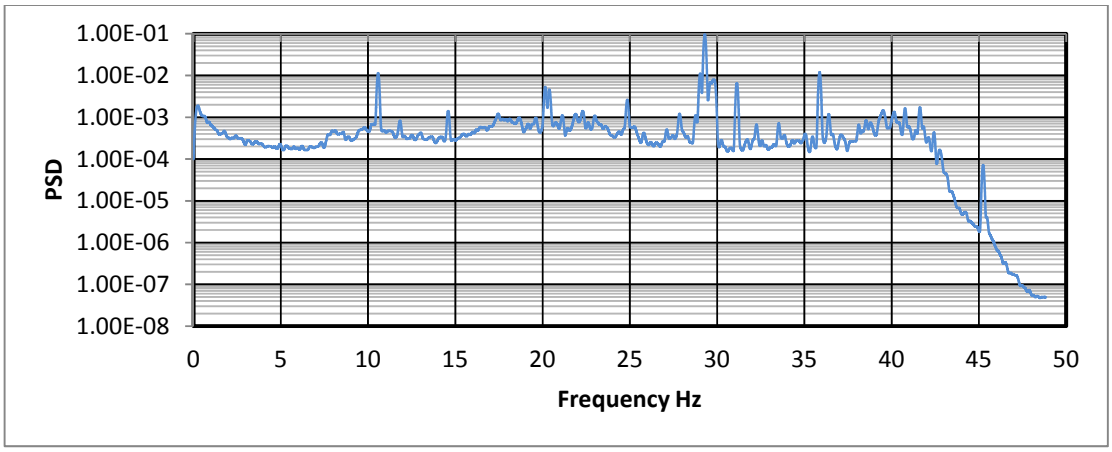

Figure B.3.9 Log-normal PSD plot for vertical direction at Location 3

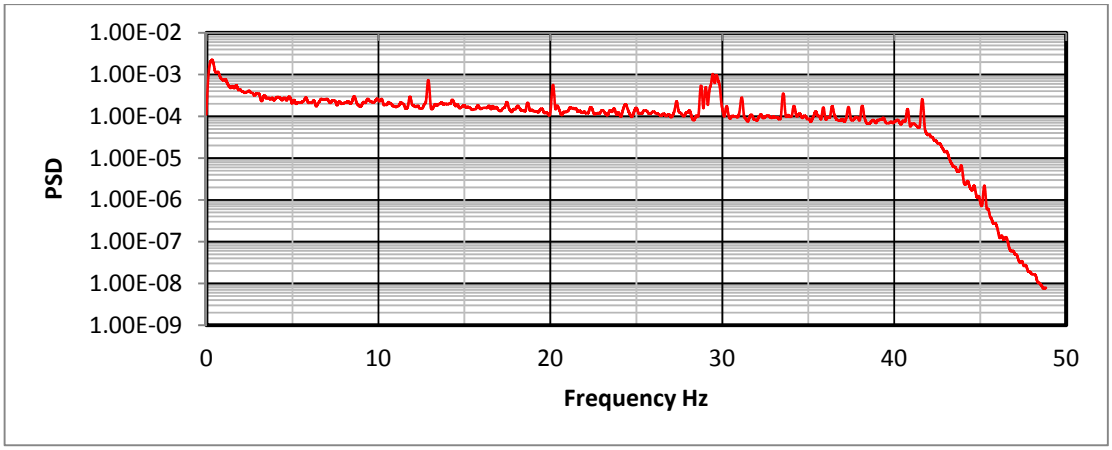

Figure B.3.10 Log-normal PSD plot for N-S direction at Location 4

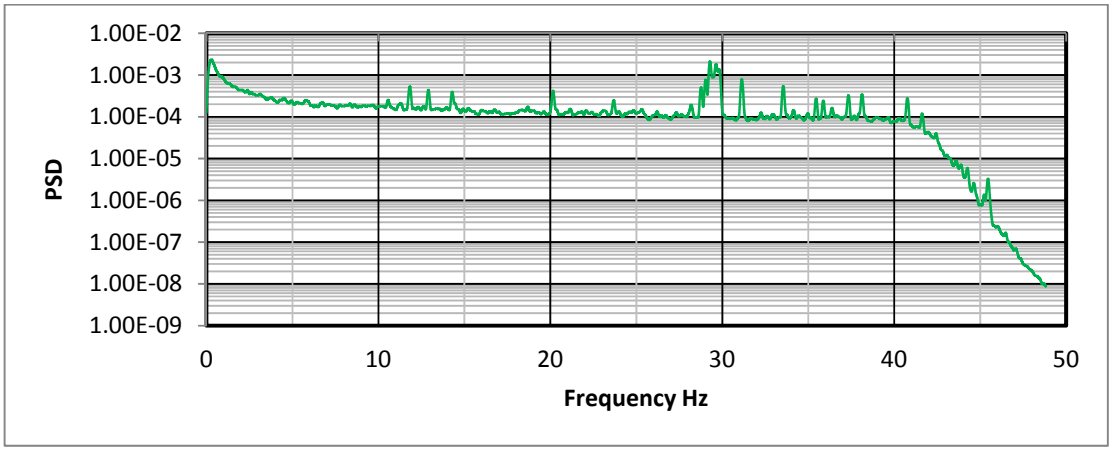

Figure B.3.11 Log-normal PSD plot for E-W direction at Location 4

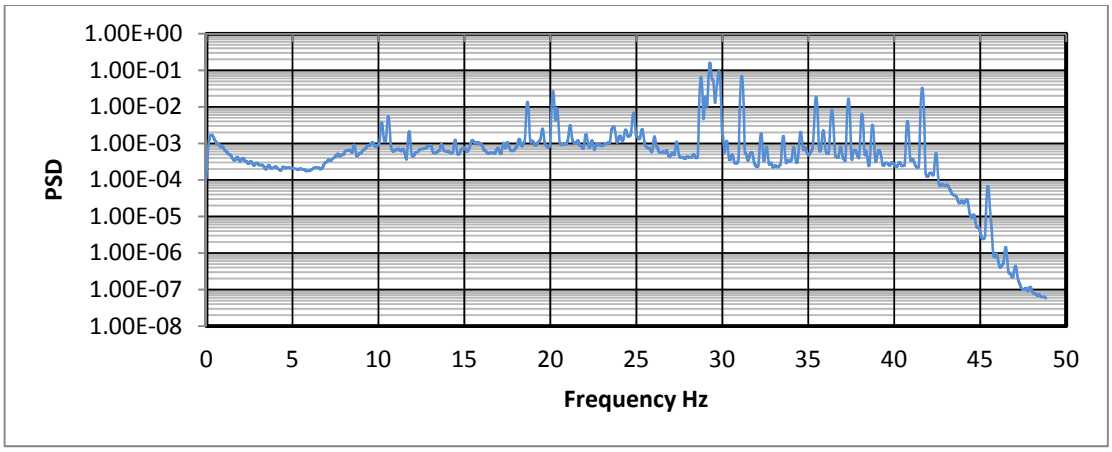

Figure B.3.12 Log-normal PSD plot for vertical direction at Location 4

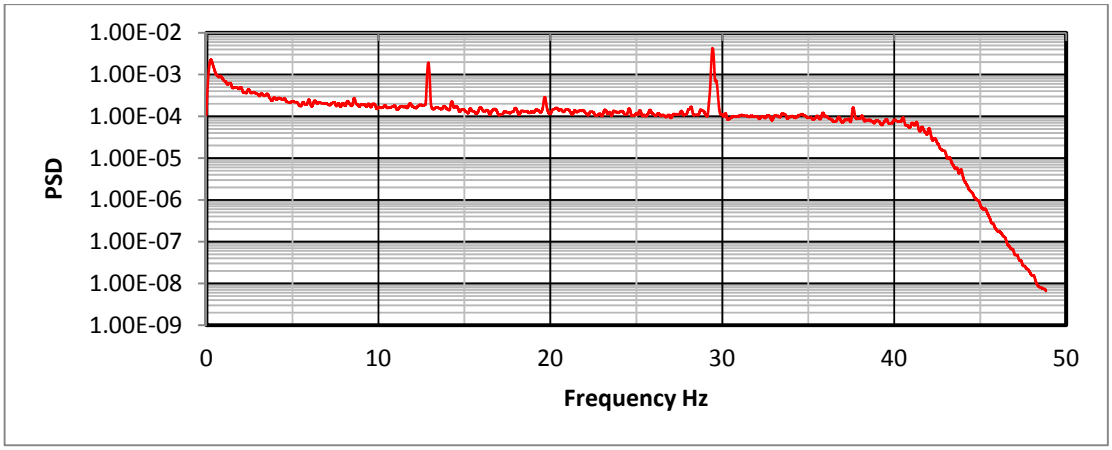

Figure B.3.13 Log-normal PSD plot for N-S direction at Location 5

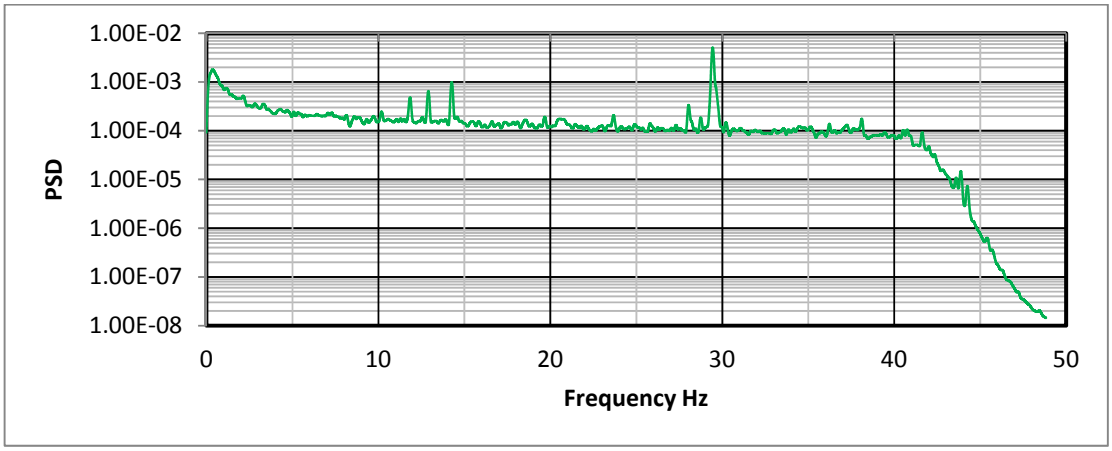

Figure B.3.14 Log-normal PSD plot for E-W direction at Location 5

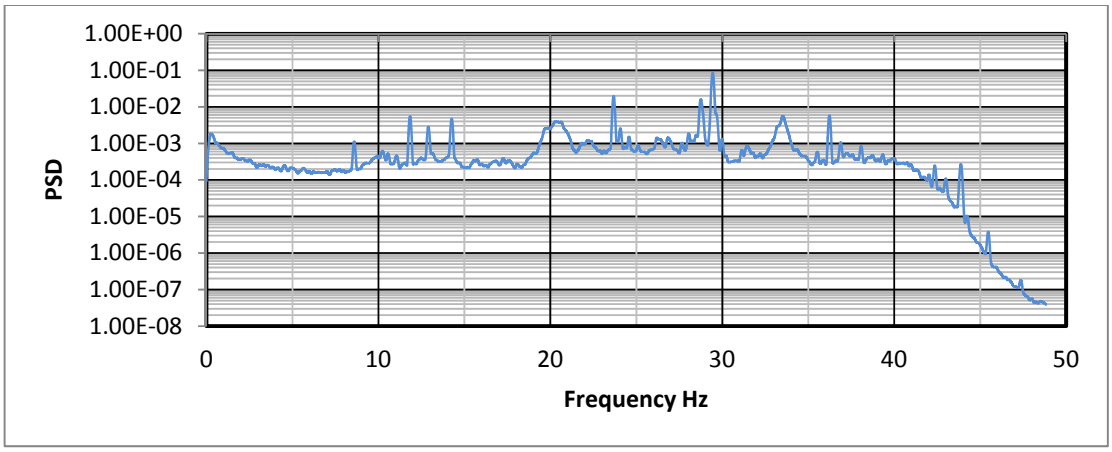

Figure B.3.15 Log-normal PSD plot for vertical direction at Location 5

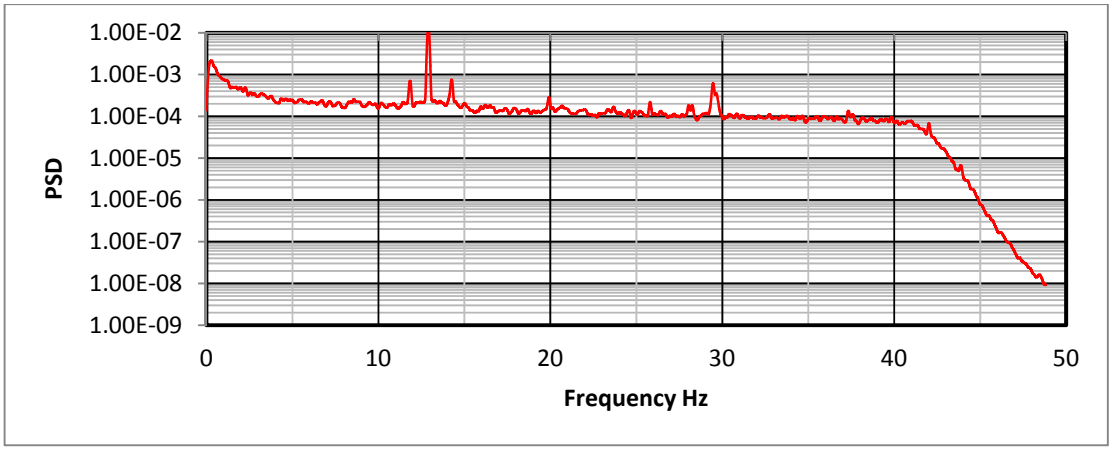

Figure B.3.16 Log-normal PSD plot for N-S direction at Location 6

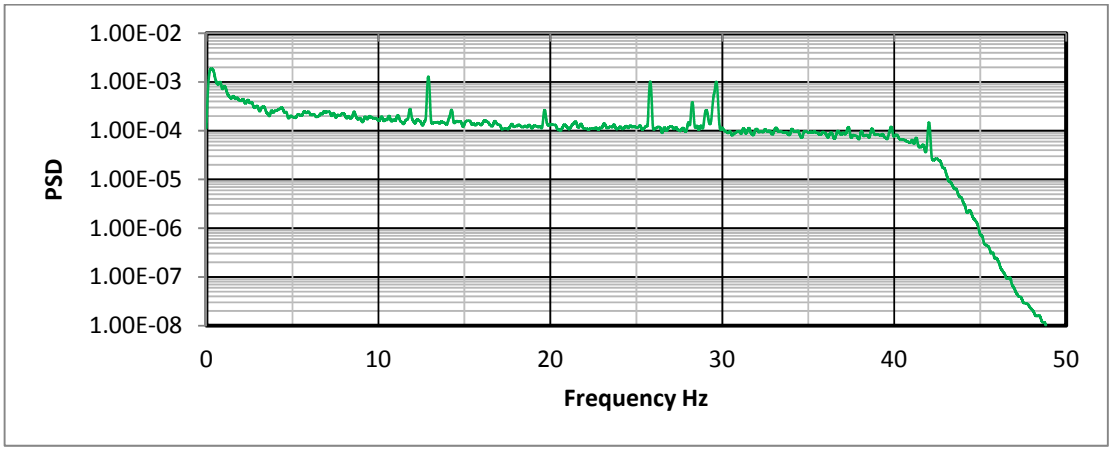

Figure B.3.17 Log-normal PSD plot for E-W direction at Location 6

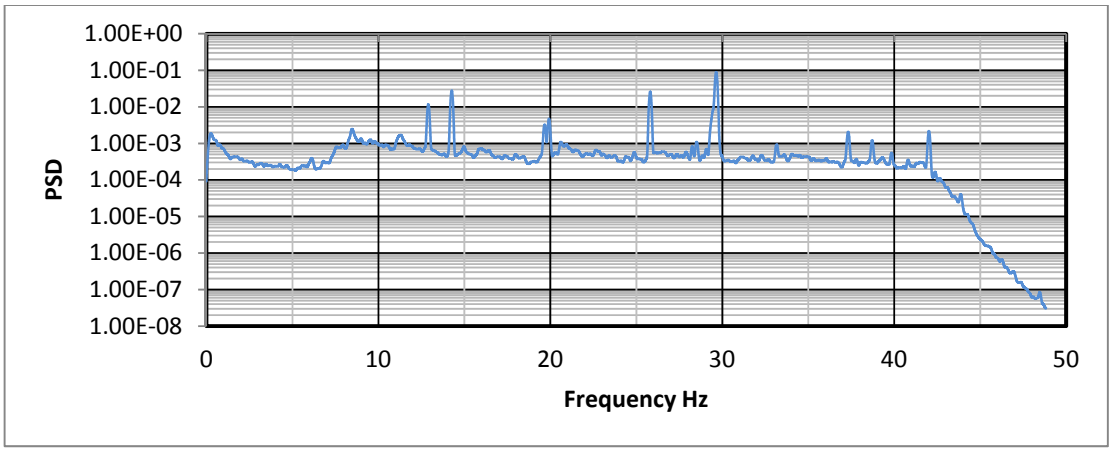

Figure B.3.18 Log-normal PSD plot for vertical direction at Location 6

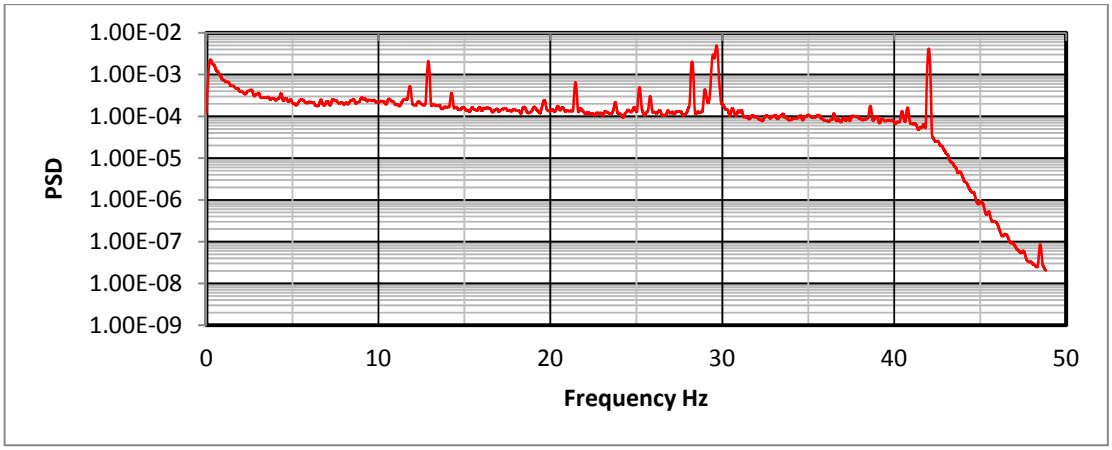

Figure B.3.19 Log-normal PSD plot for N-S direction at Location 7

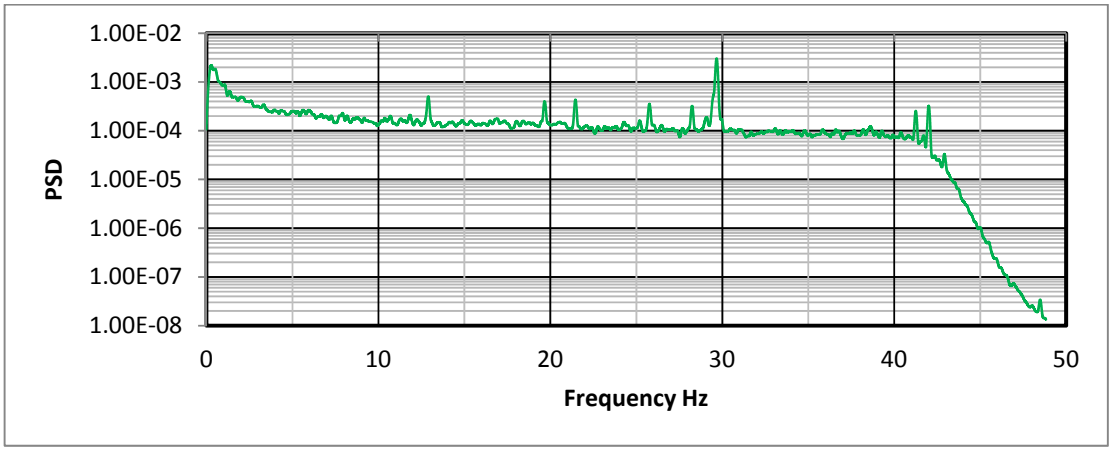

Figure B.3.20 Log-normal PSD plot for E-W direction at Location 7

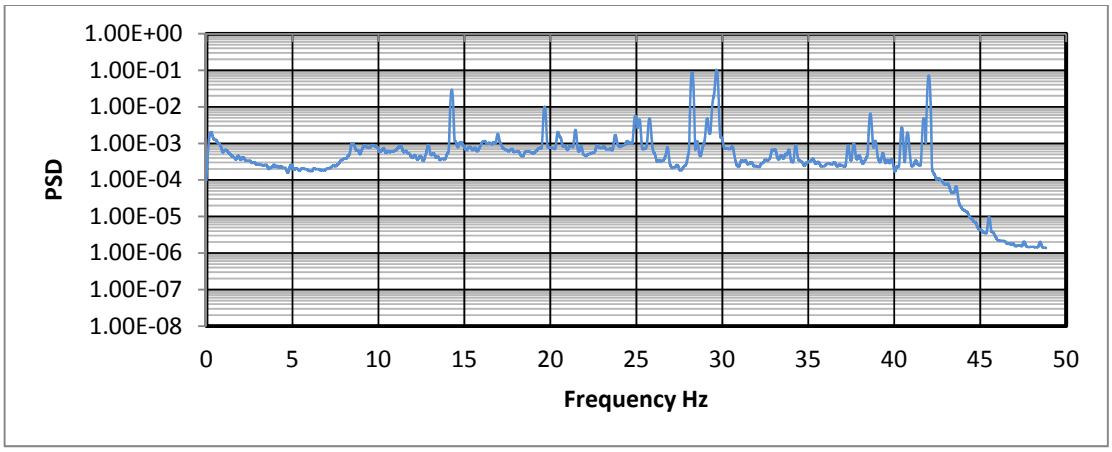

Figure B.3.21 Log-normal PSD plot for vertical direction at Location 7

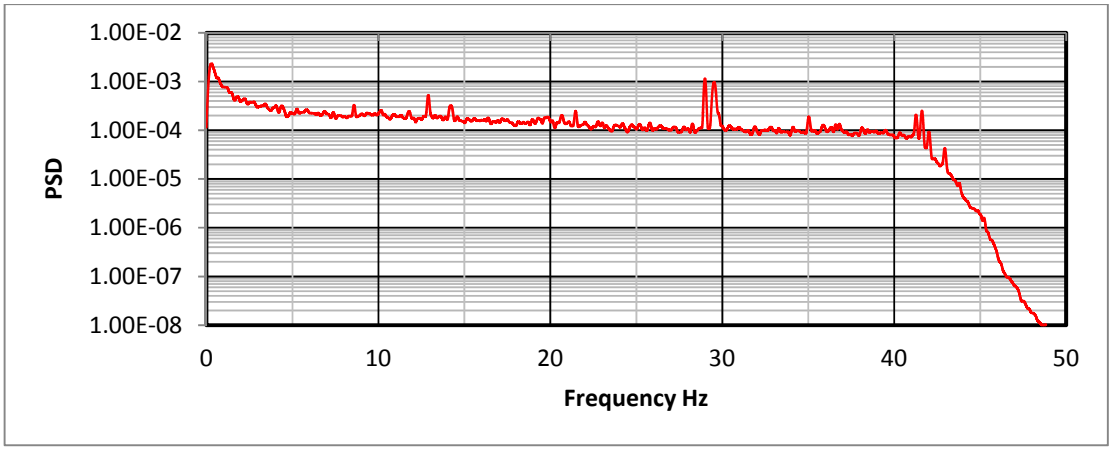

Figure B.3.22 Log-normal PSD plot for N-S direction at Location 8

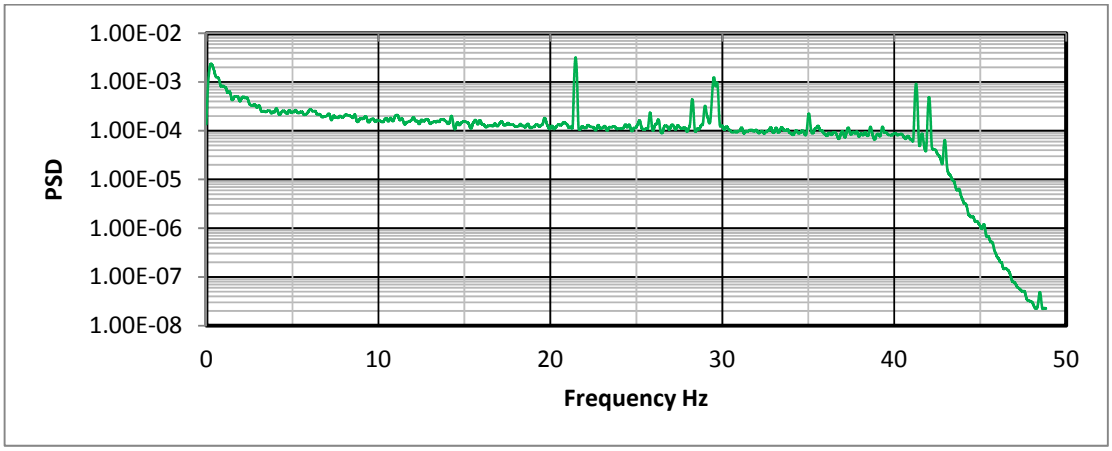

Figure B.3.23 Log-normal PSD plot for E-W direction at Location 8

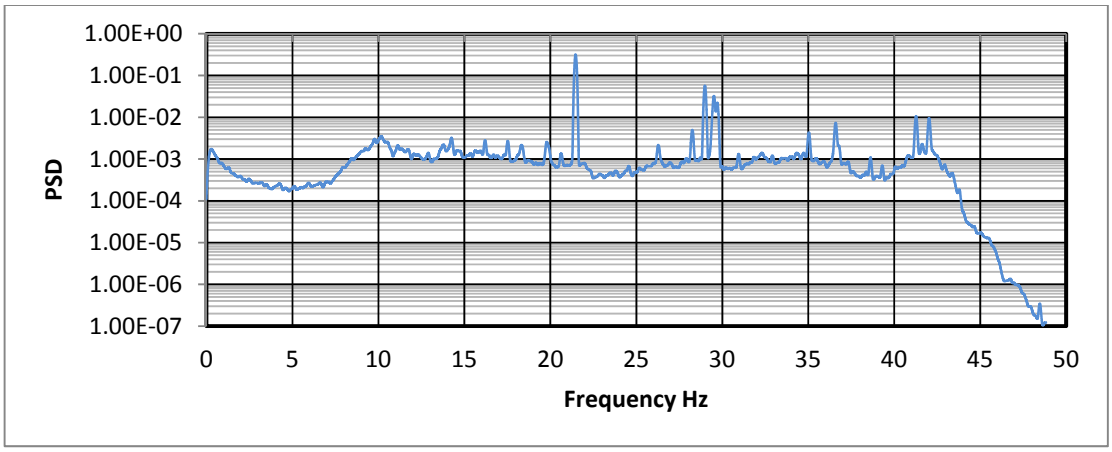

Figure B.3.24 Log-normal PSD plot for vertical direction at Location 8

B.4 Log-Log Power Spectral Density Plots for Frequency Range 1 to 10 Hz

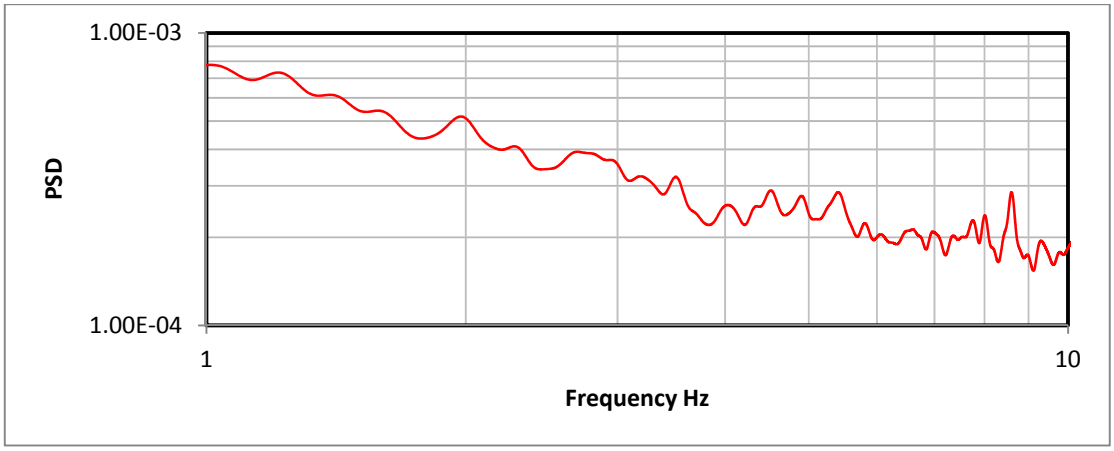

Figure B.4.1 Log-log PSD plot for N-S direction at Location 1 (1~10 Hz)

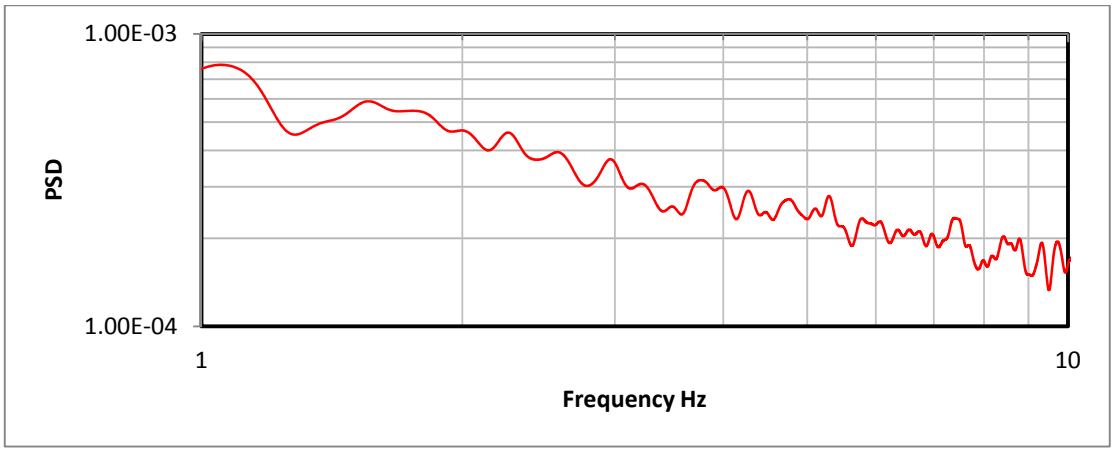

Figure B.4.2 Log-log PSD plot for N-S direction at Location 2 (1~10 Hz)

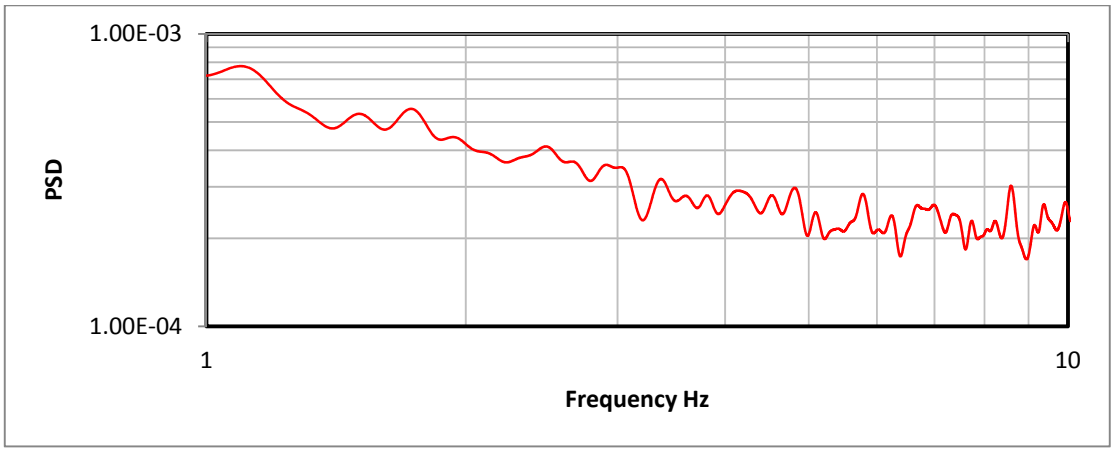

Figure B.4.3 Log-log PSD plot for N-S direction at Location 3 (1~10 Hz)

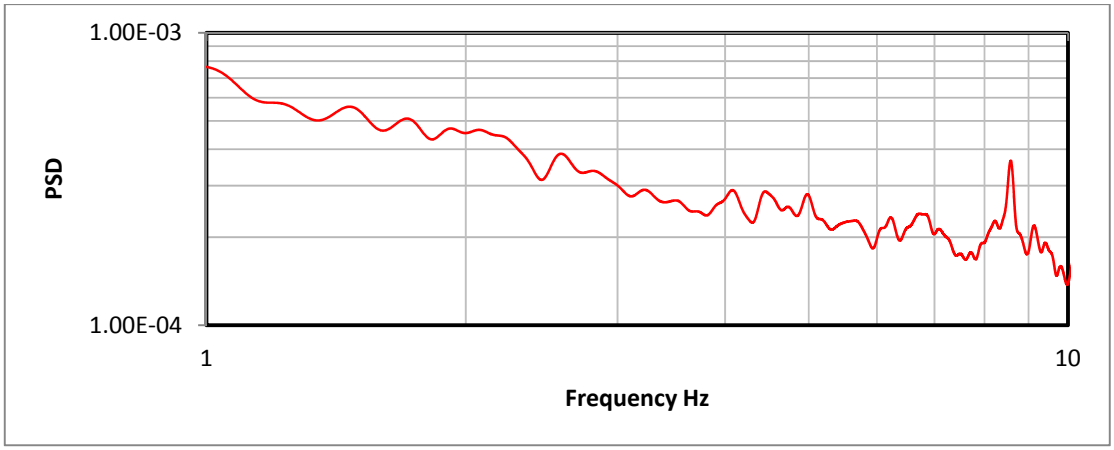

Figure B.4.4 Log-log PSD plot for N-S direction at Location 4 (1~10 Hz)

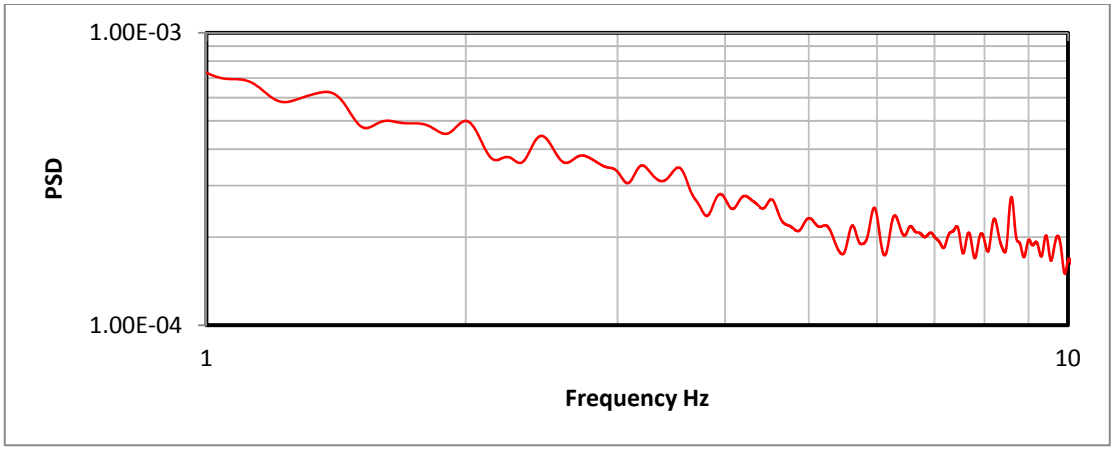

Figure B.4.5 Log-log PSD plot for N-S direction at Location 5 (1~10 Hz)

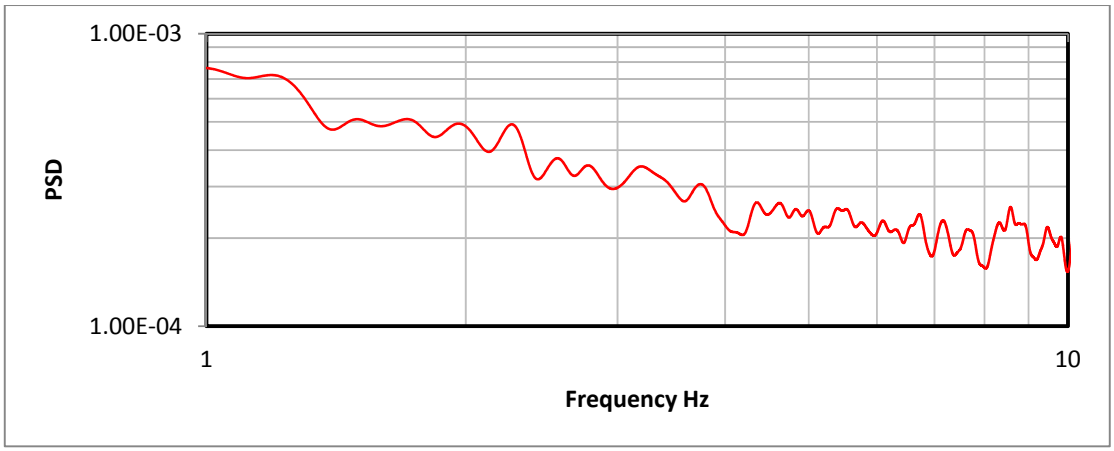

Figure B.4.6 Log-log PSD plot for N-S direction at Location 6 (1~10 Hz)

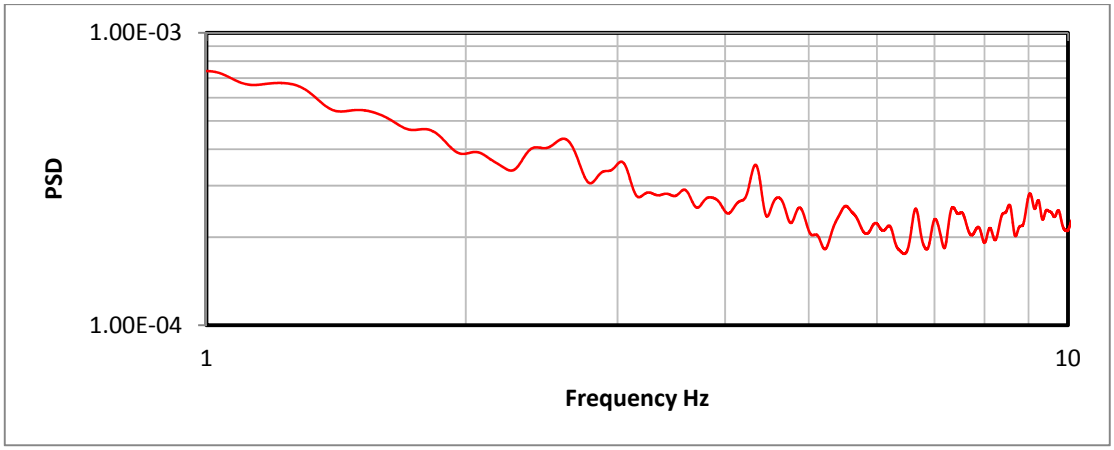

Figure B.4.7 Log-log PSD plot for N-S direction at Location 7 (1~10 Hz)

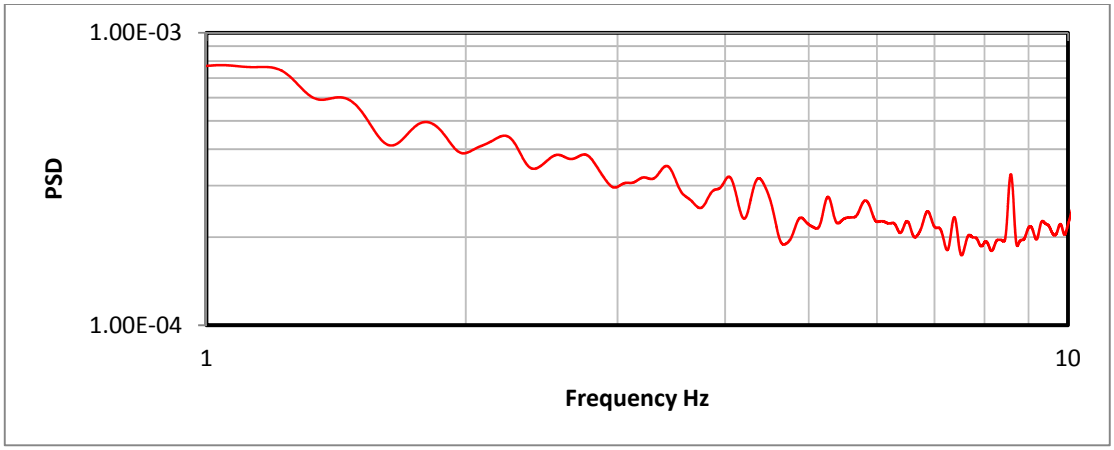

Figure B.4.8 Log-log PSD plot for N-S direction at Location 8 (1~10 Hz)

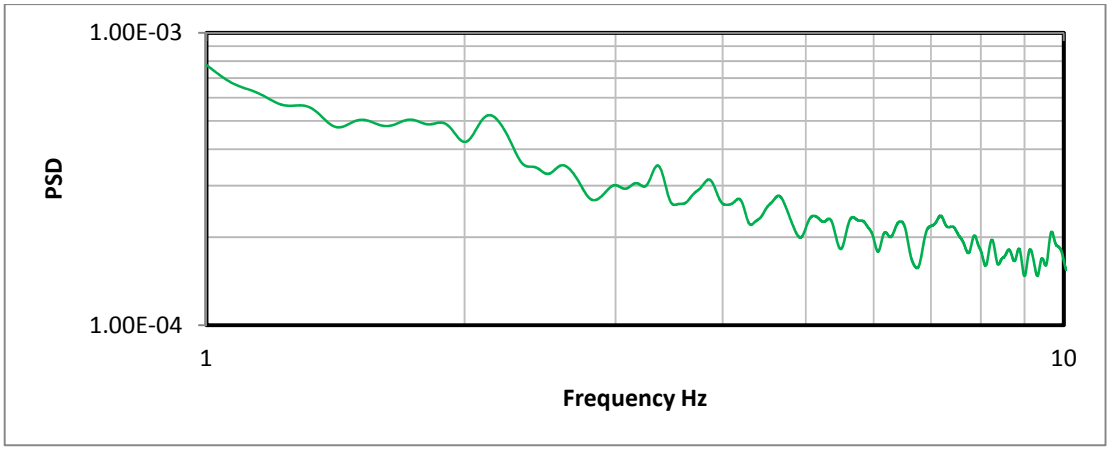

Figure B.4.9 Log-log PSD plot for E-W direction at Location 1 (1~10 Hz)

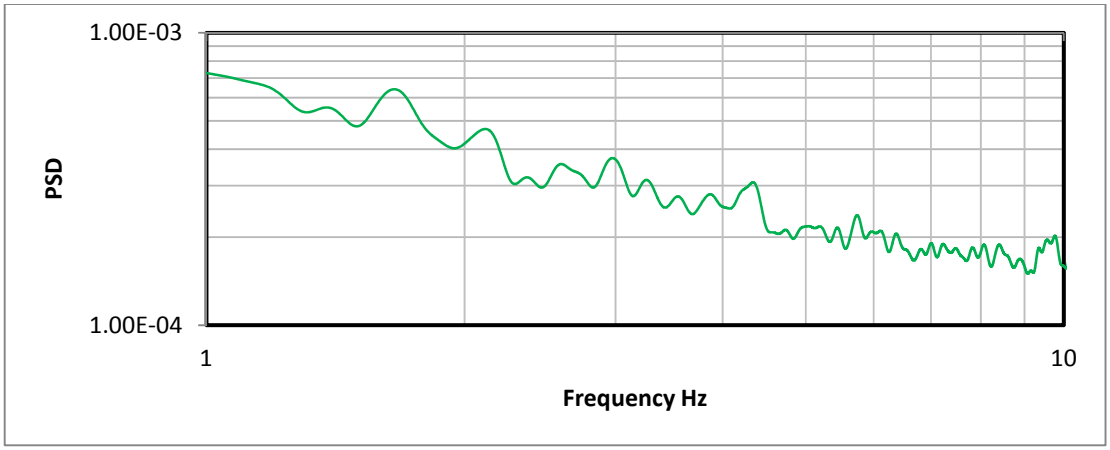

Figure B.4.10 Log-log PSD plot for E-W direction at Location 2 (1~10 Hz)

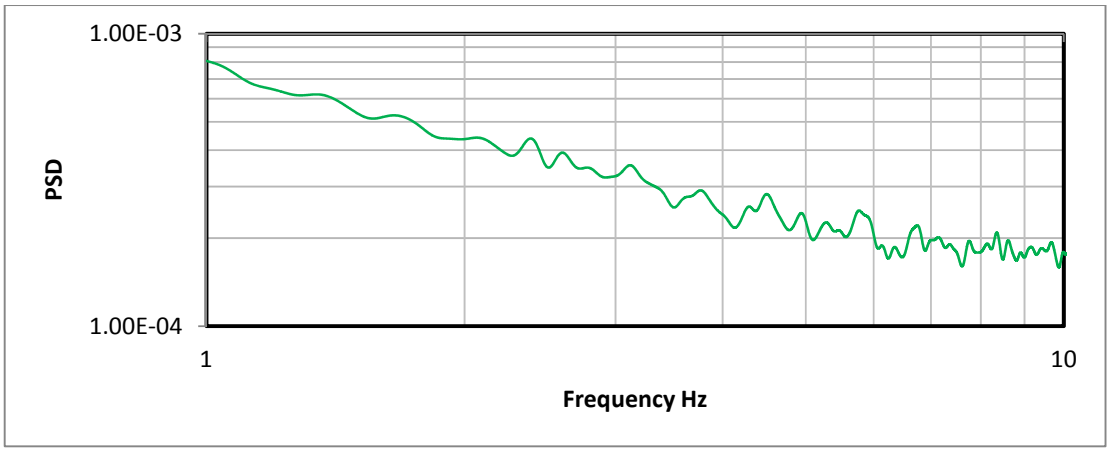

Figure B.4.11 Log-log PSD plot for E-W direction at Location 3 (1~10 Hz)

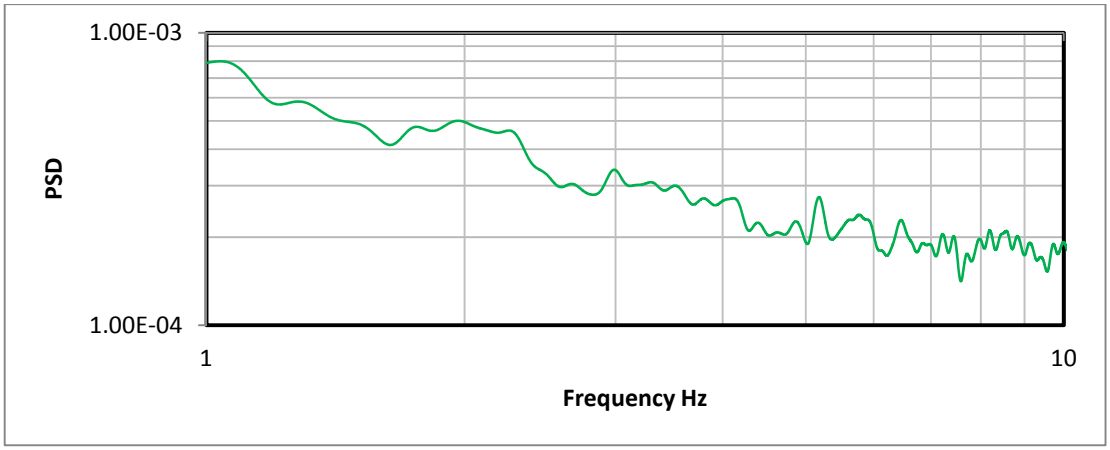

Figure B.4.12 Log-log PSD plot for E-W direction at Location 4 (1~10 Hz)

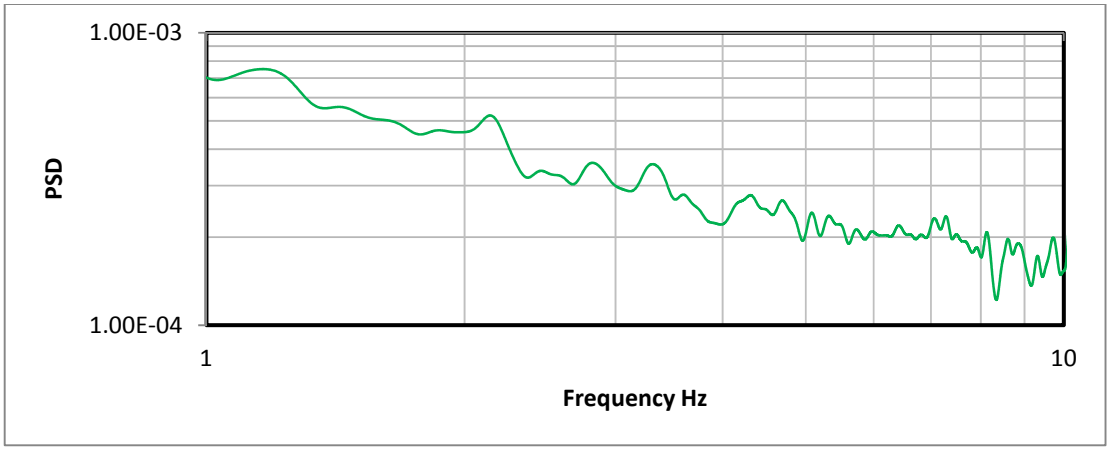

Figure B.4.13 Log-log PSD plot for E-W direction at Location 5 (1~10 Hz)

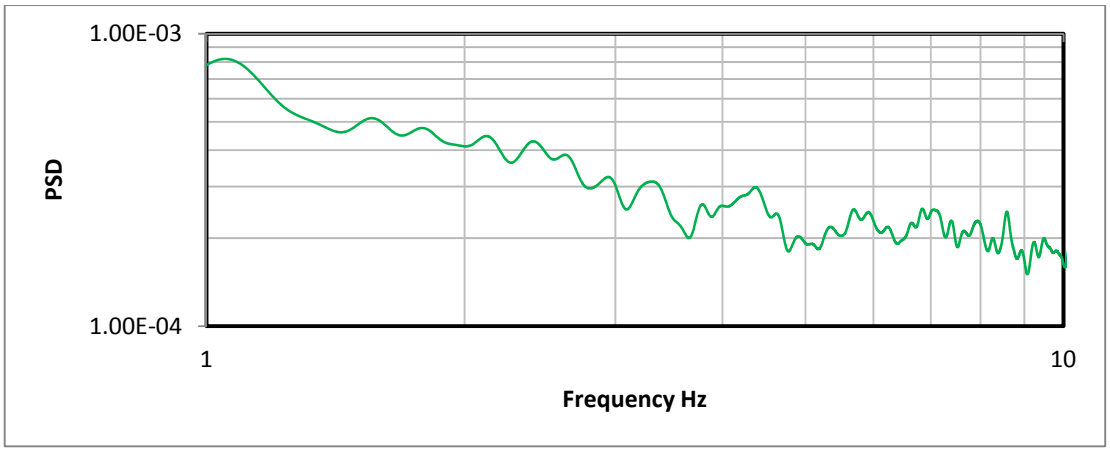

Figure B.4.14 Log-log PSD plot for E-W direction at Location 6 (1~10 Hz)

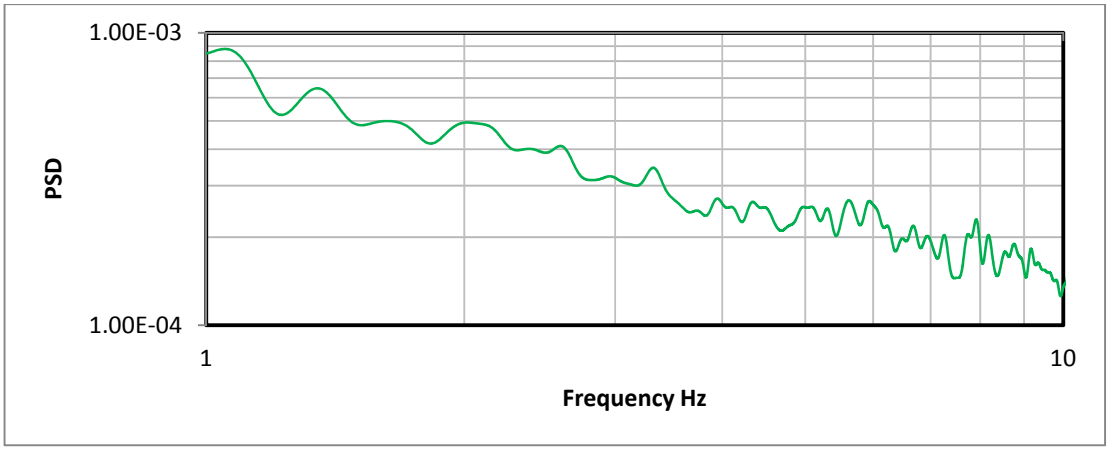

Figure B.4.15 Log-log PSD plot for E-W direction at Location 7 (1~10 Hz)

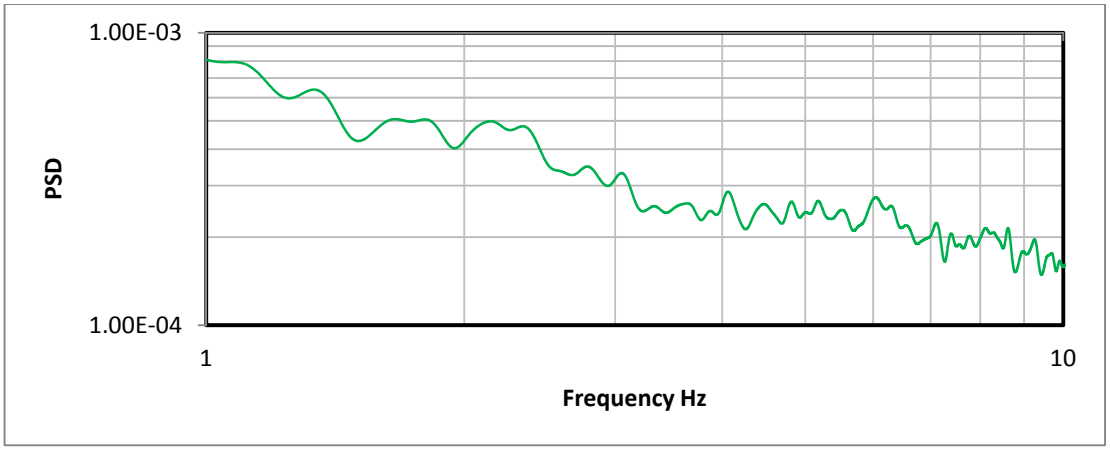

Figure B.4.16 Log-log PSD plot for E-W direction at Location 8 (1~10 Hz)

Appendix C

Input Ground Motion Time Histories and Spectra

The ground motions inputted in the SAP 2000 finite element model were generated from the PEER-Ground Motion Database (PEER, 2011). These original ground motion records were scaled to match with the target spectrum suggested by NBCC 2010 within the SeismoMatch program. The comparison between the scaled and unscaled spectra and time histories are presented in the subsequent figures

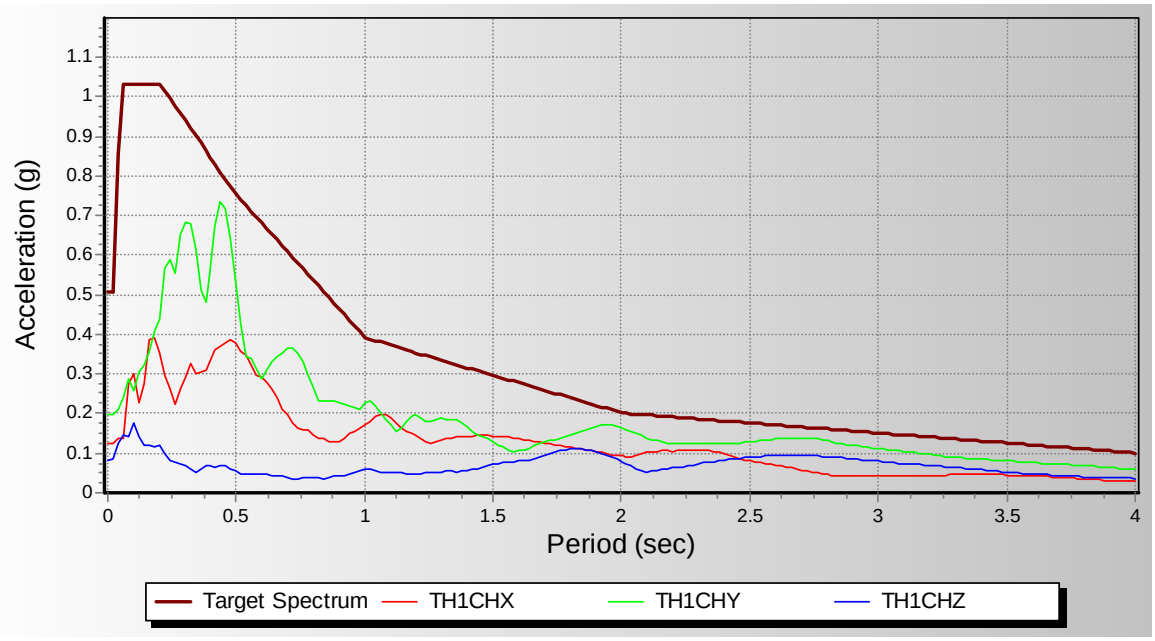

Figure C.1.1 Original spectra for TH1-Chi Chi relative to the target spectrum

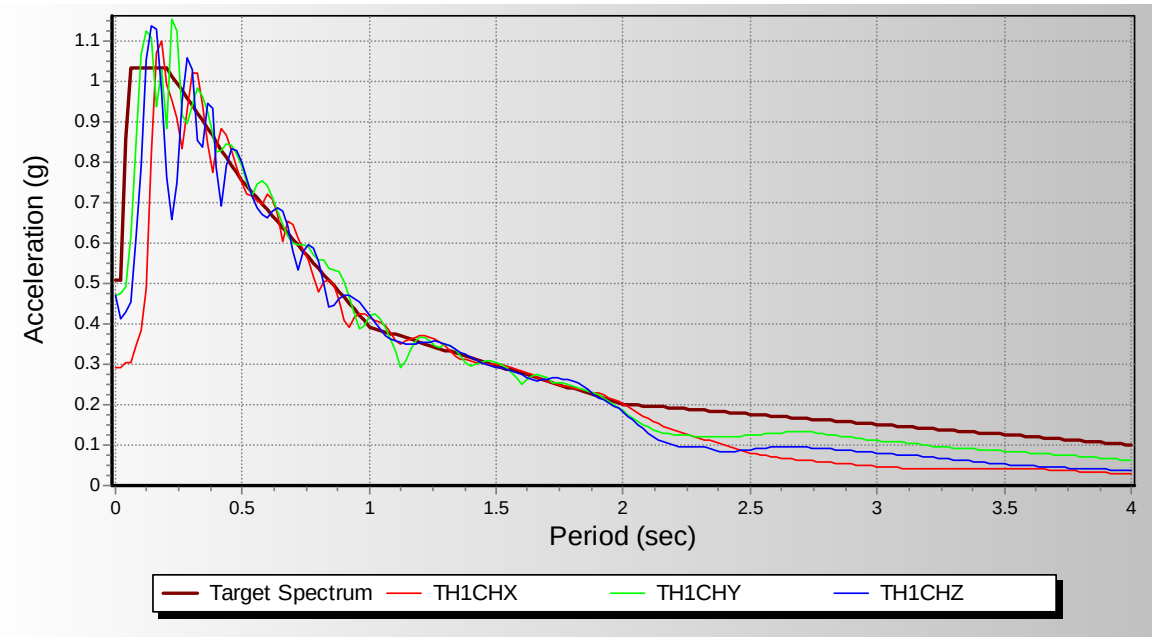

Figure C.1.2 Matched spectra for TH1-Chi Chi relative to the target spectrum

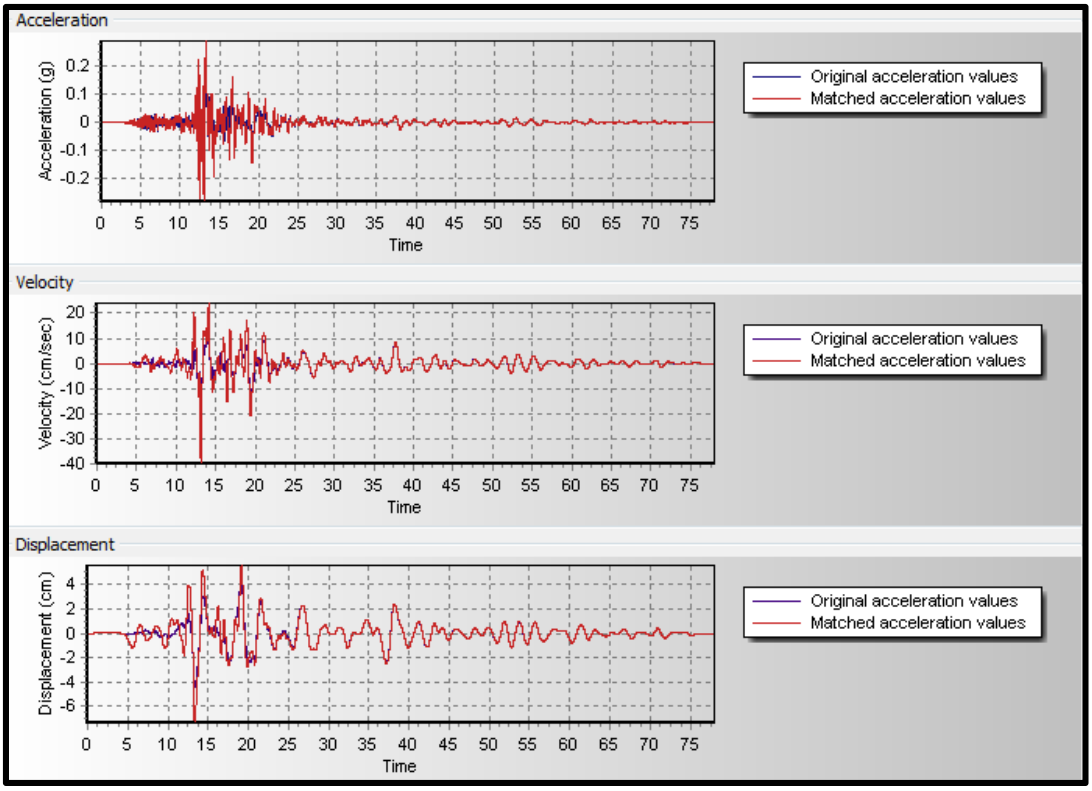

Figure C.1.3 TH1CHI_X original vs. matched acceleration, velocity and displacement time histories

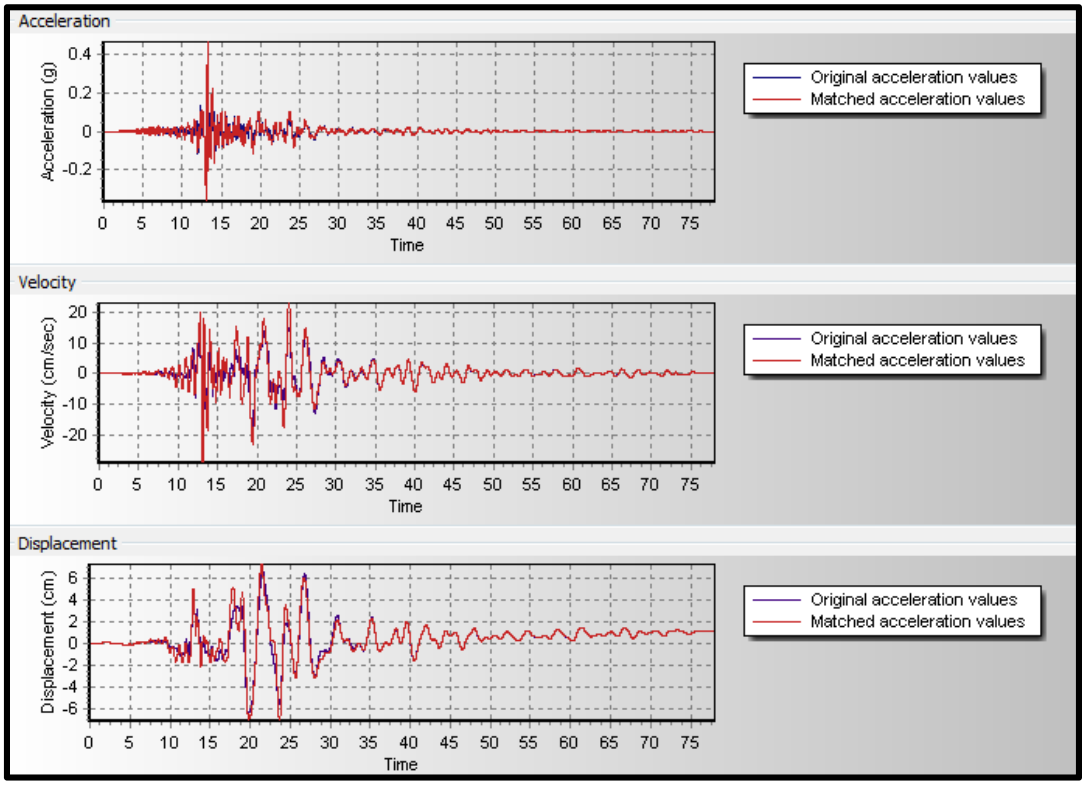

Figure C.1.4 TH1CHI_Y original vs. matched acceleration, velocity and displacement time histories

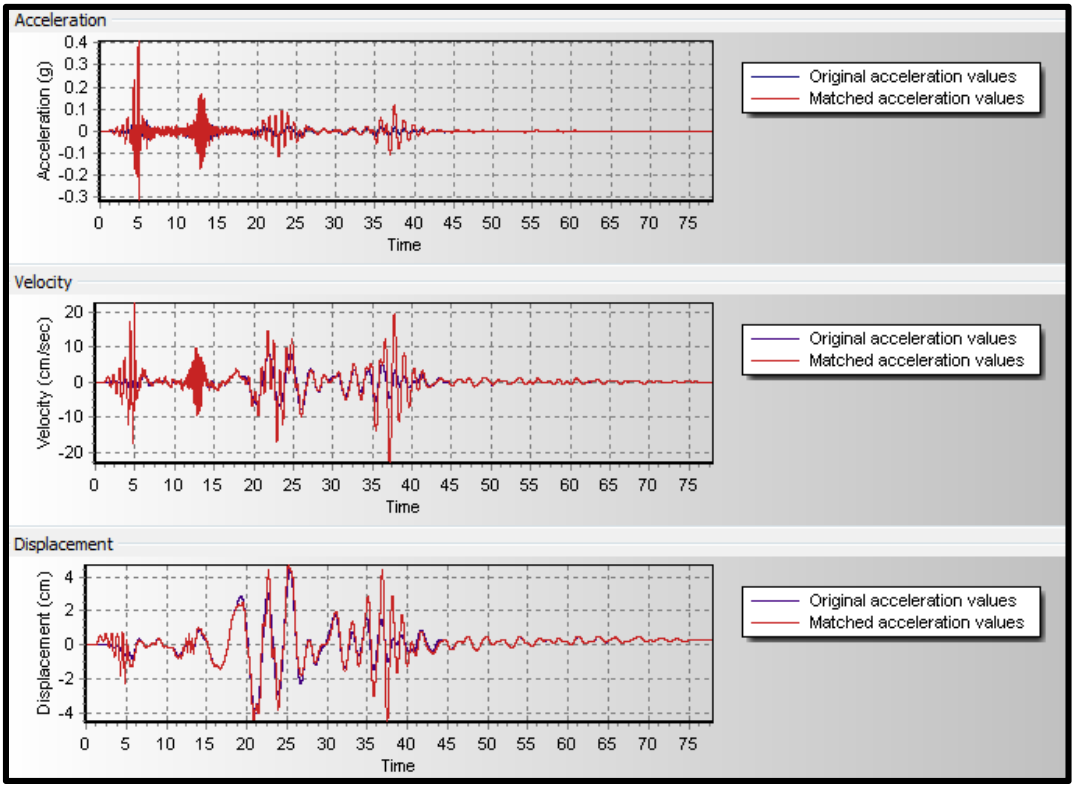

Figure C.1.5 TH1CHI_Z original vs. matched acceleration, velocity and displacement time histories

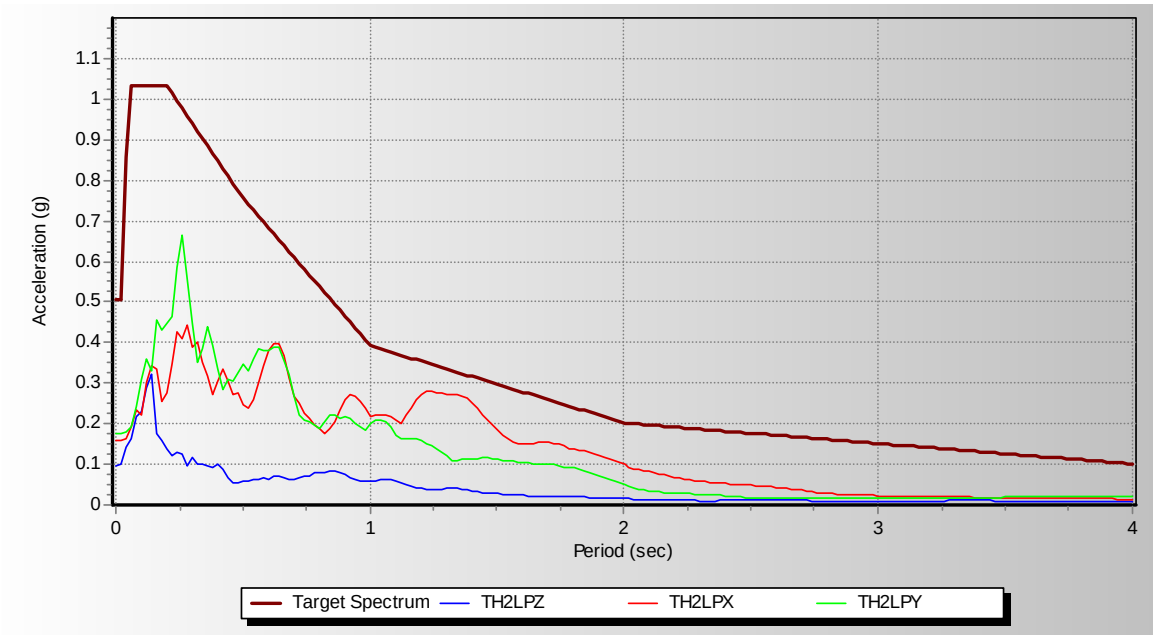

Figure C.1.6 Original spectra for TH2-Loma Prieta relative to the target spectrum

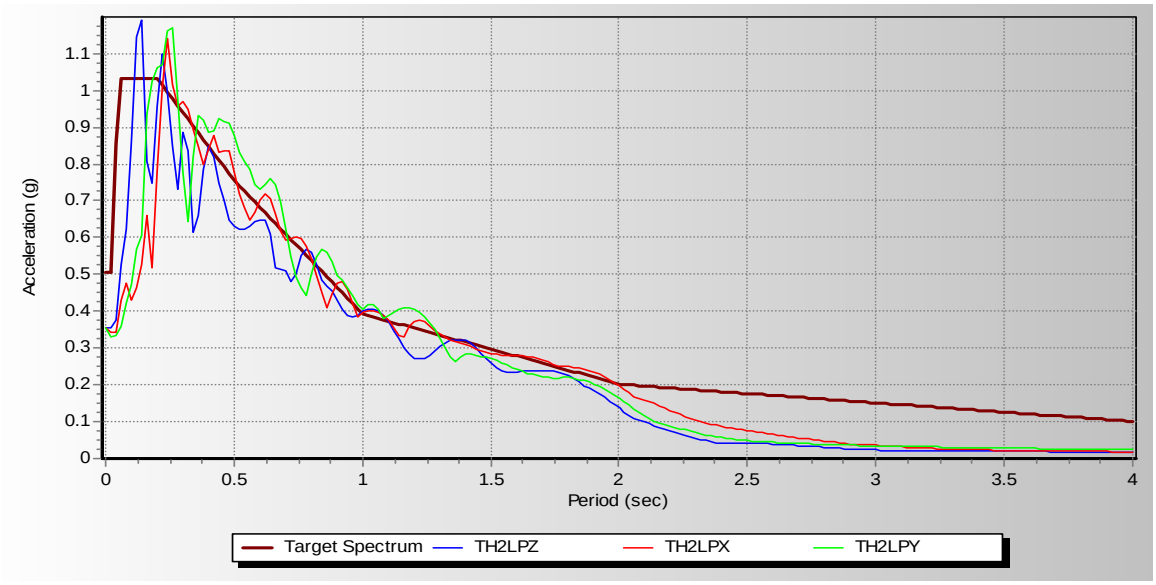

Figure C.1.7 Matched spectra for TH2-Loma Prieta relative to the target spectrum

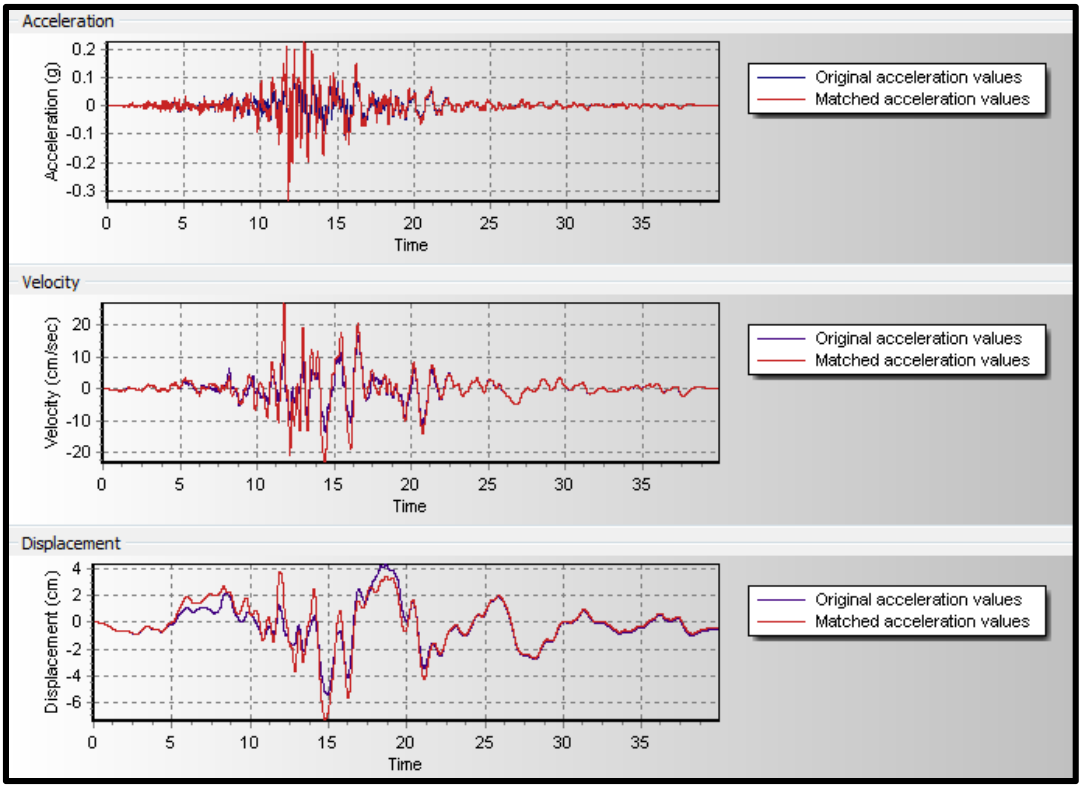

Figure C.1.8 TH2 LP_X original vs. matched acceleration, velocity and displacement time histories

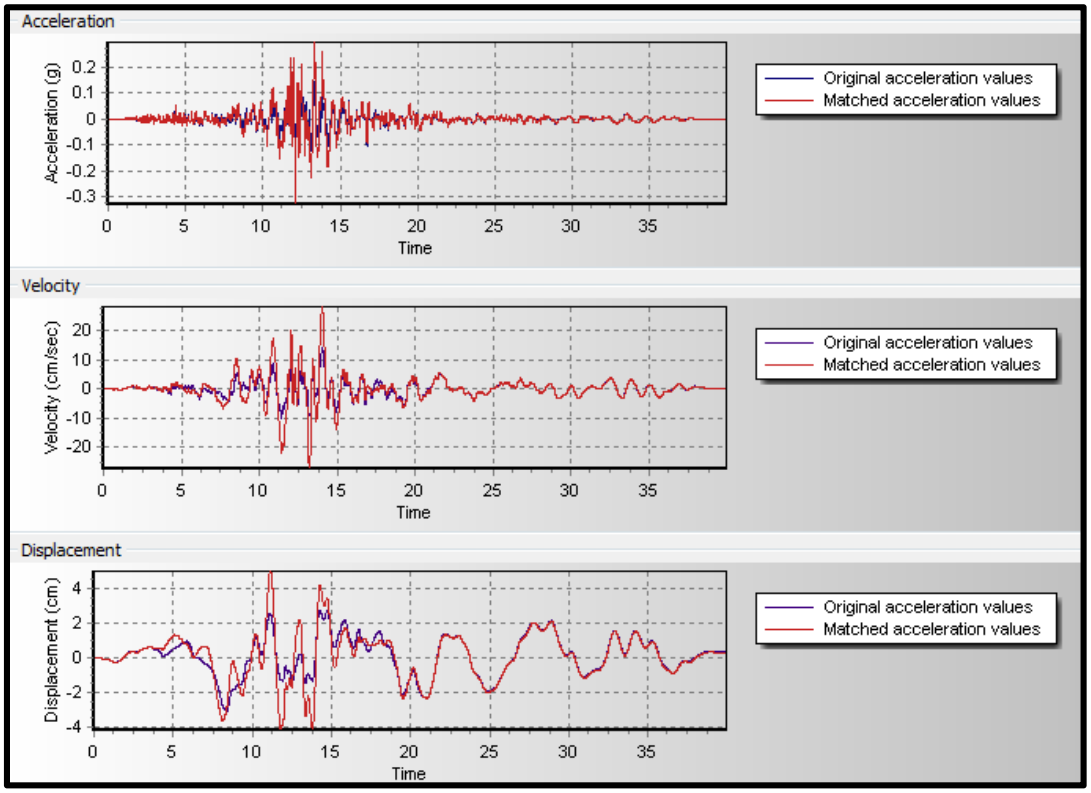

Figure C.1.9 TH2LP_Y original vs. matched acceleration, velocity and displacement time histories

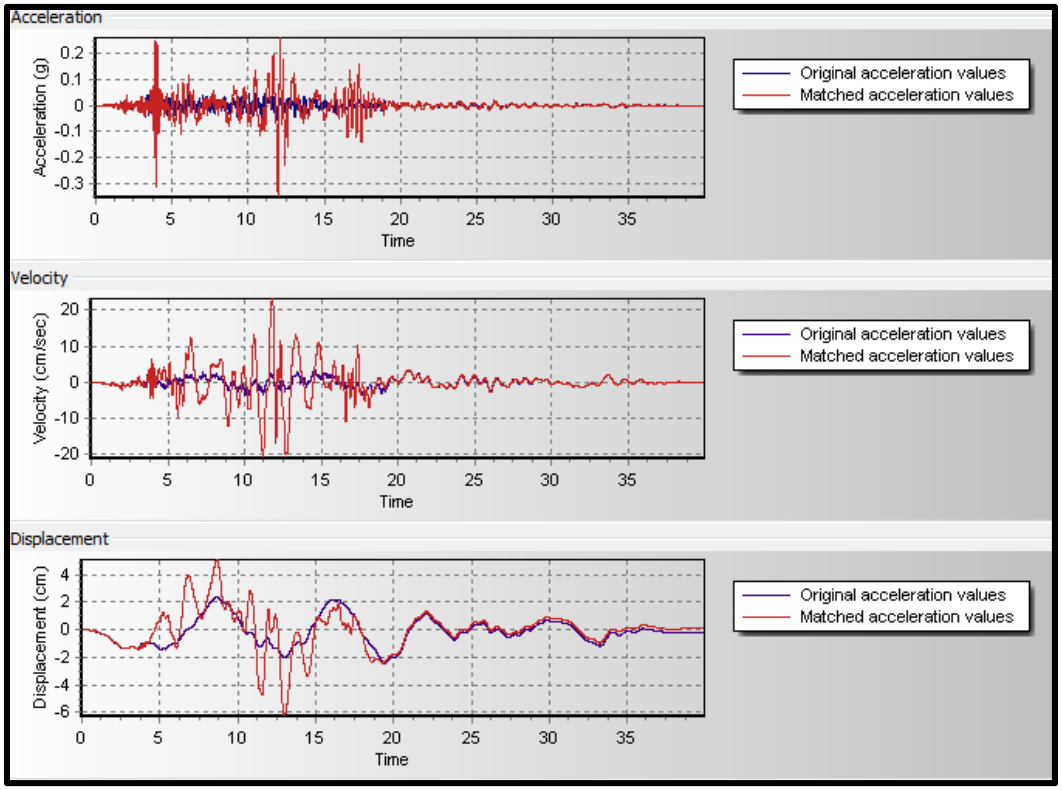

Figure C.1.10 TH2LP_Z original vs. matched acceleration, velocity and displacement time histories

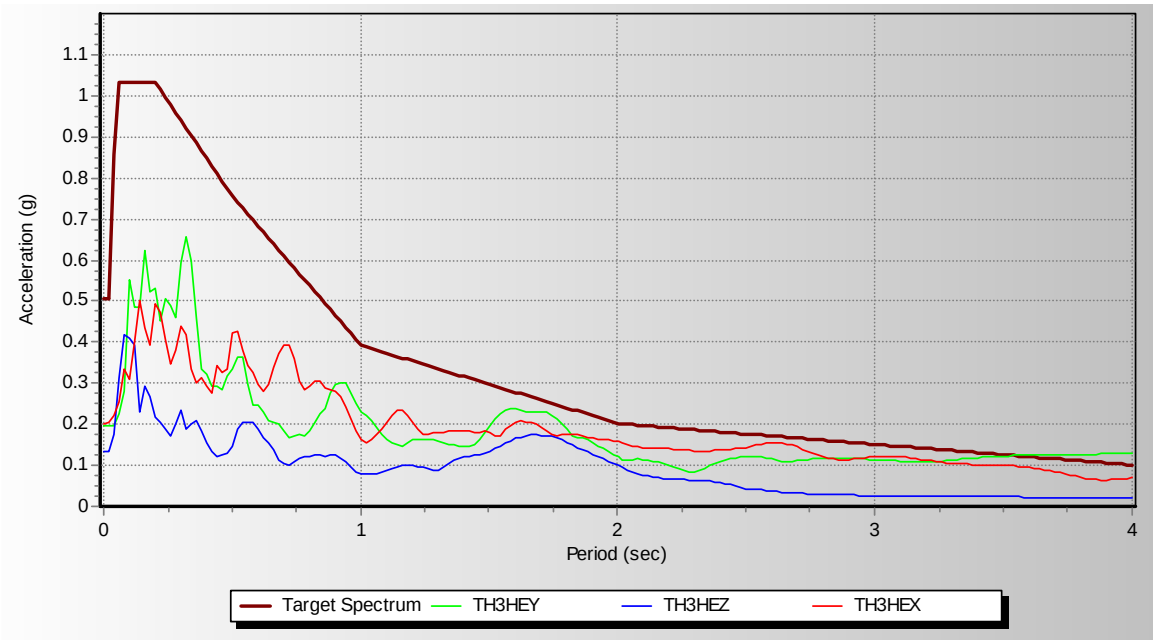

Figure C.1.11 Original spectra for TH3-Hector Mine relative to the target spectrum

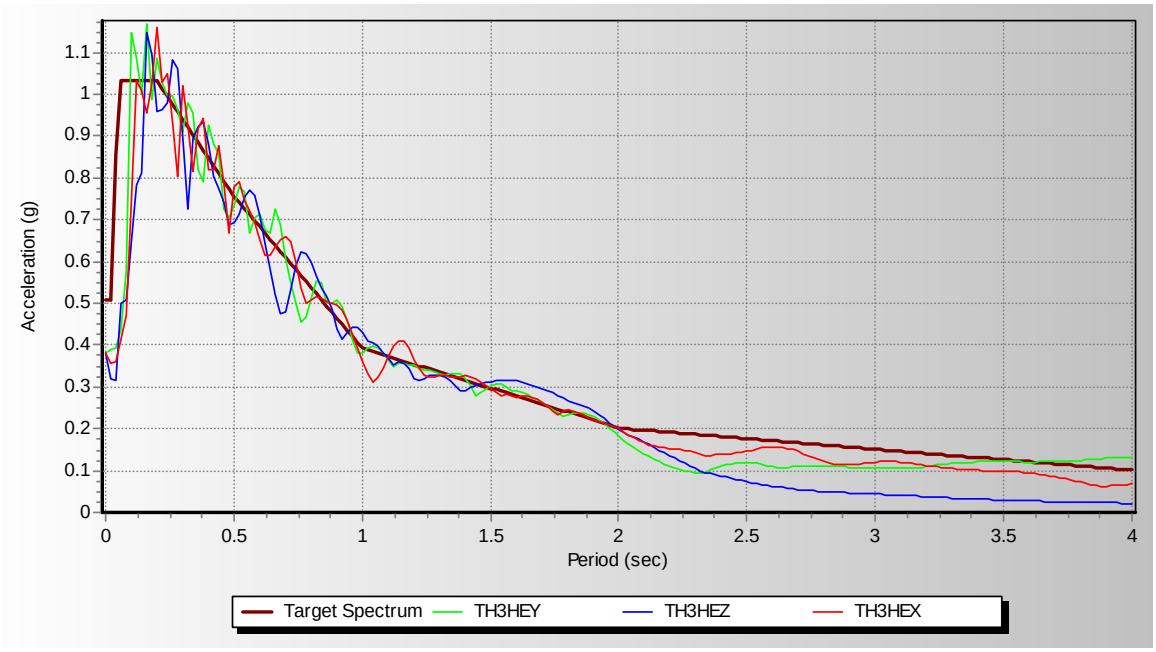

Figure C.1.12 Matched spectra for TH3-Hector Mine relative to the target spectrum

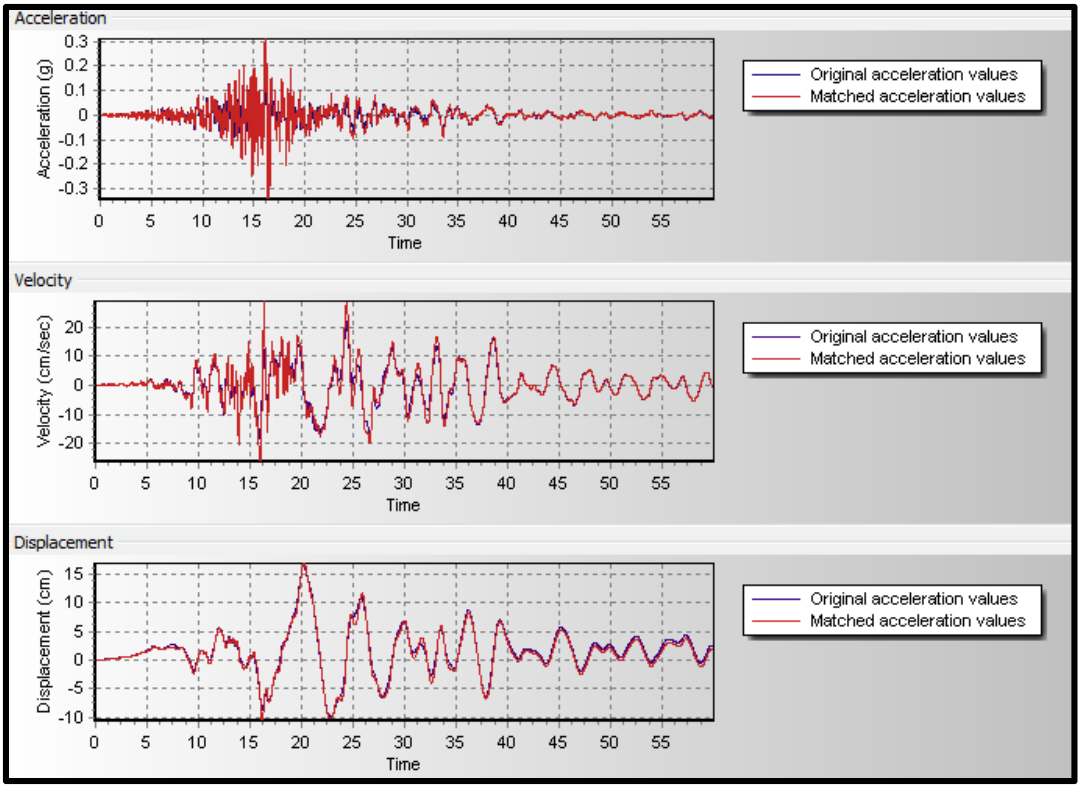

Figure C.1.13 TH3HE_X original vs. matched acceleration, velocity and displacement time histories

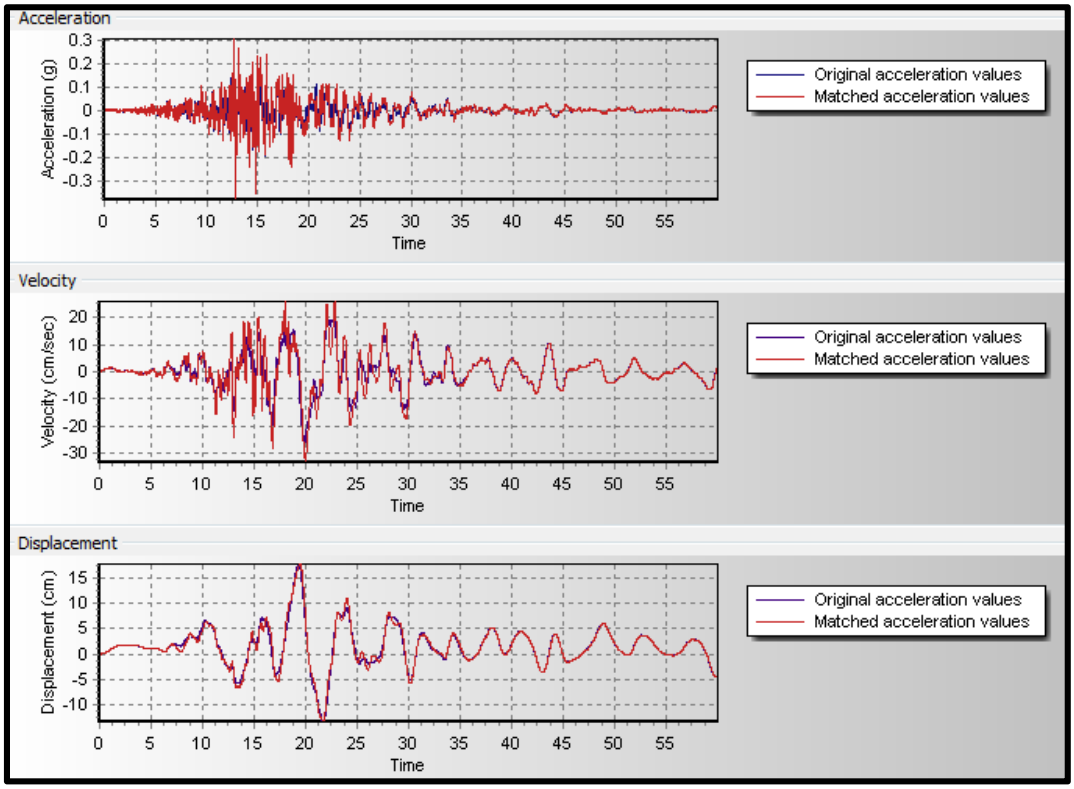

Figure C.1.14 TH3HE_Y original vs. matched acceleration, velocity and displacement time histories

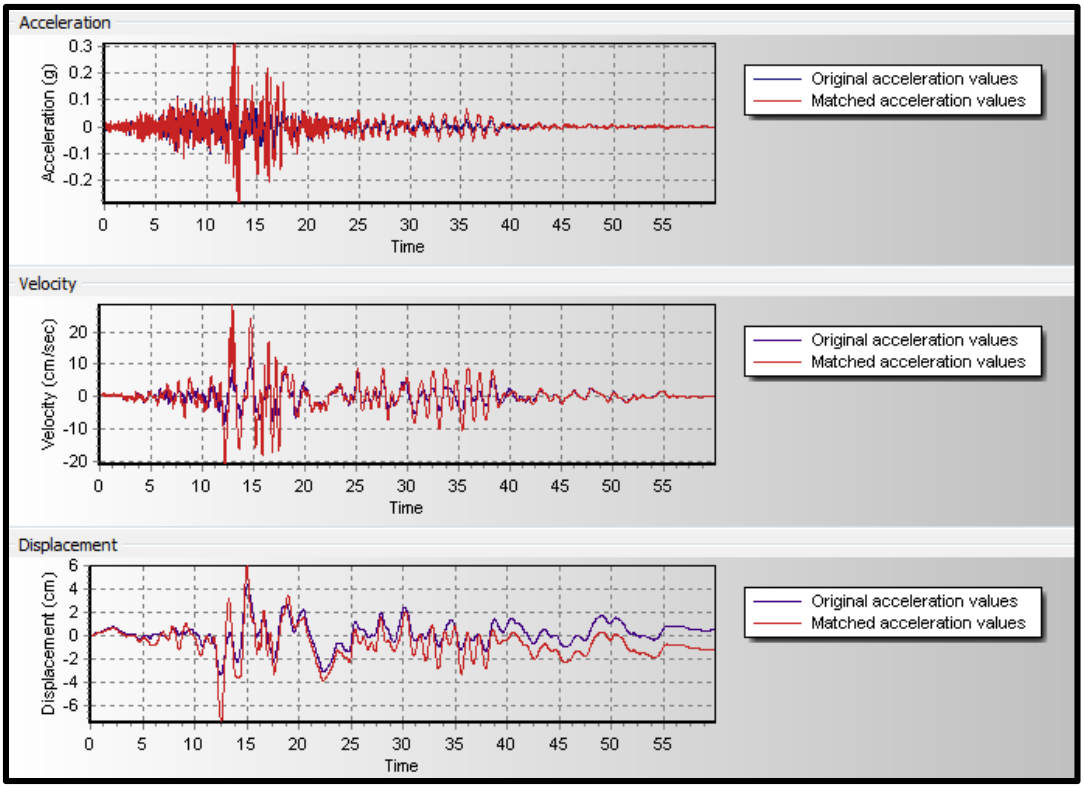

Figure C.1.15 TH3HE_Z original vs. matched acceleration, velocity and displacement time histories

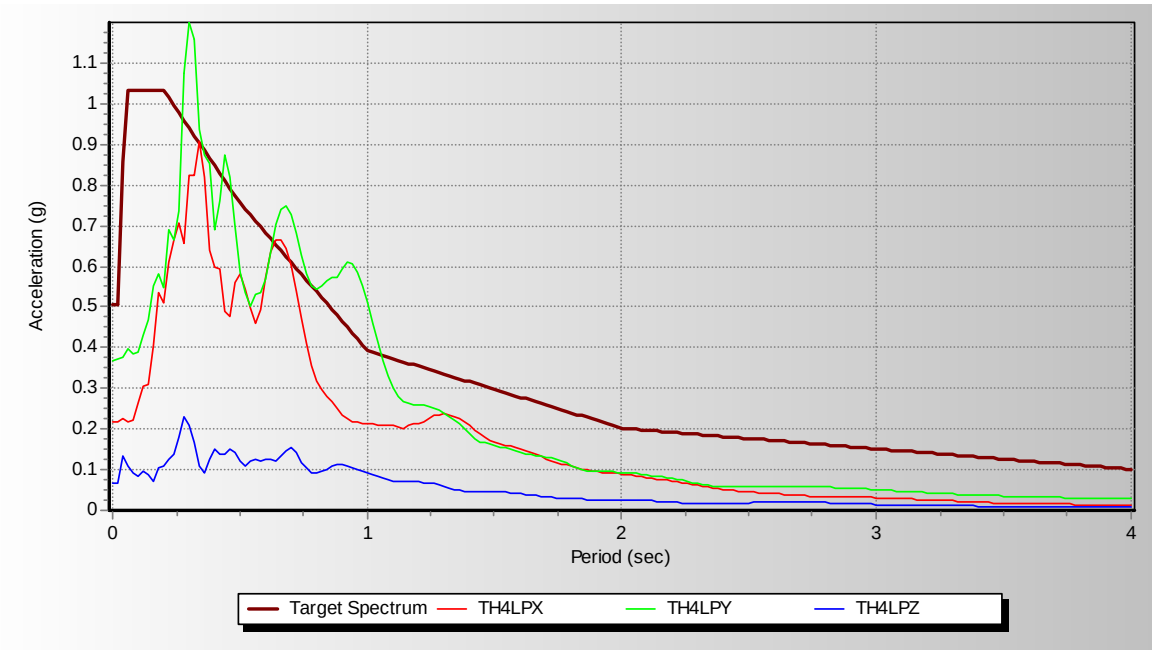

Figure C.1.16 Original spectra for TH4-Loma Prieta relative to the target spectrum

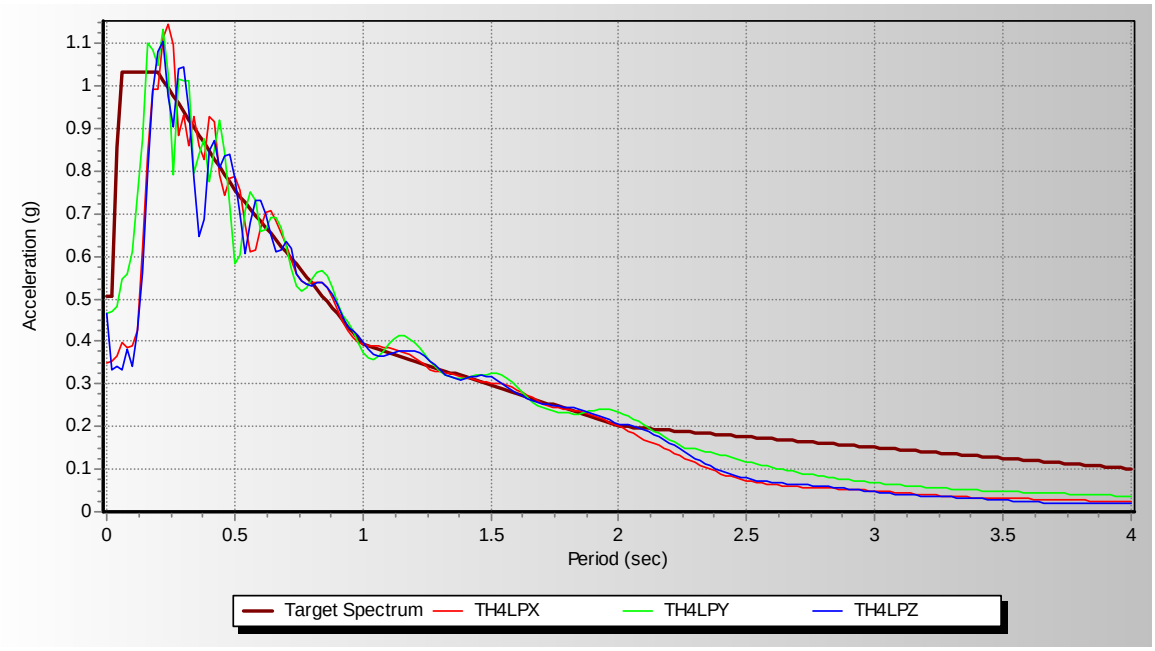

Figure C.1.17 Matched spectra for TH4-Loma Prieta relative to the target spectrum

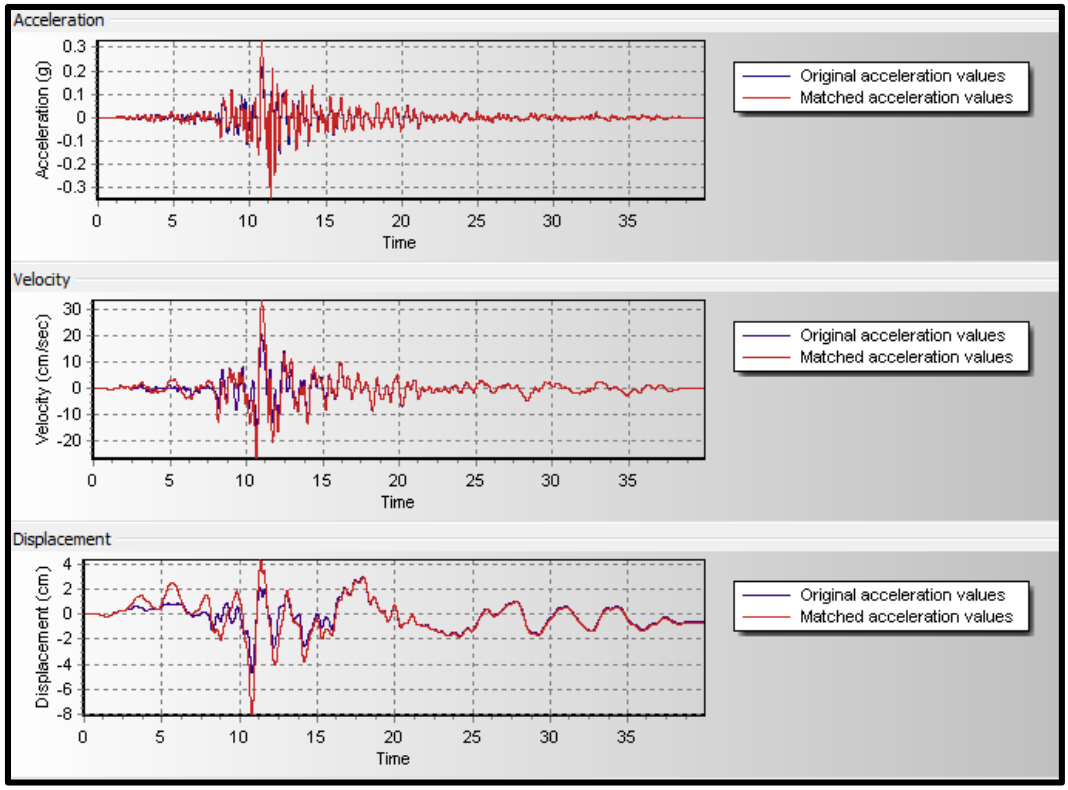

Figure C.1.18 TH4LP_X original vs. matched acceleration, velocity and displacement time histories

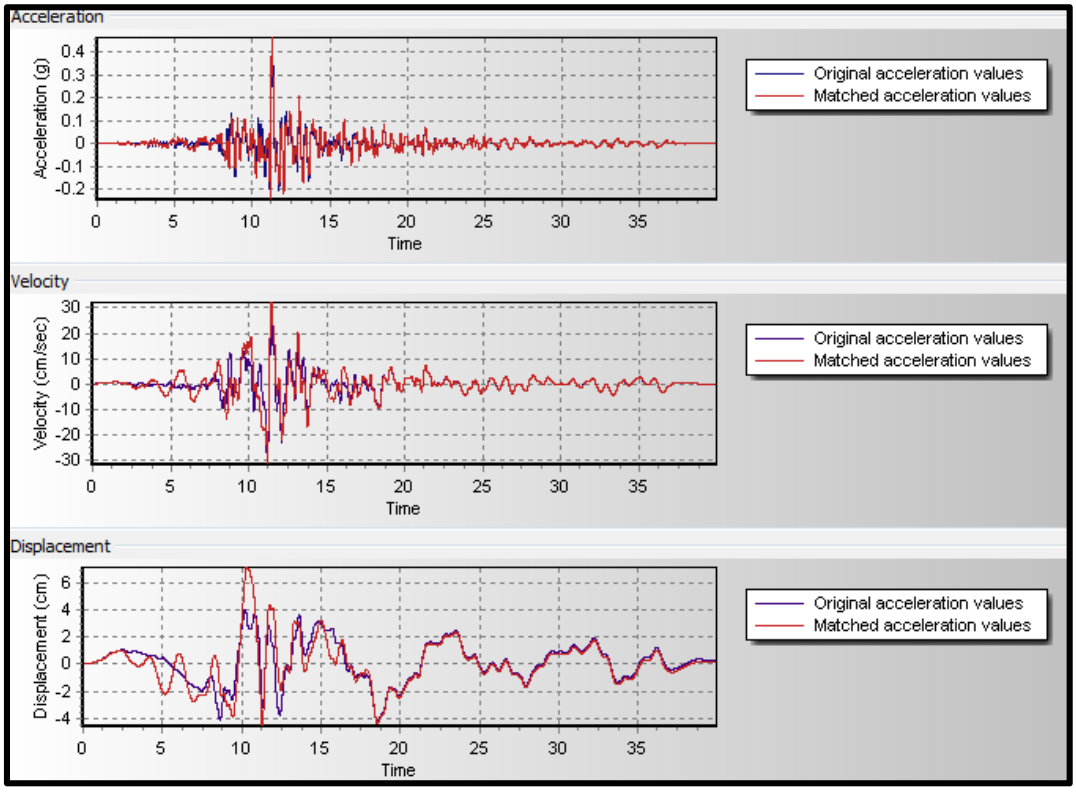

Figure C.1.19 TH4LP_Y original vs. matched acceleration, velocity and displacement time histories

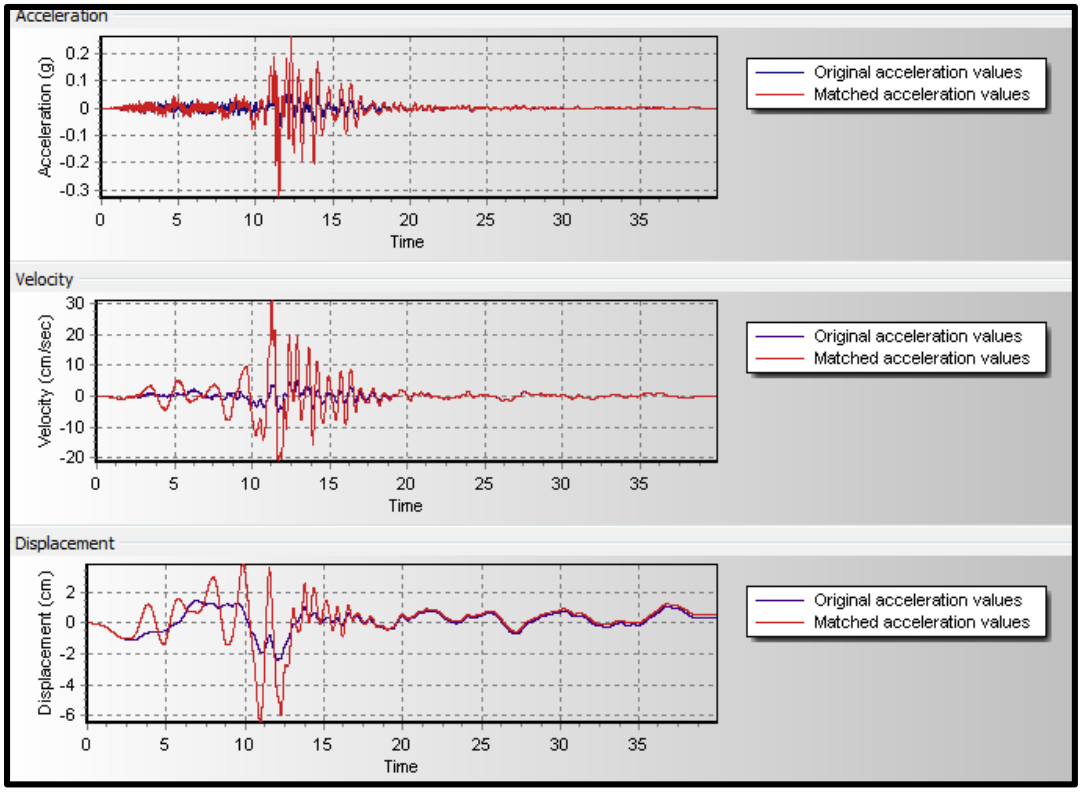

Figure C.1.20 TH4LP_Z original vs. matched acceleration, velocity and displacement time histories

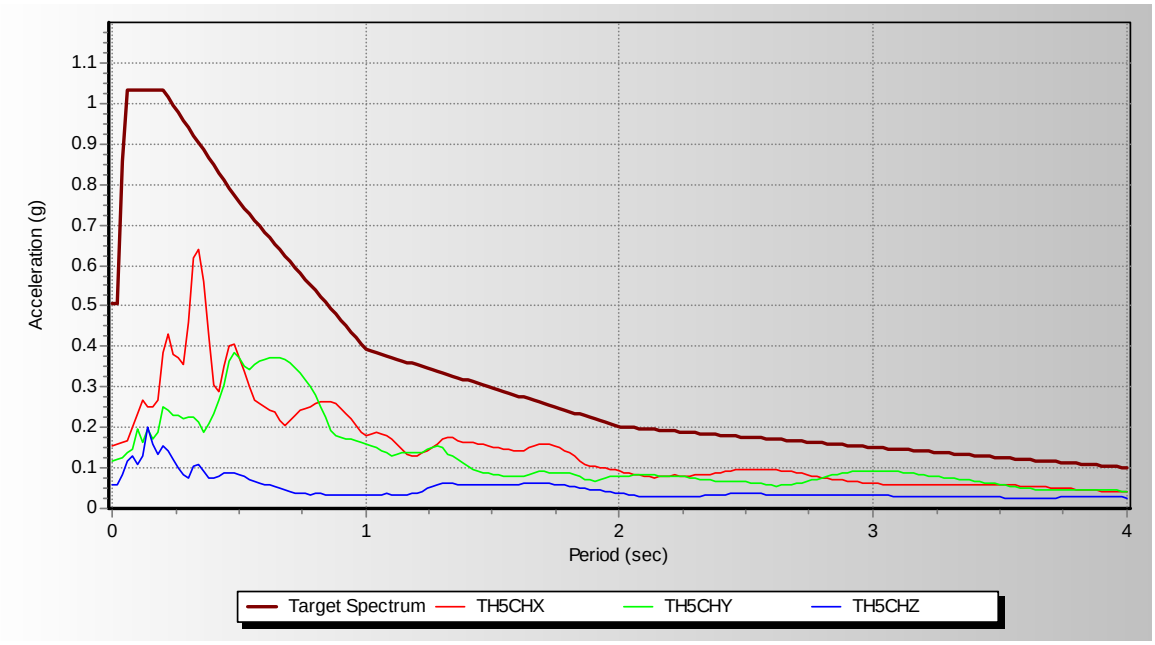

Figure C.1.21 Original spectra for TH5-Chi Chi relative to the target spectrum

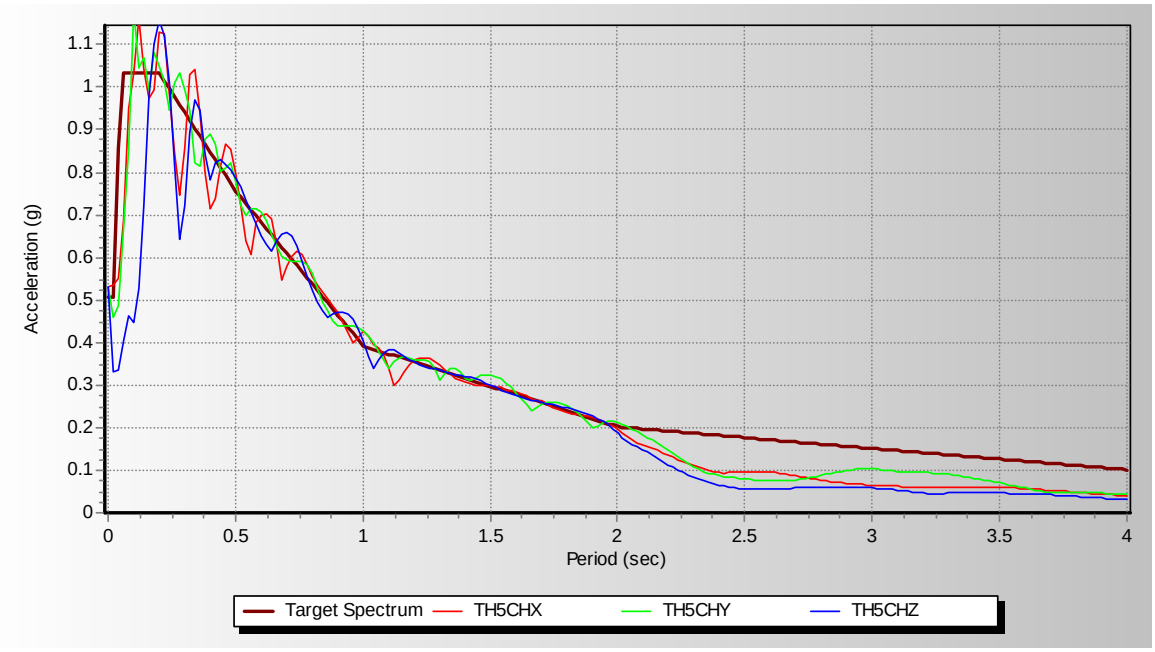

Figure C.1.22 Original spectra for TH5-Chi Chi relative to the target spectrum

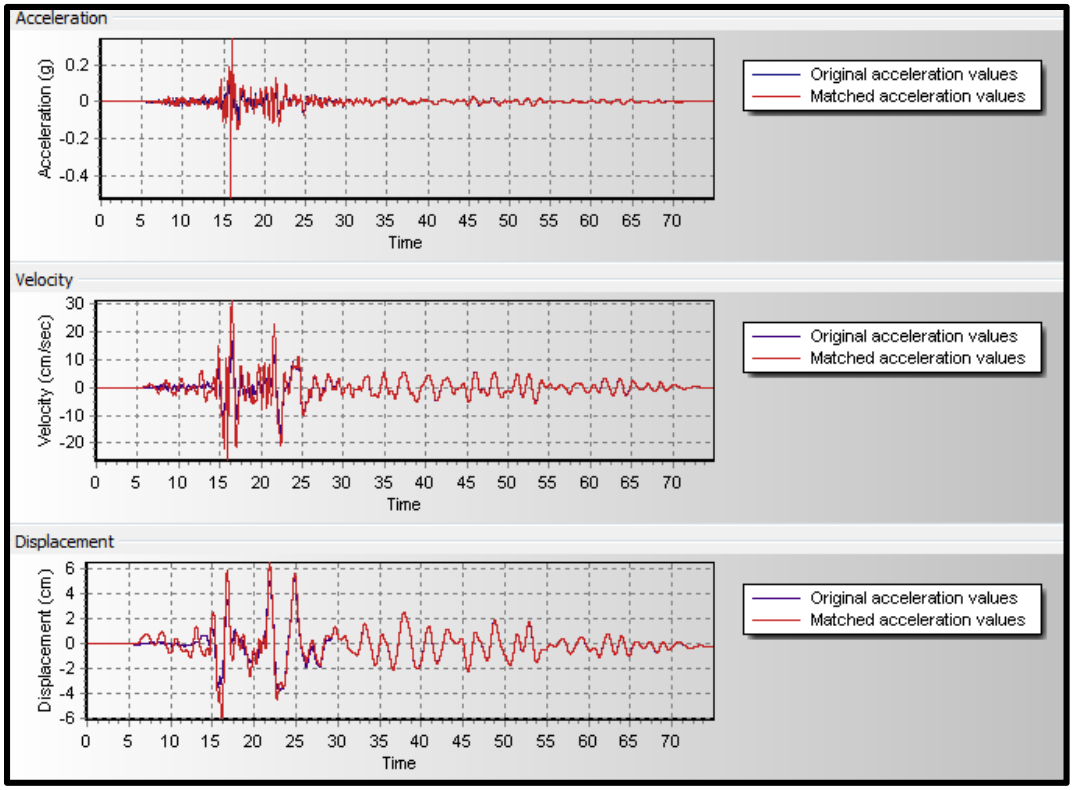

Figure C.1.23 TH5CHI_X original vs. matched acceleration, velocity and displacement time histories

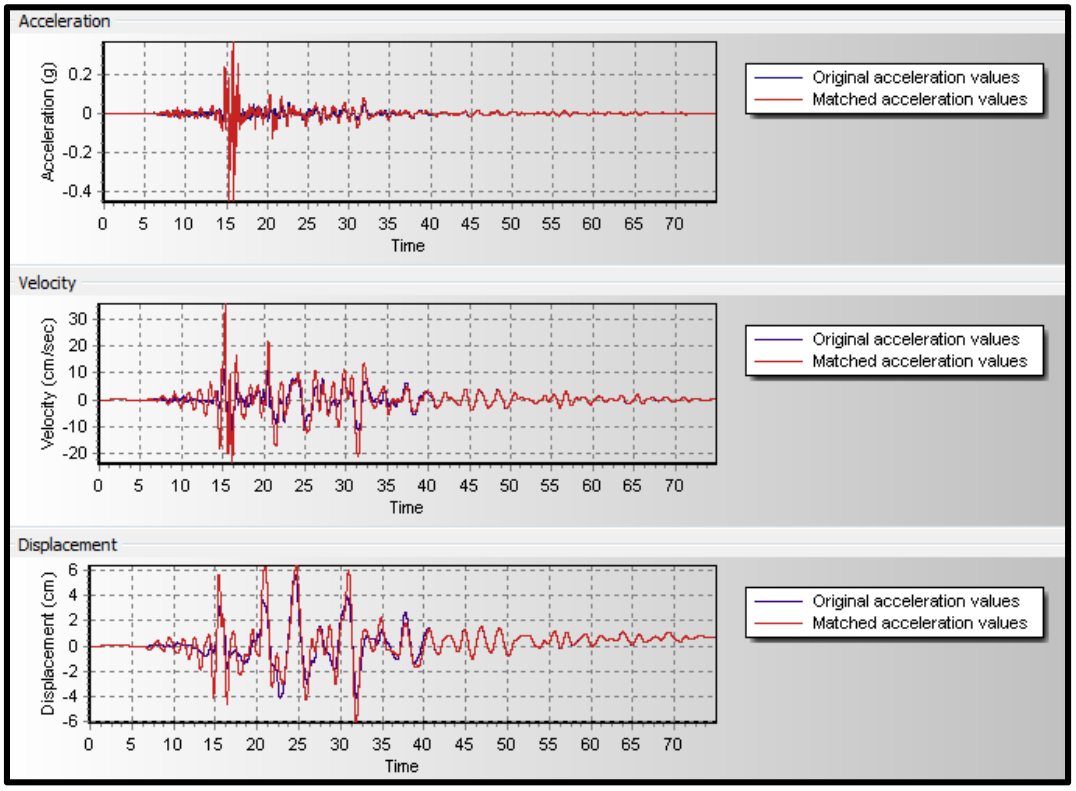

Figure C.1.24 TH5CHI_Y original vs. matched acceleration, velocity and displacement time histories

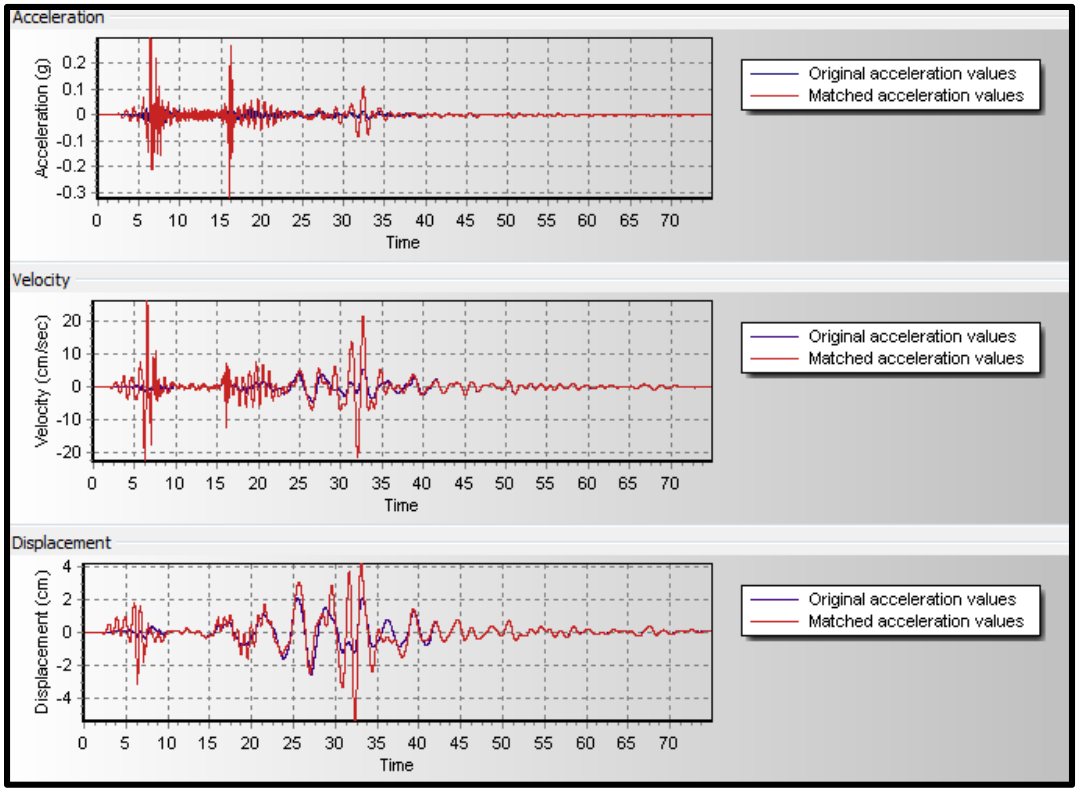

Figure C.1.25 TH5CHI_Z original vs. matched acceleration, velocity and displacement time histories

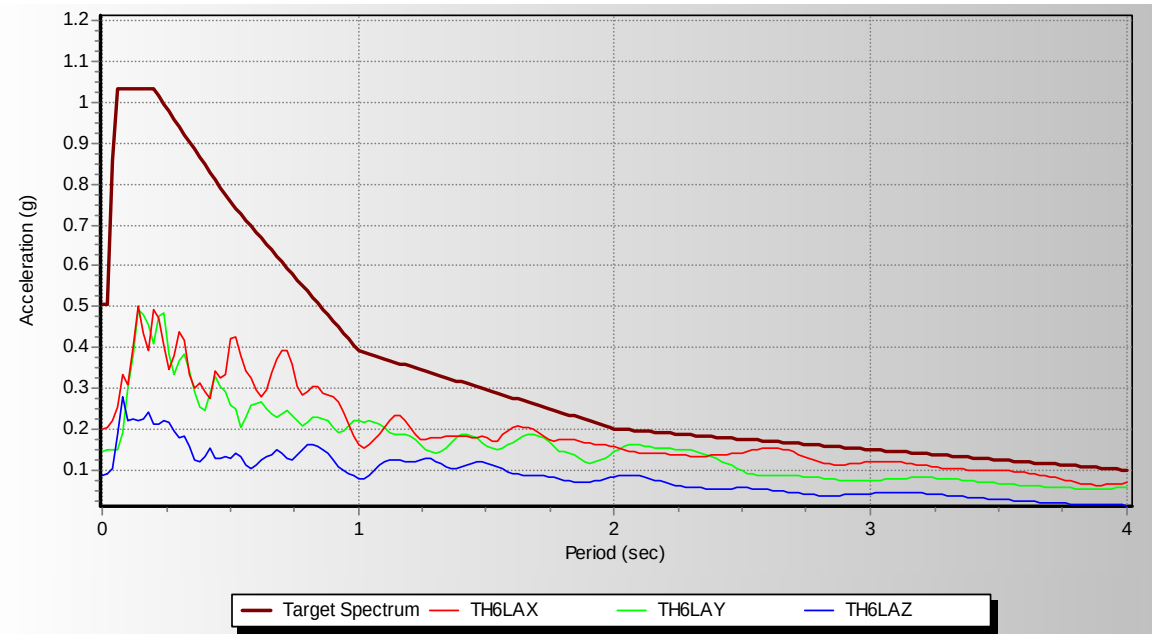

Figure C.1.26 Original spectra for TH6-Landers relative to the target spectrum

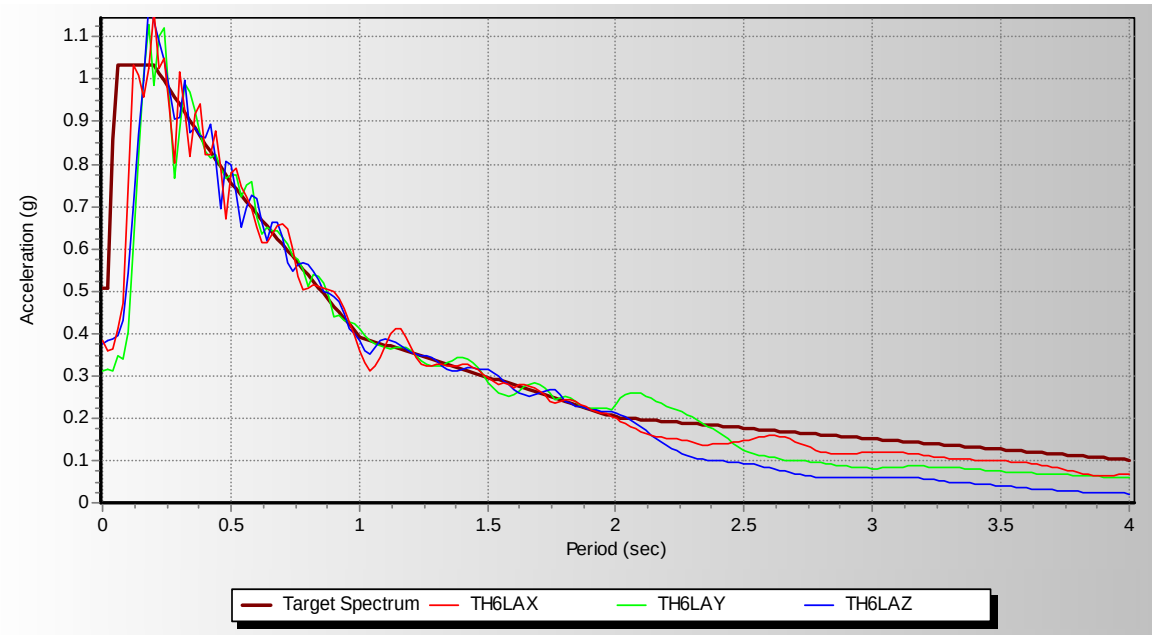

Figure C.1.27 Matched spectra for TH6-Landers relative to the target spectrum

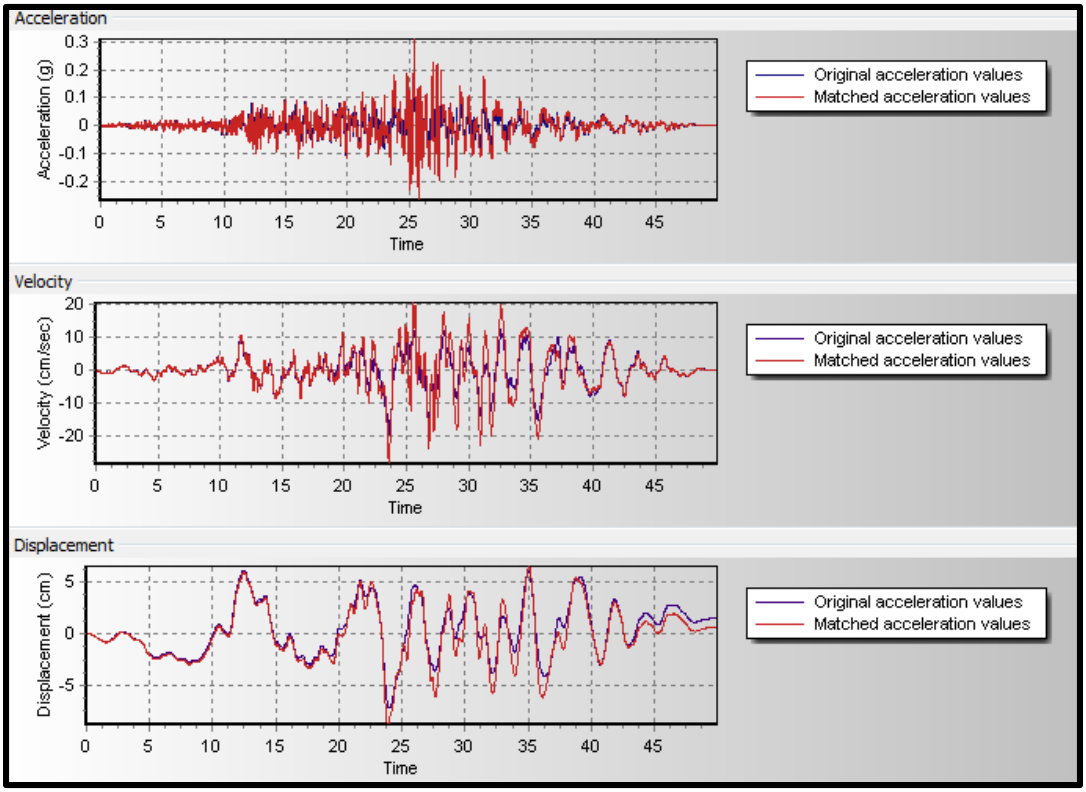

Figure C.1.28 TH6LA_X original vs. matched acceleration, velocity and displacement time histories

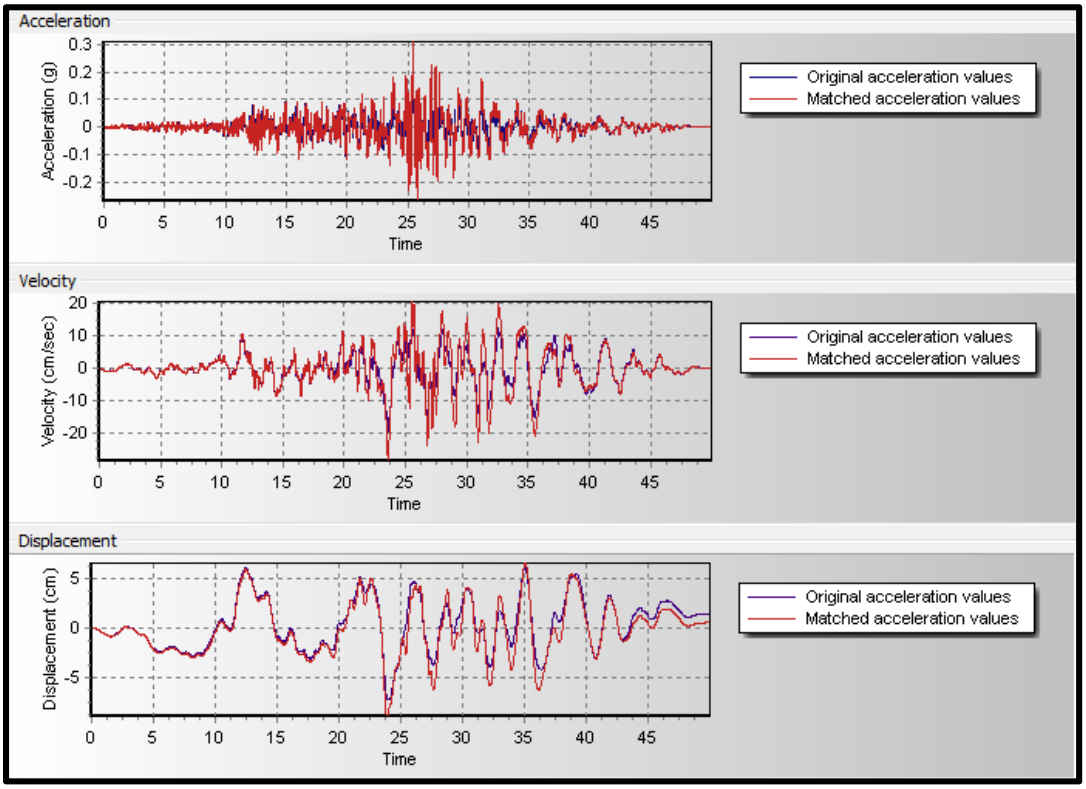

Figure C.1.29 TH6LA_Y original vs. matched acceleration, velocity and displacement time histories

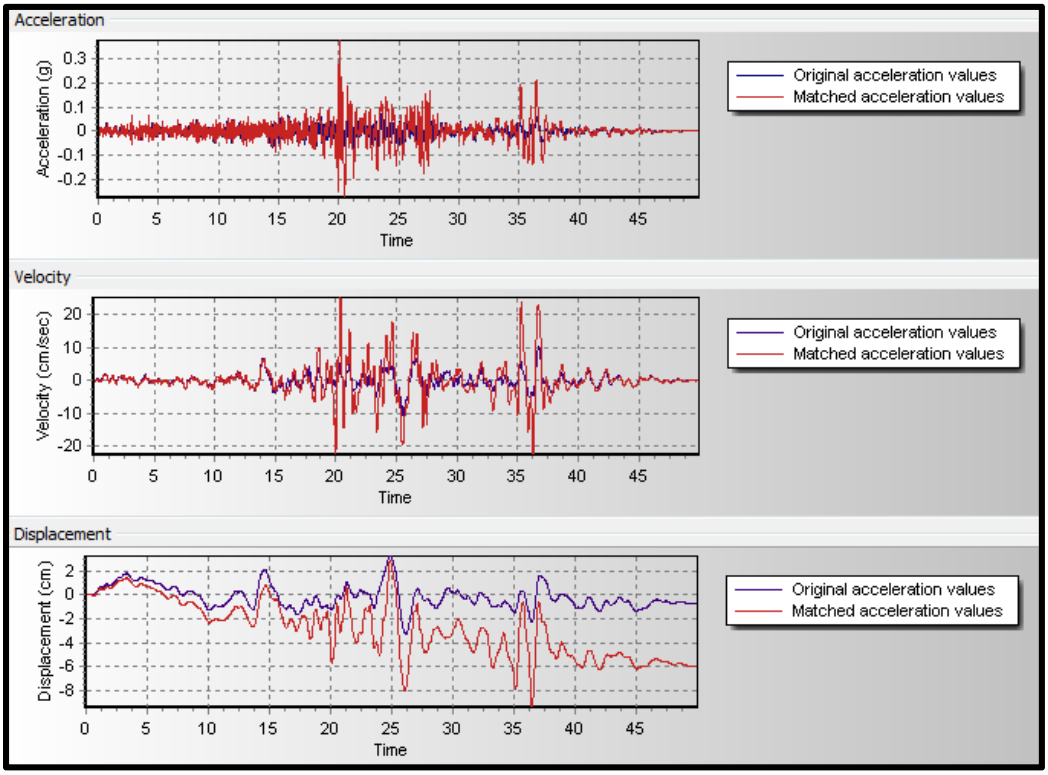

Figure C.1.30 TH6LA_Z original vs. matched acceleration, velocity and displacement time histories

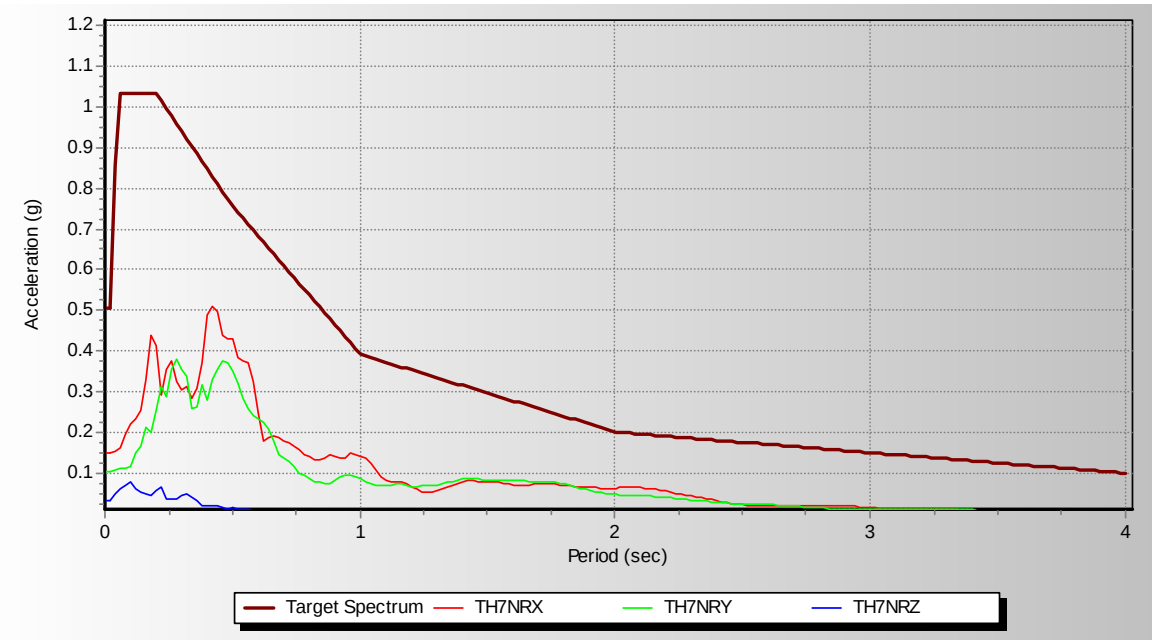

Figure C.1.31 Original spectra for TH7-Northridge relative to the target spectrum

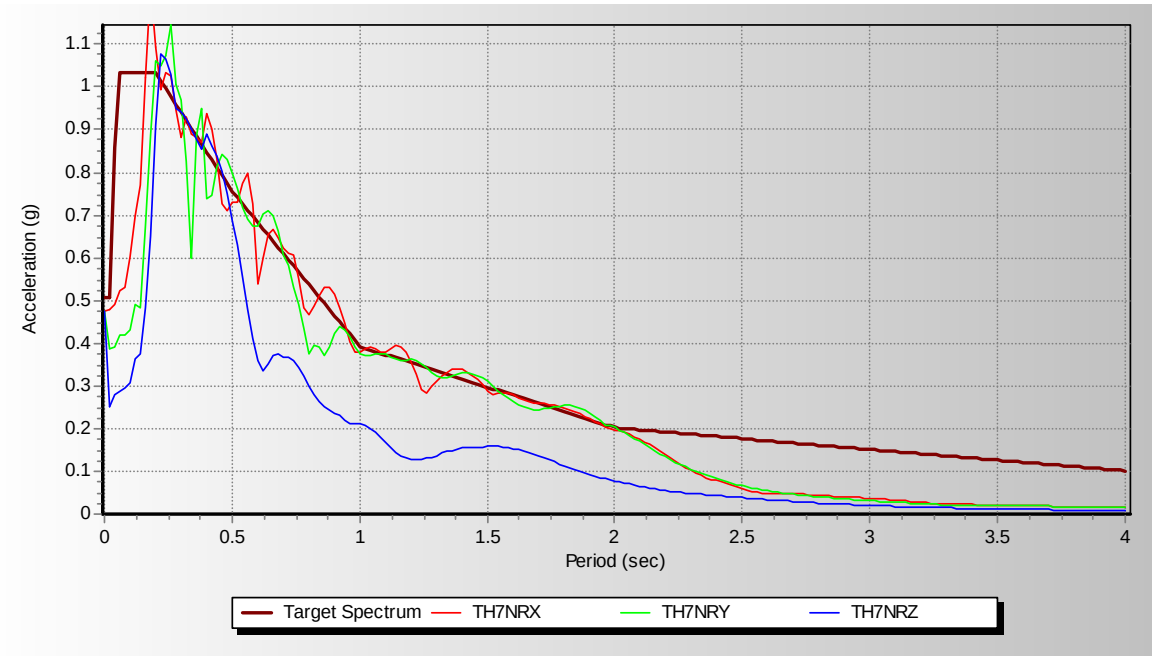

Figure C.1.32 Matched spectra for TH7-Northridge relative to the target spectrum

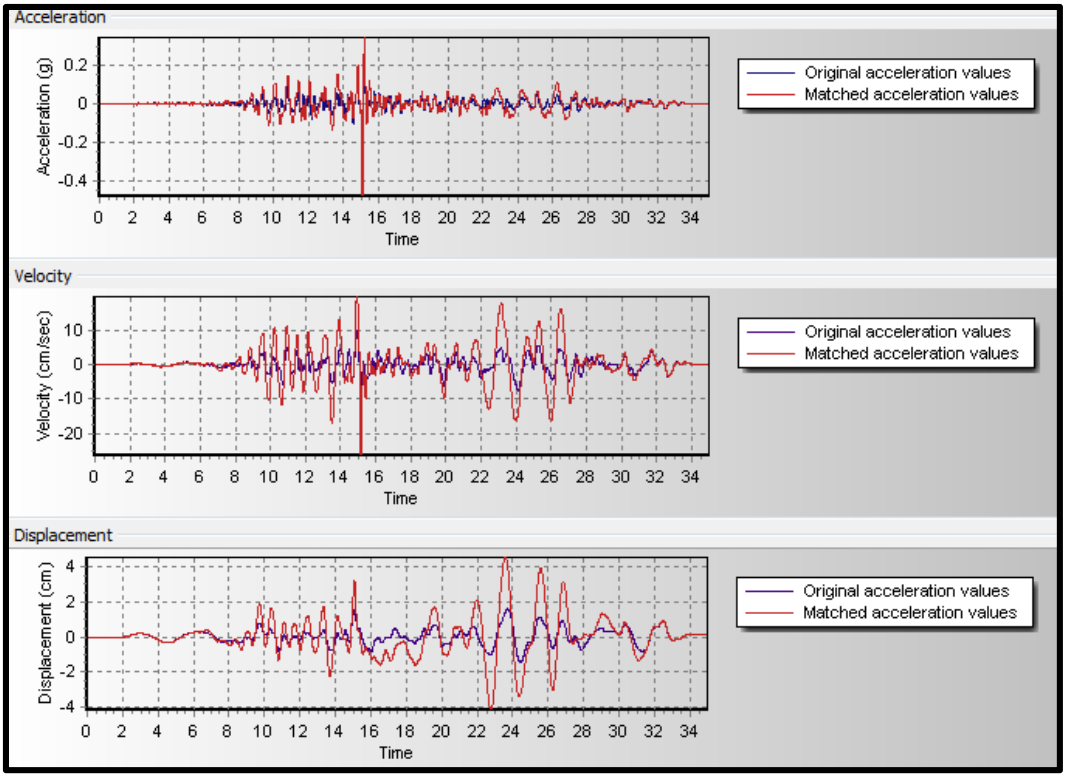

Figure C.1.33 TH7NR_X original vs. matched acceleration, velocity and displacement time histories

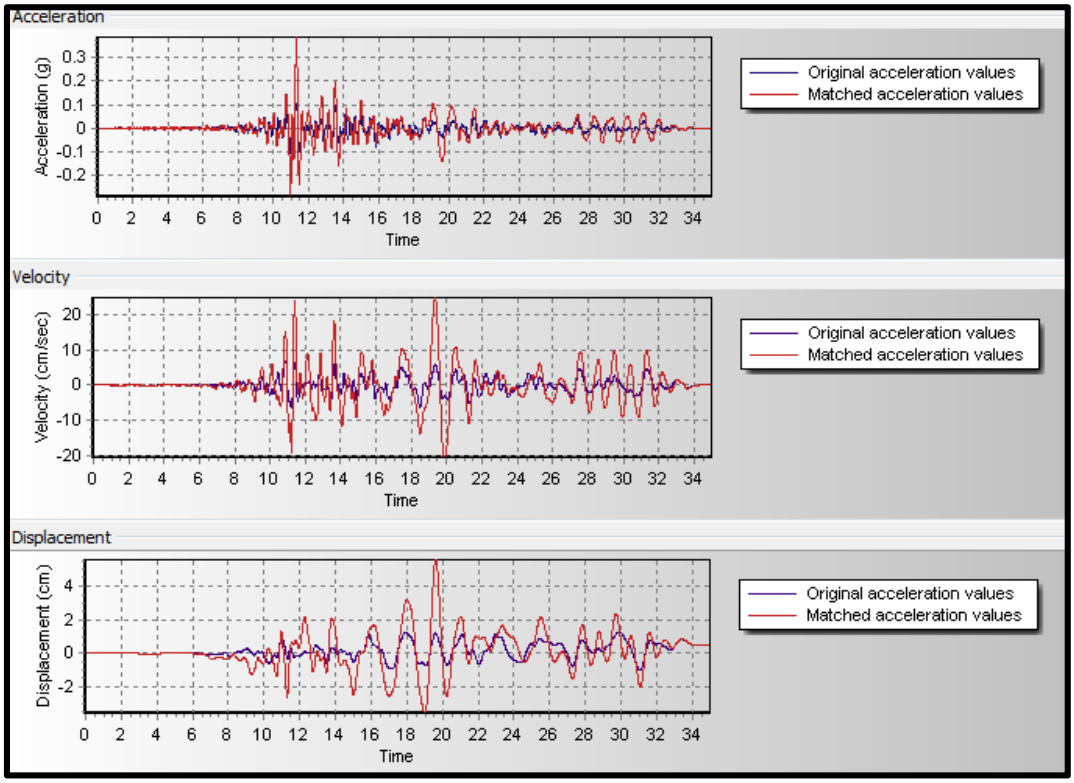

Figure C.1.34 TH7NR_Y original vs. matched acceleration, velocity and displacement time histories

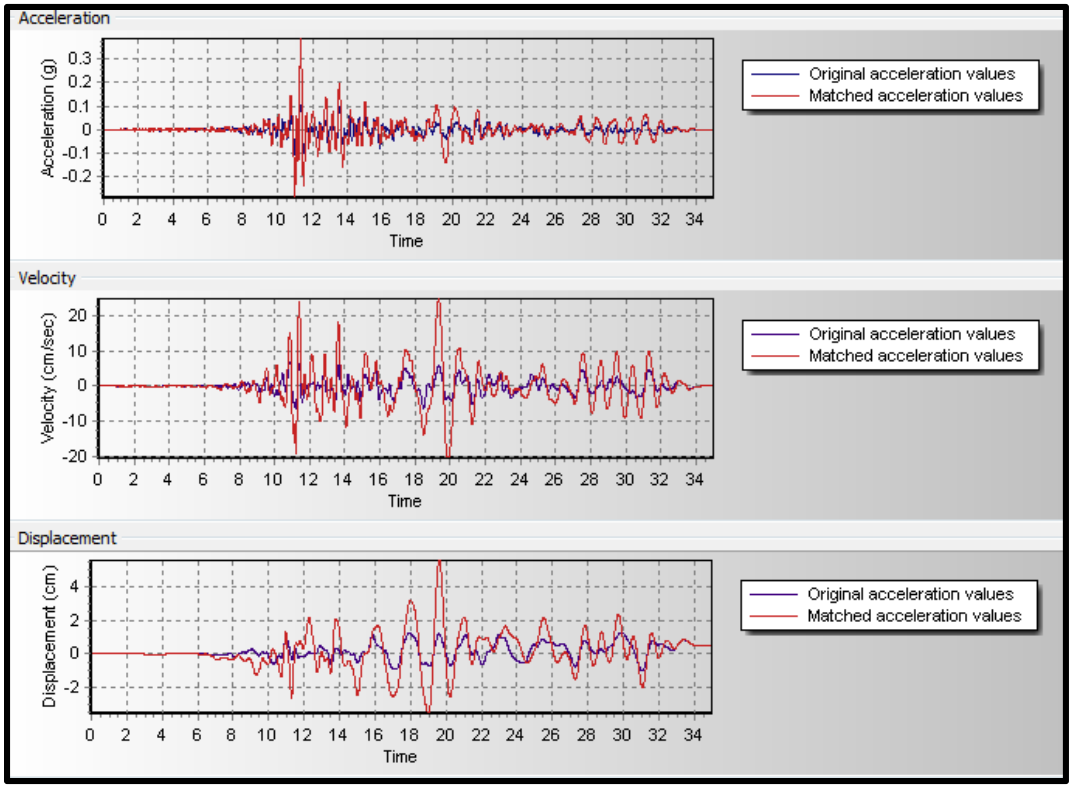

Figure C.1.35 TH7NR_Z original vs. matched acceleration, velocity and displacement time histories

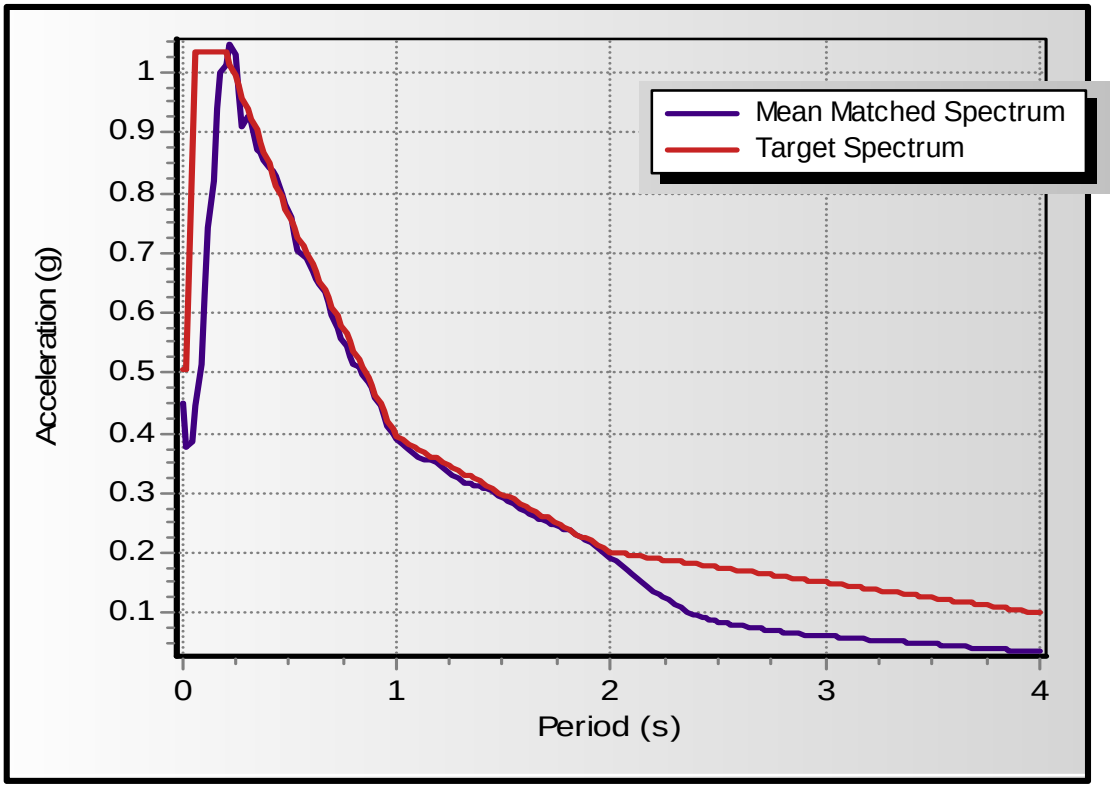

Figure C.1.36 Mean matched spectrum vs. target spectrum

Appendix D

Supporting Calculations

Sample Calculation for Dynamic Masses

AREAS.

ROOF: $(200)(260) - (72)(100) = 44800\ FT^2 = 4200\ M^2$

PH: $(200)(220) - (72)(100) = 36800\ FT^2 = 3400\ M^2$

UNIFORMLY DISTRIB. DL & SL

ROOF: 8" CONC. SLAB @ UNIT WEIGHT 150 lb/ft³

$(8/12)(150) = 100\ PSF = 4.8\ KPa$.

PARTITIONS: 1 KPa.
6"x6" STEEL COL: 96 COL 20 KN/COL

PH: 8" CONC. SLAB @ UNIT WEIGHT 150 lb/ft³
4.8 KPa.
SDL TO ACCOUNT FOR PERMANENT EQUIPMENT USE 20 PSF
1 KPa.
SNOW: $S = T_s[S_s(C_b C_w C_s C_a) + S_r]$
$= 1.25\,(1.8\,(0.8)(1.0)(1.0)(1.0) + 0.2)$
$= 2.0\ KPa$
25% SNOW = 0.5 KPa

TOTAL: $(4.8+1)(4200) + (4.8+1.0+0.5)(3400) + (96)(20)$
$= 47400\ KN$

EACH COLUMN = $47400/164 = 288\ KN/COL$

ADDED TO EACH COL. @ ROOF LEVEL

FOR A TYPICAL FLOOR

DEAD LOAD (DL): 8" CONC @ 150 lb/ft³
100 PSF = 4.8 KPa

SUPER IMPOSED DEAD LOAD (SDL): 1 KPa PARTITIONS.
1 KPa ELECTRICAL & MECHANICAL TOLERANCE

TOTAL: $(4.8 + 1.0 + 1.0)KPa\,(8000\ m^2) = 54400\ KN$
220 COLUMNS @ $\frac{54400\ KN}{220} = 248\ KN/COL.$